Author:
Mcgowan, Lucy M

Title:
Modelling the biological mechanisms underpinning healthy and pathological bone repair in zebrafish (Danio rerio)

Modelling the Biological Mechanisms Underpinning Healthy and Pathological Bone Repair in Zebrafish (*Danio rerio*)

University of Bristol

School of Physiology, Pharmacology and Neuroscience

A dissertation submitted to the University of Bristol in accordance with the requirements of Doctor of Philosophy in the Faculty of Life Sciences

by

Lucy M. McGowan

17th March 2022

Word Count: 56,434

DEDICATION AND ACKNOWLEDGEMENTS

This thesis is dedicated to Leonard Harrison; a man who loved learning new things, telling bad jokes, barbequing in the rain, and above all else, his family.

I would first like to thank the Wellcome Trust for generously funding my Ph.D., as well as members of the Dynamic Molecular Cell Biology Ph.D. Programme for their support and friendship throughout my degree.

Dr Chrissy Hammond, thank you for being an exceptionally supportive and responsive supervisor. You always allowed me to create my own path during my Ph.D. and encouraged my desire to do the research I found most fascinating. Your supervision has made my project both productive and incredibly enjoyable. I would also like to thank members of the Hammond lab and the wider zebrafish research community at the University of Bristol, from whom I have learned a tremendous amount. In particular, thank you to my colleague, mentor and friend, Dr Erika Kague, who taught me research skills too numerous to list and was always first in line with me at the pub on Fridays. Thank you also to Dr David Gurevich for engaging in spontaneous, hour-long discussions about science *every* time we bumped into each other in the corridor; our conversations always brought exciting new ideas (too many to actually investigate) and spurred me on.

Thank you to my progress panel members, Professor Paul Martin and Dr Tom Richardson, for their valuable feedback throughout my project. I would also like to thank my second supervisor, Dr Rebecca Richardson, as well as Dr Borko Amulic, for his collaboration, extra supervision and for welcoming me into his own lab.

To my incredible friends: Hatcher, Cate, Elise, Meg, Gabs, Kian, Tom, Rich, Will, Andy & Rumba. You've each supported me throughout my Ph.D. *and* made sure I never felt alone whenever it got stressful. Thank you.

To my partner, Charlie, thank you for being my rock, my biggest cheerleader and my home. You always made sure I was fed when I was too busy to stop, went on countless snack runs to the 10 O'clock shop and switched on the light every time I didn't notice it had gone dark (literally, and metaphorically). I'm so grateful to have had you by my side throughout my Ph.D. Also, thank you for proposing 3 weeks before my thesis deadline – that wasn't *at all* distracting. If this writing process didn't put you off, nothing will.

Finally, to my adoring family, thank you for your unconditional love, unwavering support, and countless words of wisdom. You are better than the best family I could ever ask for. Mum, Dad, Ailsa and Grandma: You'll be glad to know that this means I'm *finally* finishing school. I couldn't have done it without you.

ABSTRACT

Bone is a dynamic, living tissue, maintained by an elaborate and interconnected network of different cell types. These cells synthesise and remodel a highly specialised, mineralised extracellular matrix (ECM). Tightly coupled communication between bone synthesising osteoblasts, bone resorptive osteoclasts and innate immune cells is required to maintain optimal bone turnover and respond to fracture. Osteoporosis is an increasingly prevalent disease with complex aetiology, characterised by reduced bone deposition in relation to bone resorption. This leads to bone fragility and fracture susceptibility; symptoms which carry an extensive socioeconomic impact and high morbidity in the population. Currently, osteoanabolic treatments to promote osteoblast activity in bone are lacking. During healthy fracture repair, osteoblasts precursors rapidly proliferate and differentiate into highly active, bone synthesising osteoblasts. Therefore, studying optimal fracture repair may elucidate the molecular mechanisms which promote osteoanabolic activity, thereby helping to identify new targets for the treatment of osteoporosis and fracture. Here, I employ zebrafish (*Danio rerio*) as a model system to explore genetic and immunological factors underpinning optimal bone repair. Zebrafish show remarkable genetic, skeletal and immunological similarities with humans, allowing for clinically relevant study of bone. However, unlike mammalian systems, zebrafish display high genetic tractability, fecundity, and fast generation time. Moreover, the translucent caudal fin of adult zebrafish serves as an ideal tissue for live imaging multicellular responses during repair and regeneration of mature bone. Therefore, I explored three factors, with poorly characterised influences on bone repair: Wnt16, neutrophils and Tnf-α. I demonstrate that Wnt16 elicits a protective effect against fracture and supports bone repair by regulating osteoblast differentiation. Furthermore, I highlight a novel, pro-reparative role for neutrophils in fracture stabilisation and rapid ECM production during early bone repair. Finally, I demonstrate that *tnf*α is expressed by differentiating osteoblasts in regenerating bone and explore the pleiotropic effects of Tnf-α on osteogenesis.

COVID-19 IMPACT STATEMENT

Between March 2020 and June 2020, access to lab facilities was prohibited by the University of Bristol due to the UK government's COVID-19 "stay at home" order. Though lab access resumed in July 2020, access remained restricted, with maximum occupancy rules in place for the remainder of the year, through to Spring/Summer 2021. As such, alternating working week patterns were established, meaning some experiments were delayed until equipment, lab space or aquarium space were available to book in line with new COVID protocols. COVID-19 self-isolation rules meant that some experiments were disrupted or had to be rescheduled. Moreover, some zebrafish lines were bred prior to the pandemic for adult experiments due to take place when lockdowns were enforced. This meant that some zebrafish stocks aged, and new stocks had to be bred before experiments could be performed. Thankfully, disruption resulting from the pandemic was largely mitigated by the Wellcome Trust, who generously granted me a 6 month extension to my Ph.D. However, progress on some experiments (namely FACS, confocal imaging and import and breeding of *tnfα* line) were slowed due to reduced access to facilities, minimal face-to-face training or staff absences (including ASU staff shortages), during and after the lockdown.

AUTHOR'S DECLARATION

I declare that the work in this dissertation was carried out in accordance with the requirements of the University of Bristol's *Regulations and Code of Practice for Research Degree Programmes* and that it has not been submitted for any other academic work. Except where indicated by specific reference in the text, the work is the candidate's own work. Work done in collaboration with, or with the assistance of, others, is indicated as such. Any views expressed in the dissertation are those of the author.

SIGNED: ……. DATE: ……17th March 2022……

TABLE OF CONTENTS

LIST OF FIGURES

LIST OF TABLES

LIST OF APPENDICES

LIST OF ABBREVIATIONS

ABBREVIATION	DEFINITION
AL	Amplicon Length
ALP	Alkaline Phosphatase
ANOVA	Analysis of variance
APC	Adenomatous Polyposis Coli
ARS	Alizarin Red Stain
ASU	Animal Scientific Unit
AWERB	Animal Welfare and Ethical Review Body
BMD	Bone Mineral Density
BMP	Bone Morphogenic Protein
BMU	Basic (Bone) Multicellular Units
bp	Base pair
BSP	Bone Sialoprotein
CCR2	CC Chemokine Receptor 2
CD XX	Cluster of Differentiation XX
CIC-7	Chloride Ion Channel 7
COL10	Type 10 collagen
COL2	Type II Collagen
CPED1	Cadherin Like And PC-Esterase Domain Containing 1
CRISPR	Clustered Regularly Interspaced Short Palindromic Repeats
CSFR1	Colony Stimulating Factor Receptor 1
CT	Computed Tomography
CTSK	Cathepsin K
CXCR1/2	C-X-C motif chemokine receptors 1 and 2
DAMP	Damage Associate Molecular Patterns
DAPI	4′,6-diamidino-2-phenylindole
DC-STAMP	Dendritic Cell-Specific Transmembrane Protein
DD	Death Domain
DEPC	Diethyl Pyrocarbonate

DEXA	Dual Energy X-ray Absorptiometry
DKK-1	Dickkopf-related protein 1
DMEM	Dulbecco's Modified Eagle Medium
DMSO	Dimethyl Sulfoxide
DNA	Deoxyribonucleic Acid
dpa	Days post amputation
dpf	Days post fertilisation
dpi	Days post injury
dpr	Days post removal
eBMD	Estimated BMD
ECM	Extracellular Matrix
EDTA	Ethylenediaminetetraacetic acid
eGFP	Enhanced Green Fluorescent Protein
Ekk	Ekkwill
eQTL	Expression Quantitative Trait Loci
EtOH	Ethanol
FAB	Fibroblast Activating Protein
FACS	Fluorescence Activated Cell Sorting
FAP	Fibroblast Activating Protein
FBS	Foetal Bovine Serum
FGF	Fibroblast Growth Factor
FSC	Forward Scatter
GFP	Green Fluorescent Protein
gRNA	Guide RNA
GSK3β	Glycogen synthase kinase 3β
GTP	Guanosine Triphosphate
GWAS	Genome-Wide Association Studies
HBM	High Bone Mass
HEPES	4-(2-hydroxyethyl)-1-piperazineethanesulfonic acid
HIF	Hypoxia Inducible Factor
hpi	Hours post injury
HSC	Haematopoietic Stem Cell

IHC	Immunohistochemistry
IL	Interleukin
JNK	c-Jun kinase
KOH	Potassium Hydroxide
LEF	Lymphoid-Enhancing binding Factor
LRP-5	Low-density lipoprotein Receptor-related Protein 5
Lyz	Lysozyme
M-CSF	Macrophage Colony Stimulating Factor
MAPK	Mitogen-Associated Protein Kinases
MCC	Mander's Correlation Coefficient
MCP-1	Macrophage Chemotactic Protein 1
MeOH	Methanol
MGC	Multinucleated Giant Cell
MIA	Modular Image Analysis
MMP	Matrix Metalloproteinase
mo	Months old
MPX	Myeloperoxidase
MR	Mendelian Randomization
MS222	Tricaine methanesulphate
MSC	Mesenchymal Stem Cell
NADPH	Nicotinamide Adenine Dinucleotide Phosphate
NET	Neutrophil Extracellular Trap
NFP	Nifurpirinol
NFκB	Nuclear Factor kappa B
NK Cell	Natural Killer Cell
NLR	Neutrophil to Leukocyte Ratio
NOS	Nitric Oxide Synthase
NTR	Nitroreductase
OI	Osteogenesis Imperfecta
OPC	Osteoprogenitor Cell
OPG	Osteoprotegerin
OPN	Osteopontin

OPPG	Osteoporosis-Pseudoglioma Syndrome
OR	Oestrogen Receptor
OSX	Osterix
PAM	Protospacer Adjacent Motif
PAMP	Pathogen Associated Molecular Pattern
PBS	Phosphate buffered saline
PBS-Tw	0.1% Tween 20 in phosphate buffered saline
PBS-Tx	0.02% TritonX in phosphate buffered saline
PCC	Pearson's Correlation Coefficient
PCNA	Proliferating cell nuclear antigen
PDK1	Pyruvate Dehydrogenase Kinase 1
PFA	Paraformaldehyde
Phe-WAS	Phenome-Wide Association Study
PRR	Pathogen Recognition Reeceptor
PTH	Parathyroid Hormone
RANK-(L)	Receptor activator of NFκB - (ligand)
RNA	Ribonucleic acid
ROCK	Rho-associated protein Kinase
ROI	Region Of Interest
ROS	Reactive Oxygen Species
RUNX	Runt-related transcription factor
SD	Standard Deviation
SNP	Single Nucleotide Polymorphhism
SOST	Sclerostin
SOX	SRY-transcription factor
SSC (wash)	Saline Sodium Citrate (wash)
SSC (FACS)	Side Scatter (FACS)
TACE	TNF-α Converting Enzyme
TCF	T-Cell Factor
TGF- β	Transforming Growth Factor β
TL	Tüpfel Long fin
TMD	Tissue Mineral Density

Tnf-α	Tumour necrosis factor α
TNFR	TNF-α Receptor
TNFSF(R)	TNF Super Family (Receptor)
TRADD	TNFR1-Associated Death Domain
TRAF	TNFR-Associated Factor
TRAP	Tartrate-resistant acid phosphatase
TUNEL	Terminal deoxynucleotidyl transferase dUTP Nick End Labelling
VEGF(A)	Vascular Endothelial Growth Factor (A)
WHO	World Health Organisation
Wnt	Wingless-type MMTV integration site family member
WT	Wild Type
yo	Years old
zr	Zebrafish recombinant

PRELIMINARY TABLES

Table 1. Species Gene and Protein Nomenclature. *When referring to genes or proteins in a non-species-specific manner, human nomenclature is used.*

Species	Common Name	Gene Nomenclature	Protein Nomenclature
Homo Sapiens	Human	*WNT16*	WNT16
Mus musculus	Mouse	*Wnt16*	WNT16
Rattus norvegicus	Rat	*Wnt16*	WNT16
Danio rerio	Zebrafish	*wnt16*	Wnt16

CHAPTER 1: MAIN INTRODUCTION

Versions of some figures, text and tables included within this chapter have been published within a review article, in the peer-reviewed journal, JBMR (Dietrich et al., 2021 (1)). As a joint lead author, I contributed equally towards the creation and revision of this review article with my co-authors. Any published figures included in the chapter were originally created and revised solely by me, with edits made based on feedback from co-authors and reviewers. The published tables included within this chapter were researched and drafted by me and were edited by Dr Chrissy Hammond and Dr Franziska Knopf prior to manuscript submission. Any text included within this chapter that was published in the review was written solely by me. Throughout this thesis, where reference is made to this review, the publication has been cited accordingly to ensure credit is given to all co-authors. Moreover, some text included within this chapter was included within the introduction of an original research article published in the peer-reviewed journal, JBMR Plus (McGowan et al., 2021 (2)). As the lead author of this research article, I prepared the manuscript in full, including all text. Dr Chrissy Hammond and Dr Erika Kague provided manuscript feedback prior to submission for publication. Text has been amended wherever appropriate for inclusion into this thesis.

1.1 SKELETAL BIOLOGY

1.1.1 THE CELLULAR COMPOSITION OF BONE

Skeletal homeostasis is central to a vast number of essential processes in the body; in addition to facilitating movement and protecting vital organs, our bones regulate mineral reserves, house haematopoiesis and influence systemic hormone levels (3). Despite its strong and protective structure, bone is a highly dynamic, complex, and responsive tissue. Skeletal homeostasis is maintained by numerous cell types such as chondrocytes, osteoblasts, osteocytes, osteoclasts and innate immune cells (Figure 1) (4, 5). These cells work in synergy to maintain an optimal balance between bone deposition and bone resorption under steady state conditions, maintain joint integrity and to respond to acute skeletal damage such as fracture (6, 7).

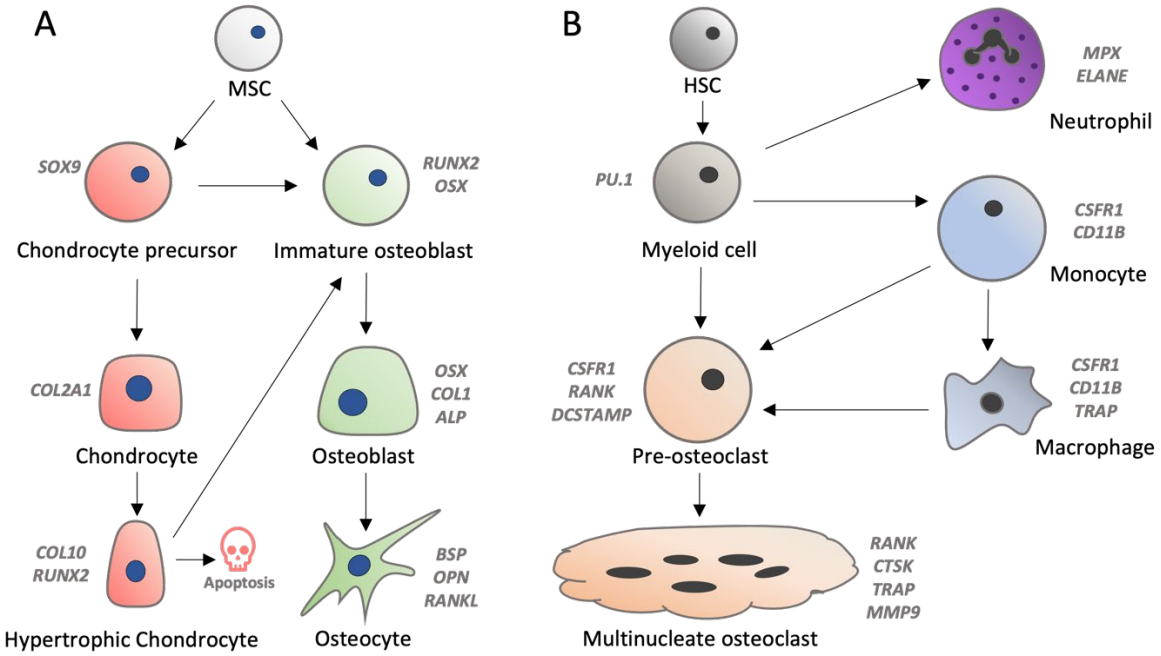

Figure 2. The Cellular Composition of Bone. A: *Chondrocytes, osteoblasts and osteocytes differentiate from a mesenchymal stem cell precursor (MSC). Chondrocyte precursors express SOX9 (SRY-transcription factor 9), whereas immature osteoblasts initially express RUNX2 (runt-related transcription factor 2) and then OSX (Osterix). Chondrocyte precursors may transdifferentiate into immature osteoblasts via expression of RUNX2, or upregulate expression of COL2A1 (Type II collagen) and secrete vast quantities of ECM which is modelled into cartilage. Mature chondrocytes become hypertrophic, expressing COL10 (Type X collagen), and either undergo apoptosis or transdifferentiate into osteoblasts via upregulation of RUNX2 and OSX. Osteoblast precursors mature into osteoblasts via the downregulation of RUNX2 and upregulation of COL1 (Type I collagen) and ALP (Alkaline phosphatase); these cells synthesise bone matrix. Osteoblasts become trapped in the osteoid and differentiate into stellate osteocytes. Osteocytes are mechanosensitive cells which are interconnected via fluid-filled lacunae.* ***B:*** *Osteoclasts and myeloid immune cells differentiate from a haematopoietic stem cell precursor (HSC) expressing the PU.1 transcription factor. Myeloid cells may differentiate into neutrophils (expressing MPX (myeloperoxidase) and ELANE (elastase), monocytes and macrophages (expressing CSFR1 (Colony stimulating factor receptor 1), CD11B (Cluster of differentiation 11B) and TRAP (Tartrate-resistant acid phosphatase) or pre-osteoclasts (expressing CSFR1, RANK (Receptor activator of NF-κB) and DC-STAMP (Dendritic cell-specific transmembrane protein)). Monocytes and macrophages expressing RANK may differentiate into osteoclast precursors. Pre-osteoclasts fuse into multinucleate osteoclasts expressing MMP9 (Matrix metalloproteinase 9), CTSK (Cathepsin K), TRAP and RANK which resorb bone along their ruffled borders.*

1.1.1.1 CHONDROCYTES

Cartilage is a type of avascular connective tissue, with major roles in skeletal development and homeostasis, joint mobility, and bone repair. Chondrocytes are the cells which form and maintain cartilage by secreting vast quantities of a rich Extracellular Matrix (ECM) that is comprised of collagens, glycoproteins, proteoglycans, and hyaluronic acid (8). Type II collagen α 1 (encoded by *COL2A1*) is the most abundant protein within cartilage, closely interacting with other collagens and ECM proteins to form a dense fibrillar network (9). This complex fibrillar network traps water molecules, giving rise to the structural, load bearing and lubricating properties of cartilage. Chondrocytes are derived from Mesenchymal Stem Cells (MSCs) (Figure 1. A). The transcription factor SRY-box 9 (SOX9) induces the differentiation of MSCs into proliferating chondrocytes which express *COL2A1* and produce cartilaginous ECM (10). Chondrocytes may undergo further differentiation into mature pre-hypertrophic and hypertrophic chondrocytes, induced by Runt related transcription factor 2 (RUNX2). Hypertrophic chondrocytes are post-mitotic, display increased cell volume and synthesise proteins such as Vascular Endothelial Growth Factor A (VEGFA), Matrix Metalloproteinase 13 (MMP-13), type X collagen (COLX) and Nitric Oxide Synthase (NOS) to promote mineralisation (10, 11). This transition allows for the migration and differentiation of osteoblasts into the chondrocyte lacunae, which synthesise bone. However, pools of immature chondrocytes are maintained within joint sites and growth plates to allow for skeletal growth, repair and joint function; continued *SOX9* expression supresses the differentiation of these proliferative chondrocytes into hypertrophic chondrocytes, partly by promoting glutamine metabolism and enabling continued ECM production and chondrocyte survival within the avascular cartilage (12). Chondrocyte differentiation is largely governed by the dynamic control of SOX9, COLX, RUNX2 and bone morphogenic protein (BMP) signalling (11).

1.1.1.2 OSTEOBLASTS AND OSTEOCYTES

The strong structural properties of the skeleton can be attributed to ossification, a carefully balanced process in which osteoblasts secrete and mineralise bone matrix. Osteoblasts are cuboidal bone synthesising cells that are also derived from the mesenchymal lineage but differentiate from 2 distinct populations of cells (Figure 1. A). Osteochondral progenitor cells expressing *SOX9*, or hypertrophic chondrocytes expressing *COLX*, may differentiate into pre-osteoblasts in response to high levels of RUNX2 (13). Type X collagen is a marker of hypertrophic chondrocytes undergoing osteogenic differentiation, that is highly conserved in vertebrates (14, 15). Osteoblast precursors may also differentiate directly from MSCs which proliferate in response to osteopontin (OPN, also known as SPP1), before condensing and

upregulating expression of *RUNX2*. The proliferation and cell specification of pre-osteoblasts from MSCs is largely governed by reciprocal signalling between β-catenin, downstream of canonical Wnt (Wingless / Intergrated) signalling, and RUNX2 (16-18). Pre-osteoblasts, originating from either population, must then express the osteoblast transcription factor, osterix (OSX, also known as SP7), in order to supress Wnt/β-catenin signalling and differentiate into mature osteoblasts capable of synthesising bone matrix (19, 20). As these osteoblasts differentiate, they exit the cell cycle and upregulate the production of COL1A1, Bone Sialoprotein (BSP) and Alkaline Phosphatase (ALP) (13). Although these pre-mature osteoblasts are post-mitotic, they further differentiate into mature osteoblasts by adopting their characteristic cuboidal shape with a basophilic cytoplasm, and produce osteocalcin and calcium phosphate to facilitate bone mineralisation (13).

As the ECM mineralises around them, osteoblasts become entombed within bone and terminally differentiate into *OPN* and *BSP* expressing osteocytes (Figure 1. A); these cells comprise over 90% of the cellular content of bone (21). As they become embedded within the osteoid, osteoblasts extend dendritic protrusions which interact with the dendrites of neighbouring mature osteocytes; thus, osteocytes form an elaborate interconnected stellate cellular network (22). Osteocytes are highly mechanosensitive cells which reside within the fluid-filled lacunae of mature bone. As master regulators of bone homeostasis, osteocytes transduce mechanical, hormonal and environmental stimuli into the secretion of osteoregulatory factors, which fine tune the activity of osteoblasts and osteoclasts in bone (21). Although mature osteoblasts are known as the major source, osteocytes also secrete Osteoprotegerin (OPG), which acts as a decoy receptor for the osteoclastogenic Receptor Activator of NF-κB Ligand (RANK-L) (22, 23). On the other hand, osteocytes produce the protein Sclerostin (SOST), which negatively regulates Wnt signalling to supress osteoblast differentiation, and promote osteoclastogenesis (24). A balance between these osteoanabolic and osteocatabolic signals helps mature bone to self-regulate its turnover during homeostasis and in response to stress or injury.

1.1.1.3 OSTEOCLASTS

Osteoclasts are large, multinucleate bone-resorptive cells derived from the myeloid lineage (Figure 1. B). During development, Haematopoietic Stem Cells (HSCs) expressing the transcription factor, PU.1, and Colony Stimulating Factor Receptor 1 (CSFR1) begin differentiating into primitive macrophages, which also serve as osteoclast precursor cells (25). Macrophage Colony Stimulating Factor (M-CSF) is a pro-osteoclastogenic protein produced by osteoblasts, osteocytes and stromal cells. M-CSF binds to CSFR1 on

the surface of mononucleated osteoclast precursors, which then upregulate expression of RANK. The production of soluble RANK-L by immune and skeletal cells is crucial to induce osteoclastogenesis from myeloid precursors (26). Under the influence of RANK-L, $RANK^+$ osteoclast precursors differentiate into mature osteoclasts, cluster together and begin expressing Dendritic Cell-Specific Transmembrane Protein (DC-STAMP) (27, 28). Signalling via DC-STAMP allows osteoclast precursors to undergo fusion, forming giant, multinucleate, mature osteoclasts (29). Cathepsin K, Tartrate-Resistant Acid Phosphatase (TRAP) and MMP-9 are classical markers of mature osteoclasts, which facilitate the breakdown of mineralised bone matrix (30). Osteoclasts possess a distinctive ruffled border which is polarised towards the bone surface; here osteoclasts secrete proteolytic and demineralising enzymes (31, 32). As a result, osteoclasts leave a trail of resorptive pits and trenches on the surface of bone (33). Interestingly, a novel intermediate cell type, termed an "osteomorph", was recently discovered in mice (34). Osteomorphs are formed via the fission of mature multinucleate osteoclasts into non-resorptive, transcriptionally distinct, daughter cells. Remarkably, RANK-L induces the refusion of these daughter cells into mature osteoclasts at different locations, whilst OPG has been shown to inhibit this recycling process (34). As members of the myeloid lineage, many of the molecular signals which act on innate immune cells also regulate osteoclastogenesis (35). Therefore, osteoclast differentiation is closely intertwined with inflammation.

1.1.1.4 OSTEOIMMUNOLOGY

In addition to defending the body from invading pathogens, the immune system is a key regulator of musculoskeletal homeostasis (36). The emerging field of osteoimmunology examines the relationship between the immune system and bone. Similarly to osteoclast precursors, mature macrophages are capable of cell fusion, forming Multinucleated Giant Cells (MGCs) (37). Within the bone microenvironment, pro-inflammatory conditions are generally thought to suppress osteoblast differentiation, whilst promoting osteoclastogenesis (38). Along with stromal cells, activated immune cells, including neutrophils, macrophages and T lymphocytes, provide a major source of osteoclast promoting proteins such as RANK-L and M-CSF (39, 40). It is now accepted that osteoclasts do not only differentiate from immature myeloid precursors; they also arise from monocytes, mature macrophages, MGCs and potentially dendritic cells (35). The cytokine Tumour Necrosis Factor alpha (TNF-α), which is expressed by pro-inflammatory macrophages, is known to promote RANK expression by macrophages and monocytes, priming them for

RANK-L mediated transdifferentiation into osteoclasts (41). Moreover, TNF-α can directly stimulate the production of RANK-L by osteocytes and stromal cells (42).

Despite strong links between inflammation and bone resorption, immune cells also play an immunoregulatory role in bone. Bone-resident macrophages, termed "osteomacs", have been described in the homeostatic control of bone (43, 44). Osteomacs are specialised bone-resident macrophages, which maintain osteal tissue via efferocytosis of apoptotic osteoblasts, as well as modulating healthy bone turnover and repair (44, 45). Even less is understood about the long-term role of neutrophils in bone health and disease. High numbers of pro-inflammatory neutrophils in peripheral blood are associated with decreased bone mineral density (BMD) (40). However, chronic neutropenia (low blood neutrophil counts) is also associated with pathological bone loss, suggesting that neutrophils contribute to the homeostatic regulation of bone turnover (46). Despite their crucial role in innate immunity, the role of neutrophils in maintaining bone health has been relatively understudied. Thus, more research is required to elucidate the immunoregulatory and pathogenic contributions of innate immune cells in bone.

1.1.2 BONE DEVELOPMENT AND REMODELLING: AN OVERVIEW

From an evolutionary perspective, bone should be strong and shock absorbent, whilst also being as lightweight as possible. Therefore, skeletal development and homeostasis are finely-tuned processes which are optimised to provide these properties. Throughout life, skeletal cells must orchestrate three main processes: developmental osteogenesis, bone modelling throughout growth and remodelling of mature bone (13). During development, the paraxial mesoderm, the neural crest and the lateral plate mesoderm migrate throughout the developing embryo to give rise to the axial skeleton, the craniofacial skeleton and the limbs, respectively (47). Once in position, MSCs condense into either osteoblasts or chondrocytes, to give rise to three types of bone tissue, via two main routes: intramembranous ossification and endochondral ossification (48). Dermal bone is formed via intramembranous ossification, which is mainly found in the skull, jaw and clavicle in humans (49). However, most bone, including all long bones, arises via endochondral ossification during skeletal development, which forms trabecular (spongey / cancellous) bone and cortical (compact) bones (50). Cortical bone is strong, providing structural support for movement, and accounts for the majority of the mature skeleton. Trabecular bone is porous in appearance, and is found at the centre and distal ends of long bones (e.g. femur), or in the vertebral column, where it absorbs

shock from mechanical loading (51). Cortical and trabecular bones also house hematopoietic marrow within their cavities.

1.1.1.5 ENDOCHONDRAL OSSIFICATION

Endochondral ossification is the process by which chondrocytes produce a cartilaginous scaffold, which is subsequently ossified by osteoblasts. Long bones, such as the femur, develop via this process. Throughout skeletal development, populations of condensed MSCs expressing *SOX9* differentiate into *COL2A1*$^{+}$ chondrocytes, which secrete the ECM that is assembled into mature cartilage (52). As endochondral ossification develops, pools of immature chondrocytes migrate radially outwards, leaving a gradient of mature and hypertrophic chondrocytes behind them within the cartilaginous scaffold. Gradually, this cartilage becomes vascularised as a result of VEGF production by hypertrophic chondrocytes (53). Chondrocyte differentiation favours hypoxic conditions, whereas vascularisation promotes osteoblast differentiation (50). Therefore, hypertrophic chondrocytes within the mature cartilage template either undergo apoptosis or differentiate into osteoblasts via Wnt/β-catenin mediated expression of *RUNX2* and *OSX* (10). Moreover, MSCs seeded within the cartilage template differentiate directly into osteoblasts and begin synthesising trabecular bone, which hardens as it ossifies. This region becomes the primary centre of ossification, which expands outwards as osteoblasts secrete cortical bone around the surface of the cartilage template (47). As bones elongate, secondary ossification sites appear at the ends of the tissue (forming the epiphyses), where trabeculated bone is modelled; this provides the shock-absorbing, spongey tissue within vertebrae and the femoral head, amongst other bones. Until maturity is reached, bone appositional growth is achieved by the growth plate. The growth plate is a highly organised tissue, populated with a series of chondrocytes that are arranged into zones of proliferation, then increasing maturity. Chondrocytes within the growth plate pass from proliferation, then through prehypertophy and hypertrophy, before apoptosing or transdifferentiating into osteoblasts (54). At the distal ends of the bone, articular cartilage is produced by chondrocytes within the joint; this is maintained by pools of immature chondral cells throughout life, which are essential for joint health and skeletal mobility, though cartilage has relatively limited capacity for repair. Osteoclasts shape the overall structure and density of bone, during both skeletal development and remodelling of mature bone throughout life. However, little is known about the interactions of osteoclasts with developing bone, or their role in shaping the skeleton. Prenatal osteoclasts are derived from the yolk sac, and are thought to contribute minimally towards skeletal development, whereas postnatally, osteoclasts differentiate from HSCs to resorb bone (26, 49).

1.1.1.6 INTRAMEMBRANOUS OSSIFICATION

Unlike endochondral ossification, intramembranous bone formation does not require an intermediate cartilaginous template. Intramembranous ossification is the process by which condensed MSCs differentiate directly into osteoblasts, via sequential expression of RUNX2 and OSX. This process is heavily dependent on the dynamic activation and repression of the canonical Wnt/β-catenin pathway, as well as fibroblast growth factor (FGF) pathway signalling (16). Intramembranous bones, such as calvaria found in the skull, gradually grow outwards via a continuous process of remodelling, sutural growth and the formation of secondary cartilage (49). Where neighbouring intramembranous bones meet, they are united along suture edges, which contain proliferative stem cells and osteoblast precursors (55). A sub-type of intramembranous ossification is perichondral bone formation, whereby bone is deposited onto the surface of cartilage, without replacing it (1). Perichondral ossification occurs at the interface of the growth plate and bone, either preceding or occurring alongside endochondral ossification (56).

1.1.1.7 BONE REMODELLING

As bone reaches maturity, continuous communication between skeletal cells ensures that the tissue is maintained over time and responds appropriately to mechanical or environmental stress. Under homeostatic conditions, osteocytes secrete SOST to suppress unnecessary differentiation and activity of osteoblasts (24). As already described, osteocytes sense mechanical strain via their dendritic processes as forces are applied to the skeleton. Mechanical stimulation leads to an influx of intracellular calcium in osteocytes to influence cell metabolic pathways, whilst the cell membrane receptor, piezo 1, transduces mechanical cues into the activation of canonical Wnt signalling, increased OPG and OPN production, and downregulation of SOST (57, 58). This helps to ensure that bone deposition is upregulated in regions of the skeleton that are exposed to strain.

Remodelling is the cyclical mechanism by which bone is continuously renewed via resorption of old or damage bone, followed by deposition and mineralisation of new bone matrix (6). During remodelling, osteoactive Basic Multicellular Units (BMUs, also Bone Multicellular Units) form on the surface of bone, and orchestrate bone remodelling via five distinct stages: activation, resorption, reversal, formation and termination (59). The BMU is comprised of bone resorptive osteoclasts at the leading edge which are separated from bone synthesising osteoblasts by a bridge of mononucleated (reversal) cells, all contained beneath a canopy of bone lining cells (60). The activation phase may be induced by systemic hormonal

changes (e.g. parathyroid hormone (PTH) and oestrogen), strain due to physical activity, or microdamage of bone resulting from day-to-day wear and tear (6). This results in localised bone matrix damage and osteocyte apoptosis, triggering the formation of a BMU. Osteoclast precursors are recruited to the bone, where they differentiate into osteoclasts under the influence of RANK-L and resorb bone. The reversal phase then follows bone resorption, whereby mononuclear cells remove trails of demineralised collagen, left in the wake of osteoclasts. The exact origin of reversal cells has been debated. However, it has been demonstrated that reversal cells are immature osteoblast cells, which express RUNX2 (61, 62). During the formation phase, osteoblasts differentiate and deposit fresh matrix rich in type 1 collagen in previously resorbed area, which is then mineralised. Finally, in the termination phase, osteoblasts either undergo apoptosis, or become trapped within the newly-formed osteoid and differentiate into SOST-producing osteocytes, acting to suppress bone formation (59). Whilst bone remodelling is an elegant, self-regulating cycle, dysregulated signalling at any stage of this process can lead to bone pathology. Moreover, if bone experiences unbearable force during traumatic injury, it will fracture. Fractures must be efficiently repaired to restore skeletal homeostasis and bone function.

1.2 OSTEOPOROSIS AND FRACTURE REPAIR

1.2.1 THE PATHOPHYSIOLOGY OF OSTEOPOROSIS

Bone development, growth and remodelling requires strictly coordinated reciprocal signalling to balance osteoblast and osteoclast activity. Therefore, perturbation of this balance leads to pathophysiology, a decline in bone health and impaired skeletal function. A myriad of different skeletal diseases can arise due to imbalanced bone development and homeostasis. However, here I will focus on osteoporosis, a highly prevalent bone disease.

When bone deposition by osteoblasts is reduced in relation to resorption by osteoclasts, a reduction of BMD ensues, leading to loss of bone integrity (4). Poor bone quality and low BMD are strong predictors of fracture risk (63). Osteoporosis is a chronic metabolic bone disease which is characterised by a harmful reduction in BMD, resulting in high susceptibility to fracture. Fragility fractures cause extensive morbidity and pose a significant socioeconomic burden in the United Kingdom, costing the National Health Service an estimated £4.4 billion annually (64). Osteoporosis is a multifactorial disease; primary osteoporosis

occurs due to genetic, hormonal or age-related loss of bone homeostasis, whereas secondary osteoporosis is a by-product of other chronic diseases, or long-term exposure to glucocorticoids, which disrupts bone turnover (65).

1.2.1.1 AGE-RELATED OSTEOPOROSIS

Osteoporosis is predominantly an age-related disease. Currently, in the UK, an estimated 3.5 million people over the age of 50 suffer with osteoporosis, resulting in over half a million fragility fractures per year (66). Moreover, as the ageing population increases, the treatment costs associated with osteoporotic fractures are set to rise by 30% in the next decade. As many as 1 in 3 women and 1 in 5 men over 50 will experience an osteoporotic fracture in their lifetime, meaning age is the strongest predictor of osteoporosis (67). The impact of fragility fractures on quality of life in the ageing population is substantial; they cause long term pain, mobility issues and social isolation, whilst 25% of people who suffer hip fracture die within one year of the injury (66, 68).

Around the age of 50, the number of resorptive BMUs within endosteal bone increases, whilst the formation of bone at the surface declines, leading to a gradual reduction in BMD over time (69). In addition to a decline in the amount of bone, the microstructural properties of bone deteriorate with age. In trabecular bone within the vertebrae and femoral neck, trabecular number significantly decreases after 60 years, with increased separation between trabeculae (70, 71). These changes to the trabecular architecture are consistent between men and women, suggesting that they result from ageing. Moreover, increased resorption forms pores within the cortex of cortical bone, resulting cortical thinning. The diameters of individual pores further expand with age before fusing together to form giant pores (70, 72). Whilst both men and women display increased cortical porosity with age, cortical thinning is more pronounced in women (73). A study in mice demonstrated that age-related increases in endosteal remodelling were associated with increased DNA damage and cell senescence in osteocytes, as well as increased RANK-L production, in a sex steroid-independent manner (74). Adiposity has been linked to osteoporosis, as bone marrow stromal cells favour differentiation into adipocytes, as opposed to skeletal cells, with age (75). Adipocytes can stimulate osteoclastogenesis via the production of pro-inflammatory cytokines such as TNF (76). However, the directionality of the relationship between adiposity and osteoporosis is unclear. The process of ‘inflammaging’ is also associated with age related bone loss and fracture risk (77). Inflammaging is characterised by low-grade chronic inflammation; specifically, activation of the innate immune system in the absence of infection or injury (78). Given that pro-inflammatory cytokines stimulate bone resorption,

and that chronic inflammation can also occur with age, a better understanding of how ageing, inflammation and bone are linked is required to identify new therapies to treat osteoporosis and fragility fractures (79, 80).

1.2.1.2 POST-MENAPAUSAL OSTEOPOROSIS

Oestrogen is a master regulator of bone health in both men and women, supressing bone remodelling by signalling directly to osteoblasts, osteocytes and osteoclasts via oestrogen receptors (ORs) (81). Deletion of OR-α from myeloid cells in mice suppresses osteoclast differentiation and reduces trabecular bone resorption. However, this effect is not recapitulated in cortical bone (82, 83). Crucially, oestrogen is known to protect osteoblasts and osteocytes against apoptosis, whilst also promoting osteoblast differentiation (84, 85). Expression of OR-α by osteoblast precursors has been shown to trigger canonical Wnt signalling to promote osteogenic differentiation and cortical bone formation in an oestrogen-independent manner (84, 86). Oestrogen also induces the production of the RANK-L decoy receptor, OPG, by osteoblasts (87). Throughout perimenopause, oestrogen levels decline, triggering a reconfiguration of bone at the cellular level and an overall shift towards increased bone remodelling and resorption (88). As a result, osteoporosis is particularly prevalent in post-menopausal women (89).

1.2.1.3 GENETIC AND DEVELOPMENTAL CAUSES OF OSTEOPOROSIS

Familial studies have demonstrated that between 50 and 85% of the variance in peak adult BMD is inherited, with age-related bone loss also showing a degree of heritability (90). This highlights that there is a strong genetic component to osteoporosis.

Rare genetic mutations can cause gross defects in skeletal development and remodelling, predisposing individuals to osteoporosis at a young age (91). Osteogenesis Imperfecta (OI) is the term given to a collection of rare genetic bone collagenopathies, which are characterized by sub-optimal skeletal development, aberrant bone architecture and high fracture incidence (92). There are multiple sub-types of OI, with varying degrees of severity; type I OI is the mildest form, which is underpinned by reduced production of normal type 1 collagen. Other types of OI are the result of mutations which alter the molecular structure of type 1 collagen (93). The majority of OI cases result from mutations in *COL1A1*/*A2*. (94). Some rarer forms of OI arise from mutations in collagen-processing genes such as *BMP1* and *PLOD2* (95-98), or osteoblast- related genes such as *OSX* (99, 100). Interestingly, rare mutations in genes encoding an androgen-to-oestrogen converting enzyme, as well as OR-α (*ESR1*) are also known to induce premature

osteoporosis (90). Finally, loss of function mutations in low-density lipoprotein receptor-related protein 5 (*LRP5*), which encodes a key protein in the canonical Wnt signalling pathway, causes Osteoporosis-Pseudoglioma Syndrome (OPPG) (101). OPPG is an extremely rare autosomal recessive disorder, which causes severe juvenile osteoporosis and blindness. Interestingly, gain of function mutations in the same gene leads to overproduction of OPG, causing a high bone mass phenotype (102). This highlights the need for effective Wnt signaling in healthy bone development and the prevention of osteoporosis.

More recently, large scale epidemiological studies have begun to identify hundreds of genetic loci associated with low BMD and fracture susceptibility (103, 104). Relatively common single-nucleotide polymorphisms at these loci are likely to underpin bone phenotypes which cause a predisposition to osteoporosis. Epigenetic modifications, such as DNA methylation, histone modification and activity of non-coding RNAs, are also known to alter gene expression in skeletal cells and influence bone metabolism in the pathogenesis of osteoporosis (105). One study, which assessed genome-wide DNA methylation in healthy and osteoporotic trabecular bone in humans, demonstrated that increased methylation of osteogenic genes is associated with osteoporosis (106). Investigating the genetic basis of osteoporosis will help to identify genes and pathways that are crucial for healthy bone development and maintenance, thereby revealing targets to promote increased BMD.

1.2.1.4 GLUCOCORTICOID MEDIATED BONE LOSS

Secondary osteoporosis can be induced by long-term glucocorticoid use. Glucocorticoids, such as prednisolone and dexamethasone, are common immunosuppressive drugs, used for the treatment of chronic inflammatory diseases like rheumatoid arthritis, asthma and allergy (107). Glucocorticoids inhibit osteoblastogenesis and increase osteoblast apoptosis, whilst stimulating bone resorption by osteoclasts (108). Interestingly, osteoblast expression of the glucocorticoid activating enzyme, 11 β-hydroxysteroid dehydrogenase, increases in osteoblasts with age, meaning endogenous and synthetic glucocorticoids are more readily activated within bone in older people (109). Not only does glucocorticoid-mediated immunosuppression increase fracture risk, but it also impedes bone repair and remodelling, due to impaired immune cell and osteoblast responsiveness (110, 111). On the other hand, hyperinflammation has also been associated with bone loss (77, 80). Collectively, this highlights the crucial role of immune regulation in balancing overall bone homeostasis and responding to damage.

1.2.1.5 DIAGNOSIS AND TREATMENT OF OSTEOPOROSIS

Dual Energy X-ray Absorptiometry (DEXA) is the traditional method used to measure the mineral content of bone within a defined area and calculate a T-score. An individual's T-score represents their BMD in relation to that of a healthy young adult in the population and is based on the difference in standard deviations (SDs) from the peak bone mass (65). In 1994, the World Health Organisation (WHO) defined a T-score of -2.5 SDs sufficient for the diagnosis of osteoporosis (112). However, osteoporosis is a silent disease, with most patients unaware of a decline in BMD until fragility fracture occurs. Computed Tomography (CT) imaging is a technique which is routinely used to monitor chronic diseases and assess trauma but can also be used to measure BMD. Recently, opportunistic quantitative screening of routinely acquired CT scans has been proposed as a low-cost method for early diagnosis of osteoporosis and intervention via the detection of previously unrecognised vertebral fractures (113). However, the aetiology of osteoporosis varies from patient-to-patient. Therefore, a variety of treatments are required to reflect the complexity in the pathophysiology of osteoporosis.

Historically, the treatment of osteoporosis has depended heavily on anti-resorptive bisphosphonates, such as alendronate and zolendronate, to supress osteoclast activity (114). However, long-term use of bisphosphonates can cause gastrointestinal irritation and may even lead to osteonecrosis of the jaw (115). Other anti-resorptive treatments include hormone replacement therapy, as well as a RANK-L-neutralising biologic, denosumab (114). Whilst a range of antiresorptive drugs are available, targeted and affordable osteoanabolic treatments to promote osteoblast activity are lacking. Teriparatide and abaloparatide are PTH mimicking biologics, which can stimulate osteoanabolic activity and increase BMD, in a dose-dependent manner (116). However, use of these drugs is limited to 24 months due to concerns over their long-term safety, whilst abaloparatide is only approved in the US. Romosozumab is a novel monoclonal antibody therapy which inhibits SOST activity to stimulate osteoblast differentiation, and has superior effects on BMD increase, compared to denosumab (117). However, romosozumab treatment may increase risk of severe cardiovascular disease and its efficacy is thought to wane after 12 months (118). Current osteoanabolic therapies are costly, short-term and impractical for patients as they must be injected (116). Hence, there is an urgent unmet demand to identify novel targets for therapeutic intervention in osteoporosis and promote optimal bone repair in fragility fractures.

To truly decipher the cellular and molecular underpinnings of osteoporosis and identify novel pathways for its treatment, a better understanding of osteogenesis in adult bone is required. The triggering of

inflammatory processes as well as reactivation of developmental osteogenic pathways are required during healthy fracture repair. Therefore, understanding how this process is regulated may highlight important targets for the treatment of osteoporosis.

1.2.2 HEALTHY FRACTURE REPAIR

Fractures arise when the mechanical properties of bone are overwhelmed by the force applied to it. This can occur where excessive force is applied to healthy bone (traumatic injuries), or due to the failure of poor-quality bone to withstand normal levels of mechanical force (diseased bone). Fractures range in their severity, depending on the location within the body and the degree of trauma; overall, they represent a substantial socioeconomic health burden in the population (119). Skeletal mobility and circulation around fractures are impaired (120). Therefore, efficient fracture repair is essential to restore function of the affected area in the body. Bone is one of few tissues in the adult human body that can effectively repair itself after trauma, without fibrous scarring; thus, fracture repair can be considered as a type of tissue regeneration (121). This is made possible by the coordinated retriggering of bone developmental pathways. Fracture repair is orchestrated by three overlapping processes: inflammation, bone repair and callus remodelling (Figure 2) (122).

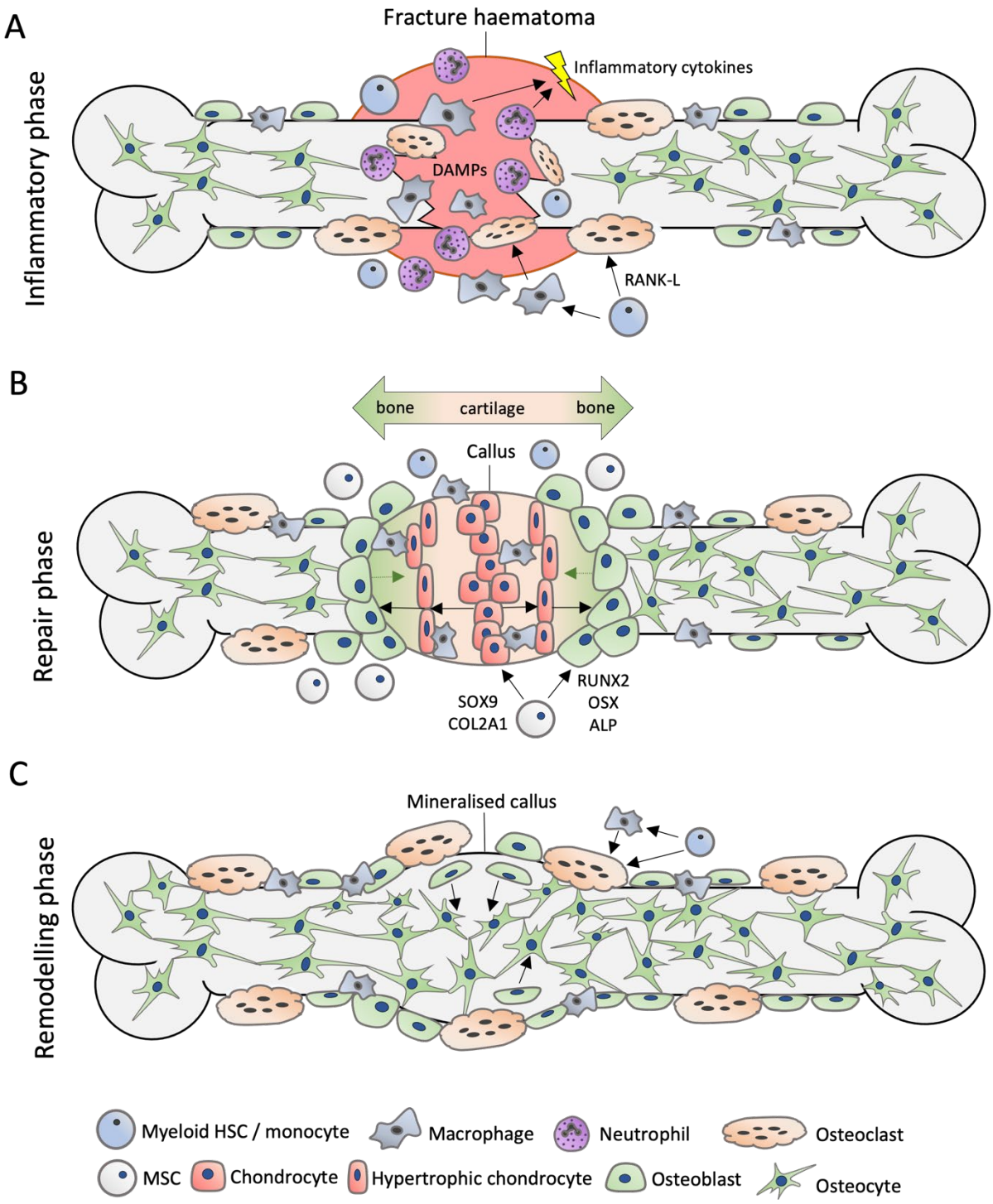

Figure 3. An Overview of Fracture Repair in Humans. *Fracture repair follows 3 phases: inflammation, repair and remodelling.* ***A:*** *Damage associated molecular patterns (DAMPs) are released immediately after fracture to recruit inflammatory cells to the fracture haematoma and secrete pro-inflammatory cytokines. Osteoclasts differentiate from either myeloid Haematopoietic Stem Cells (HSCs),*

monocytes or macrophages, in response to Receptor Activator of NF-κB Ligand (RANK-L) and resorb damaged bone. ***B:*** *Chondrocytes differentiate from Mesenchymal Stem Cell (MSC) precursors expressing SOX9 and synthesise a soft cartilaginous callus rich in type II collagen (COL2A1). At the periphery of the callus, osteoblasts differentiate from MSCs expressing Runt-related transcription factor 2 (RUNX2) and Osterix (OSX) and secrete bone matrix rich in type I collagen, which is mineralised. Chondrocytes adjacent to vascularised bone become hypertrophic and either undergo apoptosis or transdifferentiate into osteoblasts. Gradually, the cartilaginous template (soft callus) is transformed into a mineralised (hard callus).* ***C:*** *Once a hard callus of woven bone has formed, the callus is gradually remodelled via resorption by osteoclasts and deposition of mature, lamellar bone by osteoblasts. Osteoblasts become entombed within the bone and differentiate into mechanosensitive osteocytes, which orchestrate bone remodelling.*

1.2.2.1 PHASE 1: INFLAMMATION

The inflammatory phase is initiated immediately after injury; damage associated molecular patterns (DAMPs) trigger local immune and stromal cells to release pro-inflammatory cytokines and chemokines, which activate complement cascades and recruit leukocytes (123). Moreover, the rapid formation of fibrin clots at the injury site stems blood loss and results in the formation of a fracture haematoma, a temporary hypoxic tissue, which bridges damaged bone and provides a scaffold for the infiltration of inflammatory cells (124, 125). Neutrophils are the first cell type to be recruited to the fracture, accumulating at the fracture haematoma within hours of the injury. Open fractures carry a significant risk of infection, which can complicate bone repair or even lead to serious systemic inflammation (126). Therefore, as the first line of defence, neutrophils are required to provide antimicrobial protection against invading pathogens at the fracture site (127). Neutrophils also amplify inflammation via the production of pro-inflammatory cytokines, chemokines, and growth factors, such as Interleukin 1β (IL-1β), TNF-α, IL-6, Monocyte Chemotactic Protein 1 (MCP-1) and Transforming Growth Factor β (TGF-β) (128, 129). This initiates the repair process by promoting callus formation and the recruitment of other inflammatory cells such as macrophages. Early neutrophil-mediated inflammation is thought to influence osteogenic and chondrogenic differentiation of MSCs, thereby facilitating bone matrix deposition at the later stages of repair (128). However, it has also been proposed that neutrophil recruitment has a negative influence on fracture repair via the production of reactive oxygen species (ROS) and ECM remodelling enzymes (127). The exact role of neutrophils in fracture repair is still debated. It is likely that early recruitment of neutrophils to the fracture haematoma is necessary to initiate efficient and optimal fracture repair, but

excessive inflammation by neutrophils due to dysregulated granulocyte regulatory mechanisms or infection within the fracture haematoma has a detrimental effect. Further research is required to elucidate the optimal neutrophil response in fracture repair.

The role of macrophages throughout bone repair is better characterised than that of neutrophils. Both tissue resident and circulating cells of the macrophage / monocyte lineage are recruited to fractures slightly later than neutrophils, contributing not only towards the initial inflammatory phase, but also the repair and remodelling phases (43). In mice, ablation of macrophages at various time points post fracture impairs early soft callus formation, as well as endochondral ossification and formation of a hard bony callus (130). Moreover, in zebrafish, nitroreductase-mediated and glucocorticoid-induced apoptosis of macrophages impairs fin regeneration and fracture repair, with increased fracture susceptibility (111, 131). Thus, the role of macrophages and monocytes in orchestrating fracture repair is significant. Initially, classical pro-inflammatory macrophages (M1) provide further antimicrobial activity, clearance of necrotic cells and stimulate inflammation at the fracture site, whilst pro-reparative macrophages (M2) stimulate osteogenesis (132). Moreover, it has been proposed that M1 macrophages recruited to fractures can differentiate directly into osteoclasts under inflammatory conditions, which are required for the clearance of dying bone fragments prior to initiation of the repair phase (133). Excessive or prolonged inflammation during the inflammatory phase of fracture is known to impede efficient bone repair, and can lead to fracture complications (134).

1.2.2.2 PHASE 2: BONE REPAIR

As the inflammatory phase resolves, the repair phase is initiated. During the repair phase, osteoblast precursors must proliferate and differentiate into bone synthesising osteoblasts, which infiltrate the fracture haematoma and permanently fuse damaged bone together via the formation of a mineralised callus. In mammals, this occurs via retriggering of endochondral and intramembranous bone formation pathways; repair of diaphyseal bone (the shaft of long bones) involves both ossification pathways, whilst metaphyseal or epiphysial bone repair (at the growth plate) occurs only via the intramembranous route (134, 135). Moreover, repair of metaphyseal and epiphysial bone occurs much faster compared to diaphyseal fractures; osteoblasts rapidly infiltrate the injury where they directly synthesise woven bone and new trabeculae (135). Under optimal conditions, woven bone can be transformed into lamellar bone within a week of injury (134).

During diaphyseal fracture repair, osteoblast precursors can differentiate directly into osteoblasts in peripheral regions of the fracture haematoma, adjacent to intact bone, to perform intramembranous ossification. This is in part due to the intact vasculature providing the sufficient oxygen and nutrient supply required for osteoblast differentiation and bone deposition. However, the centre of diaphyseal fractures haematomas is hypoxic, favouring chondrocyte differentiation and the formation of a cartilaginous soft callus, which is then used as a template for endochondral ossification (136, 137). Interestingly, chondrocyte hypertrophy within the callus is also known to create mechanical pressure which acts like a jack to push the fractured bone back into alignment (138). It is thought that macrophages recruited to the fracture haematoma induce soft callus formation and stabilization of the damaged bone by promoting chondrogenic differentiation of MSCs, whilst osteomacs promote endochondral ossification and ongoing remodelling (43, 130, 139). Gradually, the soft callus is invaded by blood vessels which promote chondrocyte hypertrophy and apoptosis, or transdifferentiation of chondrocytes into osteoblasts via re-entry into the cell cycle and the expression of RUNX2 (140). Monocytes are also recruited to the soft callus via the vasculature and differentiate into cartilage-degrading osteoclasts, termed “chondroclasts” (134, 141). Simultaneously, osteoblasts expressing OSX migrate inwards and replace the cartilaginous matrix with mineralised bone, before further differentiating into mature osteoblasts or osteocytes, embedded within the osteoid (122). By the end of the repair phase, a hard, vascularised callus of woven and endochondral bone has formed at the fracture site. Skeletal homeostasis is restored via the resolution of repair and remodelling of the callus into mature bone.

1.2.2.3 PHASE 3: CALLUS REMODELLING

During bone repair, osteoblasts at the periphery of the injury synthesise disorganised woven bone via intramembranous ossification, whilst endochondral ossification also ensues in the centre of diaphyseal fractures. During the latest phase of fracture repair, bone is remodelled to restore its original functional, structural and mechanical properties, as much as possible (122). Treatment with anti-resorptive bisphosphonates does not affect fracture union or callus formation but does result in delayed callus resolution and formation of lamellar bone (142-144). This demonstrates that osteoclasts are required to initiate the remodelling phase of fracture repair. Osteoclasts resorb the immature woven bone before mature osteoblasts replace it with layers of reinforced lamellar bone (121). Macrophages also contribute to this process, indirectly via the production of osteoclastogenic signals, or directly, by differentiating into osteoclasts themselves (145). Mice deficient in the CC Chemokine Receptor 2 (CCR2), which is required for macrophage recruitment, exhibit delayed bone resorption and callus resolution during remodelling post

fracture (129). The remodelling process may take years to complete in humans, with the callus remaining visible even once bone integrity has been restored. Optimal fracture repair culminates in the formation of new bone at the injury site that is physiologically and mechanically comparable to the original bone. Homeostasis is ultimately reinstated in the tissue and the repaired bone is able to withstand normal physiological forces.

1.2.3 NON-UNION FRACTURES

Though bone is capable of complete repair post fracture, in up to 10% of cases, fracture results in non-union of bone. Non-union is a common complication of fracture that is broadly characterised by the failure of timely bone repair; this substantially reduces quality of life, whilst also extending treatment duration and cost (146). The aetiology of non-union fracture is complex and has been linked to lifestyle factors (e.g. smoking, anti-inflammatory drugs), biological factors (infection, underlying disease, age, gender) or mechanical factors (e.g. fracture location, degree of trauma, fixation post fracture) (146). Though the underlying causes can be multi-faceted, ultimately, dysregulated inflammation during the early phase of fracture repair, or failure to adequately retrigger and coordinate developmental ossification pathways, underpin fracture non-union (134, 147, 148). Hypertrophic non-unions develop where the fracture haematoma forms appropriately, but the mechanical environment is too unstable for repair to progress, meaning an excessively large soft callus forms, but cannot mineralise (146). Atrophic non-unions occur due to unfavourable biological conditions within the fracture site, resulting in poor callus formation and failure of bone to refuse (149). The “Diamond Concept” was coined in 2007, and describes the need to balance mechanical support, osteoconductive bone scaffolds, osteogenic precursors and growth factors to effectively augment bone repair in non-union fractures (150).

Orthopaedic surgery is a major treatment for the prevention or resolution of non-union fracture; pins or plates are used to mechanically fix the bone, in a supportive way that stimulates repair (134). In persistent non-union fractures, natural bone grafts, sourced from healthy regions of the patient’s own skeleton, or harvested from cadavers, may be used to induce callus formation (151). Recently, synthetic bone grafts, containing pro-osteogenic factors such as VEGF and TGF-β, have been developed to provide a scaffold for callus formation (151, 152). Stem cell transplantation to deliver osteogenic precursors to fractured bone is also being explored, particularly for the treatment of atrophic non-unions (153). However, MSC differentiation must be tightly controlled.

Interestingly, osteoporosis patients are not only likely to fracture bone, but often display sub-optimal fracture healing or require orthopaedic surgery, further exacerbating the morbidity of this disease (154). Continued research is required to further elucidate which factors stimulate osteogenic differentiation and underpin optimal bone repair to further improve future osteoanabolic treatments for complex fractures and osteoporosis.

1.3 APPROACHES TO RESEARCHING HUMAN BONE PATHOLOGIES

1.3.1 RARE MUTATIONS AND PEDIGREE ANALYSIS

Some humans, possessing rare mutations in skeletal genes, exhibit extreme skeletal phenotypes. Studying rare heritable bone traits and diseases can reveal fundamental genetic regulators of healthy skeletal physiology, with causal effects in the aetiology of bone diseases. One example includes osteopetrosis, a serious and potentially fatal bone condition that was first identified in 1904 by a German radiologist, Albers-Schönberg (155). It is now known that defective osteoclast activity is the cause of aberrant skeletal development and the over-ossification of bone, joints and soft tissues in osteopetrosis. Pedigree analyses of families exhibiting either autosomal dominant or autosomal recessive osteopetrosis have revealed no fewer than 20 genetic mutations associated with the condition, including mutations in *RANK* and *RANKL* (156, 157). Targeted RANK-L inhibition is now used as an anti-resorptive treatment for osteoporosis (114). Other pedigree studies of families with extreme High Bone Mass (HBM) have been used to identify osteoanabolic drug targets. The most impactful example of this was the identification of a mutation in *SOST* within families diagnosed with sclerosteosis, a disease characterised by skeletal overgrowth and HBM (158). This eventually lead to the development of romosozumab, the SOST-inhibiting osteoanabolic drug (118). Further pedigree studies have since revealed novel osteoanabolic candidates by uncovering rare mutations in other genes associated with HBM, such as *LRP5* and *SMAD9* (159-161). At the opposite end of the spectrum, pedigree analyses have identified rare mutations in patients with diseases resulting in severely low BMD and fracture susceptibility, such as OI and OPPG, already been described in section 1.2.1.3.

The study of rare bone-related mutations has been instrumental in broadening our understanding of skeletal pathophysiology and for advancing novel therapies to treat osteoporosis. However, osteoporosis is highly-prevalent, meaning that more common genetic variants with less-extreme phenotypes are likely

to underpin disease susceptibility. Large-scale epidemiological analysis can uncover hundreds of genetic loci relevant to the aitiology of osteoporosis, at the population level.

1.3.2 GWAS AND MENDELIAN RANDOMIZATION

With the advancement of gene sequencing technologies, large-scale whole-genome and whole-exome sequencing has become possible, unlocking a treasure trove of previously inaccessible epidemiological data (162). Genome-Wide Association Studies (GWASs) are statistical analyses which leverage large-scale genetic datasets to identify associations between relatively common Single Nucleotide Polymorphisms (SNPs) and human traits of interest, in a given population. SNPs generally exert subtle effects on gene expression, rather than gross effects on protein structure or function. Thus, GWASs highlight genes of interest for prioritisation in functional analysis in further studies based on putative associations with disease phenotypes. Several important GWASs have been published since 2007, and are summarised in Zhu *et al*., 2021 (163). Measuring BMD via DEXA or CT scans can be costly and time consuming, limiting the number of samples available for GWAS. However, it has now been shown that estimated BMD (eBMD), acquired by quantitative ultrasound of the heel, can be used as a reliable proxy for true BMD in GWAS (104); using this approach Morris *et al*., recently identified 301 novel loci associated with variance in BMD, as well as 13 fracture susceptibility loci (103). Additionally, a GWAS of extreme HBM discovered associations between BMD and 4 genetic loci (two novel and two known) (164). Though GWASs provide invaluable insights into the genetic regulation of bone, these studies are purely observational, meaning follow up analyses are required to test the causal relationship between putative genes of interest and disease.

Mendelian Randomization (MR) is an increasingly popular epidemiological tool, which is used to predict causal inference between biological or environmental exposures, and pathological outcomes. Using randomly-inherited SNPs (derived from GWASs) as unconfounded proxies for a measurable exposure, MR calculates a P value that estimates the probability of a causal relationship between the exposure (e.g., circulating cytokines) and the quantifiable outcome of interest (e.g., BMD). As such, MR is considered analogous to a human randomised controlled trial (165). Furthermore, MR can be followed up by colocalization analyses using expression Quantitative Trait Loci (eQTL) data to identify the gene driving the genetic association signal (166). Indeed, MR has been used to strengthen causal inference from osteoporosis GWASs. Recently, an MR study by Zheng *et* al., demonstrated an inverse causal relationship between circulating levels of the osteoclastogenic protein SOST, and femoral neck eBMD, that is potentially

regulated by glycosylation enzymes (167). Moreover, colocalization analysis leveraging eQTL data from arterial tissue revealed common genetic signals for high levels of circulating SOST, glycosylation enzymes and reduced eBMD, revealing novel pathways of interest for the treatment of osteoporosis. MR has now been used to examine the causal relationships between a multitude of complex traits and osteoporotic bone phenotypes, with aims to perform hypothesis-free Phenome-Wide Association Studies (Phe-WASs) for the identification of novel pathways of interest in the future (168).

Despite remarkable advances in genetic epidemiological approaches to studying osteoporosis, functional validation in cell culture or *in vivo* models are still required to understand the mechanistic impact of these mutations on bone.

1.3.3 LABORATORY MODELS OF BONE REGULATION, INJURY AND DISEASE

Rodents (mice and rats) have classically been the model organisms of choice for studying osteogenesis, bone repair and skeletal disorders. The skeletons of rodents bear close resemblance to those of humans; bone develops via endochondral and intramembranous ossification, is maintained, remodelled, and repaired via similar cellular processes, and rodents develop osteoporosis, similarly to humans (169, 170). Among the many advantages of rodent models is their genetic similarity to humans. A multitude of studies using mutant mice have modelled approximately 260 genes related to aberrant skeletal phenotypes in humans (171). Recently, rapid skeletal phenotyping in mice has been used to functionally validate the effect of GWAS derived osteoporosis-related genes, highlighting those with functional relevance *in vivo* (103, 172). However, phenomics-based experiments in mice are costly, and could be considered unethical due to the large number of animals required.

Much of our current understanding of the cellular basis of fracture healing comes from assays in rodent models (134). Models of both closed and surgical tibia fractures are well established in rodents, and can be performed on animals with induced osteoporosis, to study perturbations to bone healing (173-177). The most popular assay involves the insertion of an intermedullary metal pin, followed by fracture induction via the closure of a blunt guillotine over the pin. However, variability in the quality and reproducibility of this fracture assay has been reported (173). Moreover, these injuries can cause pain and disability for the animal, increasing suffering. Crucially, most rodent studies of fracture require histological analysis of the injury, meaning multiple groups of animals must be culled for tissue harvest at each time point of interest.

Recently, two-photon intravital live imaging of uninjured tibiae in mice was used to demonstrate previously unknown dynamics of osteoclast fission and refusion via "osteomorphs", in response to RANK-L (34). Though it is possible, live-imaging of bone in mice is complex, requiring a highly-optimised imaging set up, delicate anaesthesia and open surgery to expose the bone. This makes dynamic imaging of bone in rodents inaccessible or impractical for many researchers.

Bone is a multicellular, complex tissue, which is maintained by tightly interconnected, reciprocal signalling between skeletal and immune cells. As such, it is difficult to recapitulate the environmental conditions of bone, to study osteoanabolic responses *in vitro*. Nonetheless, an increased number of insightful *in vitro* models for the study of skeletal biology have emerged, promising to reduce our reliability on rodent models (178). No immortalised osteoclast cell line currently exists. However, RAW 264.7 cells are used as a proxy for osteoclasts *in vitro*, as they are from the macrophage / monocyte lineage (179). Several immortalised osteoblast and osteocyte lineage cell lines exist, which can be used to study osteogenic processes *in vitro* (180, 181). Primary skeletal progenitor cells may also be derived from either the peripheral blood or bone marrow of rodents and humans; when cultured in osteogenic medium, mesenchymal progenitors can differentiate into osteoblasts *in vitro* (182). Tissue engineering based *in vitro* models are now being explored, with proposed applications in personalised regenerative medicine for the treatment of non-union fractures or bone metabolic diseases (183). In the future, progenitor cells harvested from humans may be expanded and differentiated *ex vivo*, assembled within a three-dimensional osteogenic scaffold, and transplanted back into patients (153). Moreover, these personalised *in vitro* models may be used to screen for effectiveness of a variety of osteoregulatory drugs to optimise treatment of bone diseases. *In vitro* models provide exciting avenues for bone tissue engineering and personalised medicine (184). However, currently, there are no *in vitro* models of osteoporosis or fracture.

Though they provide clinically-relevant insights, rodent models of skeletal biology harbour practical, ethical and financial limitations. Whilst *in vitro* models mitigate these limitations, they struggle to accurately recapitulate the complex bone environment required to model human bone pathologies. The zebrafish is an advantageous alternative model organism for the study of skeletal biology and disease, which can provide valuable insights into the genetic, molecular and cellular regulation of bone.

1.4 ZEBRAFISH AS A MODEL FOR STUDYING SKELETAL BIOLOGY, FRACTURE REPAIR AND BONE REGENERATION

Zebrafish (*Danio rerio*) are small vertebrate teleosts (bony fish), which are widely used for a broad range of scientific applications including toxicology, drug screening, developmental biology, disease modelling and regenerative medicine (185-188). Here, I will focus on the utility of the zebrafish as a clinically relevant model for accelerating the pace of discovery in the research of skeletal biology, bone disease and fracture. I will also describe skeletal injury assays in zebrafish which can reveal novel insights into bone repair and regeneration. Comparisons of human, zebrafish and rodent models of skeletal biology are summarised in Table 2 and Table 3 (1).

Table 2. Comparison of Skeletal Features and Development in Humans, Rodents, and Zebrafish. *Abbreviations: dpf = days post fertilisation, AGM = Aorta Gonad-Mesonephros, CHT = Caudal Hematopoietic Tissue. A version of this table has been published in Dietrich et al., 2021 (1), though the original draft of this was researched and created by Lucy M. McGowan.*

Basic Skeletal and Haematopoietic Development				
Process	**Human**	**Rodent**	**Zebrafish**	**Reference**
Bone Types	• Dermal • Cortical • Trabecular	• Dermal • Cortical • Trabecular	• Dermal • Cortical	(189)
Skeletal Cell Types	• Chondrocytes • Osteoblasts • Osteoclasts (multinucleate) • Osteocytes	• Chondrocytes • Osteoblasts • Osteoclasts (multinucleate) • Osteocytes	• Chondrocytes • Osteoblasts • Osteoclasts (multi and mononucleate) • Osteocytes	(189, 190)
Ossification Types	• Endochondral • Intramembranous • Periosteal	• Endochondral • Intramembranous • Periosteal	• Endochondral • Intramembranous • Periosteal	(49, 189, 191)
Development	*In utero*	*In utero*	Extrauterine (*in ovo*)	
Average Brood Size	n/a	6-8	100-150	(192)
Mineralization Begins	4-5 weeks	~ 2 weeks	3-4 dpf	(193, 194)
Skeletal Maturity Reached	Up to 30 years	4 –5 months	3-4 months	(195)
Direction of Loading	Axial	Orthogonal	Axial	(196)
Fracture Repair	Yes	Yes	Yes	(197, 198)

Appendage Regeneration	No	No	Yes	(199, 200)
Gene Conservation (vs humans)	100 %	~ 85 %	~ 75 %	(201)
Hematopoietic Bone Marrow	Yes	Yes	No	(202)
Sites of Primitive Hematopoiesis	**Embryonic**			
	• Yolk sac	• Yolk sac	• ALM • PLM	(202-204)
Sites of Definitive Hematopoiesis	**Foetal**		**Larval**	
	• AGM • Placenta • Liver • Bone marrow • Thymus • Spleen	• AGM • Liver • Bone marrow • Thymus • Spleen	• AGM • CHT • Kidney marrow • Thymus	(202-204)
	Adult			
	• Bone marrow • Thymus	• Bone marrow • Thymus	• Kidney marrow • Thymus	(202-204)

Table 3. Comparison of Experimental (205)Tractability in Humans, Rodents, and Zebrafish. Abbreviations: CT = Computed Tomography, BMD = Bone Mineral Density, DEXA = Dual-Energy X-ray Absorptiometry, n/a = not applicable, 1° = primary. A version of this table has been published in Dietrich et al., 2021 (1), though the original draft of this was researched and created by Lucy M. McGowan.

Experimental Tractability for Studying Mechanisms of Bone Disease and Repair				
	Human	Rodent	Zebrafish	Reference
Dynamic Histomorphometry	• Tetracycline	• Alizarin red stain • Calcein green/blue • Tetracycline	• Alizarin red stain • Calcein green	(206-210)
Visualising Cell Dynamics of Bone	No	Limited	• Transparent larval stages • Transparent fins for studying adult bone repair • Adult scale regeneration	(195, 199, 211-213)
BMD Assessment	• BMD from CT (fixed / live) • eBMD from ultrasound (live) • BMD from DEXA (live)	• BMD from μCT (fixed) • BMD from DEXA (live)	• BMD from μCT (fixed)	(103, 214, 215)
Experimental Drug Administration	n/a	• Injection • Ingestion • Gavage	• Immersion • Implantation • Injection	(195)
Mosaic CRISPR Mutagenesis Time	n/a	3 months	5 days – 3 months	(216, 217)
Stable CRISPR Mutagenesis Time	n/a	9 months	6-9 months	(218)

Ex vivo / In vitro Study of Bone for Osteoactive Compound Screening	• *In vitro* differentiation of stem cells • *Ex vivo* culture of cells isolated from 1° tissue	• *In vitro* differentiation of stem cells • *Ex vivo* culture of 1° cells	• *Ex vivo* whole scale culture • *Ex vivo* culture of 1° cells	(195, 219, 220)

1.4.1 ZEBRAFISH SKELETAL BIOLOGY

Over the past two decades, zebrafish have emerged as an excellent model for the study of skeletal biology, injury and disease (1, 221). During mating, zebrafish eggs are fertilised by the male externally, meaning embryos undergo extrauterine development. Moreover, optical clarity of zebrafish throughout embryonic and larval stages allows for dynamic visualisation of skeletal development, using transgenic cell labelling, or live-staining. Human skeletal cell types and bone developmental pathways are conserved in zebrafish (195). Various regions of the zebrafish skeleton is formed via endochondral (neural arches), intramembranous (cranium, operculum, vertebrae, fins) and perichondral ossification (jaw); as in mammals, these processes are orchestrated by chondrocytes, osteoblasts, osteoclasts (mono and multi-nucleated) and immune cells (1). Interestingly, unlike medaka (*Oryzias latipes*), another popular teleost model of skeletal biology, zebrafish also possess osteocytes within most of their mature bone (222).

The adult skeleton in zebrafish can be separated into two groups: the craniofacial skeleton, and the axial skeleton (comprising the vertebral column, ribs and fins). Osteogenesis commences between 2-4 days post fertilisation (dpf) in zebrafish, with the skeleton taking around 3-4 months to reach maturity (1). Craniofacial skeletal elements are the first to develop at around 2 dpf; some are initially formed of unmineralized cartilage, whilst the first bony elements develop via intramembranous ossification (191). Then, by 4 dpf, mineralisation of cartilaginous craniofacial elements occurs via endochondral or perichondral ossification. The axial skeleton is formed later, as the larvae matures into a juvenile zebrafish. Unlike humans, the zebrafish skeleton continues to grow throughout adulthood. During early skeletogenesis in zebrafish, osteoblasts differentiate under the same genetic cues as in mammals; MSCs expressing *sox9* differentiate into *col2a1*$^{+}$ chondrocytes which synthesise cartilage, before some become hypertrophic (*col10a1*$^{+}$) and differentiate into *runx2* expressing osteoblast precursors (223). Development of the zebrafish jaw involves endochondral and perichondral ossification, culminating in the formation of an ossified mandible containing articulated synovial joints, which are physiologically comparable to joints in mammals (223). Moreover, gene tracking experiments in zebrafish larvae showed sequential expression of *runx2a/b*, *osx*, *col1a1* and *osteonectin* in differentiating osteoblasts, with mature mammalian osteoblast markers expressed in ossified regions (193). Activation of canonical Wnt signalling and FGF pathways also have a conserved role in osteoblast differentiation and skeletal development (16, 193).

In zebrafish, most skeletal elements are formed via intramembranous or perichondral ossification, with endochondral ossification occurring in some regions (189). Though dermal and cortical bone are present in zebrafish, unlike humans, trabecular bone is mostly absent from the zebrafish skeleton. Moreover, the centre of hollow zebrafish bones are filled with adipocytes, fibroblasts and mesenchymal cells, as opposed to hematopoietic bone marrow (212). However, like mammals, the bone marrow is heavily vascularised. The trabeculated vertebrae of mammals are connected by intervertebral discs which are comprised of the nucleus pulposus (derived from the notochord sheath) surrounded by a fibrocartilaginous matrix. During development of the zebrafish vertebral column, osteoblasts form mineralised vertebrae directly around vacuolated notochordal cells, which are connected by ring-shaped collagenous ligaments (224).

Mechanical loading is a major factor in osteogenesis, bone damage and the development of skeletal diseases. Zebrafish live in an aquatic environment; due to water buoyancy, the degree of absolute gravitational loading experienced by the skeleton is reduced compared to terrestrial mammals (1). However, unlike rodents, zebrafish load their spine axially as they swim through water, meaning the direction of force applied to the skeleton is comparable to humans, with relative effects. Though zebrafish bone is osteocytic, whether the mechanosensitive osteocyte network orchestrates the formation of BMUs and initiates bone remodelling, in a manner similar to humans, is unclear (1). Reduced numbers of osteocyte lacunae have been associated with altered skeletal morphology in zebrafish, suggesting that osteocytes regulate bone remodelling (94). In humans, *SOST* expression by osteocytes initiates bone remodelling. A comparative study of zebrafish (osteocytic bone) and medaka (anosteocytic bone) demonstrated that bone remodelling is also orchestrated by *sost*, but that *sost* is expressed by both osteocytes and non-osteocytic cells within the bone bulk in zebrafish (225). This represents an osteocyte independent mechanism of bone remodelling in teleosts, which has not been described in mammalian models. However, remodelling is initiated in response to load in both anosteocytic bone in medaka and osteocytic bone in zebrafish (1, 225, 226). Collectively, this suggests that the mechanical and molecular cues underpinning bone remodelling pathways are conserved between zebrafish and humans. Crucially, zebrafish display bone-degenerative phenotypes with age, developing skeletal diseases such as osteoporosis, spinal deformities and osteoarthritis (224, 227, 228). Therefore, zebrafish display skeletal pathophysiology that is comparable with, and clinically relevant to, humans.

1.4.2 THE ZEBRAFISH IMMUNE SYSTEM

In addition to their skeletal physiology, the zebrafish immune system is highly conserved with mammals. Similarly, to humans, zebrafish possess both innate (complement, natural killer cells, granulocytes, phagocytes) and adaptive (B cells and T cells) immune systems (229-231). In particular, innate immune cells which are essential in governing bone homeostasis and repair, such as neutrophils and macrophages, are physiologically comparable to humans (231). The anatomical sites of early and late haematopoiesis vary between zebrafish and mammals; since they lack hematopoietic bone marrow, haematopoiesis occurs in the kidney marrow of adult zebrafish (204). However, for both zebrafish and mammals, haematopoiesis occurs via primitive and definitive waves, with the molecular pathways governing HSC development and differentiation strongly conserved (204).

Immunological functions in zebrafish are comparable with mammals. For example, in humans, neutrophils are the most abundant immune cell type in the body which act as the first line of defence against pathogens and are rapidly recruited to injuries. In both larval an adult zebrafish, granular neutrophils expressing myeloperoxidase are migrate towards injuries, infection, and cancer cells (147, 232, 233). In particular, either bone trauma via fracture or apoptosis osteoblasts via laser ablation, triggers the recruitment of neutrophils which and initiates osteogenesis (147, 234). As in humans, the recruitment of neutrophils is mediated by the chemokine interleukin 8 (IL-8 / Cxcl8) and its receptor, Cxcr2 (235, 236). Once at the site of inflammation, zebrafish neutrophils exert their pro-inflammatory effects via conserved mechanisms such as phagocytosis, ROS and cytokine production, antimicrobial granule release and release of neutrophil extracellular traps (237). Moreover, macrophages in zebrafish display both classical (M1) and alternative (M2) phenotypes, contributing to both pro-inflammatory and reparative processes (238).

The key advantage of using zebrafish to study inflammatory responses is that, with the aid of transgenic reporters and live stains, the behaviour of individual immune cells can be dynamically visualised, tracked and quantified *in vivo* (239-241). Transgenic reporter lines exist for neutrophils (*mpx* reporters) (242, 243), myeloid cells (*lyzC* reporters) (244), macrophages (*mpeg1*, *mfap4*, *cfms/csf1ra* reporters) (245, 246), as well as other cells of the innate and adaptive immune system. Due to the translucency and depth of the caudal fin, it is possible to image immune contributions to adult bone in live zebrafish, in a non-invasive manner. Many zebrafish studies of inflammation have been limited to larvae due to an incomplete understanding of markers and immune cell types in adult zebrafish (247). However, our understanding of adult immunity

in zebrafish is expanding (248-250). Therefore, the zebrafish can be used to model the dynamic interactions between the immune system and bone during skeletal repair or disease development.

1.4.3 GENETIC AND PHARMACOLOGICAL MANIPULATION OF ZEBRAFISH

Zebrafish embryos are highly amenable to genetic manipulation, meaning an ever-growing myriad of transgenic and mutant lines have been established for the study of skeletal biology (1, 211). Moreover, high fecundity, short developmental times, and low-cost makes them an advantageous model for genetic and pharmacological studies, compared to rodents.

Zebrafish display genetic conservation with 75% of the human genome; as a result, approximately 85% of human disease-related genes have an ortholog in zebrafish (201, 251). Due to an additional genome-wide duplication event, multiple copies (paralogs / ohnologs) of some skeletal genes are present in zebrafish, where only one copy is observed in mammals; examples include *COL2A1* (*col2a1a* and *col2a1b*), *SOX9* (*sox9a* and *sox9b*) and *RUNX2* (*runx2a* and *runx2b*) (252-254). However, most human orthologs show high sequence and functional conservation with at least one zebrafish paralog (255). Human epidemiological analyses and GWASs continue to rapidly identify new loci associated with skeletal health (Figure 3 A) (103, 256), yet these gene candidates require functional validation. To keep up with this pace, follow-up studies using zebrafish have evolved away from traditional forward genetic screening methods and towards modern genome editing tools such as CRISPR-Cas9 (Figure 3 B) (1). Emerging phenomics-based approaches in zebrafish now present an efficient model for the rapid validation of novel GWAS-derived genes related to bone disease, via phenotyping of F0 animals displaying genetic mosaicism (Figure 3 C) (217, 255). Stable mutagenesis in zebrafish allows for more in-depth research to elucidate the role of these genes during bone development, maintenance, and injury, dynamically (Figure 3 C) (2). Integrative, multidisciplinary studies which translate findings from human genetic epidemiological studies into *in vivo* models of bone disease in zebrafish are now appearing. Recently, pedigree analyses were used to identify rare mutations in genes such as *CLCN7* and *CTSK* which cause osteopetrosis, and *SMAD9,* which causes HBM, followed by functional validation in zebrafish (161, 195, 257). Collectively, these studies have implicated the Chloride Ion Channel 7/Cathepsin K/TGF-β/SMAD (CIC-7/CTSK/TGF-β/SMAD) signaling axis in healthy bone development, and highlighted SMAD9 as a potential osteoanabolic target.

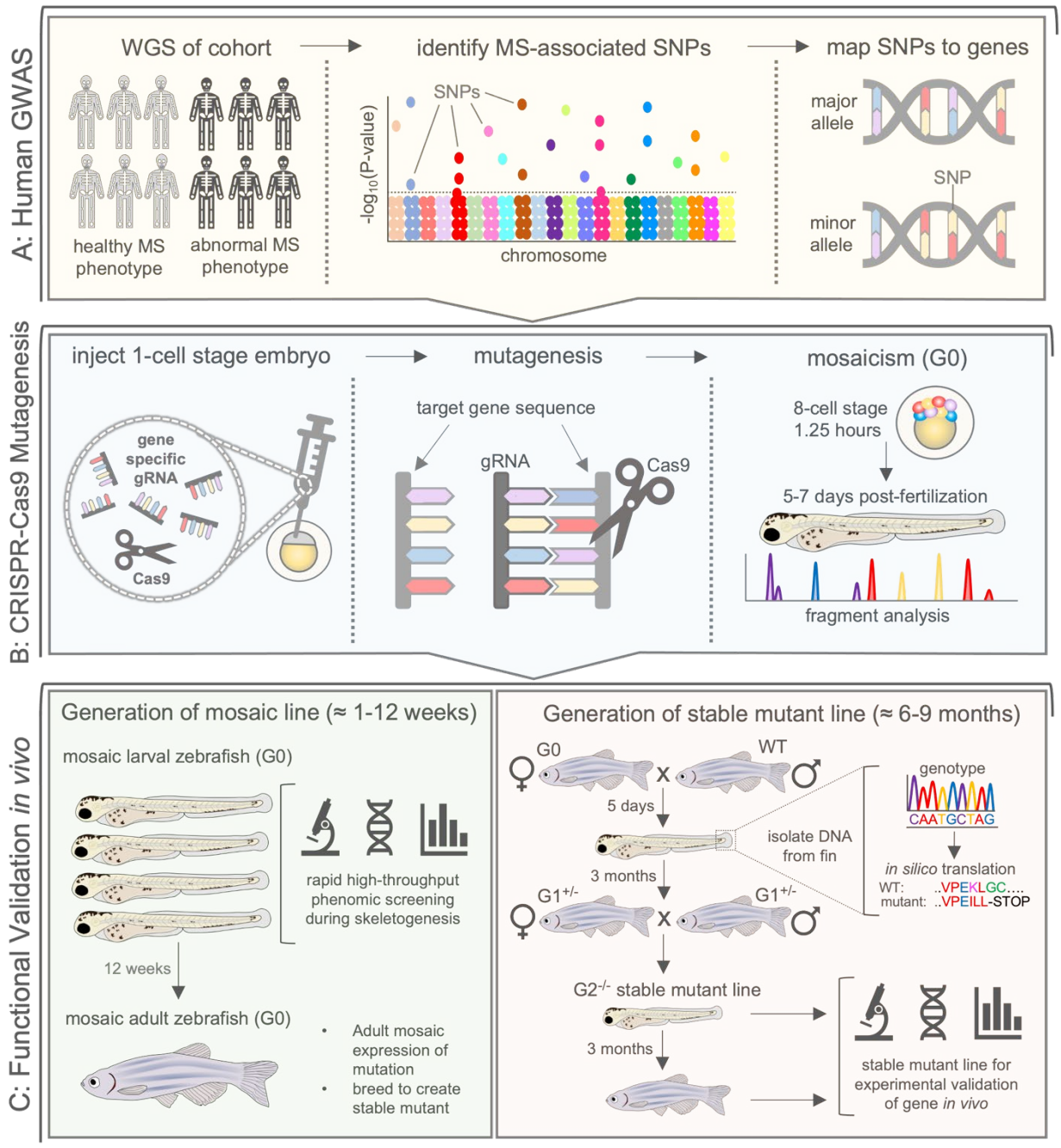

Figure 4. Zebrafish As a Tool for Rapid Validation of GWAS-Derived MS Disease-Associated Gene Candidates. A: *Human GWAS conduct WGS on large cohorts and identify SNPs in people with abnormal MS phenotypes.* ***B:*** *CRISPR-Cas9 technology can be used for targeted knockout mutagenesis in vivo. Gene-specific gRNAs are designed and injected into a one-cell stage zebrafish embryo with Cas9. Efficient gRNAs will facilitate double-strand breaks within an exon in the target gene, resulting in indel mutations. A mosaic (G0) embryo (crispant) will develop, containing a variety of mutant and WT alleles for the gene of interest that are validated through fragment analysis.* ***C:*** *(Left) mosaic*

larval zebrafish can be rapidly screened for MS phenotypes during skeletogenesis, providing a high-throughput and efficient phenomics-based approach to gene validation. Mosaic G0 zebrafish can be raised to adulthood for breeding into a stable line with a single, known mutant allele. (Right) G0 mosaic zebrafish are crossed to WT. Resulting heterozygous larvae ($G1^{+/-}$) are fin-clipped to isolate DNA for genotyping and in silico translation to identify alleles resulting in a premature STOP codon, compromising the protein. $G1^{+/-}$ with the same mutant allele are bred with each other to generate the $G2^{-/-}$ line with a stable mutation in the gene of interest. The stable mutant larvae or adults can then be used for experimental validation of the MS-associated phenotype. gRNA = guide RNA; hpf = hours post fertilization; MS = musculoskeletal; SNP = single-nucleotide polymorphism; WGS = whole-genome sequencing; WT = wild-type. This figure was created by Lucy M. McGowan and has been published (including figure legend) in a co-authored review article in Dietrich et al., 2021. JBMR (1).

Another advantage of the zebrafish model is the ease at which pharmacological compounds can be administered. In many cases, the compound of interest can be added directly to the water where it is ingested (adults and larvae) or absorbed through the skin (larvae). Compound screening may be performed on large numbers of zebrafish larvae during osteogenesis, to detect deleterious or teratogenic effects on the skeleton, or other organs (185, 191, 258). One study, in a genetic zebrafish model of OI, showed that immersion treatment with the widely-used anti-resorptive drug, alendronate, was sufficient to reduce fracture susceptibility, without impairing bone-union post fracture; similar results have also been reported in a human trail monitoring fracture outcome in patients treated with alendronate (147, 259). However, the zebrafish model also demonstrated that alendronate treatment prevents callus remodelling after union, a factor which was not monitored in the human trial. Similar approaches could be applied in future zebrafish studies to model the efficacy and safety of existing or novel osteoactive compounds in bone homeostasis, repair and disease (195).

1.4.4 MODELS OF BONE REPAIR AND REGENERATION IN ZEBRAFISH

Zebrafish are renowned for their regenerative capacity; diverse and complex organs such as the heart, skin, spinal cord, brain, retina and fin are capable of complete regeneration, whereby the affected tissues are restored to their original state, in the absence of fibrotic scarring (188). Given the genetic and cellular similarities between zebrafish and humans, zebrafish can help to elucidate which signals and cell dynamics orchestrate favourable tissue repair. Injury models have been developed in adult zebrafish for the study of

wounding, myocardial infarction, and bone, with translational applications to human medicine (1, 238, 260). Moreover, these injury assays tend to be relatively straightforward, minimally invasive and less debilitating, compared to analogous experiments in rodents, thereby reducing the pain and suffering experienced by the animal. Since zebrafish skeletal biology closely resembles that of humans, several assays to study bone regeneration and repair in adult zebrafish have now been established, as illustrated in Figure 4 (1). These assays can be used to identify both conserved and divergent mechanisms of optimal bone repair, which may be of therapeutic interest.

Skull trepanation (Figure 4 A) can be performed by micro-drilling a circular hole into the surface of the calvaria (os frontale) (1). The bone regenerates via intramembranous ossification, completely covering the lesion within 2 weeks and leaving no visible callus (198). Jaw resection is another model which can be used to decipher differences in cartilaginous, versus non-cartilaginous bone repair. Proximal to the synovial joint, the zebrafish lower jaw is comprised of a cartilage core that is surrounded by mineralised bone, whereas the distal portion contains only bone (261). Resection of the lower jaw of adult zebrafish can be performed in either the proximal or the distal regions; in either case, regeneration takes upwards of 35 days, with ectopic bone calluses forming around the resection site (Figure 4 B). However, regeneration proceeds differently depending on which portion of the jaw is resected (261). Both skull trepanation and jaw resection are traumatic injuries where accessibility to the bone for dynamic live-imaging are limited. However, alternative, less invasive models of bone repair and regeneration exist in zebrafish.

The flanks of the adult zebrafish are covered in an armour of elasmoid scales, made up of thin sheets of dermal bone (262). The zebrafish scale is a dynamic living tissue, that is developed, maintained and remodelled by osteoblasts and osteoclasts. Moreover, scales are capable of complete epimorphic regeneration post-removal and can easily be plucked from the flank to study this process over time (Figure 4 C). Within just 24 hours pools of *de novo* osteoblast progenitors form and begin regenerating (219). Complete regeneration of the scale occurs within around 14 days.

The zebrafish caudal fin is comprised of an array of segmented lepidotrichia (bony fin rays), as well as a rich network of vasculature, ECM, fibroblasts and fat, encased in a translucent epithelium. The optical clarity of this tissue allows for non-invasive dynamic live imaging of bone, making it an attractive alternative to rodent models. Perhaps one of the most studied regenerative phenomena in the zebrafish is epimorphic fin regeneration, whereby the caudal fin regenerates within 2 weeks of amputation (Figure 4 D). Within the first 48 hours of injury, inflammatory and developmental pathways trigger the formation of a blastema at the amputation plane, a proliferative mass of dedifferentiated and *de novo* MSCs (199, 212). As the tissue

regenerates, segmented lepidotrichia are reformed via intramembranous ossification. Interestingly, bone fractures within the caudal fin heal via the formation of a mineralised callus, which is then remodelled (1). This strongly suggests that fracture repair mechanisms are conserved between zebrafish and humans. Two induced caudal fin fracture assays have been developed in zebrafish (Figure 4 E) (2, 147, 197, 198). In the crush fracture assay, all lepidotrichia along the dorsoventral length of the fin are fractured, whereas in the more controlled single fracture assay, individual lepidotrichia are fractured. Recently, a study demonstrated that dynamic imaging of zebrafish caudal fin fractures over time can be used to model clinically relevant bone pathologies (147).

Collectively, a range of skeletal injury assays exist in zebrafish, highlighting the utility of this model organism for discovering the pathways which govern reactivation of osteogenesis and optimal bone repair. When applied in combination with genetic and pharmacological disruption of skeletal cells, these injury assays can help to reveal or elevate targets for prioritisation in the pursuit of novel osteoanabolic therapies.

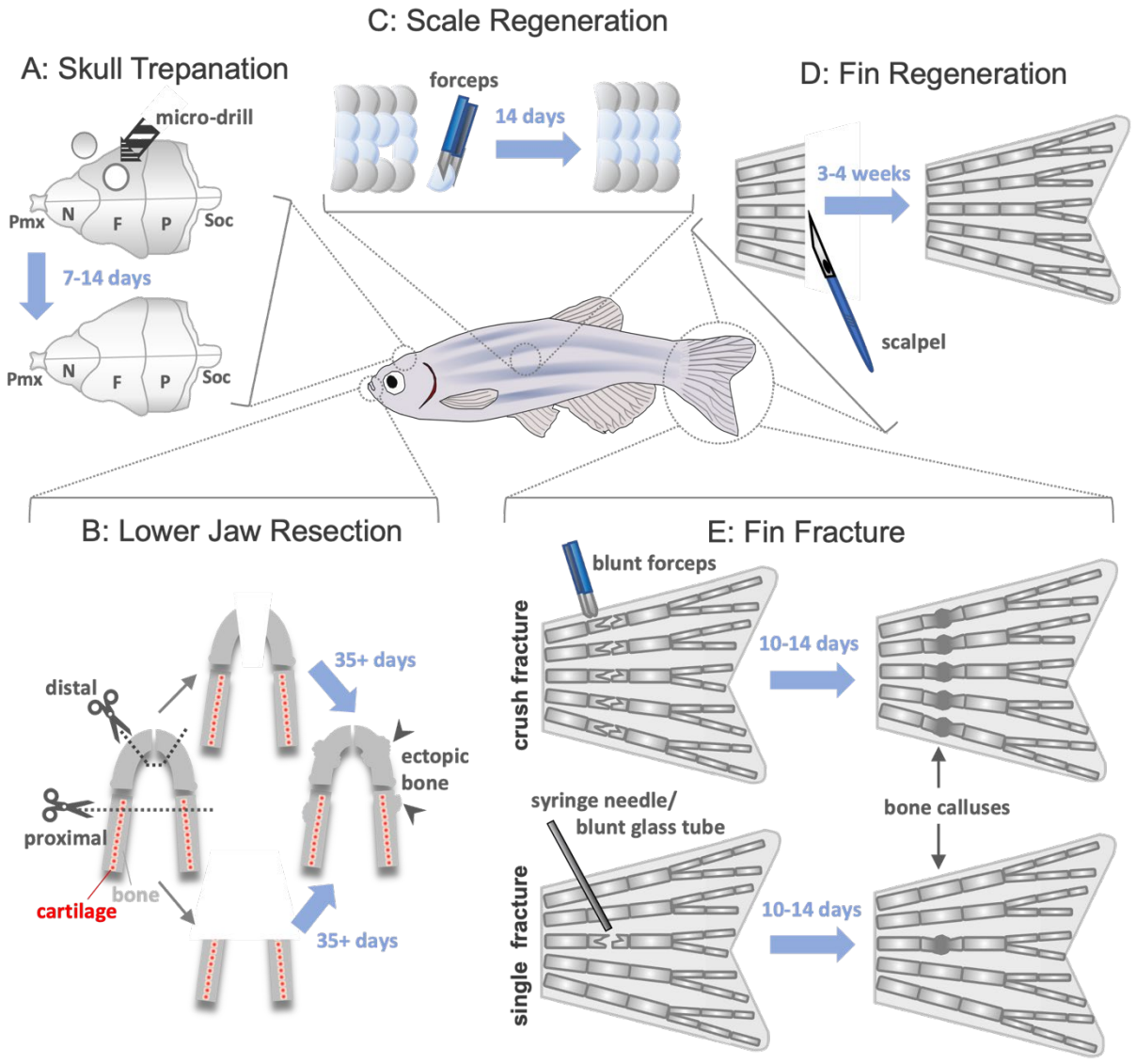

Figure 5. Models of Bone Repair and Regeneration in Adult Zebrafish. A: *During skull trepanation, a microdrill is used to destroy bone from the os frontale, which regenerates within 7 to 14 days.* ***B:*** *Two models of lower jaw resection can be performed: proximal, where both cartilage and bone are removed posterior to the synovial joint using surgical scissors (dotted line), and distal, where only the most anterior part of the bone is removed. Regeneration post resection takes upwards of 35 days and leads to ectopic bone formation in the regenerate.* ***C:*** *Scale plucking with forceps is a simple method for studying bone regeneration in vivo. Scales can be cultured ex vivo and bone regeneration easily studied dynamically in vivo due to the superficial nature of the injury.* ***D:*** *Due to its accessibility and the presence of lepidotrichia (bony fin rays), the caudal fin is an excellent model for studying bone regeneration and repair. Epimorphic fin regeneration after amputation requires 3 to 4 weeks*

until completion. ***E:*** *Fin ray fractures are bridged in 10 to 14 days and result in a bone callus, which is then remodeled. Two fin ray fracture models are available: in the crush-fracture model (top), forceps are used to introduce fractures along the entire width of the fin. In the single-fracture model, either a syringe needle or blunt glass capillary tube is used to press on an individual bone segment, introducing a single fracture in one or both hemirays. F = os frontale; N = os nasale; P = os parietale; Pmx = os praemaxillare; Soc = os supraoccipitale. This figure was created by Lucy M. McGowan and has been published (including figure legend) in a co-authored review article in Dietrich et al., 2021. JBMR (1).*

1.5 SUMMARY AND AIMS

1.5.1 SUMMARY

Bone is a dynamic, multicellular tissue, which requires constant remodelling throughout adulthood via tightly regulated reciprocal signalling between osteoblasts, osteoclasts and osteocytes. Osteoporosis and fragility fractures are highly prevalent, carrying a substantial socioeconomic health burden and greatly reducing quality of life (64). Moreover, the incidence of these pathologies is growing. The aetiology of osteoporosis is multi-factorial; though ageing is the primary cause of the disease, strong genetic links to BMD and fracture susceptibility have been demonstrated, with hundreds of genes now associated with the onset of osteoporosis (163). Despite high demand, osteoanabolic therapies to treat osteoporosis or augment fracture repair are lacking (116). Healthy fracture repair requires controlled inflammation, as well as the retriggering of developmental osteogenic processes which allow osteoblast precursors to proliferate and differentiate (134). Therefore, studying the basic science of how bone cells respond to injury may help to identify clinically relevant targets to promote bone formation. Zebrafish are an excellent model for studying bone pathologies *in vivo*, from the first stages of developmental osteogenesis in larvae, through to maintenance and repair of the mature skeleton in adults (1). Like humans, zebrafish repair fractured bone (lepidotrichia) via the formation of a mineralised callus. However, unlike humans, zebrafish are also capable of complete regeneration of bone. Live dye, fluorescent transgenic reporter lines and optical clarity of the caudal fin allow for live, dynamic imaging of mature bone in zebrafish, meaning the cell biology of bone repair and regeneration can be studied in the same animal over time. Crucially, the genome, inflammatory responses and musculoskeletal systems of zebrafish display a high degree of similarity with

humans. Zebrafish can also be used as an efficient model for functional validation of osteoporosis-associated genes via mutagenesis, or to screen the effects of pharmacological compounds on bone, *in vivo* (191, 255). Therefore, studies in zebrafish possess unique advantages compared to other models of skeletal biology and can reveal clinically relevant insights into bone.

Many factors are known to influence the elaborate process of bone repair, with many more warranting investigation. The inflammatory phase of fracture repair is triggered immediately after injury and influences the efficiency and quality of downstream osteogenesis. Therefore, I chose to focus on factors which may influence the early inflammatory response to skeletal damage, and subsequent effects on bone repair. WNT16 is a Wnt signalling ligand, with well-defined associations with osteoporosis phenotypes and bone metabolism in both human and mouse models (263-265). A study of morphant zebrafish embryos associated *wnt16* with functional haematopoiesis and immune cell development, suggesting that loss of *wnt16* may influence adult bone repair via the immune system (266). Despite this, the role of Wnt16 in fracture repair has not been investigated. Moreover, canonical, pro-inflammatory roles for neutrophils and TNF-α have been described in skeletal pathology and sub-optimal fracture repair (38, 134). However, despite evidence suggesting that these factors contribute positively to fracture stabilisation, osteogenic differentiation and repair, these potential functions have not been properly explored *in vivo* (38, 267, 268).

1.5.2 HYPOTHESIS AND AIMS

Here, I aimed to test the hypothesis that zebrafish can be used to effectively model the biological mechanisms underpinning healthy and pathological bone repair, and that subtle perturbations to these mechanisms can be detrimental to optimal bone repair. To this end, I explored the influence of three factors, with undefined roles in adult osteogenesis, on fracture healing and bone regeneration in zebrafish. I aimed to:

1. Characterise the role of *wnt16*, an osteoporosis-associated gene, in fracture susceptibility and bone repair in zebrafish.
2. Investigate a potential pro-reparative role for neutrophils in rapid ECM remodelling and fracture stabilisation during early bone repair.
3. Explore the pleiotropic effects of the pro-inflammatory cytokine, Tnf-α, on osteoblasts during bone repair and regeneration.

CHAPTER 2: MATERIALS AND METHODS

Some methods described within this chapter were included in an original research article published in the peer-reviewed journal, JBMR Plus (McGowan et al., 2021 (2)). As the lead author of this research article, I prepared the manuscript in full, including all text. Dr Chrissy Hammond and Dr Erika Kague provided manuscript feedback prior to submission for publication. Text has been amended wherever appropriate for inclusion into this thesis.

2.1 ZEBRAFISH LINES, MAINTENANCE AND HUSBANDRY

2.1.1 ZEBRAFISH HUSBANDRY, ANAESTHESIA AND ETHICAL CONSIDERATIONS

Zebrafish were maintained at the University of Bristol's Animal Scientific Unit (ASU) and cared for following standard zebrafish husbandry guidelines (269). Briefly, embryos and larvae were grown in plastic 90 mm petri dishes (Thermo-Fisher) containing 30% Danieau's solution in a 28°C incubator up to 5 days post-fertilisation (dpf), at a maximum density of 80 per dish. 100% Danieau's was comprised of: NaCl 1740 mM, KCl 21 mM, $MgSO_4$ 12 mM, $Ca(NO_3)_2$ 18 mM and HEPES buffer 150 mM in 1 L distilled H_2O. After 5 dpf, zebrafish were transferred to Tecniplast nursery tanks in the main zebrafish aquarium facility where they were fed a standard diet (powdered food 2 x daily and live food 1 x daily) and maintained at a maximum density of 20 adults per 3 L tank. Tricaine methanesulfonate (MS222) stock solution was used for all anaesthesia. Stock solution was comprised of 12 mM Tris-HCl solution (SD8146; Bio Basic Canada) and 4 g L^{-1} MS222 powder (Sigma Aldrich) dissolved in Milli-Q water (Sigma Aldrich) pH adjusted to 7.5. Aliquots of MS222 stock solution were stored at -20°C (long-term) or at 4°C (short-term). Recovery anaesthesia was performed using MS222 stock solution dissolved in Danieau's solution or aquarium water, at a final concentration of 160 mg L^{-1} for adults, or 100 mg L^{-1} for larvae. Non-recovery anaesthesia was performed using a final concentration of 640 mg L^{-1} for all stages. Post-euthanasia, death was confirmed via onset of rigor mortis (adults) or via cessation of circulation (larvae). Scientific procedures were approved by the University of Bristol's local Animal Welfare and Ethical Review Body (AWERB) and experiments conducted under a UK Home office Project License following the Animals in Scientific Procedures Act (1986).

2.1.2 TRANSGENIC LINES

All zebrafish transgenic lines used are described in Table 4. New generations of transgenic lines were generated using standard breeding protocols and sorted between 3 and 5 dpf (269); transgenic positive larvae were selected for the presence of the fluorescent protein of interest (e.g. GFP).

Table 4. Table of Transgenic Lines. *Table of all transgenic lines used, their abbreviations in the text, the description of their purpose and reference for their place of origin. Transgenic line names are italicised. When referring to the name of the transgenic line or the expression of the transgene in the text, both the gene and name of fluorescent protein is italicised (e.g. osx:GFP). When referring to fluorescent protein levels resulting from transgene expression, i.e. during observational or quantitative image analysis, the gene name is italicised and the protein name is not (e.g. osx:GFP).*

Transgenic Name	Abbreviation	Description	Reference(s)
Tg(7xTCF-Xla:Siam:nlsGFP)	Wnt:*GFP*	Canonical Wnt activity	(270)
Tg(col2a1aBAC:mCherry)	*col2a1:mCherry*	Chondrocytes	(223)
Tg(ET30:lyzC:DsRed)	*lyzC:DsRed*	DsRed^{+} neutrophils	(244)
Tg(mpeg1:mCherry)	*mpeg1:mCherry*	mCherry^{+} macrophages / myeloid cells	(245)
Tg(Ola.sp7:NLS-eGFP)	*osx:GFP*	GFP^{+} osteoblasts	(271)
Tg(osterix:mCherry-NTR)^{pd46}	*osx:mCherry (non-ablation experiments) or osx:mCherry-ntr (ablation experiments)*	Nitroreductase mediated ablation of mCherry^{+} osteoblasts	(212)
TgBAC(mpx:GFP)	*mpx:GFP*	GFP^{+} neutrophils	(242)
TgBAC(mpx:GFP)^{i114}; Tg(lyz:H2A-mCherry)^{sh530}	*mpx:GFP; lyzH2A:mCherry*	GFP^{+} neutrophil specific mCherry^{+} Histone H2A (to visualize chromatin release)	(242), (232)
TgBAC(tnfα:GFP)	*tnfα-GFP*	Tumour necrosis factor-α	(272)

2.1.3 MUTANT LINES

Generation of wnt16 mutant zebrafish line via CRISPR-Cas9 mutagenesis was performed by Dr Lucy Brunt and Dr Erika Kague at the University of Bristol, prior to the start of this Ph.D. project (273). Stable tnfα mutant zebrafish were generated by Marcus Keatinge and colleagues (Becker labs) at the University of Edinburgh and imported to the university of Bristol with the permission of the Becker labs (274).

wnt16$^{-/-}$ mutant zebrafish were generated previously by Dr Erika Kague and Dr Lucy Brunt by CRISPR-Cas9 mutagenesis at the University of Bristol (2, 273). Briefly, one-cell-stage wild type (WT) zebrafish (TL/Ekk strain) were injected with guide RNAs (gRNAs) designed to target exon 2 of *wnt16* (Merck) and Cas9 protein (Thermo Fisher Scientific). Adult mosaic (G0) zebrafish were crossed to WT zebrafish as described in Brunt *et al*., 2017 (273). Two alleles were selected: a 165 base pair (bp) insertion and a 72 bp insertion. Both mutations resulted in a premature stop codon compromising more than 85% of the protein, predicted to result in nonsense mediated decay (Figure 5 A-B) (2). Stable mutant *tnf-α* zebrafish were originally generated by the Becker labs at The University of Edinburgh and gifted to the Hammond lab at the University of Bristol (275). Briefly, CRISPR-Cas9 mutagenesis was used to target exon 4 of *tnf-α*, causing an indel mutation (5 bp deletion + 7 bp insertion) which introduced a premature stop codon at aa 97 compromising more than 58% of the Tnf-α protein sequence, predicted to result in nonsense-mediated decay (Figure 6) (275).

2.1.4 GENOTYPING OF MUTANT LINES

Where possible, zebrafish were genotyped prior to 5 dpf to minimize the number of animals raised to adulthood. 3 dpf larval zebrafish were anaesthetised in MS222 and their caudal fin resected using the pigment line as a reference point. The resected fin tissue was pipetted into a PCR tube containing 15 μl of base solution comprised of NaOH (25 mM) and EDTA (200 μM). Larvae were recovered in fresh Danieau's solution in a 24 well-plate (Thermo-Fisher) and stored in a 28°C incubator until the genotyping was complete. Adult zebrafish were anaesthetised in MS222, and a portion of their dorsal fin amputated using a sterile disposable scalpel (Swann-Morton). Amputated fin tissue was collected with tweezers and immediately placed in a 70 μl of base solution comprised of NaOH (25 mM) and EDTA (200 μM). To extract DNA from tissue, samples were heated to 95°C for 30 minutes and cooled to 4°C before adding an equal

volume of neutralising solution comprised of Tris-HCl (40 mM, pH 5.0). DNA extracts were stored in at 4 °C prior to PCR for a maximum of 7 days.

For PCR amplification, 4 μl of DNA extract was added to a well containing 1 x EmeraldAmp GT PCR master mix (Takara), forward primer (500 nM), reverse primer (500 nM) and distilled H_2O. Primers sequences: *wnt16* F- TTTTCCTCGGGCCTGGTTAT; *wnt16* R- GCCCTCTTTAACGCTCGGTA: *tnfa* F- 5'ACCAGGCCTTTTCTTCAGGT; *tnfa* R- AGCGGATTGCACTGAAAAGT. Total reaction volumes were either 10 μl or 20 μl per well. PCR was performed on a thermocycler (BioRad). PCR product from each sample underwent gel electrophoresis (1.5% agarose in Tris-acetate-EDTA + 1:10,000 SYBR Safe; Invitrogen). *wnt16* genotype was determined based on band separation due to variation in amplicon length due to mutation (Figure 5 C). Genotype of *tnfa* zebrafish was determined using Sanger sequencing from 1 μl of PCR product and 1 μl of forward primer (20 μM) diluted in 15 μl of nuclease-free water (Eurofins), (Figure 6 C). Alternatively, *tnf-α* genotype may also be determined using restriction digest; PCR product can undergo restriction with *bstXI*, according to manufacturer's instructions (New England BioLabs). Genotype can be determined based on number of bands present due to absent (*tnf*$\alpha^{+/+}$), partial (*tnf-*$\alpha^{+/-}$) or complete (*tnf-*$\alpha^{-/-}$) digestion.

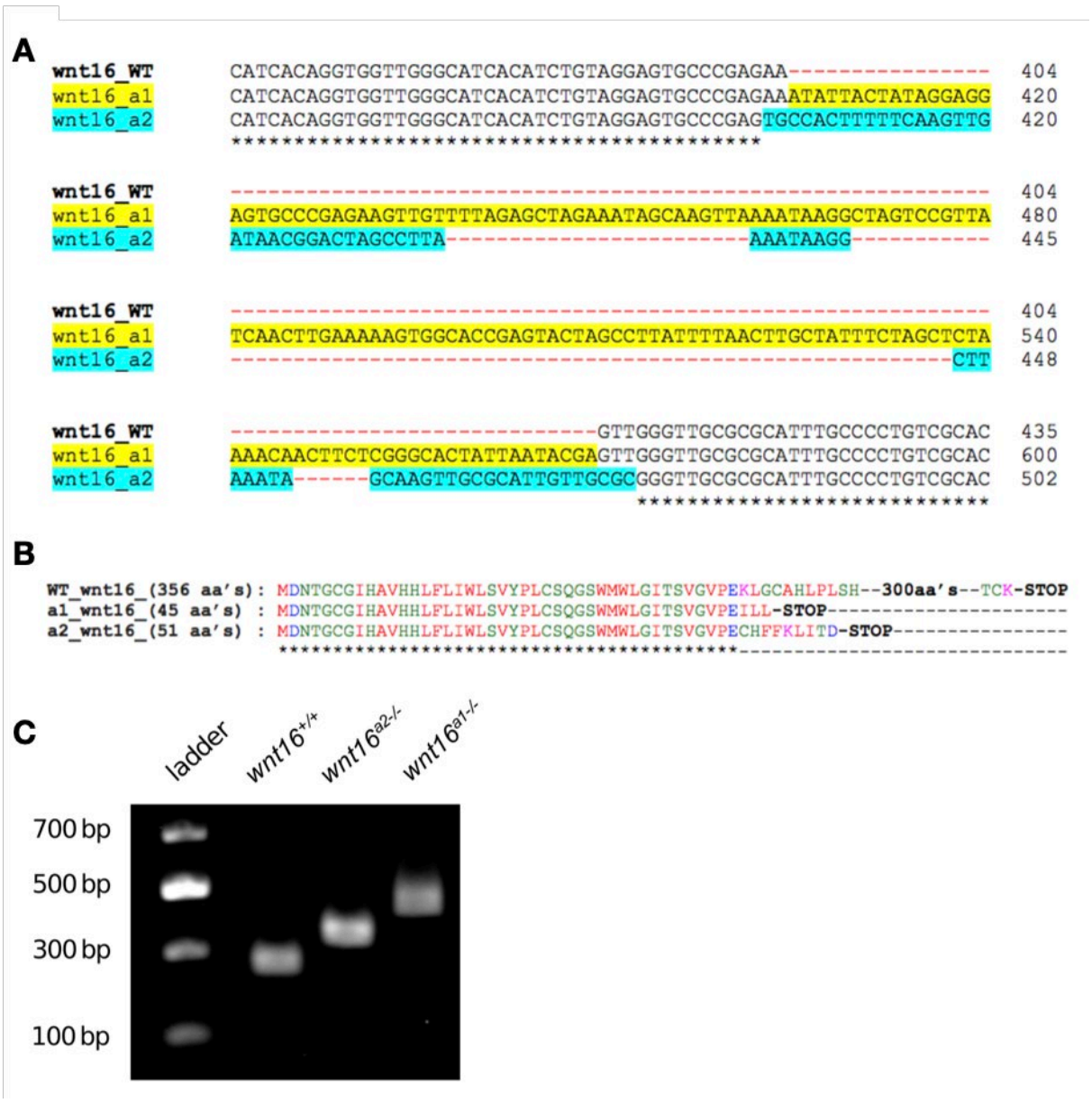

*Figure 6. CRISPR-Cas9 Mutagenesis Targeting Exon 2 Of Wnt16 Results in Large Insertion Mutations Causing the Introduction of Premature Stop Codons. A: Sequence alignment of wnt16 gene transcripts in wild type (WT), wnt16$^{a1-/-}$ and wnt16$^{a2-/-}$ zebrafish showing 165 and 72 base-pair insertions leading to frameshift mutations. * = sequence alignment with WT. B: Both mutations shown in A lead to the introduction of premature stop codons compromising > 80% of the Wnt16 protein. aa's = amino acids. C: Agarose gel electrophoresis of PCR-amplified DNA isolated from fin tissue of adult wnt16$^{+/+}$, wnt16$^{a2-/-}$ and wnt16$^{a1-/-}$ zebrafish. A version of this figure was published in McGowan et al., JBMR Plus, 2021 (2).*

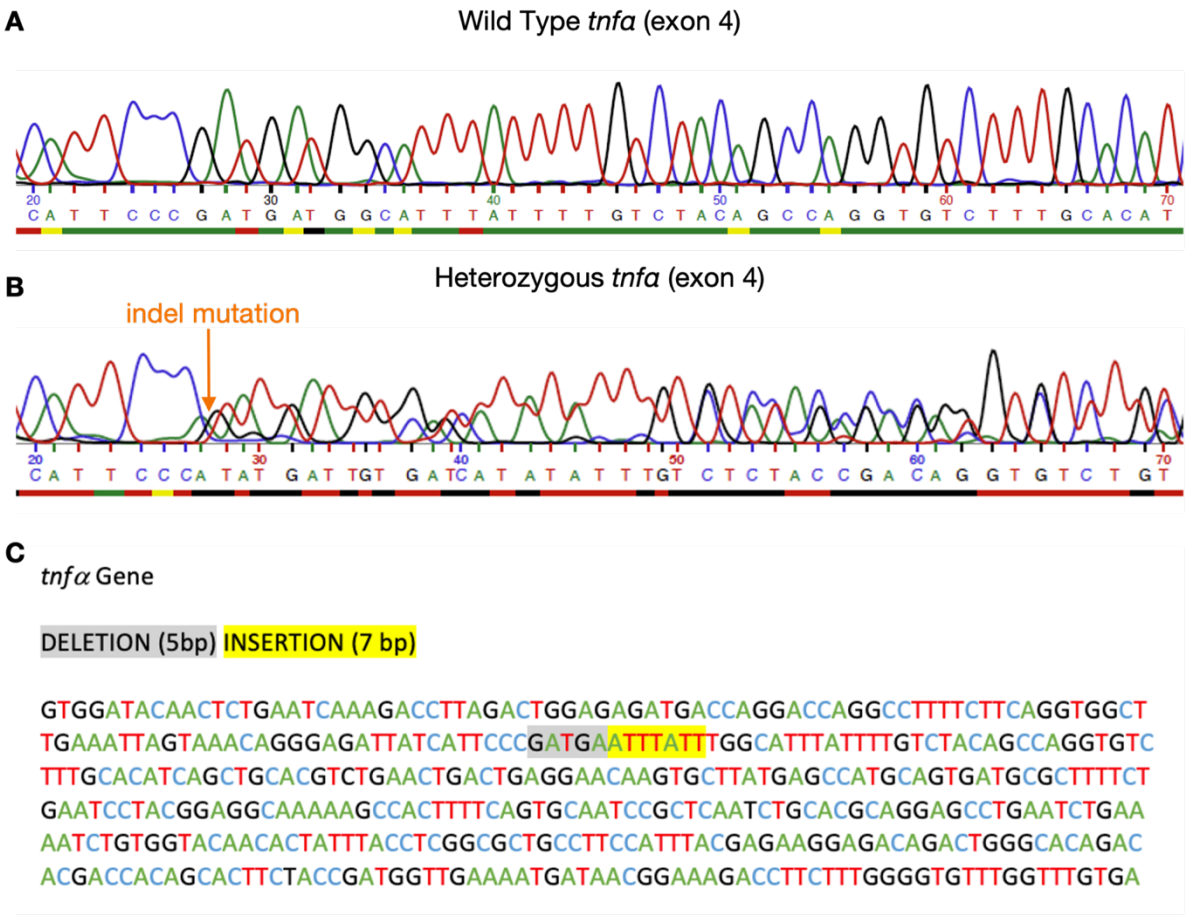

Figure 7. Genotyping of tnfα CRISPR-Cas9 Zebrafish. A-B: Sanger sequencing results of wild type (A) and heterozygous mutant ($tnf\alpha^{+/-}$, B). ***C:*** Schematic of exon 4 of tnfα with indel sequence of tnfα mutants highlighted. Mutation results in a premature stop codon compromising more that 58% of the mature protein sequence. tnfα mutant zebrafish were generated by Keatinge et al., 2021 (274).

2.2 CRISPR-CAS9 MUTAGENESIS OF *TNFα* IN ZEBRAFISH

Three gRNAs targeting either exon 1 or exon 4 of *tnfα* were designed using Chop-Chop (276) and CRISPRscan (277). gRNAs were selected based on target sequences with the highest efficiency scores (Table 5). Cas9 protein (CAS9PROT, Merck) was reconstituted according to manufacturer's instructions (500 ng μl^{-1}) and diluted at a 1:3 ratio prior to use. For each gRNA, 10 μl of injection solution was prepared and incubated at RT for 10 minutes prior to injections. Injection solutions were comprised of 1 μl Cas9 protein, 2 μl tracrRNA (TRACRRNA05N; Merck), 1 μl of 100 μM custom oligo gRNA (VC40003N; Merck), 5 μl of TE buffer (Sigma) and 1 μl of 0.5 % phenol red (Merck). WT (Ekk strain) zebrafish embryos were injected with 1 nl of injection solution at the 1-cell stage. At 3 dpf, DNA was extracted from injected and control (uninjected) larvae for PCR (section 2.1.4). Primer 3 software was used to design PCR primers which would flank the gRNA target site within the *tnfα* gene (278). An M13 pigtail sequence (5'-TGTAAAACGACGGCCAGT-3') was added to the 5' end of each of the forward primers (Table 5). To fluorescently label the PCR amplicons, a 6-carboxyfluorocein (6-FAM) labelled universal M13 primer was added to the PCR reaction at a final concentration of 500 nM (total reaction volume = 20μl), according to the methods of Carrington *et al.*, 2015 (279). To determine gRNA efficiency, the PCR product underwent fragment analysis (ABI 3500; Bristol Genomics Facility) and fragment sizes determined based on a GeneScan 500 LIZ size standard (Thermo fisher). Successful mutagenesis was verified based on the presence of multiple peaks compared to single peaks in uninjected controls (Geneious software).

Table 5. *tnfα gRNA target sequences (including protospacer adjacent motif (PAM; underlined)), exon of tnfα in which the target sequence lies, forward and reverse primer sequences for PCR, resulting amplicon length (AL) and predicted gRNA efficiency (%). Sequences are listed in the 3'-5' orientation. gRNA-1 targets the reverse stand of tnfα whereas gRNA-4 and gRNA-8 target the forward strand. The 5' end of forward primers also contained an M13 sequence (5'-TGTAAAACGACGGCCAGT-3').*

Name	Target Sequence	Exon	Forward Primer	Reverse Primer	AL	%
gRNA-1	GCTCCTGCGTGCAGATTGAGCGG	4	AGATTATCATTCCCGATGATGG	GTAGAAGTGCTGTGGTCGTGTC	285	61
gRNA-4	CGTCTGCTTCACGCTCCATAAGG	1	ATCTTCAAAGTCGGGTGTATGG	CTCACCACTTCCATCTTGTTGA	236	48
gRNA-8	GCTTGAGAGTCGGGCGTTTTTGG	1	GAACAACCCAGCAAACTCGA	GTACGGGGCAGGATTTTCAC	282	58

2.3 INDUCED FIN AND SCALE INJURIES IN ZEBRAFISH

2.3.1 LARVAL FIN RESECTION INJURY

3 dpf larvae were anaesthetised in MS222 dissolved in Danieau's solution and placed laterally on a piece of autoclave tape stuck to a small plastic petri dish. A 5 mm microsurgical knife (Wolf Laboratories) was used to resect caudal fins along the dorsoventral axis, using the ventral pigment gap as a point of reference (Figure 7 A). Larvae were recovered in fresh Danieau's solution. This simple assay can provide insights into the effects of immunomodulatory compounds on inflammatory responses to injury, prior to performing regulated procedures (bone injuries) in adult zebrafish. Though early ossified elements of the craniofacial skeleton begin developing in larval zebrafish, they lack mature bone for fracture repair studies.

2.3.2 ADULT INDUCED CAUDAL FIN FRACTURE

Adult zebrafish were anaesthetised in MS222 and placed laterally on a plastic petri dish under a brightfield stereomicroscope. The caudal fin was gently spread using a Pasteur pipette. A blunt 1 mm glass capillary tube (WPI) was used to crush a single lepidotrichium within the caudal fin, prior to the first bifurcation in the lepidotrichia, causing fracture (Figure 7 B (i)). A maximum of 3 fractures were induced in a single zebrafish, across the dorsoventral axis of the fin. Once fractured, zebrafish were recovered in fresh aquarium system water. Zebrafish were re-anaesthetised in MS222 at the time points of interest for live imaging of bone, or euthanised in MS222 and their caudal fin tissue amputated for experiments. Caudal fin fractures are optically accessible due to the translucency of the adult caudal fin, allowing for dynamic imaging of mature bone repair that follows a mechanism to humans (2, 147). The area of injured tissue is small compared to fin or scale regeneration, meaning large number of injuries would be required for RNA or protein extraction.

2.3.3 ADULT CAUDAL FIN AMPUTATION

Adult zebrafish were anaesthetised and placed under a microscope as described in 2.3.2 Caudal fins were amputated along the dorsoventral axis prior to the first bifurcation (Figure 7 B (ii)), using a sterile disposable

scalpel (Swann-Morton). Zebrafish were recovered in fresh system water and re-anaesthetised or euthanised as required, as in 2.3.2. Osteogenesis is triggered after fin amputation to regenerate lost bone. Though appendage regeneration is not possible in humans, many inflammatory and osteogenic pathways are triggered that are common with fracture repair (1). Larger amounts of regenerating bone tissue can be harvested from this injury for protein or RNA extraction compared to induced caudal fin fractures.

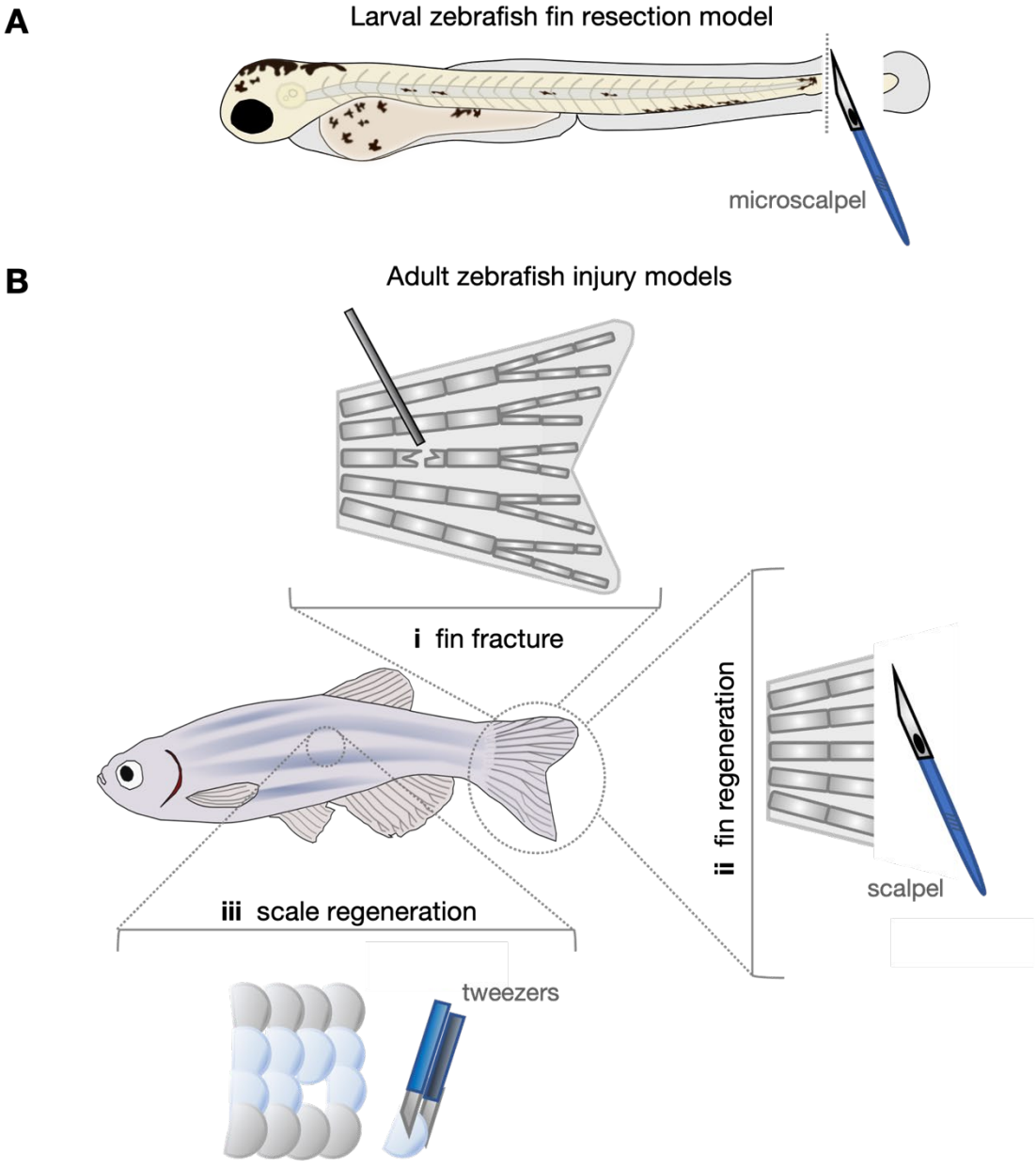

Figure 8. Injury Models Used Throughout. A: *Larvae were anesthetised at 3 days post-fertilisation and placed laterally on a microscope. Dotted line indicated where the larval fin was resected with a*

microscalpel. ***B:*** *Lateral view of anaesthetised adult zebrafish with injury models are depicted.* ***i:*** *a blunt glass tube was used to press on an individual bone within the caudal fin lepidotrichia, causing a crush fracture.* ***ii:*** *A scalpel was used to amputate the caudal fin prior to the first bifurcation in the lepidotrichia.* ***iii:*** *A maximum of 12 scales were harvested from the left flank of the zebrafish using tweezers.*

2.3.4 ADULT SCALE REGENERATION ASSAY

Adult zebrafish were anaesthetised and placed under a microscope as described in 2.3.2. Watchmaker's tweezers were used to pluck up to 12 scales from the left flank of the fish before fish were recovered in fresh system water (Figure 7 B (iii)). This injury model is optically accessible for live imaging or can be used to generate regenerating bone tissue for *ex vivo* culture assays. *Ex vivo* scale culture can be used to test the effects of osteomodulatory compounds in isolation from the whole organism. A number of genes associated with human skeletal diseases are expressed during scale regeneration highlighting the translational capacity of this model (280). Here, this model is used to examine the effect of recombinant Tnf-α on osteoblast activity, in isolation from the immune system.

2.4 LIVE STAINING OF BONE

2.4.1 ALIZARIN RED STAINING

Live Alizarin Red staining was used to label mineralised bone *in vivo*. A stock solution composed of 0.5% (w/v) Alizarin Red (Sigma Aldrich) and milli-Q water was prepared and stored at room temperature for up to one year. A working solution of Alizarin Red stain was comprised of 0.5% Alizarin Red stock solution (74 μM) and 5 mM HEPES buffer (Sigma Aldrich) dissolved in aquarium system water. Zebrafish were immersed in working Alizarin Red stain for 30 minutes (150 ml per fish) and placed in fresh aquarium system water for at least 15 minutes prior to imaging to remove excess stain (Figure 8). Working Alizarin Red stain was stored in foil-wrapped glass bottles in the dark for up to 1 month and reused a maximum of 3 times.

2.4.2 CALCEIN GREEN STAINING

Calcein green staining was used to label and quantify new bone deposition *in vivo*. A working Calcein green solution was comprised of 40 μM Calcein Green powder (Sigma-Aldrich) dissolve in aquarium system water. Calcein Green solution was placed on a metallic stirrer for one hour until all powder had dissolved and pH adjusted to 8. Zebrafish were immersed in Calcein Green stain for 30 minutes (150 ml per fish) and placed in fresh aquarium system water for at least 15 minutes prior to imaging to remove excess stain (Figure 8). Working Calcein Green stain was stored in foil-wrapped glass bottles in the dark for up to 1 month and reused a maximum of 3 times.

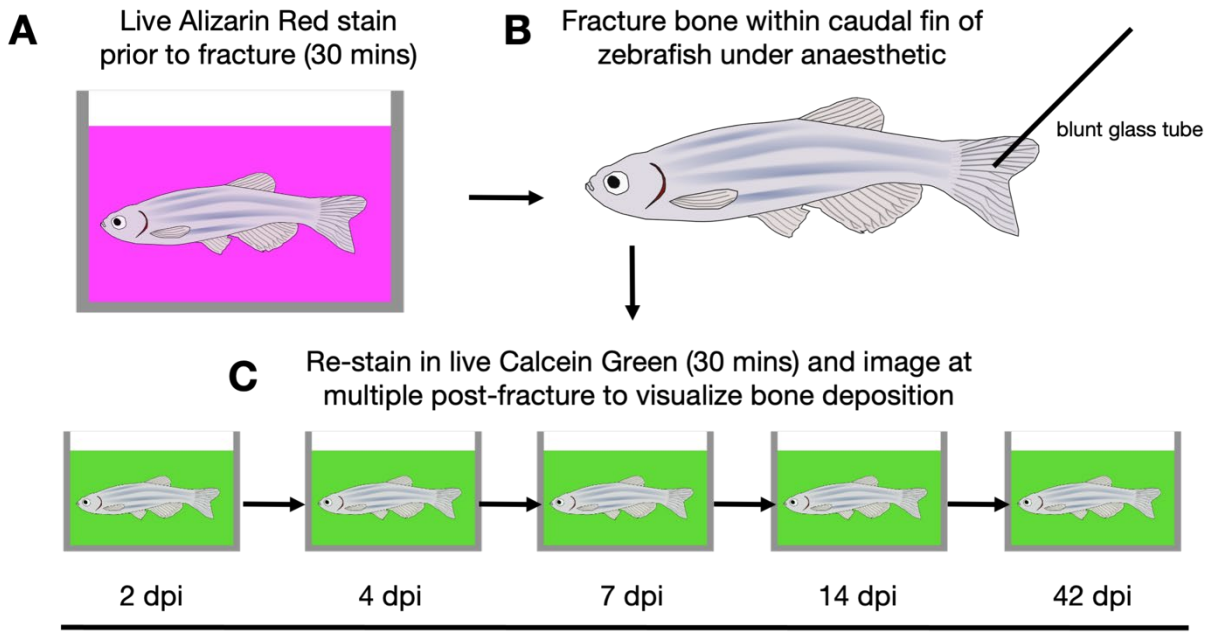

Figure 9. Schematic Overview of Live Bone Staining During Induced Caudal Fracture in Zebrafish. A: Zebrafish are live stained in Alizarin Red to label existing calcified bone prior to injury. ***B:*** *Zebrafish are removed and placed under general anaesthetic by immersion in tricaine, removed from water, and bones within the translucent caudal fin fractured by mechanical pressure using a blunt glass tube.* ***C:*** *Zebrafish are recovered and then stained in Calcein Green at various time points post injury (days post injury (dpi)), to label new bone matrix, before being re-anaesthetised and imaged. D: Stereomicroscope images show remineralisation and callus formation post fracture, which can be quantified. Figure adapted from McGowan et al., 2021 (2).*

2.5 DRUG TREATMENTS

2.5.1 SB225002 (CXCR2 ANTAGONIST)

SB225002 powder (Tocris, Bio-techne) was diluted in DMSO (Sigma Aldrich) to form a stock solution at a concentration of 100 mM which was stored in 100 μl ml aliquots at -20 °C for up to 1 year. Immediately prior to treatment, stock solution was diluted into fresh Danieau's solution or aquarium system water for final working concentrations. Larval Zebrafish were treated with 1 μM SB225002 via immersion. Adult zebrafish were treated with 5 μM SB225002 via immersion and fed a standard diet. Control zebrafish were immersed in system water containing an equivalent volume of DMSO. Treatments were refreshed daily.

2.5.2 POMALIDOMIDE (TNF-α INHIBITOR)

Pomalidomide powder (MedChemExpress) was dissolved in DMSO to form a stock solution at a concentration of 50 mg/ml and stored in 1 ml aliquots at -80 °C for up to 6 months. Immediately prior to treatment, stock solution was diluted into fresh aquarium system water to a final working concentration of 200 μM. Adult zebrafish were treated with pomalidomide via immersion and fed a standard diet. Control zebrafish were immersed in system water containing an equal volume of DMSO. Treatments were refreshed daily.

2.5.3 NITROREDUCTASE-MEDIATED OSTEOBLAST ABLATION WITH NIFURPIRINOL

Nifurpirinol powder ((NFP) Sigma Aldrich, 32439) was dissolved in DMSO to form a stock solution at a concentration of 50 mM and stored in 50 μl aliquots at -80°C in the dark, for up to one year. Double-positive *osx:mCherry-ntr*; *tnfα:GFP* zebrafish were selected at 3 dpf; these zebrafish express an mCherry^{+} bacterial nirtroreductase (NTR) under the osteoblast-specific promotor, *osterix*. Larvae were incubated in Danieau's solution containing NFP at a final concentration of 5 μM, or an equivalent volume of DMSO, for 6 hours at 28°C. The pro-drug, NFP, is reduced by nitroreductase (NTR) in osteoblasts, triggering cross-linking of DNA and apoptosis (281). Larvae were then rinsed in fresh Danieau's prior to being imaged at various time-points post-ablation (see 2.14.2).

2.6 WHOLE MOUNT IMMUNOHISTOCHEMISTRY (IHC)

2.6.1 FIXATION, WASHING AND ANTIBODIES

All tissues (larvae or adult fins) were fixed in 4% paraformaldehyde (PFA) for 2 hours at room temperature or overnight at 4°C and then dehydrated using a serial dilution of methanol (MeOH). Samples were left in 100% MeOH for 10 minutes at room temperature prior to rehydration or stored at -20°C in 100% MeOH long term. All washes were performed for 10 minutes at room temperature, unless stated otherwise. All antibodies were diluted in IHC blocking buffer (5% horse serum in PBS (Phosphate Buffered Saline)). Primary antibodies used were: chick mAb to GFP ([1:500]; ab13970; Abcam), rabbit pAb to mCherry ([1:500]; 5993; BioVision), mouse Col2a1 (1:50; M3F7; Developmental Studies Hybridoma Bank), chick α-L-plastin ([1:500]; gift from the Martin laboratory (282)), rabbit mAb to laminin ([1:250]; Abcam; ab11575, mouse m-Ab to fibronectin ([1:200]; Sigma-Aldrich; F7387). Secondary antibodies used were: goat anti-chick Alexa Fluor-488; goat anti-mouse Alexa Fluor-555; goat anti-mouse Alexa Fluor-568; donkey anti-rabbit Alexa Fluor 647 (A11039; A21137; A21124; A31573, Thermo Fisher Scientific) and goat anti-mouse DyLight 550 (SA5-10173, Thermo Fisher). Stained samples were imaged on a confocal microscope within 2 weeks of staining.

2.6.2 ADULT FIN IHC

Fins were rehydrated in a serial dilution of MeOH in PBS-Tx (0.02 % TritonX in PBS). After washing 3 times, samples were digested with Proteinase K ([1:1000]; P5568; Sigma-Aldrich) diluted in PBS-Tx for 90 minutes at 37°C. Proteinase K solution was refreshed every 30 minutes. Fins were washed 3 times in PBS-Tx and then incubated in blocking buffer at room temperature for 3 hours. Fins were then incubated with primary antibodies overnight at 4°C with gentle agitation. Fins were washed 6 times in PBS-Tx before being incubated in blocking buffer for 2 hours and then stained with secondary antibodies at room temperature for 2 hours. Fins were then washed a final 6 times in PBS-Tx. For nuclear staining, fins were incubated in DAPI ([1:5000]; D1306; Thermo Fisher) and washed a further 3 times. Stained fins were stored in PBS-Tx at 4°C.

2.6.3 LARVAL IHC

Larvae were rehydrated in a serial dilution of MeOH in PBS-Tw (0.1 % Tween 20 in PBS). After washing 3 times, samples were digested with Proteinase K ([1:1000]; P5568; Sigma-Aldrich) diluted in PBS-Tw for 25 minutes (3 dpf larvae) or 50 minutes (5 dpf larvae) at 37°C. Proteinase K solution was refreshed after 30 minutes for 5 dpf larvae. Fins were washed 3 times in PBS-Tw and then incubated in blocking buffer at room temperature for 3 hours. Fins were then incubated with primary antibodies overnight at 4°C with gentle agitation. Fins were washed 6 times in PBS-Tw before being incubated in blocking buffer for 2 hours and then stained with secondary antibodies at room temperature for 2 hours. Fins were then washed a final 6 times in PBS-Tw. Stained larvae were stored in PBS-Tw at 4°C.

2.7 ALCIAN BLUE STAINING

Fins were amputated and fixed in 4% PFA as previously described (2.6) before being dehydrated in 50 %, and then 70%, ethanol (EtOH), for 30 minutes each at room temperature. Fins were stained at room temperature overnight in alcian blue solution comprised of 0.02 % W/V alcian blue (Sigma-Aldrich), 60 mM Magnesium Chloride and 95% EtOH. Stained fins were washed 3 times for 10 minutes in 0.5% potassium hydroxide (KOH) and then bleached for 90 minutes at room temperature in solution comprised of 3% hydrogen peroxide and 0.5% KOH. Alcian blue stained fins were stored in 75% glycerol and imaged within 1 week on a stereomicroscope (2.14.1).

2.8 TARTRATE-RESISTANT ACID PHOSPHATASE (TRAP) STAINING

TRAP staining was performed using an acid phosphatase detection kit (387A, Merck). Fins were amputated and fixed for 40 minutes at room temperature in TRAP-fix solution comprised of 24% citrate solution (kit), 65% acetone, 8% formaldehyde (37%) and 3% deionised water. Fix was removed and fins were washed 3 times for 10 minutes each in PBS-Tx. TRAP staining solution was prepared fresh according to kit instructions and fins were incubated in TRAP stain at 37°C for 2 hours (300 μl stain per fin). TRAP stain was removed, and fins were washed 3 times for 10 minutes each in PBS-Tx. Fins were post-fixed in 4% PFA before washing

again in PBS-Tx (3 times, 10 minutes) and transferred to 75% glycerol. TRAP-stained fins were stored at 4°C and imaged on a stereomicroscope within 2 weeks of staining as in (2.14.1).

2.9 RNASCOPE (MULTIPLEX WHOLE MOUNT *IN SITU* HYBRIDIZATION)

RNAse-free DEPC (Diethyl Pyrocarbonate ((Thermo-Fisher) treated water was used to dilute any concentrated reagents or wash buffers. All washes were performed in SSC-Tw (0.2% SSC buffer (Thermo Fisher), 0.1% Tween 20) for 15 minutes each unless otherwise stated. All incubation steps were performed in a HybEZ II Oven (ACD, Bio-tenchne).

Fins were amputated and fixed in fresh 4 % PFA and dehydrated in a serial dilution of MeOH as previously described (2.6). 100% MeOH was removed, and samples air dried for 30 minutes. Fins were treated with Protease Plus (ACD, Bio-Techne) for 45 minutes at room temperature and then washed 3 times in PBS-Tw (0.1 % Tween 20 (Sigma-Aldrich)). RNAscope probes were heated to 40°C and cooled to room temperature before use. Probes used were: Dr-*wnt16*-C1 (894261-C1, ACD, Bio-Techne), Dr-*runx2a*-C2 (409521-C2, ACD, Bio-Techne) and Dr-*tnfrsf1b*-C1 (505601-C1, ACD, Bio-Techne). C2 probes were diluted into either C1 probe or probe diluent at a ratio of 1:50. Probes were hybridized to samples overnight at 40°C. Probes were removed and stored at 4°C to be reused (once) and fins were washed 3 times.

Samples were post-fixed in 4% PFA at room temperature for 10 minutes and washed 3 times prior to signal amplification. An RNAscope Multiplex Fluorescent V2 Kit (ACD, Bio-Techne) was used to perform signal amplification and development. Samples were incubated sequentially in Amp1, Amp2 and Amp3 reagents at 40°C for 30, 30 and 15 minutes, respectively. Samples were washed 3 times for 15 minutes each between each amplification step. A TSA Cyanine 3 and 5, TMR, Fluorescein Evaluation kit (NEL760001KT; PerkinElmer) was used in combination with the RNAscope Multiplex Fluorescent V2 Kit (ACD, Bio-Techne) to develop the fluorescent signals in each channel. A single fluorophore was assigned to each channel. A maximum of 3 channels were multiplexed in a single fin, and only the channels present were developed using the multiplex kit. Samples were incubated in HRP buffer corresponding to the correct channel (C1, C2 or C3) at 40°C for 15 minutes and then washed 3 times for 15 minutes each. The corresponding fluorophore was diluted in TSA buffer (ACD, Bio-Techne) at [1:1200] and added to samples which were incubated at 40°C for 30 minutes and then washed 3 times for 15 minutes each. HRP blocker was then added to samples

which were incubated at 40°C for 15 minutes and then washed 3 times for 15 minutes each. Developing steps were then repeated for remaining channels.

Some samples also underwent whole-mount immunohistochemistry staining to detect proteins, starting from the blocking step (2.6.2). Samples were stored in either SSC-Tw (RNAscope only) or PBS-Tw (RNAscope + immunohistochemistry) at 4°C. in the dark prior to imaging on a confocal microscope. All samples were imaged within 10 days of RNAscope protocol.

2.10 EX VIVO SCALE CULTURE

9 days prior to tissue harvesting for *ex vivo* scale culture, 12 scales were plucked from the left flank of adult Tg(*osterix:mCherry-ntr*) zebrafish, as described in 2.3.4 (Figure 7 B (iii)). At 9 days post removal, 12 regenerating scales were plucked from the left flank on the fish, whilst 12 ontogenetic scales were plucked from the right flank of the fish. Harvested scales were placed in the well of a 96-well plate (Thermo Fisher) containing 120 μl of culture medium comprised of: DMEM (31053028, Thermo Fisher) supplemented with 1% foetal bovine serum (Gibco), Pen/Strep (100 U ml^{-1}, Thermo Fisher), $CaCl_2$ (20 μM), sodium pyruvate (1 mM, Thermo Fisher), β-glycerophosphate, GlutaMAX (1 mM). Half of the wells were also supplemented with zebrafish recombinant (zr)-Tnf-α (RP1318Z-005; Kingfisher BioTech) at a final concentration of 10 ng/ml. Plates were placed in an IncuCyte ZOOM® for a total of 4 days and each well imaged every 4 hours in the brightfield and mCherry channels. Media was refreshed daily.

2.11 ALKALINE PHOSPHATASE (ALP) STAINING

Scales were rinsed in ALP buffer comprised of 100 mM Tris (pH 9.5), 100 mM NaCl, 50 mM MgCl in PBS. Staining solution was prepared by diluting NBT/BCIP stock solution (11681451001, Sigma) into ALP staining buffer at a final concentration of 1:500. Scales were incubated in freshly prepared staining solution at room temperature for 15 minutes and then immediately rinsed in Milli-Q water. Scales were mounted on glass microscope slides with FluoSave™ mounting medium (345789, Merck) and covered with a glass coverslip. Images of scales were acquired using a Leica Stereomicroscope (as in 2.14.1).

2.12 FLUORESCENCE ACTIVATED CELL SORTING (FACS)

FACS was performed with the assistance of Dr Andrew Herman and Dr Helen Rice the flow cytometry facility at the University of Bristol. All tissue preparation and analysis were performed solely by me.

2.12.1 CELL DISSOCIATION FROM FINS

Amputation injuries were performed on *tnfα:GFP;osx:mCherry* zebrafish. Uninjured or regenerating fins (4 or 6 dpa) were harvested from zebrafish via amputation and placed in ice cold PBS. Fins from 3 individual zebrafish were pooled into a single Eppendorf tube for each condition. Fins were macerated using sterile surgical scissors and tissue gently sheared using a 30 x 0.7 mm hypodermic needle (Sterican) and 1 ml syringe (BD Biosciences). PBS was removed from tissue after brief microcentrifugation. Tissue was resuspended in fresh digestion buffer (250 μl per fin) comprised of 5 mg ml^{-1} collagenase II (Thermo Fisher) and 12.5 μM $CaCl_2$ dissolved in PBS. Fins were incubated 32°C in digestion buffer on a shaker at 800 RPM for 2 hours. Tissue was disrupted every 20 minutes by gentle pipetting to aid digestion. Digestion was stopped via the addition of an equal volume of ice cold stopping buffer (250 μl per fin) comprised of 10 % foetal bovine serum (FBS, Gibco) and 12.5 μM $CaCl_2$ in PBS. Samples were incubated on ice in stopping buffer for 2 minutes, before being passed through a 40 μm cell strainer into a fresh tube. Samples were centrifuged at 300 x g for 8 minutes at 4°C, to isolate cells. Supernatant was discarded and cells resuspended in 300 μl ice cold suspension buffer comprised of 0.8 μM $CaCl_2$, 2 % FBS and Pen/Strep (50 U ml^{-1}, Thermo Fisher). Cells were stored on ice until immediately prior to FACS.

2.12.2 FACS

Single cell suspensions were ensured by passing cells through a 40 μm sieve prior to FACS to prevent clumping. Immediately prior to FACS, DRAQ7 dye (ab109202; Abcam) was added prior to FACS to allow for the exclusion of dead cells. FACS was performed on a BD Influx Fluorescence Activate Cell Sorter, under sterile conditions at 4°C. Events were gated to select for single, live cells, as depicted in Figure 9. Initial gating strategy was established based on a non-fluorescent sample of cells acquired from the regenerating fin of a wild type, non-transgenic zebrafish. GFP^+ and $mCherry^+$ gates were established using single

transgenic animals as positive controls. Cells were sorted directly into either 200 µl Trizol™ LS (Thermo Fisher) or RLT buffer (Qiagen), for RNA extraction (results not included in thesis).

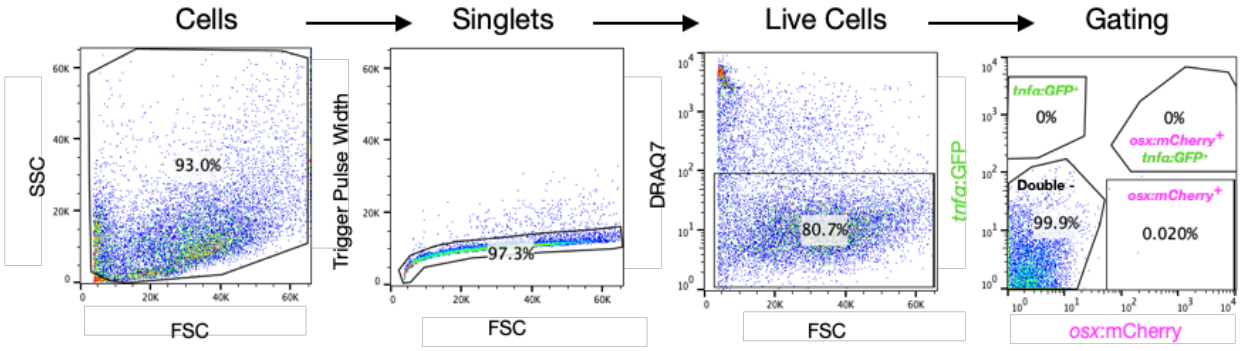

Figure 10. Fluorescence Activated Cell Sorting (FACS) Gating Strategy. *Cells from the regenerating fin of a wild type, non-transgenic zebrafish were used to establish gates for FACS. Forward (FSC) and Side Scatter (SSC) were used to gate cells, then FSC and trigger pulse width used to gate singlet cells. Live cells were gated based on exclusion of DRAQ7⁺ events. Background events in the wild type sample were gated as double⁻, and fluorescent populations (GFP⁺, mCherry⁺ and GFP⁺;mCherry⁺) gated from transgenic samples.*

2.13 RNA ISOLATION

2.13.1 RNEASY KIT METHOD OF RNA ISOLATION

For RNA-extraction of FACS-derived cells, and RNeasy Plus kit was used. Cells were sorted via FACS directly into 500µl of ice-cold RLT buffer and RNA isolation was performed exactly according to the manufacturer's instructions. The final preparation of RNA was eluted from the column using 20 µl RNAse-free water. The concentration and quality of RNA was determined via 260/280 absorption ratios after loading 1 µl sample into a NanoDrop 2000.

2.13.2 TRIZOL-LS METHOD OF RNA ISOLATION

For RNA-extraction of FACS-derived cells, the TRIzol-Chloroform method was used. Cells were sorted via FACS directly into ice-cold 500µl of TRIzol-LS (Thermo Fisher) solution. Cells were gently sheared using a 30 x 0.7 mm hypodermic needle (Sterican) and 1 ml syringe (BD Biosciences) before adding chloroform (200 µl per 750 µl TRIzol-LS). Cells were vortexed immediately and incubated at RT for 3 minutes. Samples were centrifuged at 12,000 g for 15 minutes at 4°C. The clear upper aqueous phase was removed and deposited in a new tube. Isopropanol (500 µl per 750 µl TRIzol-LS) and incubated at RT for 10 minutes before centrifuging again at 12,000 g for 10 minutes at 4°C. Supernatant was carefully removed and discarded before washing pellet in 75% ice-cold EtOH (1000 µl per 750 µl TRIzol-LS). Samples were mixed via vortex and then centrifuged at 12,000 g for 10 minutes at 4°C. All supernatant was carefully removed and discarded, and pellet left to air dry for 10 minutes. Ethanol clean-up of was then performed to improve sample purity. Pellet was resuspended in 20 µl RNAse-free water before 2 µl sodium acetate (3 M) and 100 µl of 100% ice-cold EtOH was added and samples incubated at -20°C overnight. Samples were centrifuged at 12,000 g for 30 minutes at 4°C and supernatant removed and discarded. Pellet was resuspended in a further 500 µl of 100% ice-cold EtOH before centrifuging again at 12,000 g for 10 minutes at 4°C. This step was repeated once, before supernatant was removed for a final time sample was air-dried for 10 minutes. The final RNA preparation was resuspended in 11 µl RNAse-free water and concentration and quality of RNA was determined via 260/280 absorption ratios after loading 1 µl sample into a NanoDrop 2000.

2.14 IMAGING

2.14.1 LIVE IMAGING OF INJURIES IN TRANSGENIC ZEBRAFISH

Fish were anaesthetised in MS222 at the required time-points post-injury to immobilise them and immediately placed on a plastic petri dish. Images of the fin were taken in the dark using a DFC700T camera mounted to a MZ10F Stereomicroscope (Leica Microsystems). Images were acquired using LAS X software (version 3.7.0) and saved in the *.lif* file format to preserve metadata. Fish were recovered in fresh system water after imaging.

2.14.2 CONFOCAL IMAGING

UltraPure™ Low Melting Point Agarose (Thermo Fisher) was used to mount whole mount samples for confocal imaging. Live larval zebrafish were mounted in 1% low melting point agarose in Danieau's solution supplemented with MS222. Fixed larvae or tissues were mounted in 0.3% agarose. Samples were imaged with a ×10 objective lens on a SP5 confocal microscope (Leica Microsystems). Images were acquired using LAS X software (version 3.0 or above) and saved in the. *.lif* file format to preserve metadata. For 3-dimensional imaging, confocal stacks were taken at a minimum of 1.5 μm and a maximum of 3 μm increments through the tissue.

2.14.3 MICRO COMPUTED TOMOGRAPGY (μ-CT) IMAGING

μ-CT scans were performed by Dr Erika Kague and images processed for analysis in collaboration with Dr Elis Newham at the University of Bristol.

Scans were performed and analysed as described in McGowan *et al*., 2021 (2). Briefly, prior to scanning, whole adult zebrafish were fixed in 4% PFA for 1 week and then dehydrated into 70% ethanol via transfer between a series of increasing EtOH concentrations. A Bruker SKYSCAN 1227 μ-CT scanner was used to acquire images with a voxel size of 5 μm, using an x-ray source of 60 keV, 50 W current and a 0.25 mm thick aluminium filter. Each scan acquired 1500 angular projections with 400 ms exposure time over a 180° scan. X-radiographs were reconstructed using the filtered backprojection algorithm provided by NRecon software (v. 1.7.1.0) and saved as 8-bit tiff stacks. "Phantom" samples containing known calcium hydroxyapatite concentrations (0.25 and 0.75 $g.cm^{-3}$ CaHA) were also scanned to calibrate tissue mineral density (TMD) measurements in the μ-CT fin data. Avizo image analysis software (version 8.0, Thermo Fisher Scientific) was used to generate 3D volume renders of whole caudal fins using both automatic and manual segmentation, which were saved as binary image stacks. The first 2 dorsal and ventral lepidotrichia were excluded from the analysis of all fins due to varying resolution and size. Image stacks were used to isolate the grayscale values of segmented fins from values of surrounding soft tissue and air by multiplying these binary (fin = 1; non-fin = 0) stacks against the original reconstruction stacks using image algebra in Fiji/ImageJ (283). Greyscale values were compared with the mean grayscale values of calibrated TMD values and exported for analysis.

2.15 GENERIC IMAGE ANALYSIS IN FIJI

FIJI software was used for processing, analysis and quantification of all imaging data (284).

2.15.1 QUANTIFICATION OF FIN REGENERATION

Fin regeneration was quantified using 2 methods: % area of regeneration and percentage length of regeneration. An image was taken of the whole fin prior to, and immediately after, amputation. The area and length of amputated tissue was then calculated. The total area and length of regenerated tissue was measured at various time points post-amputation and converted to a % area / length of regeneration relative to the amount of amputated tissue. This method normalises for variability in size of the fin and amount of amputated tissue.

2.15.2 FLUORESCENCE INTENSITY RATIO MEASUREMENTS

FIJI was used to quantify relative fluorescence intensity ratios in images of transgenic zebrafish. Intensity ratios were calculated by measuring the average pixel intensity of injured tissue within a region of interest (ROI), divided by average pixel intensity of uninjured tissue withing an ROI. This method of quantification normalises for any variability in reporter expression between animals or image acquisition settings from day-to-day, allowing for more reliable comparison of fluorescence intensities between zebrafish.

$$Intensity\ Ratio = \frac{Average\ intensity\ of\ X\ within\ injury}{Average\ intensity\ of\ X\ in\ uninjured\ tissue}$$

$$X = fluorophore\ or\ transgene\ reporter\ of\ interest, such\ as\ GFP$$

2.15.3 COLOCALISATION ANALYSIS

To measure colocalization between 2 colour channels, the freely available JACoP plugin was used. Images for each channel were manually thresholded within JACoP to exclude background. The same threshold value was applied to repeat images acquired for each condition or time point. The JACoP plugin calculates

both the Pearson's correlation coefficient (PCC) and Manders' correlation coefficient (MCC) values for each image. PCC accounts for pixel intensity within the colocalization analysis, whereas MCC uses an adjustable threshold measure fraction of Channel A overlapping channel B, and vice versa. For PCC values, 1 = complete colocalization between channels and 0 = no colocalization with channels. Only PCC values were used for comparison between groups.

2.15.4 QUANTIFICATION OF ALCIAN BLUE AND TRAP STAINING

To quantify glycosaminoglycan levels in the soft callus, the FIJI polygon tool was used to measure the area of alcian blue stained tissue immediately around the fracture site. TRAP activity was quantified using 2 methods: $TRAP^+$ % area and number of $TRAP^+$ punctate. The injury was centrally positioned within a defined ROI measuring 300μm x 300 μm. The number of $TRAP^+$ punctate were manually counted. To measure the % $TRAP^+$ area, the brightfield image was converted to an RGB stack montage and thresholded to detect $TRAP^+$ pixels and the area measured.

2.16 MODULAR IMAGE ANALYSIS (MIA) IN FIJI

Modular image analysis (MIA) is a freely available plugin for use in FIJI, where tailored MIA workflow files can be written and loaded into the plugin for specific image analyses. The MIA plugin and associated MIA workflow files for specific analyses were written and developed by Dr Stephen Cross in the Wolfson Bioimaging Facility at The University of Bristol. Links to all workflow and classifier files are available in Appendix 1. The development of this plugin is ongoing; the latest release of MIA along with previous versions are available to download via GitHub (285).

2.16.1 MIA OF IMMUNE CELL RECRUITMENT

To quantify the number of immune cells responding to injury in transgenic zebrafish, the MIA, 0.9.30 FIJI plugin was used with the "*2019-06-13 Cell distance to fracture_WEKA.mia*" workflow and "*2019-05-07 C2*" classifier, as described in McGowan *et al*., 2021 (2, 284, 286). Briefly, images were enhanced using the WEKA plugin and a threshold applied at a probability value of 0.5. Individual cells were separated in the

binarized image using the watershed tool. The injury site within the image was manually identified and the distance of each immune cell to the fracture site was measured. The number of cells within either a 100 μm radius or a 300 μm radius of the injury was then calculated in Microsoft Excel.

2.16.2 MIA OF *EX VIVO* SCALE CULTURE

To quantify *osterix* expression, via the *osx:NTR-mCherry* transgenic reporter, in scales during *ex vivo* culture, the MIA, 0.21.2 FIJI Plugin was used with the "*2022-01-24 Scale and spot detection_wholescale.mia*" workflow (287). Scale shape descriptors were measured via automatic detection in the bright field channel. A manually defined minmum threshold (threshold = 10) was used to detect and outline $mCherry^+$ areas of the scale. The MIA output contained the total area of each scale, the $mCherry^+$ area for each scale (in both μm^2 and as a percentage of the total area of each scale), and the mean signal intensity of mCherry. Opltimisation of this analysis workflow is ongoing.

2.16.3 MIA OF ALKALINE PHOSPHATASE STAINING IN SCALES

To quantify ALP staining in scales post-culture, the MIA, 0.21.2 FIJI Plugin was used with the "*2021-10-20 RGB scale analysis.mia*" workflow and "*2021-10-15 Scaled WB*" classifier (287). Images were corrected for chromatic aberration, an artefact of image acquisition, using channel alignment. Colour deconvolution and a manually defined threshold (threshold = 75) were then applied to all images. Individual stained regions were separated in the binarized image using the watershed tool. Scale area, width and shape descriptors were measured using a semi-automated method, whereby a reference point was added to the mid-anterior region of each scale. The area of ALP-stained region for each scale was calculated in both μm^2 and as a percentage of the total area of each scale, as well as mean signal intensity of ALP staining.

2.17 POWER CALCULATIONS AND STATISTICAL ANALYSIS

2.17.1 POWER CALCULATIONS

The freely available G*Power software (version 3.1) was used (288). Priori power calculations were performed to estimate appropriate sample sizes where α = 0.05, and power (1- β err prob) = 0.8. Effect estimates were calculated using preliminary pilot data, where available, or based on existing data from the published literature. Sample sizes for individual experiments are indicated in figure legends throughout results and are based on both power calculations and practical limitations (i.e., number of injuries which could be feasibly performed in adults or number of animals available).

2.17.2 STATISTICAL ANALYSIS

GraphPad PRISM Software (version 8) was used for all statistical analyses and graph design. Where possible ($n \geq 7$) a D'Agostino Pearson normality test was performed on data to determine whether a parametric or nonparametric statistical test should be used. Where a normality test could not be performed ($n < 7$), a non-parametric test was used. Where more than two sets measurements were compared (e.g., different fish at multiple time points), a one-way ANOVA (parametric) or Kruskall-Wallis test (non-parametric) was used. Where two or more groups (e.g., untreated and treated) and multiple measurements (e.g., time points) were compared, a two-way ANOVA was used with a Sidak test to correct for multiple comparisons. For comparison between groups at individual time points (e.g., untreated 4 dpi and treated 4dpi), but without comparison between repeated measures (e.g., untreated 2 dpi and untreated 4dpi), multiple t-tests (one per row) were performed, and statistical significance determined using the Holm-Sidak method. For comparison of frequencies between groups (e.g., frequency of fracture dissociation), a contingency analysis (Fisher's Exact Test) was performed. Where repeat measures were taken from the same animal over time, such as throughout a live time course of fracture repair, statistical tests were adjusted to account for repeated measures. Differences were considered statistically significant where $P < 0.05$, as per convention. All graphs display mean ± the standard deviation as error bars (where appropriate).

CHAPTER 3: RESULTS SECTION 1

WNT16 ELICITS A PROTECTIVE EFFECT AGAINST FRACTURE AND SUPPORTS BONE REPAIR IN ZEBRAFISH

The data described within this chapter has been published as an original research article in the peer-reviewed journal, JBMR Plus (McGowan et al., 2021 (2)). As the lead author of this research article, I collected and analysed the majority of data within it, prepared the manuscript text and figures in full and responded to reviewer's comments. Dr Chrissy Hammond and Dr Erika Kague provided manuscript feedback prior to submission for publication. Figures and text have been adapted as appropriate for incorporation into this thesis. Unless stated otherwise, data collection, analysis and interpretation were performed solely by me. Any data included within this chapter that were collected or analysed in collaboration with other authors, are clearly indicated as such throughout the text and figure legends, as well as being highlighted throughout relevant sections of the methods (Chapter 2).

3.1 INTRODUCTION

3.1.1 WNT SIGNALLING PATHWAYS IN BONE

Wnt signalling pathways are highly conserved, central regulators of skeletal development and homeostasis which act on bone throughout the lifetime of vertebrate organisms (289). Canonical Wnt pathway activation leads to the stabilisation of β-catenin and activation of T cell factor/lymphoid enhancer factor family (LEF-TCF) transcription factors, whereas the calcium-dependent and planar cell polarity non-canonical Wnt signalling pathways regulate intracellular calcium levels and Jun N-terminal kinase (JNK) activity, respectively (Figure 10) (290, 291). Activation of TCF/LEF downstream of canonical Wnt signalling has been associated with the expression of key osteoblast differentiation genes such as *RUNX2* and *OSTERIX*, in a variety of *in vitro* and *in vivo* models (292), including in zebrafish (16, 193). Tightly coordinated synergy between Wnt signalling and other key developmental pathways, such as the fibroblast growth

factor (FGF) and bone morphogenetic protein (BMP) signalling pathways, is required to establish optimal osteoblast differentiation and bone development (18, 293). Due to their central role in regulating osteoblast stemness and differentiation, the modulation of Wnt signalling pathways have become an exciting area of research in osteoanabolic therapy development for the treatment of osteoporosis and bone trauma (289) . Therefore, the influence of different Wnt signalling ligands on these complex pathways and downstream effects on bone must be investigated further.

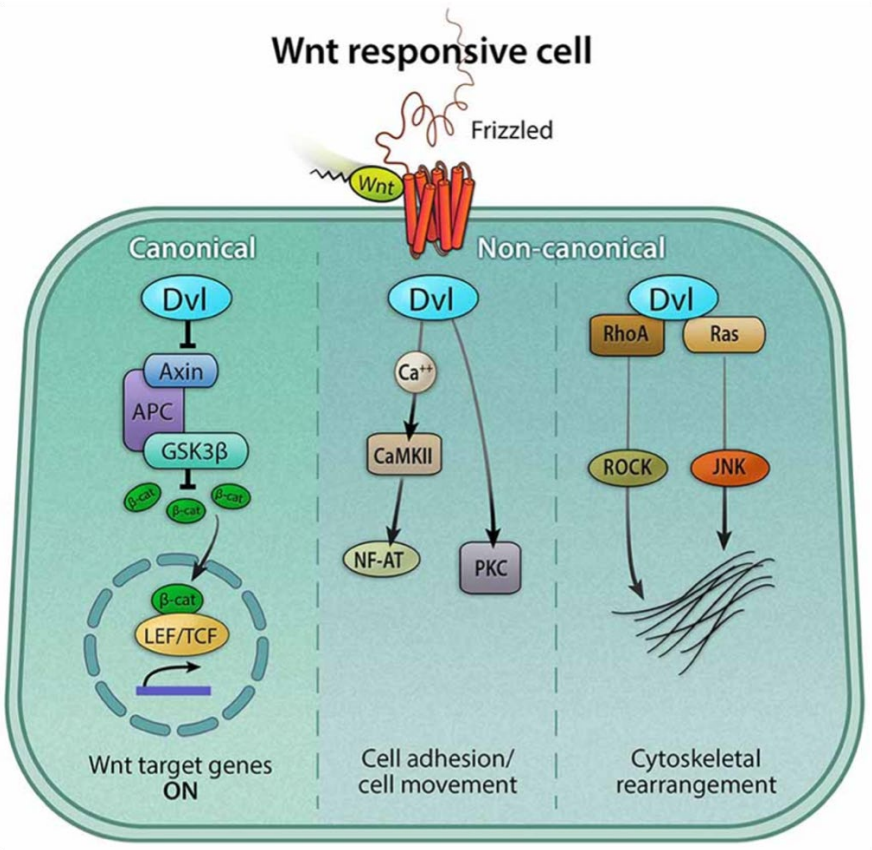

Figure 11. Wnt Signalling Pathways. *The Wnt signalling pathways are categorised as canonical (left), or non-canonical (right); either are initiated by the binding of a Wnt ligand to a frizzled receptor on the cell surface. In canonical Wnt signalling, binding of a Wnt to frizzled and the co-receptor, lipoprotein receptor related protein (LRP) 5/6 results in the activation of dishevelled (Dvl), which inhibits the β-catenin destruction complex formed of Axin, adenomatous polyposis coli (APC) and Glycogen synthase kinase 3β (GSK3β). In the absence of GSK3β-mediated phosphorylation, β-catenin becomes stabilised and translocates to the nucleus where it activates T cell factor/lymphoid enhancer factor family (TCF-LEF) transcription factors and increases Wnt target gene expression. In Ca^{2+} dependent non-canonical Wnt signalling, the activation of Dvl results in intracellular Ca^{2+} release and*

downstream activation of protein kinase C (PKC), calmodulin-dependent kinase II (CaMKII) and nuclear factor of activated T-cells (NFAT), facilitating cell migration. In the non-canonical planar cell polarity (PCP) Wnt signalling pathway, Dvl activates RhoA-Rho-associated kinase (ROCK) and c-Jun N-terminal kinase (JNK) via Rho and Ras GTPases, facilitating cytoskeletal rearrangement and cell polarity. Figure originally from Jansson et al., 2015 (291).

3.1.2 WNT16 IN BONE HOMEOSTASIS AND DISEASE

Wnt ligands are a large family of secreted glycoproteins which activate Wnt signalling pathways. The binding of Wnt ligands to membrane-bound frizzled receptors initiates downstream intracellular signalling events which influence cell stemness, proliferation, differentiation and migration (Figure 10, (291)). WNT16 is one such ligand, which is known to influence the activity of canonical and non-canonical Wnt pathways (294, 295). Recently, WNT16 has emerged as a regulator of musculoskeletal health; mutations in *WNT16* have been linked to reduced cortical bone thickness and BMD via a number of human genome wide association studies (GWAS) (103, 263, 265). Furthermore, a meta-analysis of GWAS in women aged 20-45 years also associated *WNT16* with lumbar-spine BMD, suggesting that *WNT16* influences BMD throughout life, not only in post-menopausal or ageing populations (296). In addition to population studies, current experimental evidence further supports a role for WNT16 as a key regulator of bone homeostasis and repair, as well as immune cell development. Knockout of *Wnt16* in mice has been shown to lead to decreased cortical bone thickness and up to a 61% decrease in femur and tibia bone strength compared to wild type littermates in three-point bending tests (263). Whilst loss of *Wnt16* in mice decreases bone strength, overexpression of *Wnt16* in osteoblasts (under the *Col1a1* promoter) leads to increased bone formation (297, 298). However, one study showed that *Wnt16* overexpression in osteoblasts could not counter glucocorticoid-induced osteoporosis and bone loss, suggesting that other factors play a role (298); one possible explanation could include interactions with the immune system.

Similarly to humans, glucocorticoid treatment in zebrafish has been demonstrated to suppress the innate immune system and osteoblast activity, leading to decreased bone synthesis (111). Interestingly, it has also been shown that morpholino-mediated knockdown of *wnt16* in zebrafish embryos results in impaired haematopoiesis and loss of thymic T lymphocytes at 4 days post-fertilisation (dpf) (266). Embryonic knockdown experiments demonstrated that somatic *wnt16* expression is required for the upregulation of notch ligands and subsequent expression of the haematopoietic stem cell (HSC) marker *cd41*, which is

needed for proper immune cell differentiation (266). Despite its proposed role in early HSC development, the relationship between Wnt16 and the immune system has not been explored further in adult tissues, or in stable mutant lines. Moreover, there is increasing interest in the interplay between immune cells and bone; osteoclasts and macrophages are derived from a common myeloid progenitor cell population and it is thought that macrophages can differentiate directly into osteoclasts in response to environmental molecular stimuli (133). The rapid, but tightly regulated, recruitment of innate immune cells is also required for optimal bone repair post-fracture (130, 267). In addition to promoting osteoblast activity, osteoblast-derived WNT16 has been shown to repress osteoclastogenesis, both directly via osteoclast progenitor cells and indirectly by increasing expression of Opg in osteoblasts (264). WNT16 has been linked to bone maintenance, fracture susceptibility and leukocyte differentiation. However, functional studies to elucidate the role of WNT16 in these dynamic processes are still required.

3.1.3 EXPERIMENTAL AIMS: INVESTIGATING WNT16 IN BONE HOMEOSTASIS AND REPAIR

Zebrafish serve as excellent models for studying the musculoskeletal system, innate immunity and Wnt signalling pathways (1). A large family of Wnt ligands are encoded by 19 separate genes in humans; 15 of these genes are conserved in zebrafish, including *wnt16* (266, 291). Larval zebrafish express *wnt16* in osteochondral precursor cells during jaw joint development; knockdown of *wnt16* in has been shown to perturb the proliferation and migration of these cells, altering the joint morphology (273). However, the relationship between *wnt16* and bone was not studied. Crucially, transparent zebrafish fin tissue provides optical clarity for high-quality, dynamic live imaging of adult bone injury and repair *in vivo*. This model can be used to decipher the role of *wnt16* in bone homeostasis and fracture healing in zebrafish.

Therefore, in this chapter, I aimed to:

1. Establish whether loss of Wnt16 increases susceptibility to fracture in zebrafish.
2. Develop and employ a model of induced fracture in caudal fin lepidotrichia and accompanying image analyses to further characterise fracture repair in zebrafish.
3. Use the induced caudal fin fracture model to investigate whether, and if so, how, loss of Wnt16 affects fracture repair in zebrafish.

To this end, I used a stable *wnt16*$^{-/-}$ mutant line of zebrafish, which lacks the functional Wnt16 protein, to investigate how loss of functional *wnt16* would affect bone maintenance, fracture repair and innate leukocyte function *in vivo*.

3.2 RESULTS: WNT16 IN BONE HOMEOSTASIS AND REPAIR

3.2.1 LOSS OF WNT16 ALTERS BONE TISSUE MINERAL DENSITY IN THE CAUDAL FIN

CRISPR-Cas9 wnt16$^{-/-}$ zebrafish were generated previously by Dr Erika Kague and Dr Lucy Brunt in the Hammond lab at the University of Bristol (273). μ-CT scans were performed by Dr Erika Kague (Senior Research Associate – Hammond Lab). μ-CT images were processed and analysed in collaboration with Dr Elis Newham at the University of Bristol.

WNT16 has been associated with low eBMD and increased fracture risk (103, 263, 299). Therefore, μ-CT was used to observe bone morphology and measure tissue mineral density (TMD) in whole-fins of adult WT and *wnt16*$^{-/-}$ zebrafish. Pseudo-coloured μ-CT images of WT and *wnt16*$^{-/-}$ illustrate regions of low to high TMD across the fins (Figure 11 A). Images of *wnt16*$^{-/-}$ fins showed a high frequency of bone calluses (Figure 11 A), which form post-fracture and remain visible at the injury site long-term, after the bone has repaired (147). The TMD of bone across the whole caudal fin ray was measured for each fish and plotted (Figure 11 B). The caudal fins of *wnt16* mutants show a high degree of variability in bone TMD relative to WT specimens, as well as generally lower TMD across the fin. This suggests that *wnt16*$^{-/-}$ zebrafish have weaker bone which is more susceptible to spontaneous fracture compared to WT.

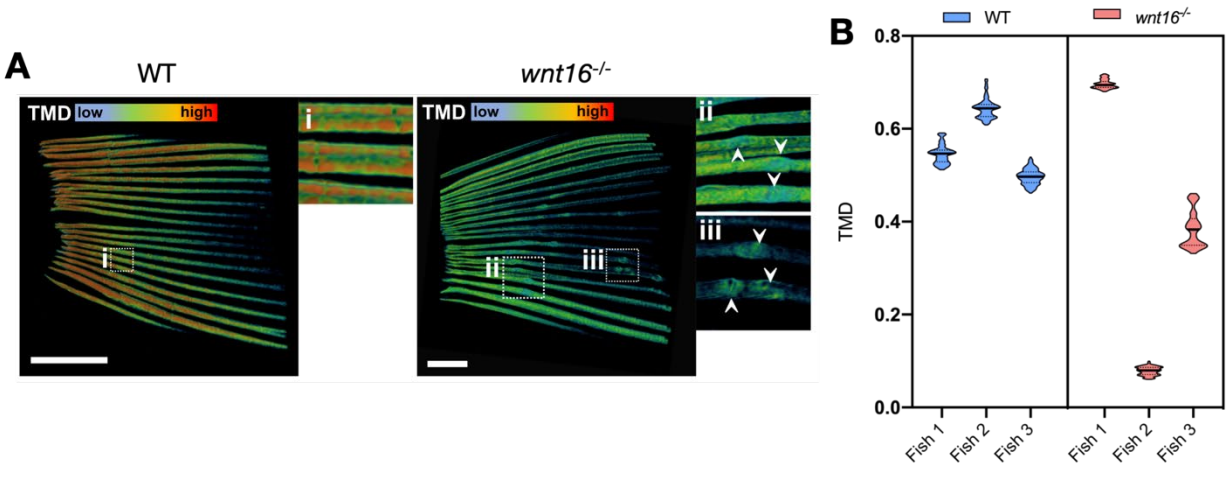

Figure 12. Loss of Wnt16 Results in Lowered and Uneven Tissue Mineral Density (TMD) in the Adult Caudal Fin. A: *representative μ-CT images taken of adult fins show generally reduced and more*

variable TMD in the lepidotrichia of mutant wnt16 zebrafish compared to WT. wnt16$^{-/-}$ zebrafish also display evidence of spontaneous fracture, resulting in bone calluses (arrowheads ii & iii), compared to WT (i). Scale bar = 1 mm. ***B:*** *TMD values across the fin were calculated for each fish (WT and wnt16$^{-/-}$) and plotted as violin plots showing distribution around the mean (black line). N = 3 per genotype. N.B.: μ-CT scans were performed by Dr Erika Kague. Images were processed and TMD measurements calculated in collaboration with Dr Elis Newham.*

3.2.2 *WNT16* MUTANT ZEBRAFISH ARE SUSCEPTIBLE TO SPONTANEOUS FRACTURE AT A YOUNG AGE

Bone calluses in the caudal fin rays can be easily visualised using live alizarin Red S (ARS), which binds to calcified tissue. Thus, ARS was used to quantify and compare the frequency of spontaneous lepidotrichia fractures within the previously uninjured caudal fins of young adult (6 month old (mo)) WT and *wnt16*$^{-/-}$ zebrafish. Bone calluses and spontaneous fractures were rarely observed in the young WT zebrafish, with only 25% of zebrafish sampled displaying a minimal number of calluses and a mean number of 0.4 calluses per fin (Figure 12 A-C). However, a significantly higher number of calluses were recorded in the caudal fins of young *wnt16*$^{-/-}$ zebrafish; 100% of *wnt16*$^{-/-}$ fins sampled contained calluses, with a mean of 8.5 calluses per fin. To test whether calluses resulting from spontaneous fracture increase with age, calluses were also quantified by ARS in moderately aged (20 mo) and severely aged (30 mo) WT zebrafish. Aged WT zebrafish were comparable in appearance and callus frequency to 6 mo *wnt16*$^{-/-}$ zebrafish (Figure 12 A-B). Statistical analysis showed no significant difference in callus frequency between young *wnt16*$^{-/-}$ and severely aged WT zebrafish (Figure 12 C). Collectively, this demonstrates that *wnt16*$^{-/-}$ zebrafish display a bone fragility phenotype which predisposes them to spontaneous fractures and the accumulation of calluses at a young age.

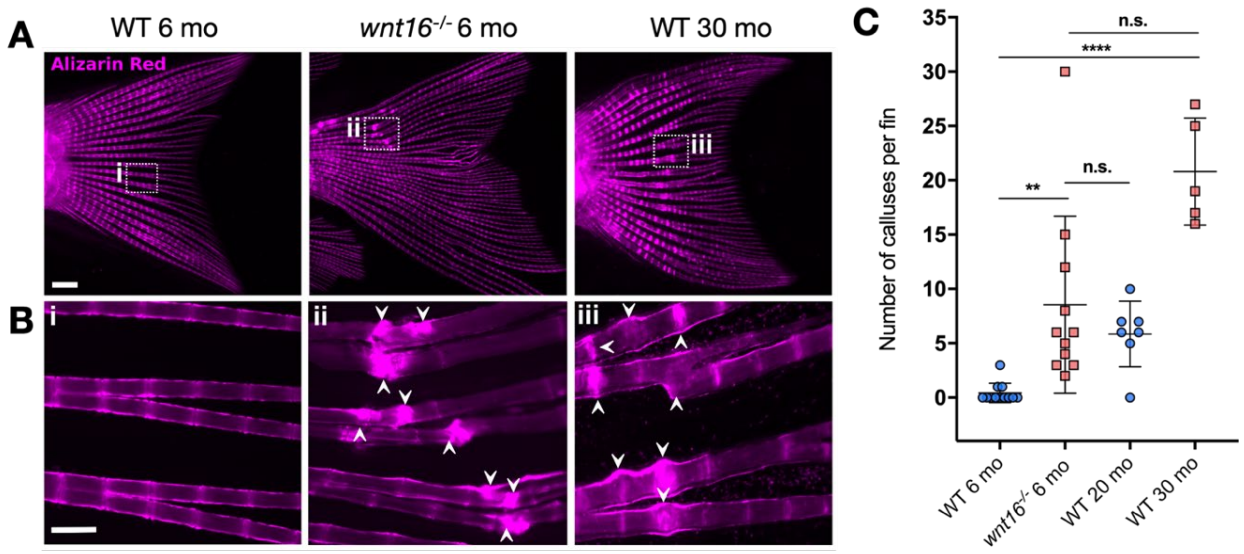

***Figure 13. wnt16 Mutants Are Susceptible to Spontaneous Fracture at a Young Age**. **A:** Representative images of the caudal fins of uninjured adult zebrafish live stained with alizarin red to label bone at 6 (young), 20 (moderately aged) or 30 (severely aged) months old (mo). Scale = 1 mm. **B:** Higher magnification images (from A) show undamaged bone in a 6 mo WT fin (i) and the presence of bone calluses resulting from spontaneous fracture (arrowheads) in 6 mo wnt16$^{-/-}$ (ii) and 30 mo WT (iii) fins. Scale = 200 μm **C:** Total number of calluses per fin were quantified for each group; young wnt16$^{-/-}$ zebrafish displayed a significantly higher number of bone calluses resulting from fracture compared to young and moderately aged WT zebrafish, but a comparable number of calluses compared to severely aged WT zebrafish. **$p < 0.01$, ****$p < 0.0001$, n.s. = no significant difference; $N \geq 5$ per group; points represent mean (± SD)*

3.2.3 WNT16 IS EXPRESSED IN BONE POST FRACTURE

Similarly to mammals, fracture repair in zebrafish comprises an inflammatory phase, a repair phase and a remodelling phase (300). Immune cells are rapidly recruited to the injury site post fracture to prevent infection and initiate the repair process, before osteoblast activity later increases to facilitate bone callus synthesis and mineralization (147). Since WNT16 has been linked to immune cell differentiation and osteoblast function (266, 297), I next investigated changes to *wnt16* expression post fracture. Fractures were induced within the lepidotrichia of adult WT zebrafish. Uninjured and fractured bone tissue was fixed between 2-14 days post injury (dpi) for whole-mount RNAScope to label *wnt16* mRNA in situ (Figure 13 A). Expression of *wnt16* was quantified by measuring the fluorescence intensity of the probe within a region of interest at the fracture site, relative to uninjured bone in the same fin (intensity ratio). *wnt16* was expressed at low levels in uninjured bone, but expression increased significantly at 4 dpi, before returning to basal levels by 10 dpi (Figure 13 B). This demonstrates that *wnt16* expression is upregulated early on post-fracture, suggesting a role for Wnt16 in the initiation of bone repair in addition to its established role in healthy bone development and homeostasis.

3.2.4 BONE REMINERALISATION IS DELAYED IN *WNT16* MUTANTS POST FRACTURE

Since *wnt16* expression is upregulated post-fracture (Figure 13), and *wnt16* mutants displayed a high number of bone calluses (Figure 12), I next tested whether fracture repair was impaired in *wnt16*$^{-/-}$ zebrafish. Adult WT and *wnt16*$^{-/-}$ fish were live stained in ARS to label existing bone and imaged prior to fracture induction. Zebrafish were then live stained in calcein green at regular intervals between 0 and 42 days dpi to label newly incorporated bone matrix at the fracture site, and re-imaged (Figure 14 A). Injured *wnt16*$^{-/-}$ zebrafish displayed significantly reduced bone callus formation within the first 7 days of fracture healing compared to WT zebrafish; the reduction in remineralisation was most apparent at 4 dpi (Figure 14 B and C). This suggests that Wnt16 promotes efficient bone remineralisation post fracture, possibly via the regulation of skeletal or immune cells in early bone repair.

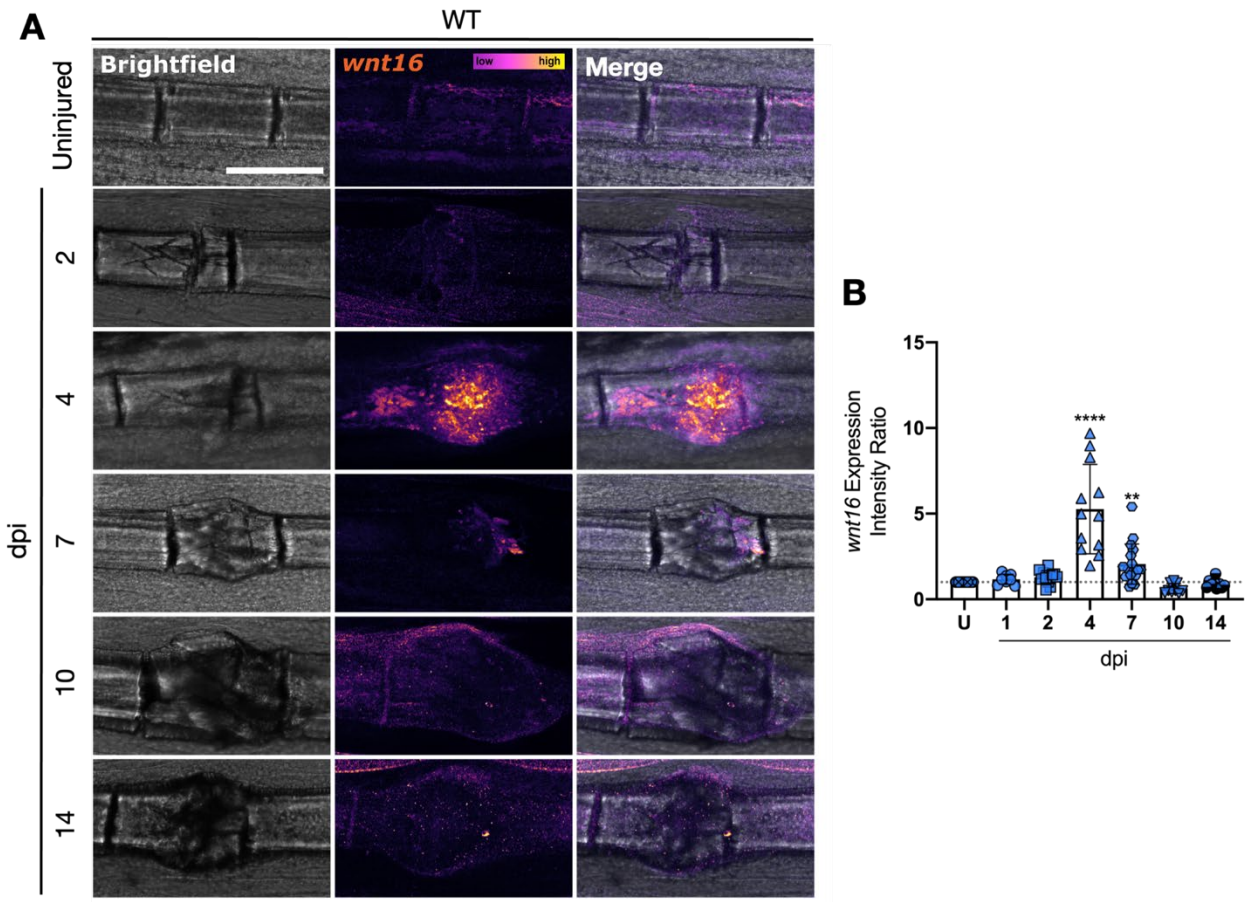

*Figure 14. wnt16 Expression Is Upregulated in Bone Post Fracture. A: Fractures were induced within the lepidotrichia of adult WT zebrafish. Uninjured and fractured bone tissue was fixed between 1-14 days post injury (dpi) for whole-mount RNAScope to label wnt16 mRNA in situ. Representative images from each time point are shown. Scale bar = 200 μm. B: The expression of wnt16 was quantified within a region of interest at the fracture site relative to the fluorescence intensity of the probe in uninjured bone (U) in the same fin (intensity ratio). The expression of wnt16 increased significantly post fracture between 4 and 7 dpi. Grey dotted line = wnt16 intensity ratio in uninjured bone. U = uninjured bone tissue. *p < 0.05, ****p < 0.0001; N ≥ 8 per time point; points represent mean (± SD).*

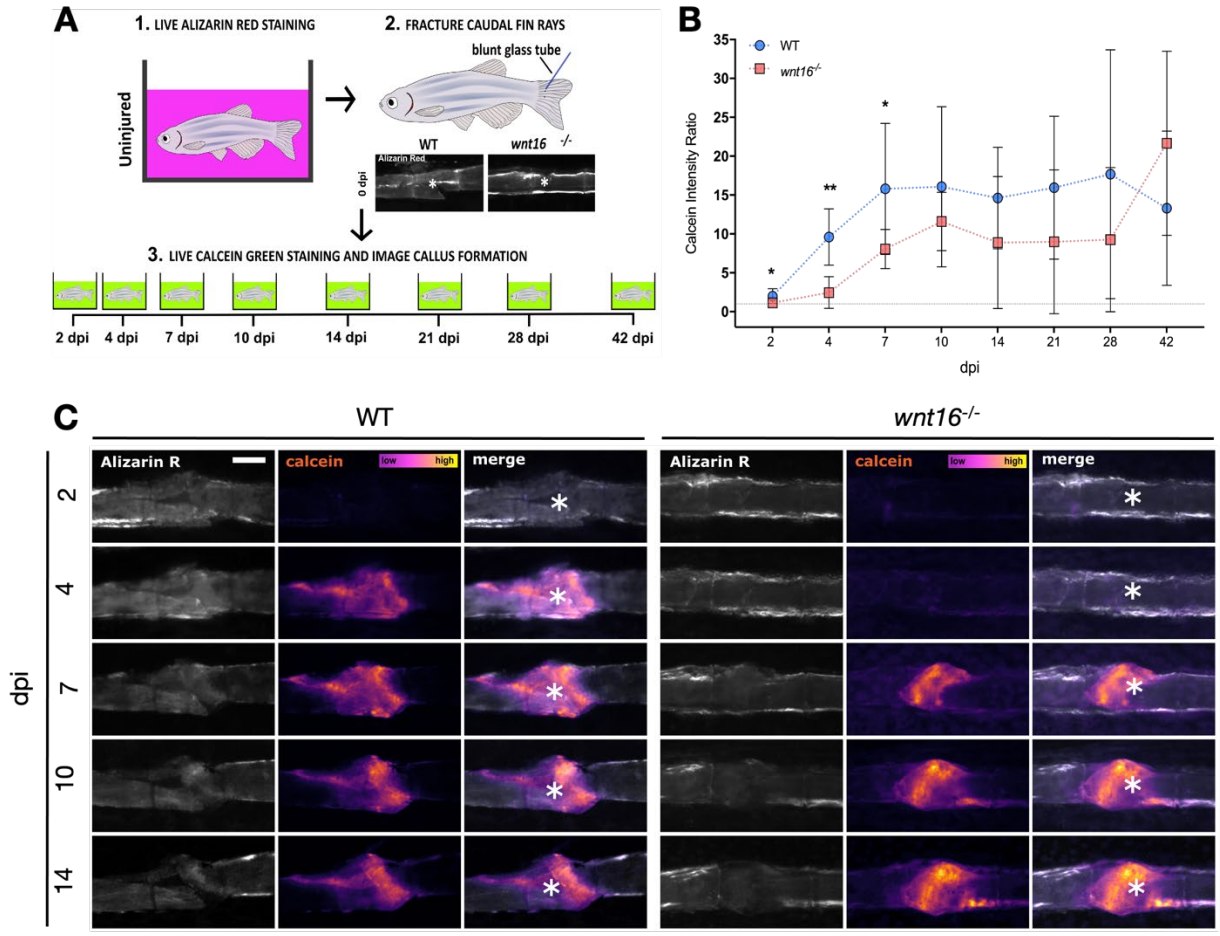

Figure 15. Bone Remineralisation is Significantly Delayed In wnt16 Mutants Post Fracture. A: Schematic illustrating the method used to measure bone remineralisation post fracture. Alizarin red was used to label bone in adult zebrafish prior to fracture, caudal fin fractures were induced, and zebrafish were restained with Calcein green to label remineralising bone throughout fracture repair. ***B:*** Callus formation was quantified by measuring the Calcein intensity ratio between the fracture site and uninjured bone. Callus formation was significantly reduced from 2 to 7 days postinjury (dpi) in wnt16 mutant fractures, compared to WT. *$p < 0.05$, **$p < 0.01$; $N \geq 5$ per group; points represent mean (± SD). Grey dotted line indicates where Calcein intensity at the fracture site = uninjured bone. ***C:*** Representative images of WT and wnt16$^{-/-}$ fractures at selected time points post injury show old bone labelled by Alizarin Red (grey) and callus formation at the fracture site, labelled by Calcein. White asterisk = centre of fracture. Scale = 200 µm.

3.2.5 SOFT CALLUS FORMATION IS NOT AFFECTED BY LOSS OF WNT16 DURING FRACTURE REPAIR

Since Wnt16 appeared to influence efficient bone repair, I next investigated whether formation of the initial soft callus differed between WT and *wnt16* mutant zebrafish post-fracture. In mammalian bone repair, the soft callus is comprised of a glycosaminoglycan-rich cartilaginous matrix and forms prior to the mineralised, hard callus (301). Alcian blue staining was performed in WT and *wnt16*$^{-/-}$ fins fixed between 0 and 7 dpi to label glycosaminoglycans. Both WT and *wnt16*$^{-/-}$ fractures showed the presence of a cartilaginous soft callus, peaking at 4dpi (Figure 15 A). However, no difference in alcian blue staining was observed between WT and *wnt16* mutant bone post-fracture at any time point. Fractures were also induced in the caudal fins of transgenic *col2a1*:mCherry zebrafish (Table 4) to study chondrocyte activity post fracture. *col2a1:mCherry* expression was almost undetectable throughout fracture repair and intensity ratios showed little variation from uninjured bone at all time-points post-injury (Figure 15 B-C). Moreover, no significant differences in Col2a1 levels were observed between WT and *wnt16* mutant fractures at any time point (Figure 15 C). This result from transgenic animals was validated using an antibody to label Col2a1 via immunohistochemistry at 4 dpi on fixed, WT fins. The 4 dpi time point was chosen as this is when soft callus formation peaked, according to the alcian blue staining of fractures (Figure 15 A). No observable increase in Col2a1 was detected at 4dpi, relative to uninjured bone (Figure 15 D). Collectively, these data suggest that soft callus formation is not affected by loss off *wnt16* and that Col2a1 is not a predominant component of the soft callus that is formed post-fracture in zebrafish lepidotrichia. This also suggests that delayed bone remineralisation in *wnt16*$^{-/-}$ zebrafish post fracture is not due to aberrant soft callus formation.

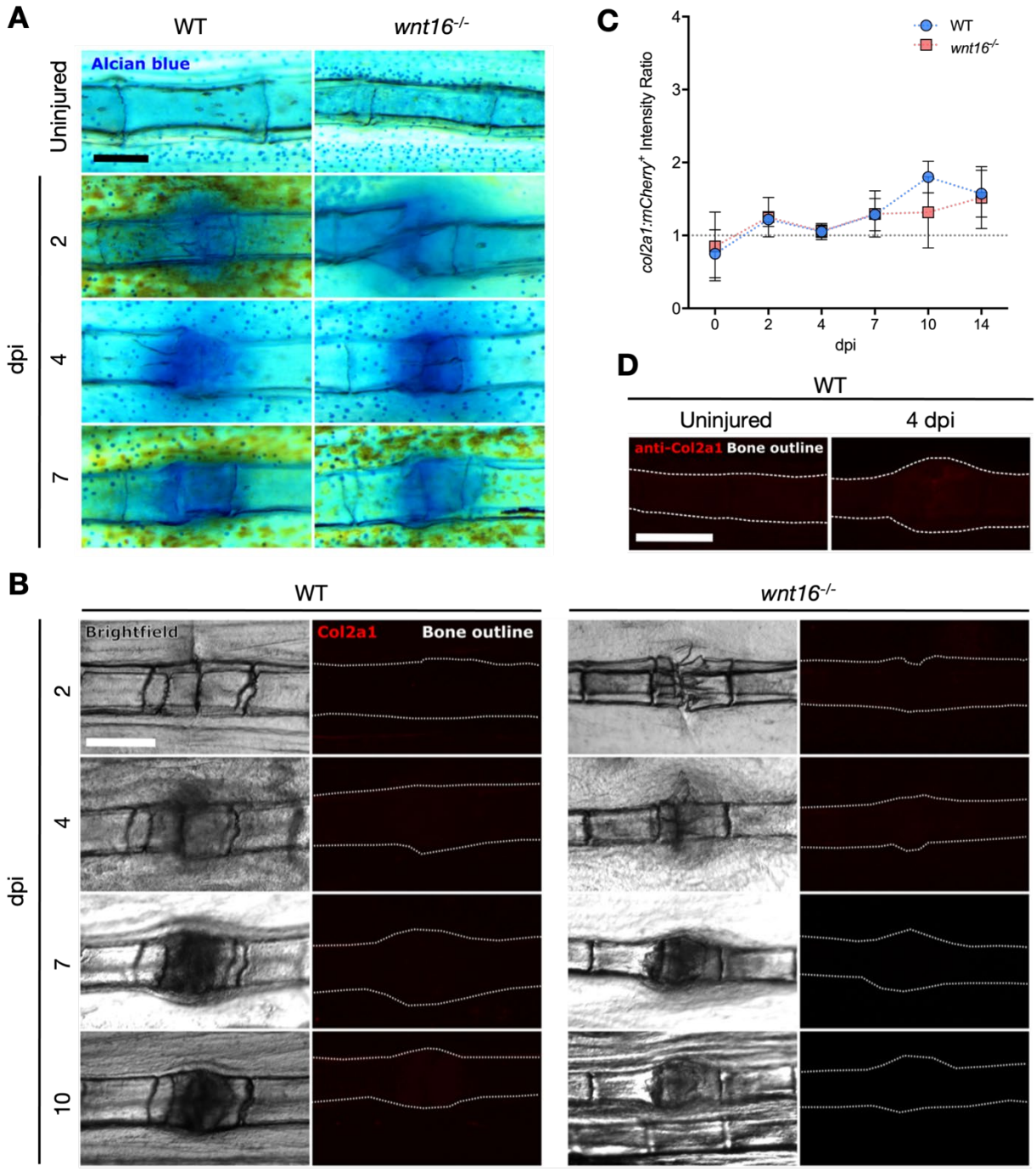

Figure 16. Soft Callus Formation is Not Affected in wnt16$^{-/-}$ Zebrafish Post Fracture. A: *Fractures were induced within the lepidotrichia of WT and wnt16$^{-/-}$ zebrafish. Uninjured and fractured bone tissue was fixed between 2-14 days post injury (dpi) for whole-mount alcian blue staining to label glycosaminoglycans within the early soft-callus, which forms post fracture. Representative images are shown. Alcian blue staining peaks at 4 dpi, but no marked difference in soft callus size was observed between WT and wnt16$^{-/-}$ zebrafish. Scale bar = 100 μm; N ≥ 9 per group.* ***B:*** *Lepidotrichia*

within the caudal fins of WT and wnt16$^{-/-}$ zebrafish carrying the col2a1:mCherry transgene were fractured and imaged from 0-14 days post injury (dpi). col2a1:mCherry remained low, at almost undetectable levels, throughout fracture repair in both WT and wnt16$^{-/-}$ zebrafish. Representative images are shown. Scale bar = 200 μm. ***C:*** *col2a1:mCherry levels were quantified within region of interest at the fracture site relative levels within uninjured bone in the same fin for each time point (intensity ratio). No significant difference between WT and wnt16$^{-/-}$ intensity ratios were measured at any time point post fracture; N≥6 per group; points represent mean (± SD).* ***D:*** *Immunohistochemistry was performed on uninjured and fractured bone at 4 dpi from WT zebrafish using a validated anti-Col2a1 antibody. No staining was detected in either group.*

3.2.6 OSTEOBLAST RECRUITMENT IS DELAYED POST FRACTURE IN WNT16 MUTANT ZEBRAFISH

Osteoblast activation is a key event in bone repair post-fracture. Osteoblasts differentiate from mesenchymal stem cell (MSC) precursors, initially expressing *runx2*, before downregulating *runx2* and expressing the transcription factor osterix (*osx*). Osteoblasts synthesise bone matrix within the initial soft callus; the callus hardens as it mineralises and is remodelled to restore the bone to a healthy state (141). Interestingly, transcriptomic analysis of osteoblast-prone clones isolated from tonsil derived MSCs showed that upregulation of WNT16 is predictive of osteogenic differentiation (302), suggesting that WNT16 may promote osteoblastogenesis. In zebrafish, osteoblasts may also dedifferentiate from a mature state by upregulating *runx2* and *osx* expression in response to bone injury, before proliferating and migrating to the damaged tissue where they initiate bone repair (198). Thus, I next investigated whether osteoblast activity was impaired post-fracture in *wnt16$^{-/-}$* zebrafish. Live AR staining was performed on WT and *wnt16$^{-/-}$* zebrafish carrying the *osx:GFP* transgene (labelling osteoblasts) prior to fracture induction in lepidotrichia within the caudal fins and imaging (Table 4). Injured zebrafish were imaged at various time points from 0-14 days post injury (dpi). Zebrafish were re-stained with live ARS prior to imaging at each time point to ensure labelling of any new bone. To quantify osteoblast density at the fracture site throughout repair, the fluorescence intensity of *osx:*GFP was measured relative to uninjured bone (intensity ratio). In WT zebrafish, the intensity ratio of *osx*:GFP at the fracture site peaked at 4 dpi, before steadily decreasing (Figure 16 A & B). However, compared to WT fractures, the intensity ratio of *osx*:*GFP* was significantly reduced at 4 dpi in *wnt16* mutants, not peaking until 10 dpi (Figure 16 A & B). Interestingly, the *osx:*GFP intensity ratio of fractured bone in *wnt16* mutants was significantly higher than in WT zebrafish at 10 dpi.

A comparable bony callus had formed at the fracture-site in both WT and *wnt16*$^{-/-}$ by 15 dpi (Figure 16 C). This demonstrates that osteoblasts in *wnt16*$^{-/-}$ zebrafish do respond to bone injury but that the recruitment and activity of these osteoblasts are significantly delayed, resulting in inefficient fracture repair. Reduced osteoblast activity at 4 dpi in *wnt16* mutants coincided with the peak of *wnt16* expression post-fracture in WT bone (Figure 13) and delayed mineralization in *wnt16*$^{-/-}$ fractures (Figure 14), suggesting that *wnt16* is required for early osteoblast recruitment and the initiation of optimal bone repair.

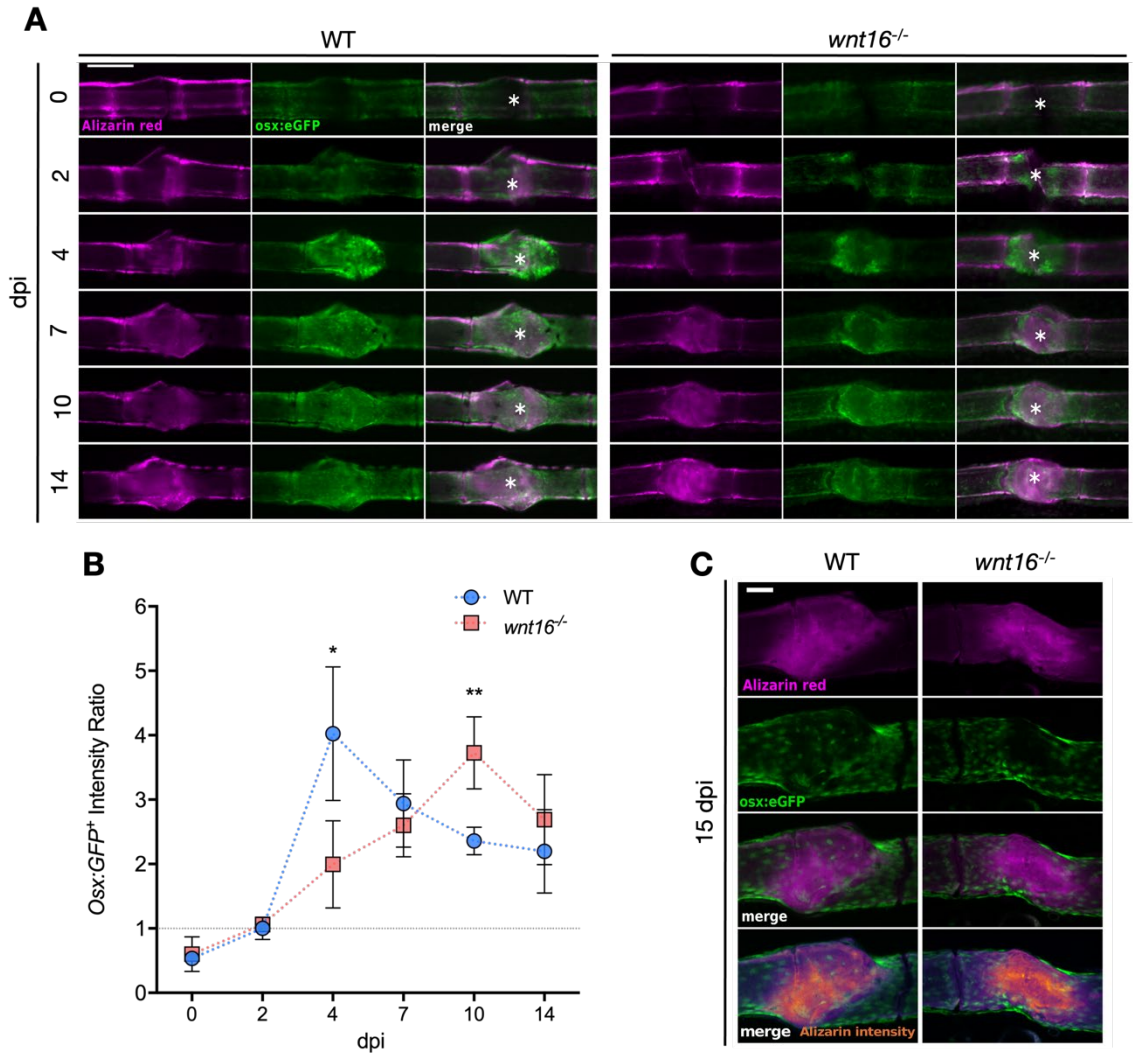

Figure 17. Osteoblast Recruitment Is Significantly Delayed Post Fracture In wnt16$^{-/-}$ Zebrafish. *Lepidotrichia within the caudal fins of WT and wnt16$^{-/-}$ zebrafish carrying the osx:GFP transgene were fractured and imaged from 0-14 days post injury (dpi).* ***A:*** *Representative images of calcified bone (Alizarin Red) and osteoblasts (osx:GFP) in WT and wnt16$^{-/-}$ fish throughout repair are shown. White asterisk = centre of fracture. Scale bar = 100 μm.* ***B:*** *Osteoblast density was quantified by measuring the fluorescence intensity of osx:GFP within a region of interest at the fracture site relative to uninjured bone in the same fin (intensity ratio). Grey dotted line indicates where osx:GFP intensity at the fracture site = uninjured bone. Osteoblast recruitment was delayed in wnt16$^{-/-}$ zebrafish, which had a significantly lower osx:GFP intensity ratio at the fracture site 4 dpi, but significantly higher osx:GFP intensity ratio at 10 dpi, compared with WT zebrafish.* ***C:*** *Confocal imaging of bone in amputated fins at the end of the time course (15 dpi) shows complete union of fractures in both WT and wnt16$^{-/-}$ zebrafish. *p < 0.05, **p < 0.01; N ≥ 6 per group; points represent mean (± SD).*

3.2.7 LOSS OF WNT16 DOES NOT AFFECT LEUKOCYTE RECRUITMENT TO BONE POST FRACTURE

Some immunohistochemical staining, as well as quantification of L-plastin^{+} cells in larval zebrafish, were performed by Alistair Vorster (Research Technician – Hammond Lab). Modular image analysis workflow files for automated analysis of leukocyte recruitment to fracture were written by Dr Stephen Cross from the Wolfson Bioimaging Facility (see section 2.16).

The controlled recruitment, activity and reverse migration of leukocytes during the inflammatory phase are known to be prerequisites for initiating osteoblast activity and optimal bone repair (134). A dysregulated inflammatory response post fracture can perturb bone repair and lead to non-union fractures in mammals (300). Neutrophils are innate immune cells which are rapidly recruited to bone post fracture, within hours of the injury (267); stimulation of the non-canonical Wnt signalling pathways with recombinant WNT5a has been shown to initiate chemotactic migration and chemokine production in human neutrophils *in vitro*, but whether WNT16 influences neutrophil recruitment to injury is unknown (303). Macrophages are another innate immune cell type which also rapidly respond to bone injury and continue to aid throughout the repair and remodelling phases in mammalian models of fracture (130). Crucially, a previous study indicated that *wnt16* expression was required for functional haematopoiesis in zebrafish embryos, suggesting that loss of Wnt16 may result in a dysregulated immune system (266).

To validate whether early leukocyte development was impaired in *wnt16* mutants, uninjured zebrafish larvae were fixed at 3 and 5 days post-fertilization (dpf). Whole-mount immunohistochemistry was used to label cartilage in the developing skeleton (Col2a1) and leukocytes (L-plastin) (Figure 17 A). Surprisingly, no significant differences in leukocyte numbers were observed at either developmental stage (Figure 17 B). This demonstrates that stable mutagenesis of *wnt16* does not lead to a significant reduction in leukocyte number during early skeletal development. However, the responsiveness of leukocytes to injury in *wnt16* mutants remained unclear.

Given that early callus formation and osteoblast recruitment were delayed post fracture in *wnt16*$^{-/-}$ zebrafish (Figure 14 & Figure 16), I also investigated whether immune cell recruitment to bone injury was affected by loss of Wnt16. In order to study neutrophil responsiveness to bone injury in zebrafish, fractures were induced in the caudal fins of WT and *wnt16*$^{-/-}$ carrying the *lyzC*:*DsRed* transgene (Table 4). Neutrophil

recruitment was quantified relative to the fracture site over time using modular image analysis (MIA). The number of neutrophils (*lyzc*$^{+}$ cells) within a 100 μm radius and 300 μm radius of the fracture was calculated (Figure 18 A). In both WT and *wnt16*$^{-/-}$ fish, neutrophils were rapidly recruited to the fracture, peaking between 8 and 24 hpi (Figure 18 B). No significant differences in the number of neutrophils recruited to the fracture sites of WT and *wnt16*$^{-/-}$ zebrafish were detected at any time point post-injury (Figure 18 C-D). However, at 8 hpi higher levels of *lyzc*$^{+}$ cells could be observed between 100-300 μm from the fracture in *wnt16*$^{-/-}$ fish (Figure 18 B). Higher mean number of neutrophils were also measured 300 μm from the fracture site at 4 and 8 hpi, though this difference was not statistically significant from WT.

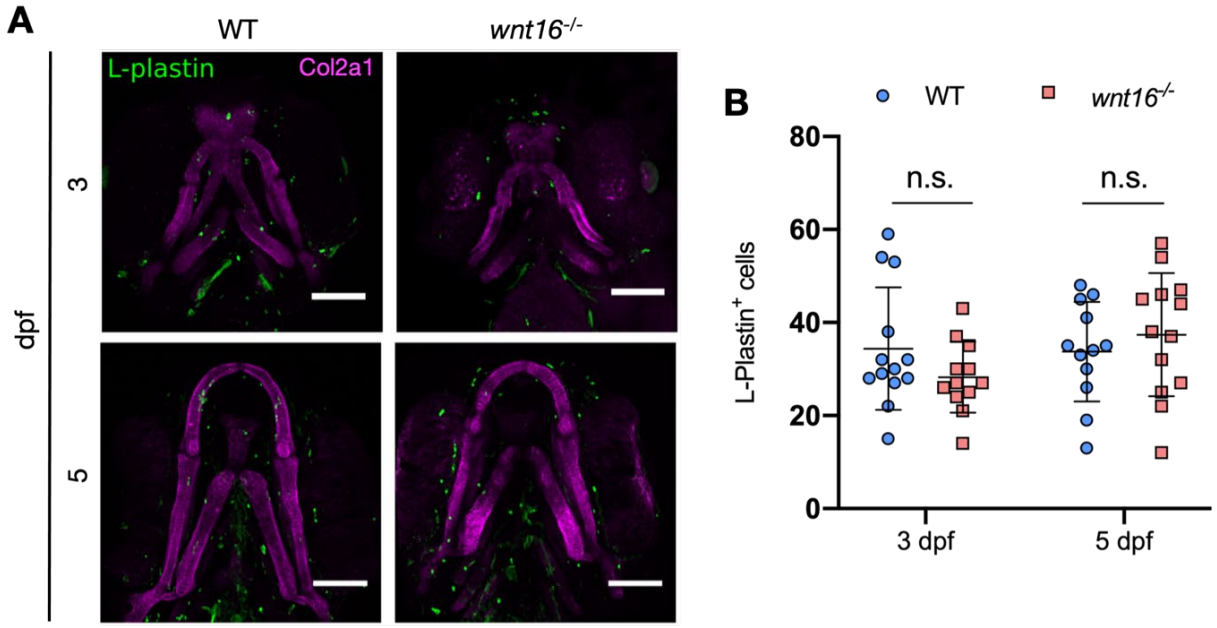

Figure 18. Leukocyte Number Is Not Altered In wnt16$^{-/-}$ Zebrafish Larvae During Early Craniofacial Skeletal Development. *WT and wnt16$^{-/-}$ larval zebrafish were fixed during early skeletal development at 3 and 5 days post fertilization (dpf) for whole mount immunohistochemistry.* ***A:*** *Representative images of each genotype at 5 and 3 dpf show the ventral view of the developing jaw in zebrafish labelled with Col2a1 (cartilage) and L-plastin (pan-leukocyte marker). Scale bar = 200 μm.* ***B:*** *The number of L-plastin^{+} immune cells in the jaw region (A: Col2a1) were quantified per larva. Comparison of WT and wnt16$^{-/-}$ larvae showed no significant difference in immune cell number at either developmental stage. n.s = no significant difference; N≥12 per genotype; points represent mean (± SD). N.B. L-Plastin^{+} cell numbers were quantified by Alistair Vorster (research technician).*

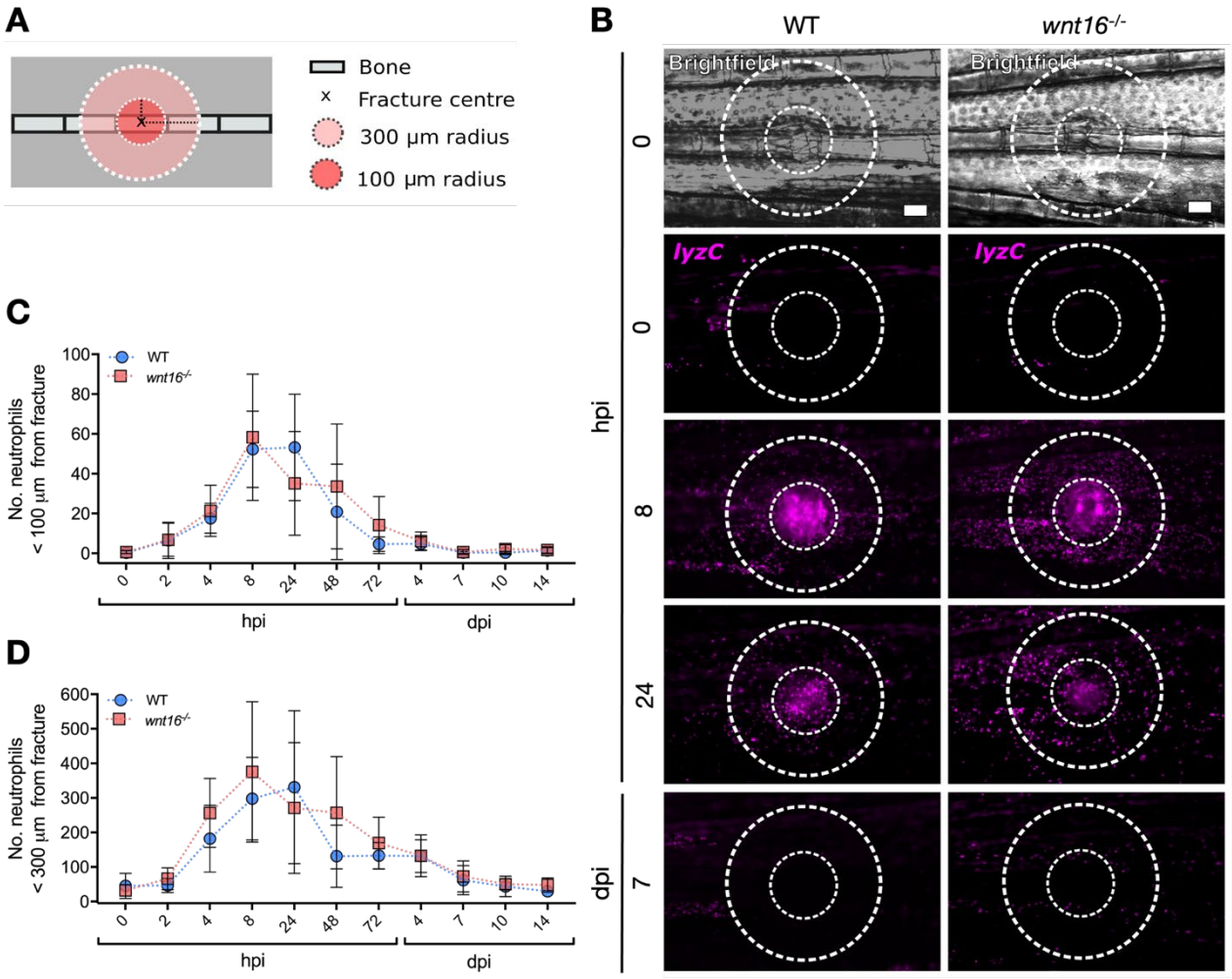

Figure 19. Loss of Wnt16 Does Not Affect Neutrophil Recruitment to Bone Post Fracture. *Lepidotrichia within the caudal fins of WT and wnt16$^{-/-}$ zebrafish carrying the lyzc:DsRed transgene were fractured and imaged at regular intervals from 0-14 days post injury (dpi).* ***A:*** *Schematic depicting 100 µm radius and 300 µm radius regions of interest around the fracture site where neutrophil recruitment was quantified.* ***B:*** *Representative images of fractures from WT and wnt16$^{-/-}$ zebrafish show neutrophil (lyzc^{+} cells) recruitment to fractured bone at 0, 8, and 24 hours postinjury (hpi) and 7 days postinjury (dpi). Scale bar = 100 µm.* ***C-D:*** *The number of neutrophils within 100 µm (C) and 300 µm (D) radii of the fractures were quantified in an automated manner using modular image analysis from 0 hpi to 14 dpi. WT and wnt16 mutants displayed comparable numbers of neutrophils at the fracture site at all time points post injury. N ≥ 5 per genotype; points represent mean (± SD).*

Similarly, fractures were induced in the caudal fins of WT and *wnt16*$^{-/-}$ zebrafish carrying the *mpeg1*:*mCherry* transgene to study the influence of Wnt16 on *mpeg1*-expressing cell dynamics post fracture (including macrophages). The number of *mpeg1*$^{+}$ cells within a 100 μm radius and 300 μm radius of the fracture was calculated (Figure 19 A). Like neutrophils, *mpeg1*$^{+}$ cells were also rapidly recruited to fractures in the first 24 hpi (Figure 19 B). Notably, I observed that *mpeg1*$^{+}$ cells responded to fracture in a biphasic pattern, decreasing in number from 2-4 dpi, before peaking in number for a second time around 7 dpi (Figure 19 C-D). This suggests that phenotypically distinct populations of *mpeg1*$^{+}$ cells may be required at different stages post-fracture to contribute to efficient bone repair. Comparison of between WT and *wnt16*$^{-/-}$ zebrafish showed no significant difference in the number of *mpeg1*$^{+}$ cells recruited to the fracture throughout repair, apart from a significant increase in *mpeg1*$^{+}$ cell number in *wnt16*$^{-/-}$ zebrafish at 8hpi (Figure 19 C-D). Collectively, these data suggest that, overall, leukocyte recruitment to fractures is not impaired in *wnt16* mutants and is unlikely to be the cause of delayed bone repair resulting from loss of Wnt16.

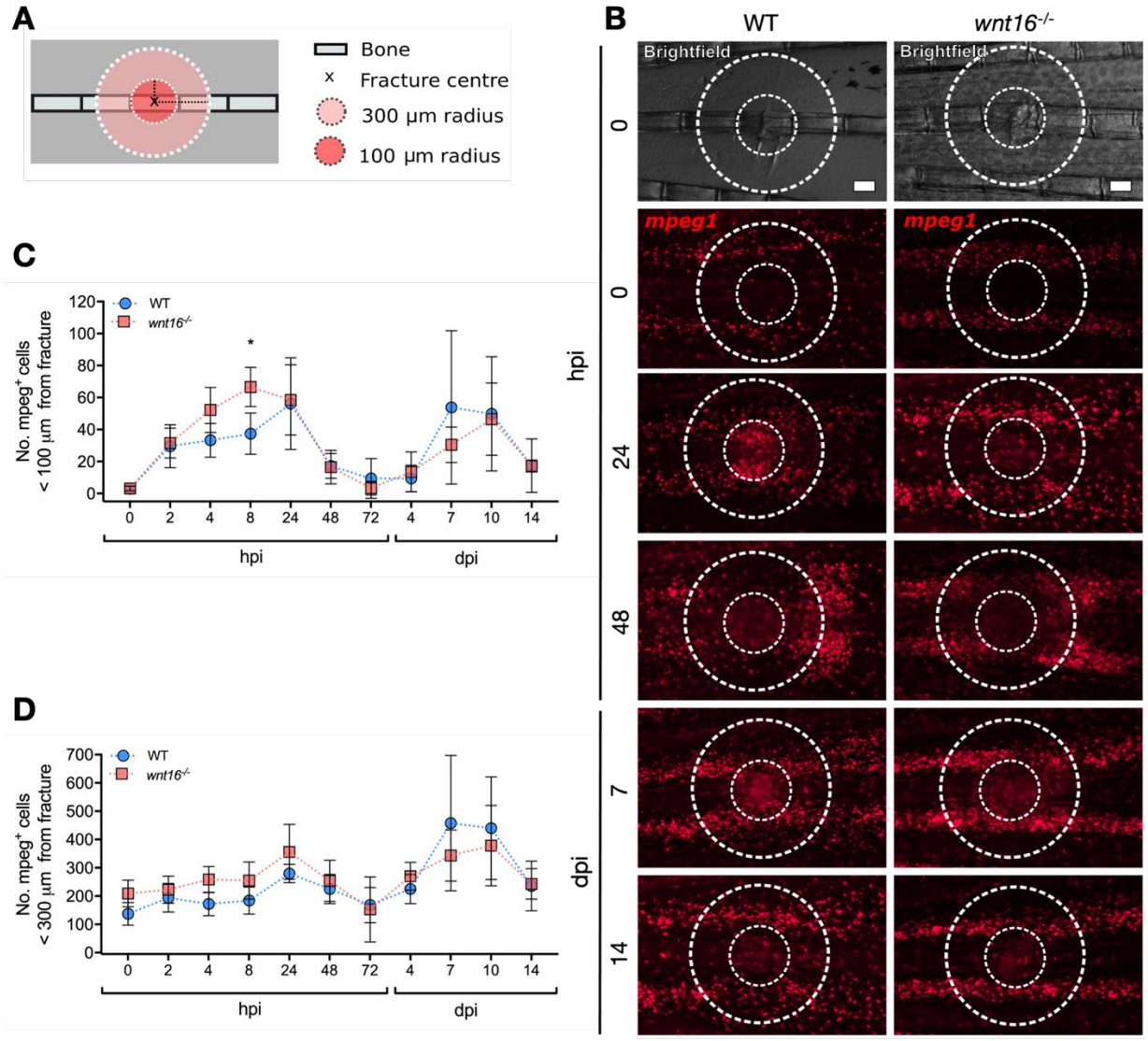

Figure 20. Loss of Wnt16 Does Not Affect mpeg1⁺ Cell Recruitment to Bone Post Fracture. *Lepidotrichia within the caudal fins of WT and wnt16$^{-/-}$ zebrafish carrying the mpeg1:mCherry transgene were fractured and imaged at regular intervals from 0-14 days post injury (dpi).* ***A:*** *Schematic depicting 100 µm radius and 300 µm radius regions of interest around the fracture site where neutrophil recruitment was quantified.* ***B:*** *Representative images of from WT and wnt16$^{-/-}$ zebrafish show mpeg1⁺ cells (including macrophages) recruited to fractured bone at selected time points from 0 to 14 dpi. Scale bar = 100 µm.* ***C-D:*** *The number of mpeg1⁺ cells within 100 µm (C) and 300 µm (D) of the fractures were quantified using modular image analysis from 0 hpi to 14 dpi. WT and wnt16 mutants displayed comparable numbers of mpeg1⁺ cells at all time points post injury, with the exception of 8 hpi, when wnt16 mutants had recruited significantly more mpeg1⁺ cells to within 100 µm of the fracture site (C). *p < 0.05; N ≥ 5 per genotype; points represent mean (± SD).*

3.2.8 TRAP-STAINED PUNCTAE ACCUMULATE CLOSE TO FRACTURE SITES IN *WNT16* MUTANT ZEBRAFISH

Tartrate resistant acid phosphatase (TRAP) is a multi-faceted enzyme, which plays a central role in bone metabolism (304). TRAP-synthesising osteoclasts are required to maintain healthy bone homeostasis via the resorption of damaged bone, but must be regulated to prevent osteoporosis (264). Recombinant WNT16 has been shown to supress osteoclastogenesis and TRAP activity *in vitro* by regulating osteoprotegerin (OPG) expression in osteoblasts (305). The uptake of osteoblast-derived extracellular vesicles by immature osteoclasts has been shown to promote osteoclast differentiation in zebrafish scale fractures, demonstrating that intercellular communication between osteoblasts and osteoclasts regulates osteoclastogenesis in response to bone damage (220). Osteoclasts and macrophages are derived from a common myeloid lineage, with peripheral blood monocytes showing higher osteoclastic potential compared to bone marrow derived monocytes (306). Moreover, a previous study established that cells expressing the osteoclast marker cathepsin K infiltrate the lepidotrichia fracture site where TRAP is detected by 24 hpi in zebrafish (147); this coincides with the recruitment of the initial wave of *mpeg1*-expressing cells to the fracture, observed in this study (Figure 19). Therefore, I investigated whether TRAP activity was associated with the recruitment of *mpeg*$^{+}$ cells post-fracture, and whether loss of Wnt16 affected levels and patterning of TRAP at the fracture site.

Fractures were induced in *mpeg1*:*mCherry*$^{+}$ WT and *wnt16*$^{-/-}$ zebrafish and live-imaged prior to amputation and fixation of the fin for TRAP staining at 0 hpi, 24 hpi, 4 dpi and 7dpi. Overall levels of TRAP activity were measured by calculating percentage area of TRAP^{+} stained tissue within 300 µm radius of the fracture site. TRAP levels increased rapidly at 24 hpi and remained high before gradually decreasing by 7 dpi (Figure 20 A-B). This demonstrates that bone resorption occurs in the early stages of bone repair post fracture, coinciding with delayed bone remineralisation and osteoblast recruitment in *wnt16* mutants (Figure 14 & Figure 16). No significant difference in overall levels of TRAP at the fracture site (TRAP^{+} % area) was detected between WT and *wnt16*$^{-/-}$ fractures (Figure 20 B). However, the overall patterning of TRAP staining was altered at 24 hpi and 4 dpi; *wnt16*$^{-/-}$ zebrafish displayed a significantly higher number of TRAP^{+} punctae around the fracture, whereas WT fractures tended to display fewer punctae, with continuous, diffuse areas of TRAP^{+} tissue (Figure 20 A & C). Comparable patterning of TRAP^{+} punctae was not observed in uninjured bone from either WT *wnt16* mutants. Interestingly, similarities in the patterning of TRAP^{+} punctae and *mpeg1*$^{+}$ cells were observed, with punctae colocalising with *mpeg1*$^{+}$ expression in some regions (Figure 20

A). Collectively, these data suggest that *mpeg1*-expressing cells may contribute to bone remodelling and TRAP-synthesis post fracture, and that dysregulated patterning of TRAP in *wnt16*$^{-/-}$ zebrafish may contribute to delayed bone remineralisation during fracture repair.

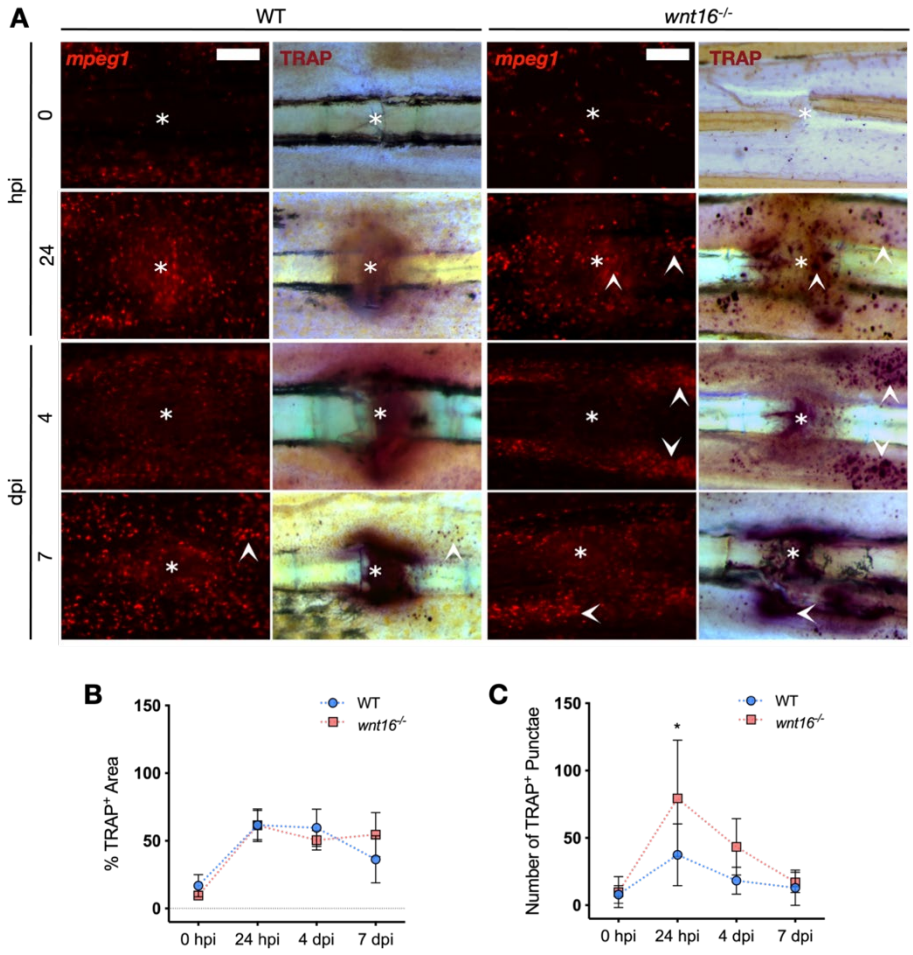

Figure 21. TRAP⁺ Punctae Accumulate Near to Fractures and Regions of mpeg⁺ Cells in wnt16$^{-/-}$ Zebrafish Post Fracture. *Lepidotrichia within the caudal fins of WT and wnt16$^{-/-}$ zebrafish carrying the mpeg1:mCherry transgene were fractured and tissue and imaged before fixing at 0 hours post injury (hpi), 24 hpi, 4 days post injury (dpi) and 7 dpi. Tissue underwent staining to detect the presence of the bone resorptive enzyme, tartrate-resistant acid phosphatase (TRAP).* ***A:*** *Representative images of mpeg1⁺ cells recruited to WT and wnt16$^{-/-}$ fractures and corresponding TRAP-staining in the same tissue at each time point post injury. Regions where TRAP⁺ punctae accumulate coincide with regions where mpeg1⁺ cells accumulate (arrowheads). White asterisk = centre of fracture; Scale bar = 100 µm.* ***B:*** *Overall coverage of TRAP was measured by calculating the total % area stained within a 300 µm^2 region of interest around the fracture site. No significant difference in the percentage area of TRAP⁺*

stained tissue was observed between WT and wnt16$^{-/-}$ fractures. ***C:*** *The number of TRAP^{+} punctae present within a 300µm2 region of interest around the fracture site were quantified. Fractures from wnt16$^{-/-}$ zebrafish showed a significantly higher number of TRAP^{+} punctae at 24 hpi and 4 dpi compared with WT. *p<0.05; N≥6 per genotype; points represent mean (± SD).*

3.2.9 PRECOCIOUS ACTIVATION OF THE CANONICAL WNT SIGNALLING PATHWAY MAY UNDERPIN DELAYED FRACTURE REPAIR IN WNT16 MUTANT ZEBRAFISH

Wnt signalling proteins regulate the stemness, differentiation and proliferation of MSCs and osteoblasts. Moreover, previous studies in mice have indicated that WNT16 may buffer levels of canonical Wnt signalling in response to injury (10). Therefore, I next investigated how loss of Wnt16 affected levels of canonical Wnt activity at the fracture site post injury, using *wnt16$^{-/-}$* and WT zebrafish carrying a β-catenin-responsive transgene (Wnt:GFP (Table 4)); in this transgenic line, cells responding to canonical Wnt pathway signalling fluoresce green. Fractures were induced in the caudal lepidotrichia of the fish and images acquired at regular intervals from 0-14 dpi (Figure 21 A). To quantify changes to canonical Wnt pathway activation at the fracture site throughout repair, the fluorescence intensity of Wnt:GFP was measured relative to uninjured bone (intensity ratio). A significant increase in the intensity ratio of canonical Wnt-responsive cells at the fracture site was observed in *wnt16$^{-/-}$* zebrafish at 2 dpi compared to WT (Figure 21 A-B). Canonical Wnt signalling remained elevated in *wnt16$^{-/-}$* fractures through to 4 dpi, where WT Wnt:GFP intensity ratios became comparable to *wnt16$^{-/-}$* zebrafish fractures. Wnt:GFP intensity ratios then gradually decreased to homeostatic levels, in both groups, by 10 dpi (Figure 21 A-B). This suggests that enhanced canonical Wnt signalling early on post fracture may contribute towards delayed callus formation and osteoblast recruitment during bone repair in *wnt16$^{-/-}$* zebrafish. However, these data indicate that precocious canonical Wnt activation occurs at 2 dpi in *wnt16* mutants, prior to when *wnt16* expression is normally upregulated post-fracture (4 dpi). Hence, it is plausible that loss of Wnt16 influences canonical Wnt activity indirectly, by governing the differentiation of proliferating pre-osteoblasts into osteoblasts.

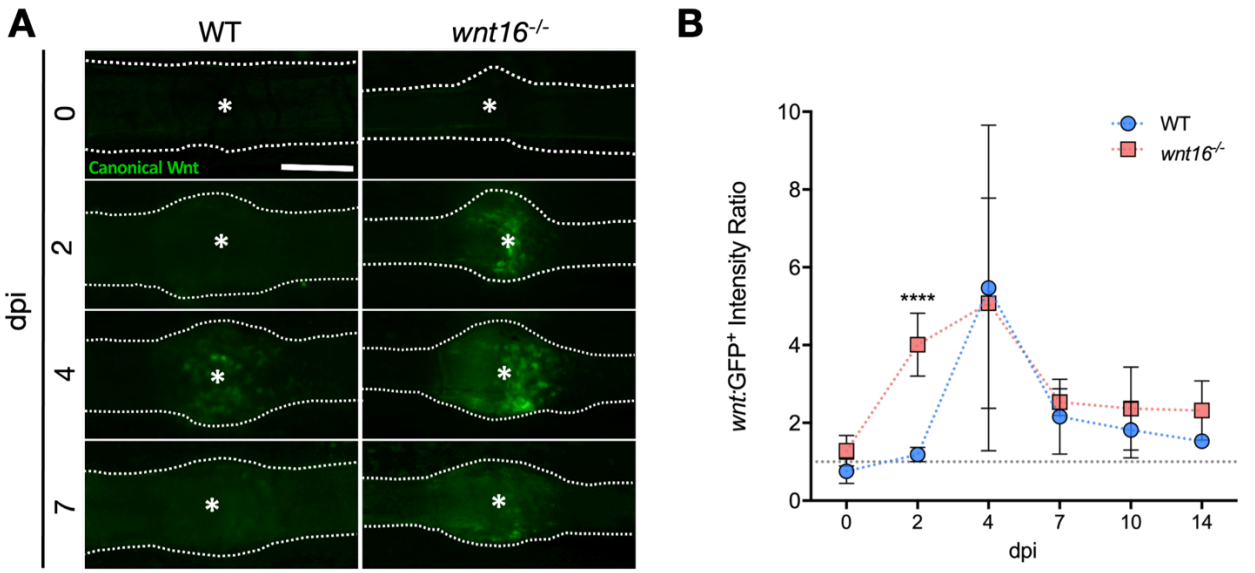

Figure 22. wnt16$^{-/-}$ Zebrafish Display Precocious Activation of The Canonical Wnt Signalling Pathway During Early Fracture Repair. *Lepidotrichia within the caudal fins of WT and wnt16$^{-/-}$ zebrafish carrying the Wnt:GFP transgene were fractured and imaged at regular intervals from 0-14 days post injury (dpi). Wnt:GFP transgenics express GFP in cells where TCF is active, downstream of canonical Wnt signaling.* ***A:*** *Representative images are shown from 0 to 7 days post fracture (dpi). White asterisk = centre of fracture; Scale bar = 200 μm* ***B:*** *Levels of canonical Wnt pathway activation throughout fracture repair were quantified by measuring the fluorescence intensity of Wnt:GFP within the fracture site relative to uninjured bone in the same fin (intensity ratio). Grey dotted line indicates where canonical Wnt activity at the fracture site = uninjured bone. wnt16$^{-/-}$ zebrafish displayed significantly higher levels of canonical Wnt activity at 2 dpi compared with WT fractures. High levels of Wnt:GFP. N ≥ 6 per genotype; points represent mean (± SD).*

3.2.10 PRECOCIOUS CANONICAL WNT SIGNALLING ACTIVITY COINCIDES WITH PREOSTEOBLAST DIFFERENTIATION POST-FRACTURE

Runx2 is a transcription factor which is strongly expressed by osteoblast precursors and is required for the proliferation and differentiation of pre-osteoblasts from MSCs (307). Runx2 directly increases the expression of canonical Wnt pathway target genes such as *tcf7*, whilst reciprocal signalling between canonical Wnt pathway genes and *runx2* induces the commitment of mesenchymal cells into osteoblasts (17). Moreover, the sequential expression of *runx2*, *tcf7, osx*, *osteonectin* and *col1a1* in skeletal elements has been visualised throughout development in larval zebrafish, further suggesting that the dynamic and spatiotemporal control of canonical Wnt target genes is required for normal osteoblast differentiation and bone mineralisation (193). Therefore, due to the close relationship between the canonical Wnt signalling pathway and osteoblast differentiation, I next sought to characterise the spatiotemporal dynamics of *runx2a* expression, relative to canonical Wnt pathway activation and *wnt16* expression during fracture repair in WT zebrafish.

Using RNAscope, whole-mount *in situ* hybridization was performed on uninjured and fractured fin tissue fixed between 2-7dpi. Expression of *runx2a* was quantified by measuring the fluorescence intensity of the probe within a region of interest at the fracture site, relative to uninjured bone in the same fin (intensity ratio). The expression of *runx2a* increased significantly relative to uninjured bone between 2-7 dpi, peaking at 4 dpi (Figure 22 A-B). Interestingly, this peak in *runx2a* expression coincided with the height of canonical Wnt activity and *wnt16* expression within the fracture site post injury, that I had already observed (Figure 21, Figure 13, respectively). This suggests that the cells within the fracture site responding to canonical Wnt pathway activation are likely to be proliferative osteoblast precursors. Indeed, at 7 dpi, as levels of Wnt:GFP decreased, the merged expression of *wnt16*, *runx2a* and Wnt:GFP was observed (Figure 22 C). This suggests that *wnt16* promotes the differentiation of osteoblast progenitor cells into osteoblasts post fracture.

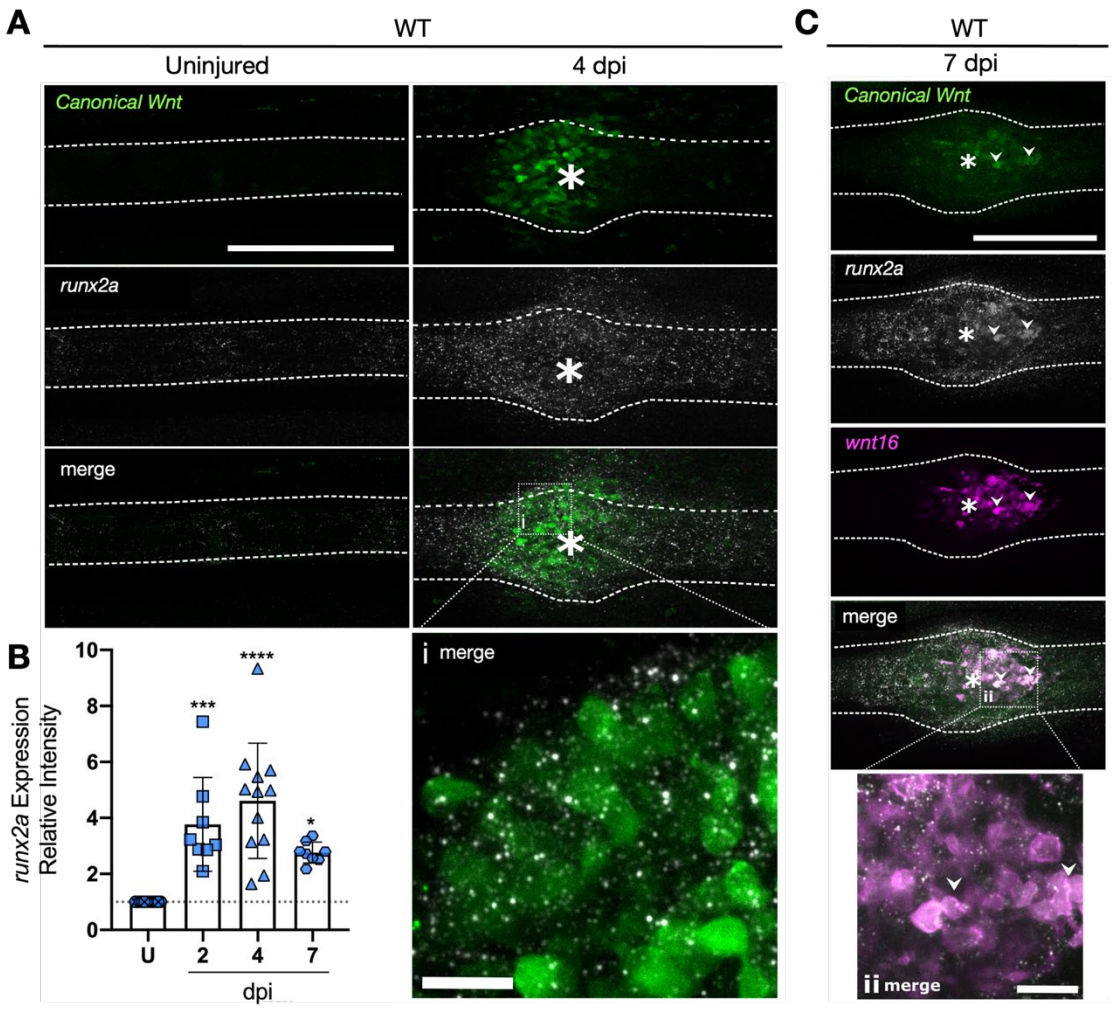

Figure 23. Precocious Activation of The Canonical Wnt Signalling Pathway in wnt16$^{-/-}$ Zebrafish Post Injury Coincides with Preosteoblast Proliferation and Differentiation. *During Fracture Repair. Lepidotrichia within the caudal fins of WT and wnt16$^{-/-}$ zebrafish carrying the Wnt:GFP transgene were fractured and fixed at various intervals from 2-7 days post injury (dpi) for whole-mount RNAScope to label runx2a and wnt16 mRNA in situ, relative to canonical Wnt pathway activation post fracture.* ***A:*** *Representative images of uninjured and 4 dpi bone from WT fins show increased levels of runx2a and Wnt:GFP post-fracture and colocalization within the fracture site.* ***B:*** *Expression of runx2a was quantified by measuring the fluorescence intensity of the runx2a probe within the fracture site relative to uninjured (U) bone in the same fin (intensity ratio). Expression of runx2a increased significantly by 2 dpi, peaking at 4 dpi, before decreasing at 7 dpi. U = Uninjured control, $n \geq 8$ per time point; points represent mean (± SD).* ***C:*** *WT fractures showed the colocalization (ii) of runx2a, wnt16 with low levels of Wnt:GFP, at 7 dpi. ****$p < 0.0001$, ***$p < 0.001$, *$p < 0.05$. Dotted lines = bone outline; white asterisk = centre of fracture; scale bars: main = 200 μm, outsets (i-ii) = 20 μm.*

3.3 DISCUSSION

3.3.1 SUMMARY OF RESULTS

Multiple studies have associated mutations in *WNT16* with osteoporosis and fracture susceptibility phenotypes in mice and humans (103, 263, 296), but no previous study had explored the influence of WNT16 during fracture repair. Moreover, the demand for models to study the influence of GWAS-derived fracture-susceptibility candidate genes on bone dynamically *in vivo* has increased in recent years. In this study, I demonstrated that the caudal fin fracture model in adult zebrafish can serve as a simple but insightful model for the dynamic study of genes associated with skeletal diseases. I used this model to further investigate the role of Wnt16 in the pathophysiology of osteoporosis and sub-optimal fracture repair. Loss of Wnt16 zebrafish leads to variable TMD in the caudal fin and the accumulation of bone calluses within lepidotrichia, resulting from fractures at an early age (Figure 11 and Figure 12); this is comparable with mammalian models, in which loss of WNT16 leads to reduced BMD and increased fracture susceptibility (263). Induction of fractures within caudal fin lepidotrichia of adult zebrafish showed that the expression of *wnt16* is significantly upregulated at the fracture site between 4 and 7 dpi (Figure 13). Wnt16 was also required for timely recruitment and differentiation of osteoblasts and efficient bone remineralisation post fracture (Figure 16 and Figure 14). Alcian blue staining showed that soft callus formation was unperturbed in *wnt16* mutants, as was the development of leukocytes or the responsiveness of neutrophils and macrophages to bone injury (Figures 15, 17,18 and 19, respectively). No significant difference in the overall levels of TRAP were detected in *wnt16*$^{-/-}$ zebrafish compared to WT, at any time point between 0-7 dpi post fracture. However, loss of Wnt16 did alter the patterning of TRAP staining at the fracture site (Figure 20). I demonstrated that delayed fracture repair coincided with precocious activation of the canonical Wnt signalling pathway in *wnt16* mutants at 2 dpi (Figure 21). In WT fractures, elevated expression of *runx2a* and canonical Wnt activity both peaked at 4 dpi, before colocalizing with *wnt16* expressing cells at reduced levels at 7 dpi, suggesting that *wnt16* promotes the optimal differentiation of Wnt:GFP^{+} osteoblast progenitors into mature osteoblasts (Figure 22).

3.3.2 THE ROLE OF WNT16 AND CANONICAL WNT SIGNALLING IN OSTEOBLAST DIFFERENTIATION

Canonical Wnt signalling culminates in the accumulation of β-catenin in the cell which translocates to the nucleus where it binds to and activates the transcription factors, TCF and LEF. In zebrafish, canonical Wnt signalling activity is known to upregulate *osx* expression directly via the Wnt/β-catenin pathway, and via interactions with the FGF pathway, during developmental osteoblastogenesis (16). However, disordered activation of the canonical Wnt signalling pathway has been linked to the pathogeneses of many age-related diseases, including osteoporosis (290). Whilst canonical Wnt signalling is required for osteogenesis, LEF-1 is downregulated in the early stages of fracture repair during soft callus formation (308). Crucially, it has been shown that constitutive β-catenin mediated activation of LEF-1 represses the transcriptional regulator of osteoblast precursors, Runx2, and subsequent maturation of osteoblasts (309). Furthermore, OSX has been shown to negatively regulate canonical Wnt activity during osteoblast differentiation (310). In WT fractures, I observed increased expression of *runx2a* from 2 dpi, continuing to 4 dpi, where both canonical Wnt activity and *runx2a* expression peaked. Colocalization of Wnt:GFP and *runx2* with *wnt16* at 7dpi, as levels of all reduce, implies that *wnt16* promotes the suppression of canonical Wnt activity in pre-osteoblasts and their differentiation into osteoblasts, potentially via regulation of *runx2* and *osx*. WNT16 is known to act on both the canonical and non-canonical signalling pathways. In the absence of Wnt16, levels of canonical Wnt activity were increased at 2 dpi. Functional redundancy between canonical Wnt ligands has been described, suggesting precocious Tcf activation results from dysregulated expression of other canonical Wnt ligands (311, 312). However, further investigation into other Wnt ligands in *wnt16*$^{-/-}$ zebrafish is required. Interestingly, overexpression of canonical Wnt signalling ligands (*WNT3A*, *WNT9A* and *WNT8B*) have been associated with down regulation of *WNT16* and other non-canonical Wnt ligands (311). Morover, WNT16 was found to be protective against excessive activation of canonical WNT and severe cartilage degeneration in a murine model of induced osteoarthritis, suggesting that WNT16 may antagonise canonical Wnt activity post-injury (295). Collectively, this suggests that delayed callus formation post-fracture in *wnt16*$^{-/-}$ zebrafish may be due to precocious and prolonged activation of the canonical Wnt signalling pathway, and that Wnt16 may optimally regulate canonical Wnt activity during fracture repair.

Precocious activation of the canonical Wnt pathway may act to suppress the expression of *runx2a* at 2 dpi, thereby delaying the differentiation of osteoprogenitor cells into mature, bone matrix-synthesizing osteoblasts. However, *wnt16* did not peak until 4 dpi in WT zebrafish. Therefore, the premature increase

in Wnt:GFP^{+} cells at 2 dpi in *wnt16*$^{-/-}$ zebrafish preceded the time point post injury where *wnt16* is normally upregulated. Despite this, low levels of *wnt16* could also be observed in uninjured bone, which may help to suppress canonical Wnt activity in homeostatic bone or during the early stages of fracture repair. Regulation of canonical Wnt activity by *wnt16* may occur either directly, or indirectly via *runx2a* and *osx*, to promote osteoblast maturation. Further studies will be required to establish whether delayed bone repair in *wnt16*$^{-/-}$ zebrafish can be completely or partially rescued via pharmacological modulation of the canonical Wnt signalling pathway, which may be possible using Wnt inhibitor compounds such as IWR-1 (313).

3.3.3 THE ROLE OF WNT16 IN THE INFLAMMATORY RESPONSE TO FRACTURE

Morpholino knockdown of *wnt16* has been shown to result in severe impairment of haematopoiesis in zebrafish embryos (266). However, loss of Wnt16 had no effect on the overall number of leukocytes detected in larvae during early skeletogenesis, nor did it have an overall effect on the recruitment of neutrophils and macrophages (*mpeg1*$^{+}$ cells) post fracture. Evidence has shown that off-target effects of morpholinos during gene knockdown may show more extreme phenotypes compared to stable mutant lines (314). These data demonstrate that targeted, stable mutagenesis of Wnt16 via CRISPR-Cas9 does not impair primitive haematopoiesis, or the innate immune response to bone injury in adult tissues. However, further investigation into HSC line markers is required to conclusively determine whether stable mutagenesis of *wnt16* shows aberrant effects on early haematopoiesis, comparable to those observed in *wnt16* morphants. Moreover, subtle differences in the number of inflammatory cells recruited to fracture could be observed, with higher mean numbers of *lyzc*$^{+}$ and *mpeg1*$^{+}$ cells observed within 300 μm of the fracture site across the first 24 hpi (Figure 18 and Figure 19, respectively). Statistical analysis revealed that only the number of *mpeg1*$^{+}$ cells were significantly higher in *wnt16*$^{-/-}$ zebrafish at 8 hpi compared to WT. However, given the observed difference in the number of immune cells across these early time points, other methods of analysis such as measuring fluorescence intensities of the immune cell reporters around the fracture site, or comparing area under the curve throughout the time course, may reveal subtle differences not detected by comparison between WT and *wnt16* mutants that are not detected by MIA.

One crucial modulator of bone repair that was not explored here is angiogenesis. Vascularization of injured bone is crucial for the metabolically demanding process of fracture repair (315). Clements *et al*., also demonstrated that Wnt16 is required for somatic expression of Notch ligands (266); Notch signalling is a known, central regulator of angiogenesis (316). It is known that ischemia can influence osteoblast

differentiation during fracture repair, with more severe, hypoxic fractures thought to favour the differentiation of MSCs into chondrocytes, rather than osteoblasts (136). Indeed, hypoxic conditions are associated with endochondral ossification post fracture (as opposed to intramembranous ossification), where the formation of a temporary cartilaginous callus precedes the invasion of blood vessels and bone mineralising osteoblasts. It is thought that this may be due to the reduced metabolic demand of chondrocytes compared to osteoblasts (136, 137). As the fracture site becomes revascularised, bone mineralisation transforms the cartilaginous callus to a more stable, hard callus. Therefore, assessing angiogenesis post-fracture using endothelial transgenic lines and measuring the expression of vascular endothelial growth factors may shed further light on the mechanisms underpinning delayed bone repair in wnt16 mutants. However, no existing studies have shown a role for Wnt16 in angiogenesis, suggesting that it is unlikely that vascularization is altered in *wnt16* mutants.

3.3.4 THE ROLE OF WNT16 IN OSTEOCLAST RECRUITMENT AND ACTIVITY POST FRACTURTE

Data from this study further supports the dogma that fracture repair in zebrafish lepidotrichia comprises 3 phases, similarly to mammals (300). The first is an initial inflammatory phase (~4-48 hpi) whereby neutrophils and macrophages infiltrate the fracture. This is proceeded by a repair phase (~2-10 dpi) whereby a glycosaminoglycan-rich soft callus initially forms. Then, osteoprogenitor cells are recruited and differentiate into osteoblasts which synthesise new bone matrix to unionise the fracture with a callus. Ultimately, the bone enters an ongoing remodelling phase (>10 dpi) in which, like humans, the repaired bone remains marked with a calcified callus.

Interestingly, the biphasic recruitment of macrophages post-fracture, which was observed for the first time in zebrafish here, is reminiscent of mammalian bone repair. In mammals, M1-like macrophages are observed during the inflammatory phase and replaced by reparative M2-like macrophages which contribute towards bone matrix synthesis and remodelling of bone (130, 139, 306). The *mpeg1* gene has been widely used as a macrophage-specific promoter in the generation of zebrafish transgenic lines. However, a number of recent studies have provided novel evidence to demonstrate that *mpeg1* expression is not restricted to macrophages in adult zebrafish. One study found a proportion of *mpeg1*$^{+}$ cells to be B cells (249), whereas another identified a population of injury responsive lymphoid cells within *mpeg*$^{+}$ populations (248). Interestingly, I observed the presence of the TRAP^{+} punctae at the fracture site, which

coincided with the recruitment of *mpeg1*$^{+}$ macrophages. Monocytes are known to differentiate into osteoclasts under pro-inflammatory conditions in mammals, whilst WNT16 has been shown to inhibit the differentiation of bone marrow cells into osteoclasts *in vitro* (133, 305). In medaka, Rank-l induction via a heat shock promotor initiates the recruitment of *mpeg*$^{+}$ cells to bone, which then differentiate into osteoclasts (317). Additionally, the number of TRAP^{+} punctae at the fracture site 24 hpi and 4 dpi was significantly higher in *wnt16* mutants compared to WT. Taken together, this data poses the possibility that *mpeg1* is expressed by other HSC-derived lineages such as osteoclasts, the differentiation of which may be regulated by Wnt16. However, this cannot be concluded from the limited data presented here. Therefore, whether distinct sub-populations of macrophages contribute differentially throughout fracture repair, and whether *mpeg1* is expressed by osteoclasts in zebrafish, warrants further investigation.

3.3.5 CONCLUSIONS AND FUTURE DIRECTIONS

In conclusion, these results help to further establish zebrafish as a useful model for studying factors influencing the dynamic behaviour of the multiple cell-types underpinning fracture repair and bone pathologies *in vivo*. In addition, this highlights the utility of the zebrafish as an emerging model for the dynamic study for rapid validation of human osteoporosis-associated genes. By studying the lepidotrichia in the transparent fins of live zebrafish, I visualised bone fragility phenotypes in a novel *wnt16*$^{-/-}$ mutant, as well as the influence of *wnt16* on bone repair in a dynamic, longitudinal manner. Using this model, I found evidence to suggest that the osteoporosis-associated gene *wnt16* elicits a protective effect against fracture susceptibility at a young age. Indeed, since publication, this result has been independently corroborated in another study, where CRISPR-Cas9 was used to create a separate *wnt16* mutant line of zebrafish, resulting in skeletal deformity and reduced bone BMD in young adults (318). More recently, Watson *et al*., used CRISPR-Cas9 to generate zebrafish with stable mutations in either *wnt16* or *cped1* (Cadherin Like And PC-Esterase Domain Containing 1), genes which reside within the same pleiotropic locus in the genome that has been associated with musculoskeletal phenotypes in human GWASs (319). Analysis of *wnt16* and *cped1* zebrafish mutants demonstrated that *WNT16* is likely to be the major gene responsible for the pleiotropic effects of the *CPED-WNT16* locus on bone and lean muscle mass (319). This study further highlights how zebrafish are accelerating our functional understanding of GWAS-derived osteoporosis gene candidates.

Finally, I also demonstrated that Wnt16 promotes bone repair, potentially by buffering levels of canonical Wnt activity and promoting optimal osteoblast differentiation via *runx2a* and *osx*. Collectively, this data strongly supports a pro-osteogenic role for Wnt16 in efficient fracture repair, via the regulation of the canonical Wnt signalling pathway. This highlights modulation of the canonical Wnt pathway, or stimulation of Wnt16, as potential osteo-anabolic candidates for further exploration in osteoporosis and fracture therapy development.

CHAPTER 4: RESULTS SECTION 2

INVESTIGATING THE PRO-REPARATIVE FUNCTIONS OF NEUTROPHILS IN FRACTURE

The data described within this chapter is currently unpublished. However, larval fin resection experiments were carried out in collaboration with an undergraduate MSci student, Mary Appleton (MA), under my training and supervision in the Hammond lab at the University of Bristol. Larval resections were performed by MA and larval time course images collected by MA. Data collected by MA was included in their MSci dissertation (submitted 2020). Any images from those experiments included in this chapter were processed and analysed by me. Any data included within this chapter that were collected in collaboration with MA are clearly indicated as such throughout the text and figure legends. MIA pipelines were written by Dr Stephen Cross from the Wolfson Bioimaging Facility at the University of Bristol (see section 2.16). Unless stated otherwise, data collection, analysis and interpretation included in this chapter were performed solely by me.

4.1 INTRODUCTION

4.1.1 NEUTROPHILS: THE FIRST LINE OF DEFENCE

Neutrophils are polymorphonuclear innate immune cells, which are the most abundant type of leukocyte in the body, and the first line of defence against pathogens. The lifespan of a neutrophil is short, existing only from around 5 hours to 5 days (320). Therefore, constant neutrophil turnover is essential to protect against infection and disease (321, 322). Upon injury or infection, conserved damage associated molecular patterns (DAMPs), or pathogen associated molecular patterns (PAMPs), act as pro-inflammatory triggers, respectively. These signals activate pathogen recognition receptors (PRR) in local epithelial, endothelial and immune cells, as well as systemically via the bloodstream (323, 324). This results in the release of cytokines and chemokines to promote inflammation and recruit neutrophils to the site of damage or infection. Interleukin 8 (IL-8) (also known as CXCL8) is one such chemokine which mediates the chemotaxis of

neutrophils via engagement with the G protein-coupled receptors, C-X-C motif chemokine receptors 1 and 2 (CXCR1/2), on the cell surface (325). Downregulation in the expression of CXCR2 by neutrophils has been linked to their decreased migration, reduced responsiveness to infection and incidence of sepsis in humans (326).

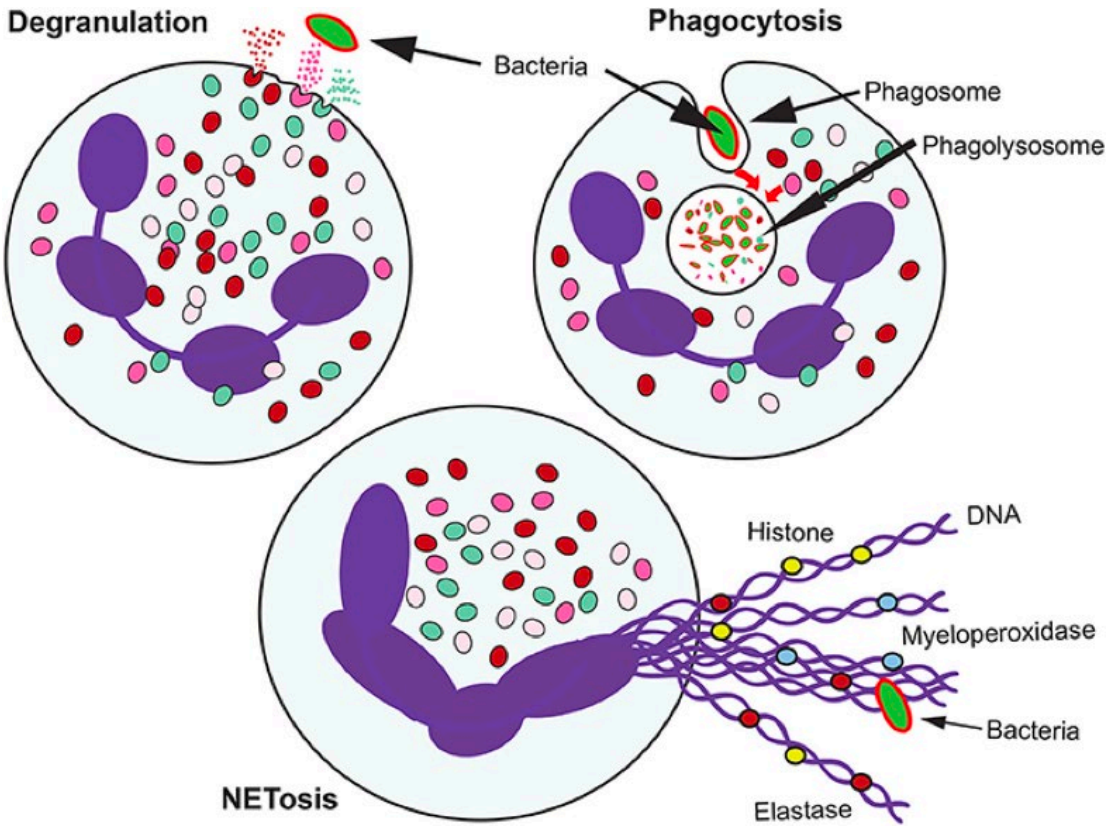

Figure 24. Mechanisms of Neutrophil Function. *Neutrophils release antimicrobial granules which kill pathogens and promote inflammation. Neutrophils engulf pathogens via phagocytosis; a phagosome is formed around bacteria which fuses with lysosomes to become a phagolysosome, where bacteria are destroyed. Neutrophils also release NETs in response to inflammatory stimuli. Chromatin, laced with antimicrobial enzymes, is fired into the extracellular space in a web-like structure which can entangle and kill pathogens. Figure from Rosales, 2018 (327).*

Once at the site of injury or infection, neutrophils elicit their protective effect against pathogens via 3 major mechanisms: degranulation, phagocytosis and Neutrophil Extracellular Trap (NET) release (Figure 23). Mature neutrophils contain granules packed with antimicrobial enzymes such as myeloperoxidase, elastase, defensins and matrix metalloproteinases (MMPs) (327). Upon degranulation, these enzymes are released and kill microbes. Like other phagocytes, such as macrophages, neutrophils can recognise and engulf microbes via phagocytosis. The neutrophil forms a vacuole, termed a phagosome, around the microbe, which then fuses with a lysosome to become a phagolysosome. Proteolytic enzymes within the phagolysosome destroy the microbe (328). Perhaps the most intriguing defence mechanism employed by neutrophils is NETosis; neutrophils are capable of unravelling their chromatin and firing DNA into the extracellular environment as a web-like structure, termed a NET. NETs are laced with antimicrobial enzymes such as neutrophil elastase and myeloperoxidase to entangle and destroy microbes (329). This process can occur via the "suicidal" pathway, resulting in neutrophil cell death, "vital NETosis", where the neutrophil retains some functional viability as an anuclear cytoplast, or "mitochondrial NETosis", where only mitochondrial DNA is released (329). These pro-inflammatory mechanisms are mediated and enhanced by the oxidative burst, a process by which neutrophils generate and release reactive oxygen species (ROS) via the Nicotinamide Adenine Dinucleotide Phosphate (NADPH) oxidase complex (330). Whilst they provide an essential first line of defence against pathogens, the pro-inflammatory activity of neutrophils must be tightly controlled to prevent excessive tissue damage or disease due to chronic inflammation (331, 332). However, sterile tissue injury resulting from blunt trauma or ischemia also induces the recruitment and activity of neutrophils, suggesting that neutrophils possess pro-reparative roles beyond antimicrobial activity and pathogen clearance (331, 333). These alternative functions of neutrophils require further study, given the high degree of interest in targeting neutrophils with therapies to treat chronic inflammatory diseases.

4.1.2 NEUTROPHILS AS MEDIATORS OF DISEASE

Dysregulated neutrophils have been implicated in the pathogeneses of many diseases including cancer (334), severe COVID-19 (335), inflammatory bowel disease (166), arthritis (332) and osteoporosis (80). Inhibition of CXCR2 has been shown to supress neutrophil recruitment and disease severity in a murine model of inflammatory induced arthritis (336). Moreover, inhibition of NETosis or degradation of NETs has been proven to be beneficial in wound healing and scar resolution in mice (337). Understandably, an

increasing number of therapies to modulate or reprogramme neutrophils are being investigated for the treatment of chronic inflammatory diseases (338). However, given the central role of neutrophils in initiating inflammation, and their potential pro-regenerative properties, further characterisation of the role of neutrophils in tissue repair is required to ensure treatment suitability for patients. Moreover, this may uncover previously unknown functions of neutrophils and reveal new targets for improving tissue repair and regeneration.

4.1.3 NEUTROPHILS IN BONE INJURY AND REPAIR: FRIEND OR FOE?

Controlled neutrophil-mediated inflammation is required to initiate bone repair and prevent infection post-injury, but without rapid resolution of neutrophil effector mechanisms, efficient tissue repair cannot proceed. As detailed in section 1.2.2, fracture healing comprises 3 phases: inflammation, repair and remodelling (134). Like with other forms of tissue damage, neutrophils are the first immune cells to be recruited to bone post fracture, mobilising within minutes of the injury. The antimicrobial activity of neutrophils prevents infection within the fracture, whilst they also release cytokines and growth factors, which drive controlled inflammation and trigger repair processes (339). Hyper-inflammation is known to impair fracture healing; high numbers of neutrophils can inhibit bone matrix mineralization *in vitro* (340). *In vivo*, this may be caused by existing comorbidities, such as diabetes (341), or infection within the fracture (126). Bacterial infection in a zebrafish caudal fin fracture model resulted in increased neutrophil recruitment to injury, with neutrophils retained at the fracture for several days compared to uninfected fractures; this resulted in failure to repair bone, likely due to hyperinflammation (147). Interestingly, increased peripheral neutrophil counts have been associated with decreasing bone density in ageing populations (342, 343). Increased neutrophil to leukocyte ratio (NLR) in peripheral blood is predictive of more severe fracture trauma and mortality within one year of hip fracture in elderly patients with osteoporosis (344, 345). Moreover, bisphosphonates, used to treat osteoporosis, have been shown to depress neutrophil chemotaxis and NADPH oxidase activity in mice, which may contribute to bisphosphonate-related osteonecrosis of the jaw (BRONJ) (346). Similar effects on neutrophils have been reported in humans undergoing bisphosphonate therapy, suggesting that reduced neutrophil function may be a useful biomarker for the development of BRONJ (347). Whilst the pro-inflammatory roles of neutrophils have been studied extensively, far less is known about their potential roles in tissue repair and

regeneration. However, our view of neutrophils is evolving, with increasing evidence emerging to support diverse, pro-regenerative roles for neutrophils in tissue repair, including in fracture healing (333).

Knockout of the CXCR2 homolog in mice (*mCXCR*$^{-/-}$) lead to a bone fragility phenotype due to decreased BMD, bone mass and thickness, in both cortical and trabecular bones (348). Mutant *mCXCR*$^{-/-}$ mice also showed reduced bone ingrowth in response to a cranial trepanation injury, when compared to wild type littermates. However, bone histomorphometry of the injury showed no difference in either osteoblast or osteoclast activity markers. This suggests that CXCR2 may regulate bone development and repair via other cell types. One possible contributor to CXCR2 mediated bone homeostasis and repair is neutrophils, given that CXCR2 plays a central role in neutrophil recruitment and activity.

Indeed, it has been shown that depletion of neutrophils prior to injury leads to impaired fracture repair in mice (268). Moreover, transplantation of fracture haematomas enriched with inflammatory cells has been shown to promote ectopic bone formation, highlighting the inherent osteogenic potential of this tissue (349). Strikingly, neutrophils recruited to human fracture hematomas have been reported to synthesise a fibronectin-rich emergency extracellular matrix (ECM), proposed to assist in stabilising the bone, prior to osteoblast-mediated repair (267). Interestingly, NETs can remodel laminin within the ECM and facilitate integrin-mediated cell adhesion and proliferation (350, 351); these properties facilitate cancer growth and metastasis. However, given that cancer mirrors many of the molecular hallmarks of wound healing (352), these properties may also facilitate healthy tissue repair. Moreover, anti-inflammatory properties for NETs have been described; under high neutrophil densities, NETs aggregate and are able to degrade pro-inflammatory chemokines and cytokines, helping to resolve inflammation by preventing further neutrophil recruitment (353). Despite these intriguing findings, the potential pro-reparative functions of neutrophils in fracture healing have not been explored further and warrant proper investigation. Current evidence suggests that neutrophils may facilitate bone repair by stabilising fractures, supporting the infiltration of other cells required for bone repair within the fracture haematoma, or by aiding in the resolution of inflammation. Studies utilising *in vivo* models which allow for dynamic, live imaging of bone repair are required to further elucidate the mechanisms by which neutrophils contribute positively to fracture healing.

4.1.4 ZEBRAFISH AS A MODEL FOR STUDYING NEUTROPHIL BIOLOGY

Over the past two decades, zebrafish have been established as a key model organism for the study of inflammation in health and disease (231). In particular, the study of the zebrafish innate immune system has provided many novel insights into neutrophil biology (203). Much of this research was made possible by the pioneering work of Renshaw *et al.*, and Mathias *et al.*, whereby neutrophil specific reporter transgenic lines were created (242, 243); expression of GFP under the myeloperoxidase (*mpx*) promoter allowed for live visualisation and dynamic imaging of neutrophils in zebrafish for the first time. Use of these lines, in hundreds of studies since their creation, has revealed novel behaviours of neutrophils in response to injury or infection (354).

In zebrafish, haematopoiesis occurs initially via a "primitive" wave, beginning at around 12 hours post fertilisation (hpf). From this, functional neutrophils and macrophages begin emerging by 30 hpf (203). Primitive haematopoiesis is then followed by a "definitive" wave, in which pools of self-renewing hematopoietic stem cells (HSCs) are generated; these HSCs are responsible for maintaining the supply of myeloid, lymphoid and erythroid cells throughout adulthood (204). In mammals and birds, neutrophils are constantly produced under homeostatic conditions by the bone marrow and released into the circulation, where they survive for between 5 hours and 5 days (320, 321). In contrast, adult zebrafish lack bone marrow; neutrophils are produced by the caudal hematopoietic tissue (CHT) in larvae, and subsequently by the kidney marrow as they mature (355). The half-life of tissue neutrophils in zebrafish larvae is thought to be around 5 days (356); whether this is maintained in adult zebrafish or reflective of mammalian tissue neutrophils is unclear, due to limited accessibility to adult tissue *in vivo*. Despite some differences in their developmental origin, zebrafish neutrophils bear striking resemblance to human neutrophils, both in their cellular physiology and function (357).

Neutrophils are rapidly recruited to bone damage in larval and adult zebrafish, in either sterile osteoblast ablation or induced traumatic bone injury models (2, 147, 234). Like in humans, Cxcl8 (IL-8) mediates the chemotaxis of neutrophils to sites of inflammation via Cxcr2 (358); knockdown of *cxcr2* has been shown to reduce entry of neutrophils into the circulation in response to injury (235). Moreover, pharmacological inhibition of Cxcr2 has been shown to significantly reduce neutrophil recruitment to larval fin resection wounds (359).

Mature zebrafish neutrophils express *mpx* and *lyz* (lysozyme C) (242, 244); these encode enzymes which promote inflammation and facilitate microbial clearance. Infection models using zebrafish have

demonstrated that their neutrophils can engulf bacteria or dying cells via phagocytosis (354). Recently, a benzochalcone fluorescent probe (HAB) was developed for use in live zebrafish; this allows for imaging of neutrophil granule dynamics within the cell and in response to phagocytosis (360). Moreover, ROS production can be imaged within transparent zebrafish tissues *in vivo* via labelling with live-dyes (361, 362). Whilst some studies have described NETosis in zebrafish (363, 364), whether teleost neutrophils are able to form true NETs has been debated. Recently, chromatin release from pioneer neutrophils recruited to wounds was visualised in a novel transgenic line, in which neutrophil histone 2 A (H2A) was tagged with mCherry (232). Neutrophils were also shown to release extracellular DNA in response to stimulation with known chemical and microbial NET inducers *in vitro*. This study provided definitive evidence of chromatin release from zebrafish neutrophils *in vivo* and strong evidence suggests that zebrafish neutrophils are capable of NETosis that is comparable to mammals. Collectively, this demonstrates the utility of zebrafish as a model for studying impaired neutrophil responsiveness and function during fracture repair *in vivo*.

4.1.5 EXPERIMENTAL AIMS: INVESTIGATING PRO-REPARATIVE FUNCTIONS OF NEUTROPHILS IN FRACTURE

Dynamic *in vivo* studies investigating the pro-reparative properties of neutrophils in fracture stabilisation and repair are lacking. The zebrafish caudal fin fracture model provides an excellent platform to address this. Therefore, in this chapter, I aimed to:

4. Establish whether neutrophils recruited to fracture in zebrafish synthesise or remodel ECM.
5. Determine whether chromatin release from neutrophils (indicative of NET production) occurs post fracture in zebrafish
6. Investigate the effect of Cxcr2 inhibition on neutrophil recruitment to fracture and subsequent effects on bone repair.

4.2 RESULTS: PRO-REPARATIVE PROPERTIES OF NEUTROPHILS IN FRACTURE

4.2.1 NEUTROPHILS RAPIDLY ACCUMULATE WITHIN CAUDAL FIN FRACTURES

As described in sections 1.2.2 and 3.2.7, neutrophils are the first cells to respond to fracture. In order to establish the window of time in which neutrophils are present at the fracture site post injury, I reanalysed time course data from WT *lyzC*:DsRed zebrafish (section 3.2.7, Figure 18), to measure neutrophil recruitment to induced caudal fin fracture between 0 hpi and 14 dpi. The number of *lyzC*$^{+}$ cells within 100 or 300 μm of the injury was measured automatically using MIA (Figure 24 A). A significant increase in the number of *lyzC*$^{+}$ cells were recorded at the fracture site from 4 – 24 hpi, compared to the same region within bone immediately after injury, peaking between 8-24 hpi (Figure 24 B-D). This number remained significantly higher within 100 μm of the fracture site until 48 hpi before reducing to homeostatic levels (Figure 24 D). This determined that neutrophils migrate towards fracture within 4 hours of injury in zebrafish, and peak in number between 8-24 hpi, declining again by 48 hpi. Therefore, 0-48 hpi was established as the window of time in which to investigate potential pro-reparative functions of neutrophils in the zebrafish caudal fin fracture model. However, given that *lyzC* has been reported to be expressed by other myeloid cells in addition to neutrophils (244), the remaining experiments were performed in *mpx*:GFP zebrafish (242) (Table 4). A previous study of zebrafish caudal fin fracture using this transgenic line mirrored the timescale of neutrophil recruitment to fracture shown in Figure 24 (147). Therefore, the 0-48 hpi imaging window determined here remains applicable for *mpx*:GFP zebrafish.

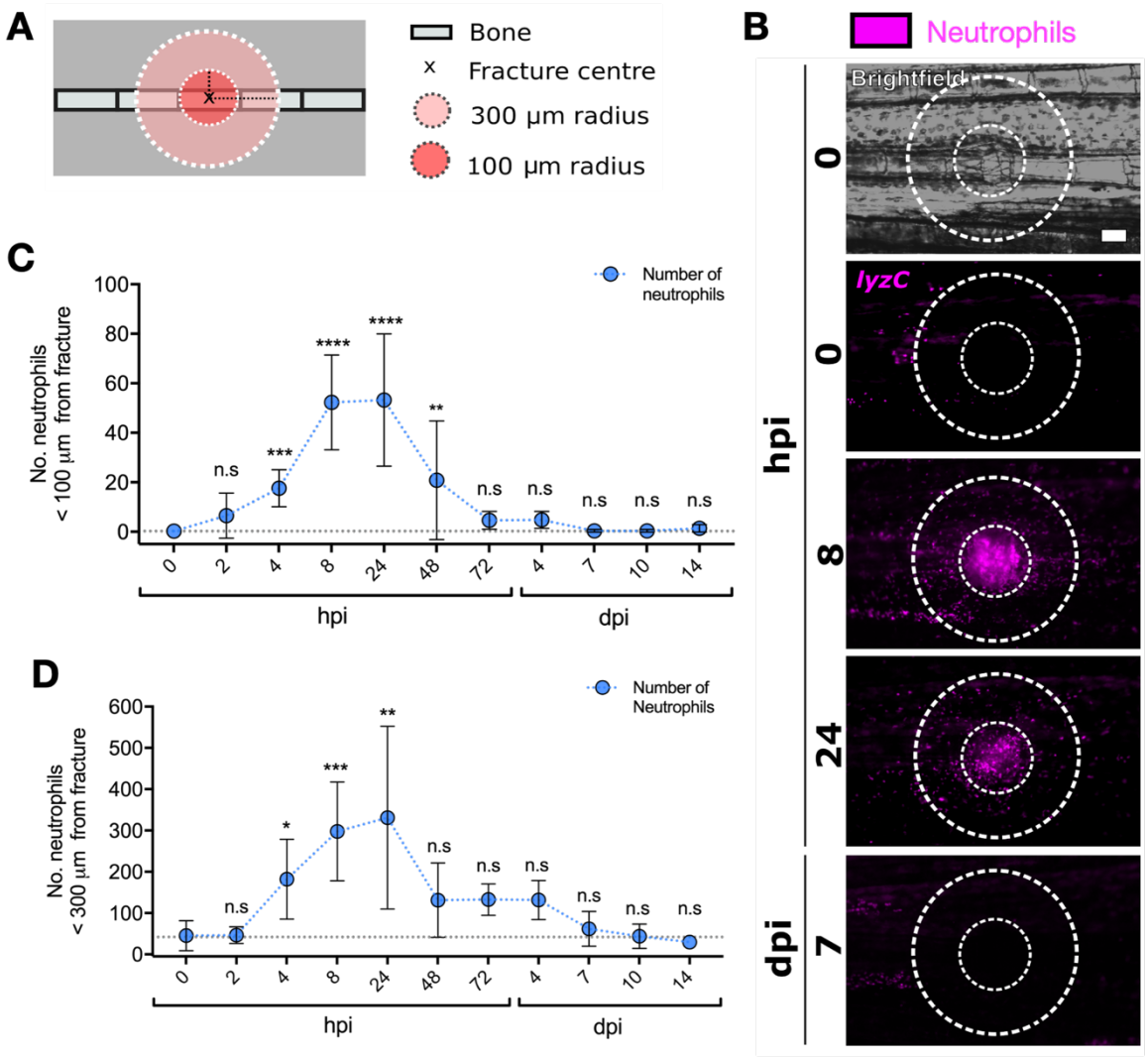

Figure 25. Neutrophils Are Rapidly Recruited to Bone Post Fracture in Zebrafish, Resolving By 72 Hours Post Injury (hpi). A: *Schematic depicts regions of interest around the fracture site where DsRed⁺ cell recruitment was imaged (B) and quantified (C-D) post fracture.* ***B:*** *Stereomicroscope images taken from the same transgenic (lyzC:DsRed) neutrophil reporter zebrafish throughout fracture repair show that neutrophils are rapidly recruited to bone post fracture and tightly pack together at the injury site. Scale bar = 100 µm.* ***C-D:*** *The number of neutrophils within 100 µm (C) and 300 µm radii of the centre of the fracture site were quantified throughout repair. The number of neutrophils recruited to the injury significantly increased between 4 hpi and 24 hpi (C), or 4 hpi and 72 hpi (D), when compared to baseline numbers of neutrophils at 0 hpi (dotted line) using a Kruskal-Wallis Test. dpi = days post injury. N ≥ 5; points represent mean (± SD). * = p < 0.05, ** = p < 0.01 *** = p < 0.001, **** = p < 0.001, ns = no significant difference (p > 0.05). Figure adapted from wild type data (section 3.2.7, Figure 18) and analysed for differences over time.*

4.2.2 NEUTROPHILS RECRUITED TO FRACTURE CONTAIN ECM PROTEINS, LAMININ AND FIBRONECTIN

The ECM environment plays a crucial role in bone repair. Laminins are a complex family of high molecular weight proteins which form a major component of the ECM and have been shown to support tissue repair by promoting cell migration and vascularisation (365). Recently, incorporation of a functional laminin α4 derived peptide into a decalcified bone matrix scaffold was shown to promote the adhesion of MSCs and their differentiation into osteoblasts (366). The laminin α4 enriched scaffold was shown to promote angiogenic differentiation via HIF-1α, highlighting the potential role of laminins in efficient bone repair. Another major component of the ECM is fibronectin. Fibronectin is a heavily conserved glycoprotein which has been shown to facilitate fracture repair by forming a 3 dimensional scaffold on which cells can migrate, and by allowing the incorporation of other ECM components, such as laminin (367). One study reported that neutrophils recruited to fracture haematomas, isolated from humans, contain fibronectin, and proposed that these neutrophils synthesise an emergency scaffold of ECM to stabilise the damaged bone and support the infiltration of stromal cells, which facilitate the latter stages of bone repair (267). However, this has not been studied in more depth. Therefore, I next investigated whether neutrophils recruited to bone injury in the zebrafish caudal fin fracture model contained ECM proteins.

Given that a high number of neutrophils infiltrate the fracture by 4 hpi, peaking in number between 8-24 hpi (Figure 24), I next investigated whether these neutrophils stained positive for the ECM proteins, laminin and fibronectin. Caudal fin fractures were performed on adult *mpx*:*GFP* zebrafish. Fractured caudal fin tissue was amputated at either 4, 8 or 24 hpi and fixed. Immunohistochemistry was performed to label anti-*mpx:GFP*, laminin and fibronectin (Figure 25). Few neutrophils could be observed in uninjured bone tissue; those that were, had rounded morphology and did not contain either fibronectin or laminin (Figure 25). Little fibronectin or laminin was detected within uninjured bone tissue. Laminin staining appeared to be restricted to blood vessels in uninjured fin tissue. As expected, at 4 hpi, an increase in anti-*mpx:*GFP staining was observed as neutrophils were recruited to fracture (Figure 25). Many of these neutrophils stained positive for both fibronectin and laminin, which appeared to be contained within the *mpx:*GFP^{+} cells. By 8 hpi, as neutrophils peaked in number, a further increase in the amount of *mpx:*GFP staining was observed. However, the distribution of this staining had changed. Some *mpx:*GFP^{+} cells retained their round morphology, whilst other regions within the fracture showed larger, more diffuse regions of *mpx:*GFP staining. Smaller, rounder *mpx:*GFP^{+} cells stained positive for fibronectin and laminin (Figure 25, white

arrowheads), whereas the more diffuse areas of *mpx:GFP* colocalised with laminin, but not fibronectin. By 24 hpi, neutrophils still present at the fracture site displayed round morphology, similar to those observed at 4 hpi. Some neutrophils stained positive for fibronectin and laminin at 24 hpi, though levels of these ECM proteins had decreased compared to earlier time points. Moreover, diffuse areas of *mpx:*GFP staining, observed at 8 hpi, were no longer present at 24 hpi. Collectively, these data demonstrate that neutrophils rapidly recruited to fracture in zebrafish contain the ECM proteins, laminin and fibronectin. This suggests that neutrophils support early bone repair, either by rapidly synthesising ECM components, or by remodelling the ECM. Moreover, the diffuse, spindle like distribution of *mpx:*GFP staining observed at 8 hpi was reminiscent of NET morphology. Therefore, I next investigated whether NET release occurs post fracture in zebrafish.

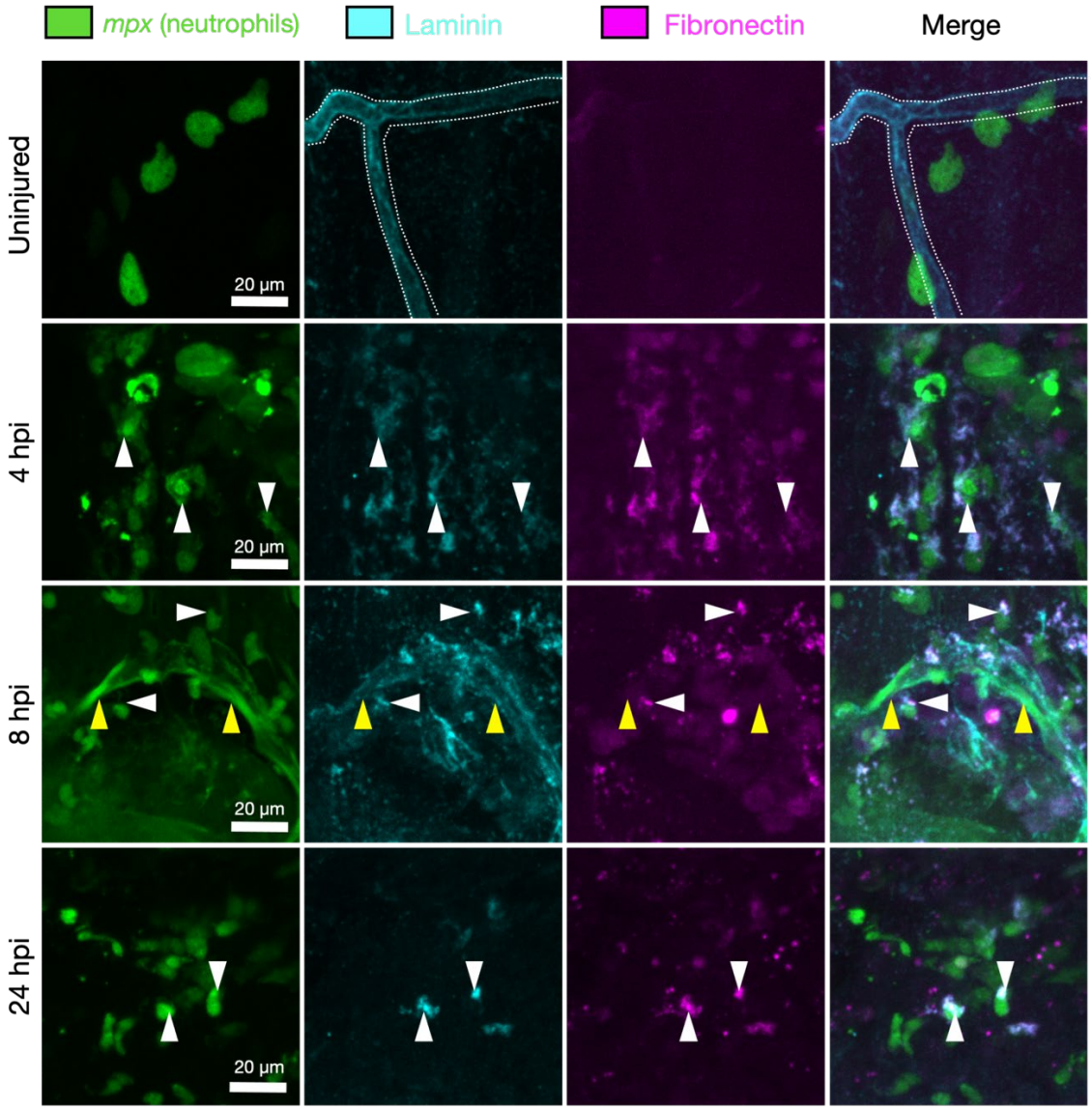

Figure 26. Neutrophils Recruited to Fracture Stain Positive for Laminin and Fibronectin and May Release Neutrophil Extracellular Traps (NETs). *Fractures were induced in the caudal fins of mpx:GFP zebrafish, harvested and fixed at 4 hours post injury (hpi), 8 hpi and 24 hpi for immunohistochemistry, and compared to uninjured (control) fins. Laminin staining appeared to be restricted to blood vessels in uninjured fin tissue (outline), with low levels of mpx⁺ cells and fibronectin observed. Neutrophils colocalise with laminin and fibronectin (white arrowheads), suggesting that neutrophils within the fracture synthesise these extracellular matrix proteins, which may promote fracture repair. At 8 hpi, mpx:GFP⁺ spindle shaped structures, which are morphologically characteristic of NETs, were also observed (yellow arrowheads). These NET-like structures colocalised with laminin. Scale bar = 20 µm. Images are representative of 2 independent repeat experiments where N ≥ 3 per time point.*

4.2.3 NEUTROPHILS RELEASE CHROMATIN WITHIN FRACTURES WHICH COLOCALISES WITH LAMININ IN ZEBRAFISH

NETs are known to remodel laminin within the ECM to promote cell adhesion and proliferation (350, 351). This suggests that NETs may facilitate early bone repair mechanisms via interactions with the ECM. I observed diffuse areas of anti-*mpx:*GFP^{+} staining, after the recruitment of neutrophils to fracture. However, this is not evidence of NET release and could represent apoptosis of neutrophils at the fracture site. Therefore, I next employed the use of a novel transgenic line of zebrafish (*mpx:GFP;lyz:H2A-mCherry*, Table 4), in which the chromatin of neutrophils is labelled with mCherry (232). This line allows for the live visualisation of neutrophil chromatin release, a hallmark of NET production. Fractures were induced in the caudal fins of *mpx:GFP;lyz:H2A-mCherry* zebrafish, and imaged at regular time points between 0 and 48 hpi (Figure 26 A). At 0 hpi, few *mpx:*GFP^{+} neutrophils can be observed around the injury. Bright *H2A*-mCherry^{+} punctae can be observed within *mpx:*GFP^{+} neutrophils. Some *lyz:H2A*-mCherry^{+} punctae do not appear to colocalise with *mpx:*GFP; however, this is likely an artefact of live imaging of these motile cells, or minor tissue movement in the live zebrafish. At 8 hpi, a peak in the levels of *mpx:*GFP can be observed; interestingly, at this time point, *lyz:H2A*-mCherry labelling appears as a more diffuse mass, with some bright punctae present. The *lyz:H2A*-mCherry colocalised with *mpx:*GFP labelling, which also appeared more diffuse. The fluorescence intensities of *mpx:*GFP (Figure 26 B) and *lyz:H2A*-mCherry (Figure 26 A) were measured relative to uninjured bone in the same fin (intensity ratio), at each of the time points imaged post fracture. As expected, levels of *mpx:*GFP and *lyz:H2A*-mCherry at the fracture site rose significantly at 4 hpi, before peaking at 8 hpi. Levels of *lyz:H2A*-mCherry remained significantly higher at 24 hpi compared to 0 hpi, whilst the intensity ratio of *mpx:*GFP had decreased (Figure 26 B-C). Colocalisation analysis of *mpx:*GFP and *lyz:H2A*-mCherry channels was performed to give a Pearson's correlation coefficient for each time point post injury. The Pearson's coefficient indicates the degree of colocalization between pixels, with 0 representing a stochastic relationship between pixels, and 1 representing complete colocalization of pixels. The heatmap in Figure 26 D illustrates the Pearson's coefficient for each injury throughout early fracture repair and shows that colocalization between *mpx:*GFP and *lyz:H2A*-mCherry increases post fracture; this increase is statistically significant at 8 hpi, before gradually declining again. This demonstrates that neutrophils release chromatin into the extracellular environment post fracture in zebrafish.

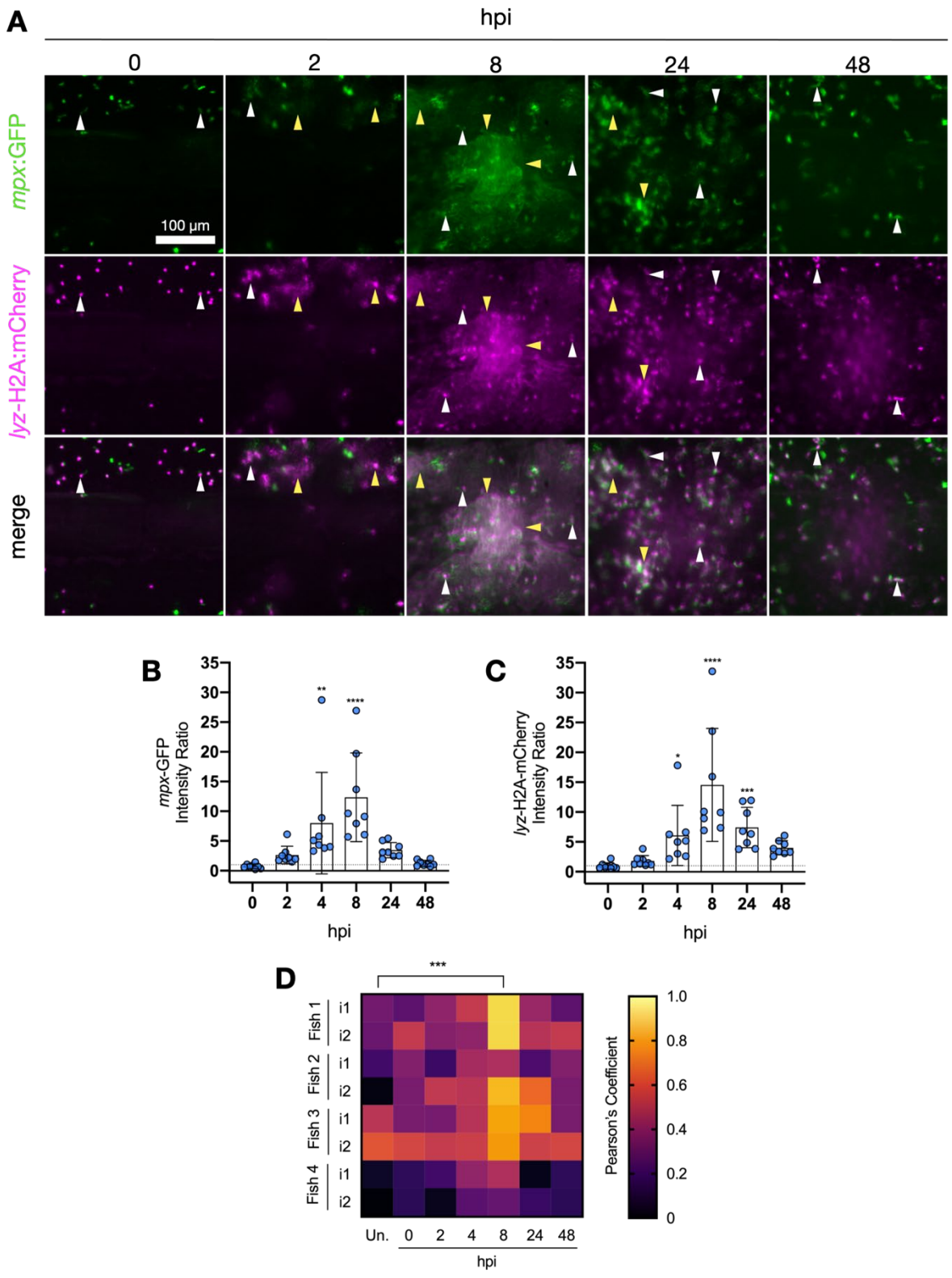

Figure 27. Neutrophils Recruited To Fracture Release Chromatin Which Colocalises With mpx:GFP.

Fractures were induced in the caudal fins of mpx:GFP;lyz-H2A:mCherry zebrafish (in which neutrophil

chromatin is labelled with mCherry) and imaged at time points from 0-48 hpi (hours post-injury). ***A:*** *Representative images of a single fracture at selected time-points throughout the time course are shown. An increase in mpx:GFP and lyz-H2A:mcherry signal can be observed at the fracture site at 8 hpi. Morphology of lyz-H2A:mcherry signal changes from distinct punctae at 0 hpi (white arrowheads), to more diffuse signal at 8 hpi (yellow arrowheads), indicating chromatin release from neutrophils.* ***B-C:*** *The intensity ratio for mpx:GFP (B) and lyz-H2A:mcherry (C) was measured relative to uninjured bone at each time point and plotted. Points represent mean (± SD).* ***B:*** *A significant increase in mpx:GFP intensity ratios at 4-8 hpi compared to 0 hpi.* ***C:*** *Similarly, lyz-H2A:mcherry intensity ratios increased significantly compred to 0 hpi from 4 hpi, but remained significantly higher at 24 hpi. Centre of image = centre of fracture. Scale bar = 100 μm.* ***D:*** *Colocalisation analysis was performed using the JACoP plugin in FIJI to measure colocalization between mpx:GFP and lyz-H2A:mCherry signals at each time point post injury. Pearson's colocalisation coefficient of 0 indicates no correlation, whereas 1 indicates complete colocalization between signals. A significant increase in colocalization can be onbserved at 8 hpi compared to uninjured bone in the same fish, suggesting NET production occurs post-fracture. N ≥ 6 fractures. * = p < 0.05, ** = p < 0.01 *** = p < 0.001, **** = p < 0.001.*

Though repeat, live time course images acquired on a stereomicroscope provides insightful data on the same fracture post injury, the resolution of these images is limited. Therefore, I next performed caudal fin fractures on *mpx:GFP;lyz:H2A-mCherry* zebrafish and fixed them at 8 and 24 hpi, when chromatin release from neutrophils was observed (Figure 27). A range of representative images of uninjured and fractured bone immunostained for DAPI, anti-GFP, anti-mCherry and laminin are presented in Figure 27. Consistent with data previously shown (Figure 25), there were few, round *mpx:*GFP^{+}*;lyz:H2A*-mCherry^{+} cells present in uninjured bone tissue, with laminin mainly restricted to the vasculature. However, at 8 hpi, levels of *mpx*:GFP, *lyz:H2A*-mCherry and laminin all increased. Strikingly, the morphology of neutrophil-derived chromatin changed to appear more web-like in structure and covered larger areas than expected by an intact nucleus. Anti-*lyz:H2A-mCherry* staining also colocalised with DAPI, demonstrating that these structures do represent extracellular DNA. Whilst much of the *lyz:H2A:*mCherry^{+} labelled chromatin colocalised with *mpx:*GFP, some of the larger, web-like structures did not. Interestingly, some regions where *lyz:H2A*-mCherry colocalised with *mpx*:GFP also stained positive for laminin (Figure 27, white arrowheads). By 24 hpi, *lyz-H2A:*mCherry staining still colocalises with *mpx:*GFP. Though some neutrophils still display some chromatin extrusions (Figure 27, yellow arrowheads), chromatin morphology generally becomes more rounded and comparable to uninjured bone.

This data demonstrates that neutrophils recruited to zebrafish caudal fin fractures release chromatin into the extracellular space within the first 8 hpi, probably via NETs. Extracellular chromatin can be observed colocalising with *mpx:GFP* and laminin at the fracture site at 8 hpi. Collectively, this suggests a role for chromatin release in early fracture stabilisation and bone repair.

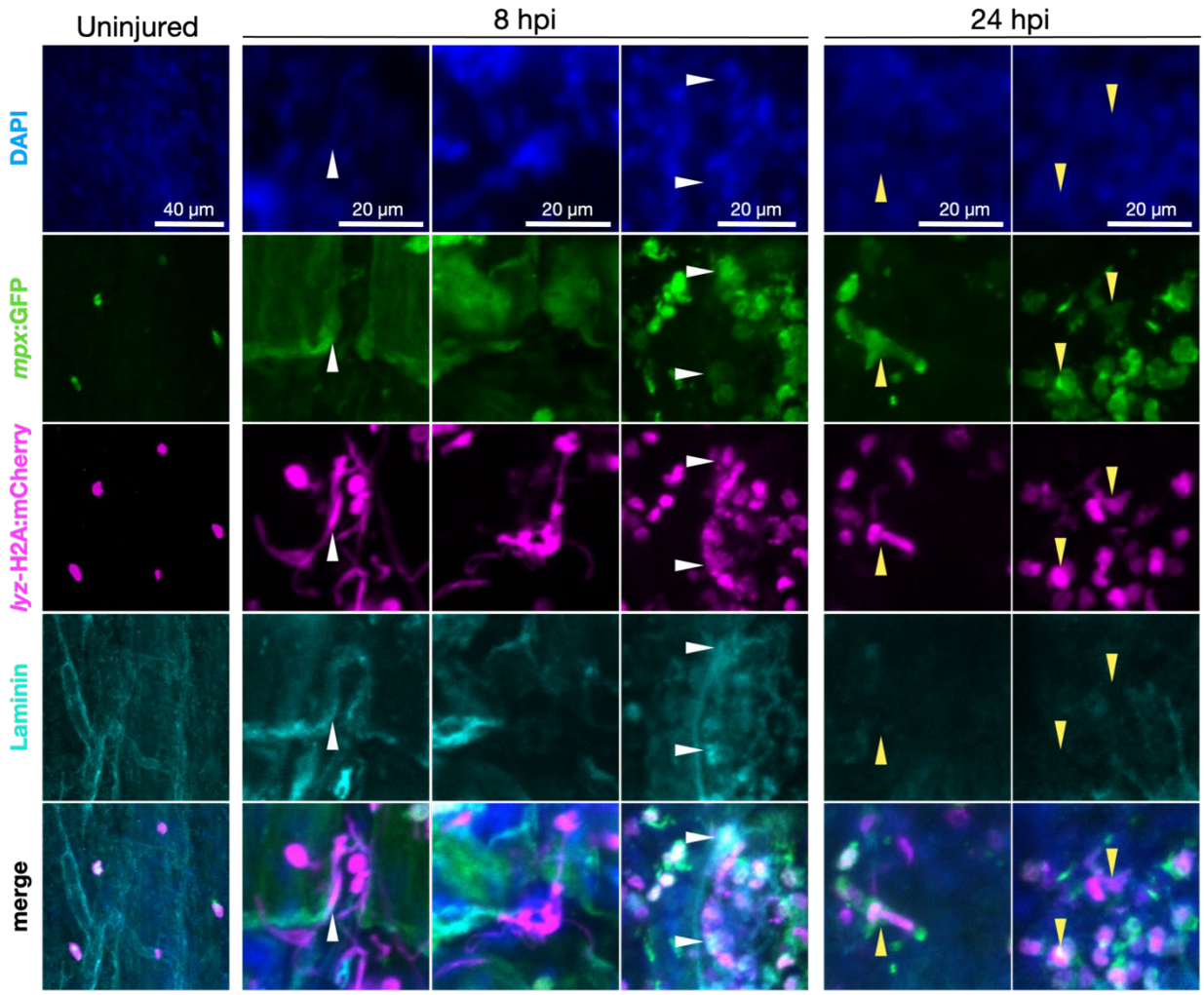

Figure 28. Morphology of Neutrophil Derived Chromatin Is Altered Post Fracture and Colocalises With Laminin and mpx:GFP. *Fractures were induced in the caudal fins of mpx:GFP;lyz-H2A:mcherry zebrafish, harvested and fixed at 8 hours post injury (hpi) and 24 hpi. Immunohistochemistry to detect DAPI, mpx:GFP, lyz-H2A:mcherry and laminin was performed. A selection of representative images from uninjured and fractured bone are shown. Uninjured tissue contained few neutrophils with mCherry^{+} punctate (chromatin), and low levels of laminin, mainly in blood vessels. At 8 hpi, levels of mpx:GFP and lyz-H2A:mcherry increase due to neutrophil recruitment. At 8 hpi, the morphology of both mpx:GFP and neutrophil derived chromatin becomes more diffuse and spindle like, compared to uninjured tissue. Some images (arrowheads) show colocalization between mpx:GFP, lyz-H2A:mcherry, suggesting the presence of NETs; these structures also colocalise with laminin in some instances. At 24 hpi, lyz-H2A:mcherry staining still colocalises with mpx:GFP; chromatin structure becomes more rounded, though can still display some extrusions (yellow arrowheads). Scale bars are indicated in DAPI images. Images representative of N ≥ 7 fractures from a one experiment.*

4.2.4 CXCR2 INHIBITION REDUCES NEUTROPHIL RECRUITMENT TO LARVAL RESECTION INJURY

Caudal fin resection experiments described in the following section were performed in collaboration with an undergraduate MSci student, Mary Appleton (MA). MA performed the majority of the caudal fin resections and well as acquiring proceeding time course images under my direct training and supervision. This data was included in MA's MSci dissertation, submitted to the University of Bristol (2020). Any data acquired in collaboration with MA that is presented here was processed and analysed solely by me.

Though a role for neutrophils in the early stabilisation of fractures and initiation of bone repair has been proposed, this has not been investigated dynamically (267). Given that neutrophils recruited to zebrafish fractures contain ECM proteins (Figure 25) and release chromatin (Figure 26), I next sought to characterise whether inhibition of neutrophil recruitment to fracture would affect bone repair in the zebrafish induced caudal fracture model. CXCR2 is a major chemokine receptor expressed on the surface of neutrophils, which facilitates chemotaxis to sites of inflammation in vertebrates. SB225002 is a potent and specific chemical antagonist of CXCR2, which has previously been shown to reduce neutrophil recruitment to wounds via Cxcl8 (IL-8) (359). A larval fin resection model was used to ensure the efficacy of SB225002 in inhibiting neutrophil recruitment, prior to performing adult caudal fin fracture experiments. Fin resections were performed on larval *mpx:GFP* zebrafish at 3 dpf, treated with either 1 μM SB225002, or an equivalent volume of DMSO (negative control). Figure 28 A illustrates the amputation point on the larval caudal fin, and the region in which neutrophil recruitment was quantified post fracture. Representative images of the counting regions from a single SB225002 or DMSO treated larva are shown between 0 and 48 hpa (Figure 28 B). Neutrophils were recruited to the fin resection by 3 hours post amputation (hpa), appearing to peak at 6 hpa, before reducing in number again by 24 hpa. Fewer neutrophils appeared to be present at the fin resections of SB225002 treated zebrafish; this was confirmed by quantifying the number of *mpx:*GFP^{+} cells recruited to the injury within the counting region (Figure 28 C). Significantly fewer *mpx:*GFP^{+} neutrophils were present within the counting region in SB225002 treated larvae at 3-6 hpa, compared to DMSO treated larvae. This demonstrates that SB225002 reduces, but does not completely inhibit, neutrophil recruitment to larval fin resection injury. This suggests that SB225002 may be used to reduce neutrophil recruitment to fracture, to study the role of neutrophils in early bone repair.

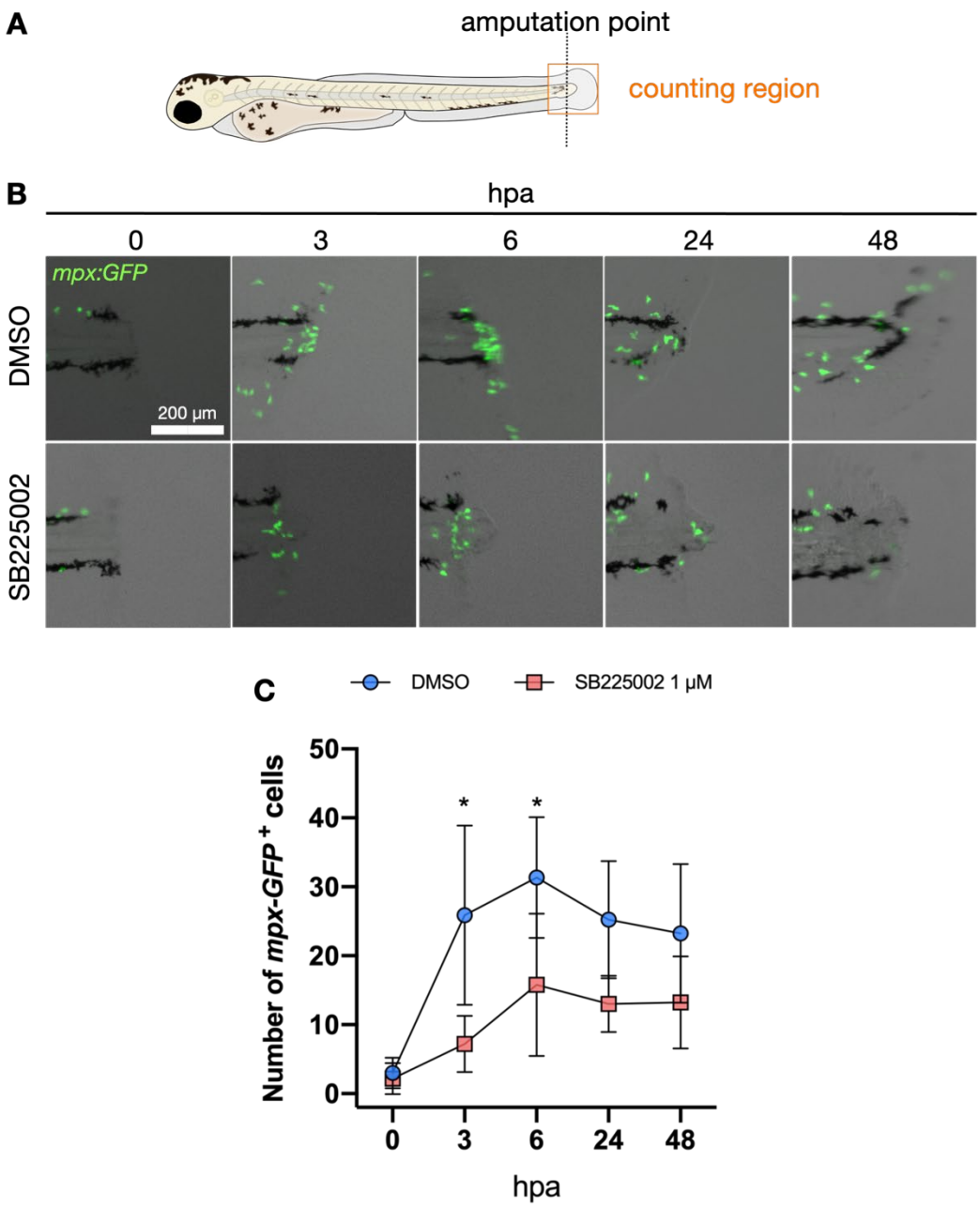

Figure 29. Cxcr2 Inhibition Significantly Reduces Neutrophil Recruitment to Injury in a Larval Resection Assay. *From 2 days post-fertilisation (dpf), larvae were treated with 1 µM of the Cxcr2 inhibitor, SB225002, or DMSO.* ***A:*** *At 3 dpf, the developing caudal fins of mpx:GFP larvae were resected along the dotted line. Over the proceeding 48 hours, live images were taken of the injury site and the number of neutrophils (mpx:GFP⁺ cells) within the counting region were quantified.* ***B:*** *Representative images of counting regions from SB225002 or DMSO treated larvae each time point post-injury are shown.* ***C:*** *The mean number of neutrophils recruited to the resection site was lower in SB225002*

*treated larvae compared to DMSO treated. Statistical analysis showed that significantly fewer neutrophils were present in the counting region early on post-injury in SB2250002 treated versus DMSO treated larvae. N≥4 larvae per time point; points represent mean (± SD); * = p < 0.05. Larval resections and image acquisition were performed in collaboration with an undergraduate MSci project student, Mary Appleton. Final data analysis and figure preparation was performed solely by Lucy McGowan.*

4.2.5 CXCR2 INHIBITION RESULTS IN A SIGNIFICANT INCREASE IN FRACTURE DISSOCIATION, WITHOUT IMPAIRING NEUTROPHIL RECRUITMENT

Having confirmed that SB225002 treatment significantly reduces the recruitment of neutrophils to larval fin resections, I next sought to determine the impact of Cxcr2 inhibition on neutrophil recruitment to fracture and early bone repair. As depicted in Figure 29 A, zebrafish were pre-treated with 5 μM of SB225002, or an equivalent volume of DMSO for 24 hours prior to fracture. Fractures were then induced in the caudal fins of the zebrafish and imaged at regular time points post injury, with treatments refreshed every 24 hours. Upon fracture, bone within the zebrafish caudal fin should remain intact (Figure 29 B), and bone repair proceeds in a manner comparable with mammals. However, in some instances, the bone distal to the fracture dissociates (Figure 29 B), then fin regeneration proceeds in place of repair. This phenomenon is not entirely predictable or well-studied, though it appears to be triggered by certain conditions such as irreparable trauma, infection to the injury or mutation resulting in impaired fracture healing (147). Fin dissociation seems to be a response to an unfavourable environment for fracture repair, meaning regeneration is preferred. Strikingly, treatment with SB225002 resulted in a high percentage of fracture dissociation events within the first 24 hpi (Figure 29 C). Fracture dissociation occurred in only around 8% of DMSO treated zebrafish within the first 48 hpi, the incidence of fracture dissociation increased significantly in SB225002 treated zebrafish, with 42% of fractures being lost within the first 48 hpi (Figure 29 D). This indicates that Cxcr2 signalling is required for the early stabilisation of fractures in the zebrafish caudal fin.

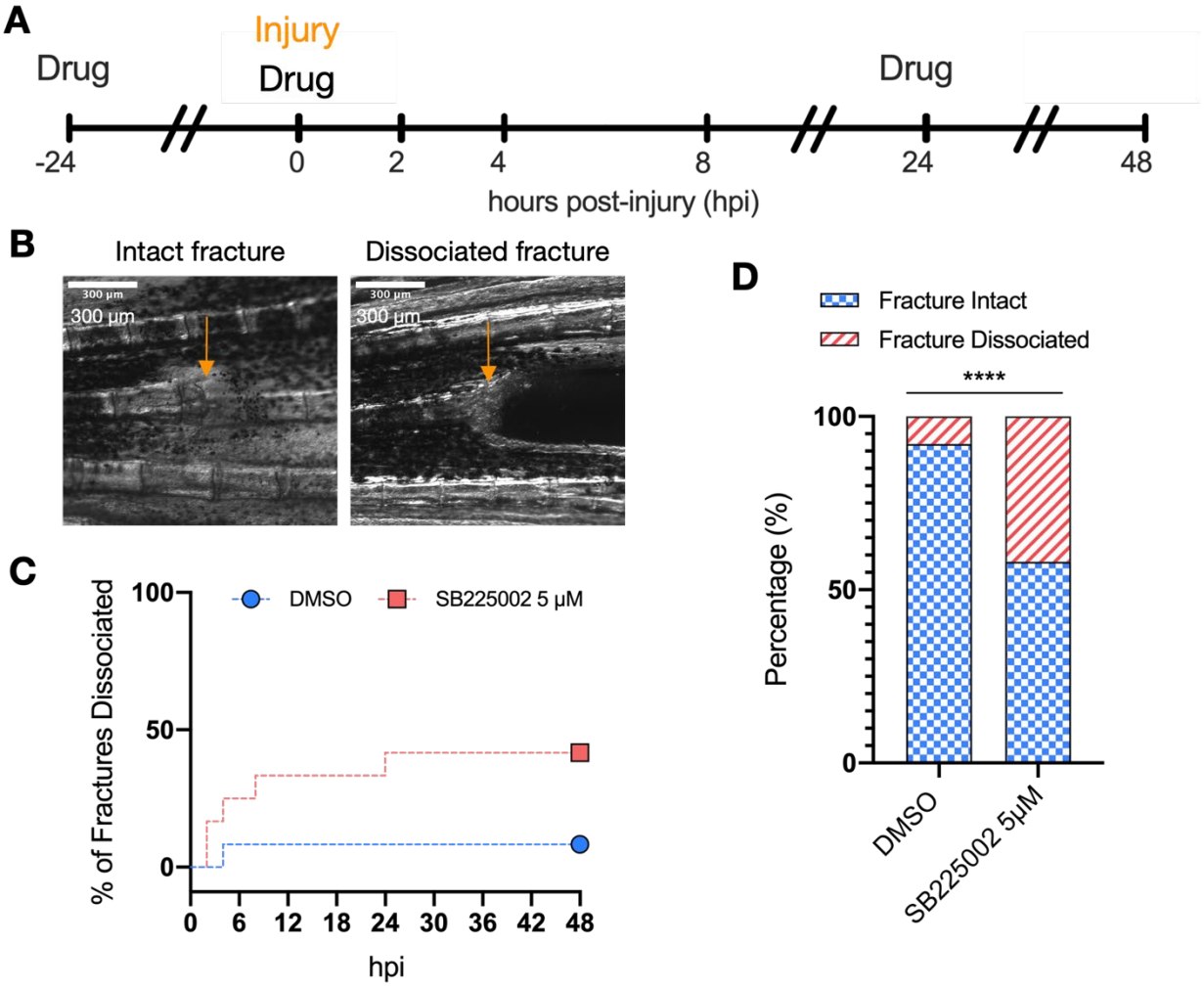

Figure 30. Cxcr2 Inhibition Results in Significantly Increased Incidence of Fracture Dissociation in First 48 Hours Post Injury (hpi). A: *Schematic depicting time course of drug treatment. Adult mpx:GFP zebrafish were treated with 5 µM SB225002, to inhibit Cxcr2, or DMSO, from 24 hours prior to injury and then every 24 hours thereafter. Numbers on timeline indicate time points when injuries were live imaged.* ***B:*** *Example bright field images of an intact fracture and a dissociated fracture 48 hours post injury (hpi). Similarly to non-union fractures in mammals, dissociated fractures have failed to begin healing and bone will regenerate instead.* ***C:*** *Survival curve showing the proportions and time points post injury that fractures in SB225002 and DMSO treated zebrafish dissociate. D: Treatment with the Cxcr2 inhibitor, SB225002, significantly increases the incidence of fracture dissociation within 48 hours of injury (42%) compared to DMSO treatment (8%). N ≥ 11 per treatment group. **** = p < 0.001.*

Considering the role of Cxcr2 in neutrophil chemotaxis, Cxcr2-dependent fracture stabilisation is likely mediated by neutrophils. Also, fracture dissociation most commonly occurred at the time points whereby neutrophils are ordinarily recruited to fracture, contain ECM proteins and release chromatin (between 4-8 hpi) (Figure 25, Figure 26). Therefore, *mpx:GFP* zebrafish were treated with either DMSO or 5 μM SB225002 before caudal fractures were induced and imaged, as previously described (Figure 28 A). Representative images of DMSO (intact) and SB225002 (intact and dissociated) fractures appear to show fewer neutrophils recruited to injury at 4 hpi in SB225002 treated zebrafish, compared to DMSO. At 8 hpi, a high number of neutrophils could be observed in both SB225002 and DMSO treated zebrafish, which had localised to the injury site (Figure 30). Surprisingly, though a trend towards reduced neutrophil recruitment could be observed at early time points post injury, no significant difference in the number of neutrophils recruited to the fracture site (within either 100 or 300 μm of the injury) was detected between 0-24 hpi as a result of SB225002 treatment (Figure 30 B-C). Significantly fewer neutrophils were detected within 100 μm of the fracture in SB225002 treated zebrafish at 48 hpi (Figure 30 B), but not within 300 μm of the injury (Figure 30 C). However, given that neutrophilic inflammation has largely resolved in untreated or DMSO treated zebrafish by 48 hpi (Figure 24, Figure 30), and that fracture dissociation tends to occur within the first 24 hpi in SB225002 treated zebrafish (Figure 29), this reduction in neutrophil number at 48 hpi is likely not biologically significant. This suggests that Cxcr2-mediated fracture stabilisation is not underpinned by gross impairment of neutrophil recruitment, but possibly via the regulation of neutrophil activity post fracture.

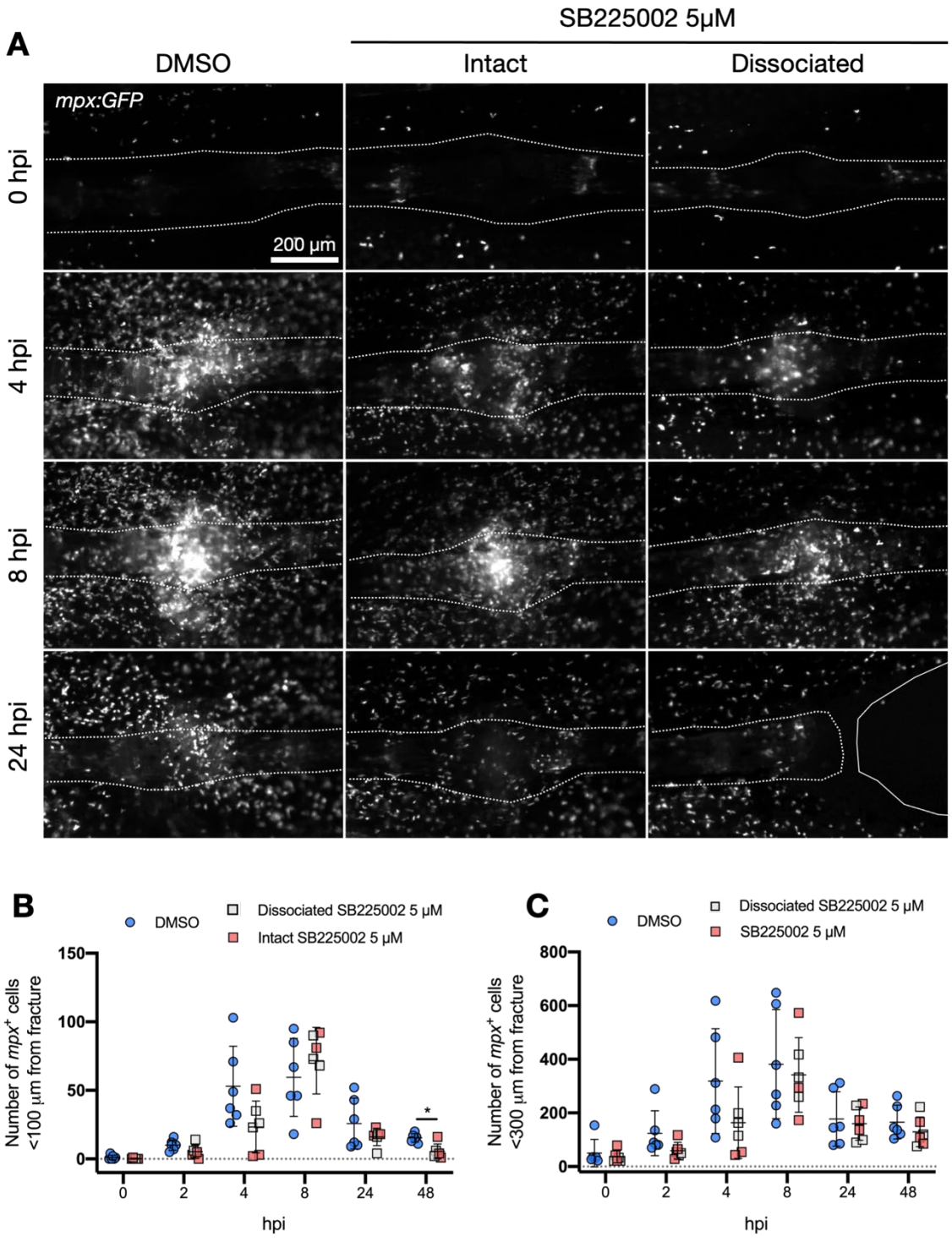

Figure 31. SB225002 Treatment Does Not Significantly Impair Neutrophil Recruitment to Fracture. *Adult mpx:GFP zebrafish were treated with 5 μM SB225002, to inhibit Cxcr2, or DMSO, from 24 hours prior to injury and then every 24 hours thereafter, as illustrated in Figure 29 A.* ***A:*** *Representative images of the same injury throughout fracture repair are shown for DMSO treated, intact SB225002*

treated and dissociated (by 24 hours post injury (hpi)) SB225002 treated zebrafish. Lower numbers of neutrophils can be observed at the fracture site at 2 and 4 hpi but are comparable at 8 hpi. Dotted line = bone outline. Solid line = blastema edge where fracture has dissociated. ***B-C:*** *The number of neutrophils recruited to within 100 μm (B) or 300 μm of the fracture site were calculated using MIA analysis. A lower mean number of neutrophils were recruited to the fractures of SB225002 treated zebrafish at 2 and 4 hpi, though not significantly fewer. SB225002 treated fracture has significantly fewer neutrophils at the fracture site at 48 hpi compared to DMSO treated zebrafish. N=6 per treatment group; points represent mean (± SD); * = p < 0.05.*

4.2.6 INHIBITION OF CXCR2 MAY ALTER THE ECM AT THE FRACTURE SITE WITHIN FIRST 24 HOURS POST INJURY

Since Cxcr2 inhibition did not significantly alter neutrophil recruitment to fractures, but did result in increased fracture dissociation, I next investigated whether alterations to the ECM were likely to underpin failure to repair fractures in SB225002 treated zebrafish. Therefore, caudal fin fractures were performed on adult *mpx*:*GFP* zebrafish, treated with 5 μM SB225002 or DMSO, as previously described. Fractured caudal fin tissue was amputated at either 8 or 24 hpi and fixed. Immunohistochemistry was performed to label DAPI, anti-*mpx:*GFP, laminin and fibronectin; unfortunately, fibronectin staining was unsuccessful in this instance, therefore, it was excluded from the final images (Figure 31). Images of DMSO treated and SB225002 treated (intact and dissociated) fractures are shown at 8 (Figure 31 A) and 24 hpi (Figure 31 B). At 8 hpi, no observable difference in the staining of *mpx:*GFP can be seen at 8 hpi (Figure 31 A); similarly, distribution and levels of laminin staining appear comparable in DMSO and SB225002 treated (intact and dissociated) fractures. Regions of laminin colocalising with diffuse *mpx:*GFP staining can be observed in all instances at 8 hpi (arrowheads, Figure 31 A); in dissociated SB225002 treated fractures, this staining localised to the edge of the bone, where the dissociation had occurred. Levels and distribution of *mpx:*GFP staining were comparable at 24 hpi in intact DMSO treated and SB225002 treated fractures (Figure 31 B), colocalizing with laminin in some areas (arrowheads). However, Cxcr2 inhibition resulted in more intense laminin staining at 24 hpi, observable in both intact and dissociated injuries, compared to DMSO treated fractures. In dissociated SB225002 treated fractures, bright, diffuse areas of *mpx:GFP* colocalize with bright laminin staining, which continues to localize to the injury border at 24 hpi. This suggests that SB225002 treatment alters levels and distribution of laminin at the fracture site at 24 hpi.

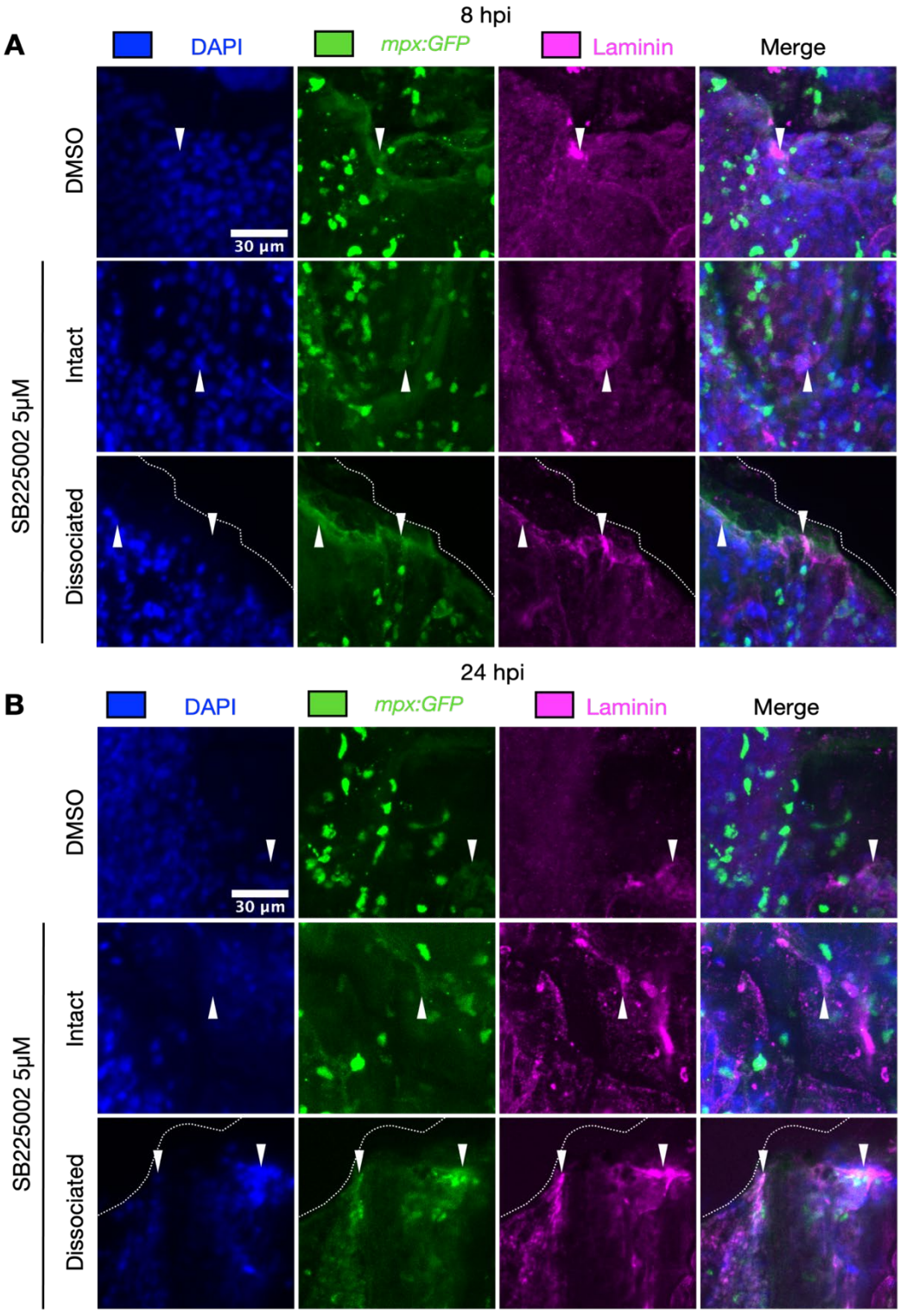

Figure 32. Cxcr2 Inhibition Does Not Alter Neutrophil Morphology but May Alter Laminin Levels and Distribution at The Fracture Site Post Injury. *Adult mpx:GFP zebrafish were treated with 5 μM SB225002, to inhibit Cxcr2, or DMSO, 24 hours prior to injury and then every 24 hours thereafter, as*

illustrated in Figure 29 A. Fins were fixed at 8 hours post injury (hpi) (A) or 24 hpi (B) and immunostained. Images of DMSO treated and SB225002 treated (intact and dissociated) fractures are shown. Images are taken at the fracture site (intact) or at the injury border (dissociated), denoted by the dotted line. Arrowheads = regions of interest where mpx:GFP staining colocalizes with laminin ***A:*** *At 8 hpi, in all conditions, bright mpx:GFP^{+} punctae as well as dimmer, more diffuse areas of mpx:GFP can be observed. Levels and distribution of laminin appear comparable in intact DMSO and SB225002 treated fractures.* ***B:*** *Levels and distribution of mpx:GFP staining were comparable at 24 hpi in intact DMSO treated and SB225002 treated fractures, colocalizing with laminin in some areas (arrowheads). However, Cxcr2 inhibition resulted in more intense laminin staining, observable in both intact and dissociated injuries, compared to DMSO treated fractures. In dissociated SB225002 treated fractures, brighter, diffuse areas of mpx:GFP localize to the injury border and colocalize with brighter laminin staining at both 8 and 24 hpi. Images represent N ≥ 2 fractures for DMSO treated zebrafish and N ≥ 5 fractures for SB225002 treated zebrafish from a single experiment.*

The ECM is formed by intricate interactions between many different proteins including laminin, but also fibronectin, collagen, and elastin. Glycosaminoglycans form covalent bonds with proteoglycans, constituting a major component of the ECM, and can regulate chemokines, cytokines and growth factors (368). Recently, interactions between glycosaminoglycans at inflamed tissue sites and G Protein Coupled receptor signalling in neutrophils has been described, as well as playing a role in CXCL8 (IL-8) mediated chemotaxis of neutrophils (369). Alcian blue staining is a method of detecting glycosaminoglycan levels in fixed tissue, which can indicate areas of high ECM content, such as in cartilage or soft callus formation post-fracture. Moreover, alcian blue staining can be performed on whole-mount zebrafish caudal fin fractures. Therefore, alcian blue staining was performed on fixed fractures (8 and 24 hpi) taken from zebrafish treated with either DMSO or SB225002 (Figure 32). Only weak alcian blue staining was detected at the fracture site within the first 24 hpi, and no difference in the levels of alcian blue staining can be observed between DMSO and SB225002 treated (intact and dissociated) fractures, at either time point post injury (Figure 32). This shows that glycosaminoglycan levels at the fracture site levels are not affected by Cxcr2 inhibition. However, since alcian blue staining appears weak within the first 24 hpi, it is unlikely that the fracture contains high levels of glycosaminglycans within this window.

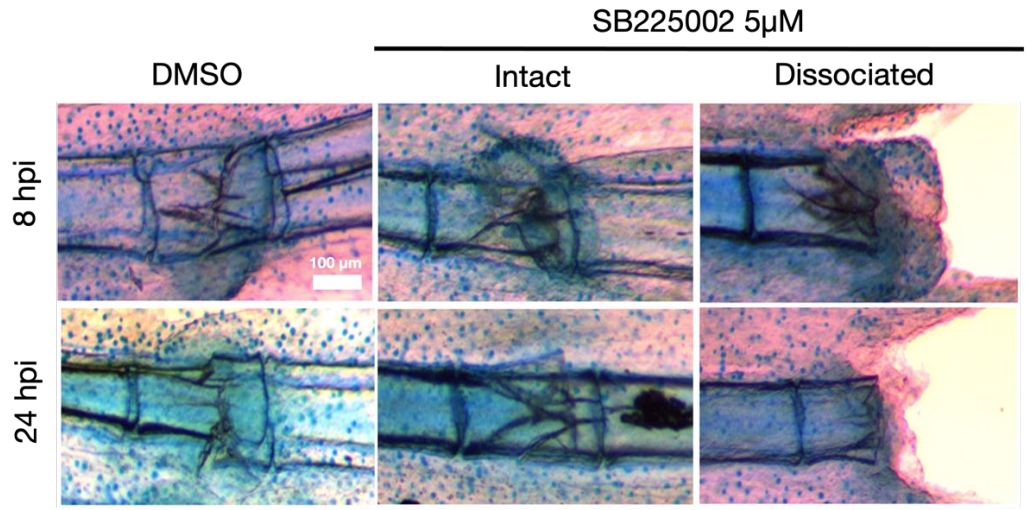

Figure 33. Cxcr2 Inhibition Does Not Alter Glycosaminoglycan Levels at The Fracture Site at 8 Or 24 Hours Post-Injury (hpi). *Adult mpx:GFP zebrafish were treated with 5 μM SB225002 or DMSO from 24 hours prior to injury and then every 24 hours thereafter, as illustrated in Figure 29 A. Fins were fixed at 8 or 24 hpi and alcian blue staining performed. Representative images from each group are shown. No marked difference in alcian blue labelling between DMSO and SB225002 treated fractures can be observed at either time point. Scale bar = 100 μm, N = 6 per treatment group.*

4.2.7 CXCR2 INHIBITION REDUCES NEUTROPHIL CHROMATIN RELEASE POST FRACTURE

In addition to playing a role in neutrophil recruitment, CXCR2 signalling has also been implicated in NETosis. Tumours have been shown to produce CXCR2 agonists which induce the release of NETs to shield cancer cells from cytotoxic lymphocytes (370). Moreover, CXCR2 inhibition has been shown to reduce pathogenic NETosis in chronic obstructive pulmonary disease (COPD) and severe asthma (371, 372). However, given the cental role of CXCR2 in neutrophil recruitment to sites of inflammation, this may be an indirect effect resulting from reduced chemotaxis of neutrophils, rather than via inhibition NETosis in neutrophils already recruited (236, 336, 373). I previously demonstrated that neutrophils recruited to zebrafish caudal fin fractures release chromatin (Figure 26), and that this chromatin colocalises with laminin (Figure 27). Therefore, I sought to determine whether fracture dissociation due to Cxcr2 inhibition was likely to be underpinned by alterations to NETs in zebrafish.

Fractures were induced in the caudal fins of *mpx:GFP;lyz:H2A-mCherry* zebrafish that were treated with either 5 μM SB225002 or DMSO, as previously described (Figure 29 A), and imaged at regular time points between 0 and 24 hpi. This experiment was halted at 24 hpi, therefore no data for the 48 hpi time point is available (see discussion, Section 4.3.5). Representative images of fractures appear to show a reduction in the intensity and distribution of *lyz:H2A*-mCherry at the fracture site in intact and dissociated SB225002 treated fractures, compared to DMSO treated fractures, throughout the first 24 hpi (Figure 33 A). Moreover, *lyz:H2A*-mCherry appears less diffuse at the fracture site between 4-24 hpi in SB225002 treated zebrafish, retaining the punctate morphology observed at 0 hpi. The fluorescence intensities of *mpx:*GFP (Figure 33 B) and *lyz:H2A*-mCherry (Figure 33 A) were measured relative to uninjured bone in the same fin (intensity ratio), at each of the time points imaged post fracture. Though the intensity ratio of *mpx:*GFP was reduced by SB225002 treatment, this reduction was not significant at any time point between 0 and 48 hpi (Figure 33 B). This was consistent with a previous experiment demonstrating that treatment with the Cxcr2 antagonist does not significantly reduce neutrophil recruitment to fracture (Figure 30). However, the mean intensity ratios of *lyz:H2A*-mCherry in SB225002 treated fractures remained low at each time point, compared to mean *lyz:H2A*-mCherry fluorescence intensities for DMSO treated fractures (Figure 33 C). Statistical analysis of *lyz:H2A*-mCherry intensity ratios comparing DMSO and SB225002 treated fractures was performed; the intensity ratio of *lyz:H2A*-mCherry was significantly lower in SB225002 treated

zebrafish at 2, 4 and 24 hpi, compared to DMSO (Figure 33 B). This suggests that inhibition of Cxcr2 reduces chromatin release from neutrophils post fracture.

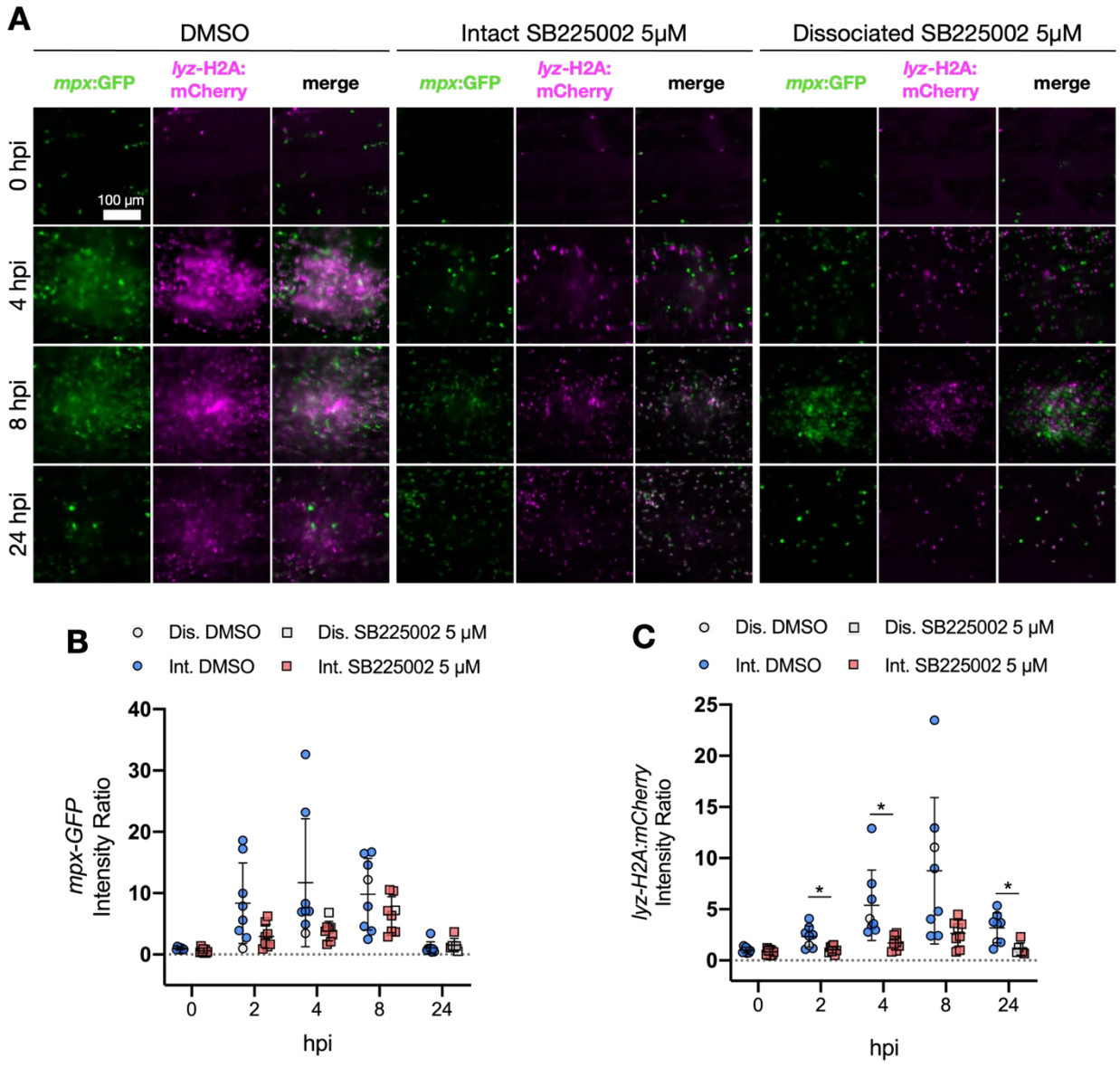

Figure 34. Cxcr2 Inhibition Significantly Reduces Chromatin Release from Neutrophils Post Fracture. *mpx:GFP;lyz-H2A:mcherry zebrafish were treated with 5 μM SB225002, to inhibit Cxcr2, or DMSO, 24 hours prior to injury and then every 24 hours thereafter, as illustrated in Figure 29 A. Fractures were induced in the caudal fins of treated zebrafish and imaged at time points from 0-24 hpi (hours post-injury).* ***A:*** *Representative images of the same injury throughout fracture repair are shown for DMSO treated, intact SB225002 treated and dissociated (by 24 hours post injury (hpi)) SB225002 treated*

zebrafish. Cxcr2 inhibition appears to lower mpx:GFP and lyz-H2A:mcherry signal at the fracture site between 4-24 hpi. Scale bar = 100 μm. ***B-C:*** *The intensity ratios for mpx:GFP (B) and lyz-H2A:mCherry (C) were measured relative to uninjured bone at each time point and plotted.* ***B:*** *Though the mean intensity ratio of mpx:GFP was lowered, Cxcr2 inhibition resulted in no significant reduction in mpx:GFP intensity ratios at the fracture site post injury.* ***C:*** *SB225002 treatment resulted in significantly decreased lyz-H2A:mCherry intensity at the fracture site compared to DMSO treatment at 2, 4 and 24 hpi . Centre of image = centre of fracture. Scale bar = 100 μm. N ≥ 6 fractures per group; points represent mean (± SD); * = p < 0.05.*

Previously, I demonstrated that chromatin released from neutrophils at the fracture site colocalised with laminin 8 hpi (Figure 27). Therefore, I also investigated whether treatment with the Cxcr2 antagonist altered the localisation of laminin, relative to *lyz:H2A*-mCherry. To this end, caudal fin fractures were performed on *mpx:GFP;lyz:H2A-mCherry* zebrafish, treated with either DMSO or 5 μM SB225002, and fixed at 8 hpi, when chromatin release from neutrophils peaks and colocalises with laminin (Figure 26, Figure 27). Tissue was stained for DAPI, anti-*mpx:*GFP, anti-*lyz:H2A*-mCherry and laminin. No obvious difference in staining was observed between SB225002 and DMSO treated fractures; as with previous immunostaining experiments, there were few, round *mpx:*GFP^{+} *lyz:H2A*-mCherry^{+} cells present in uninjured bone tissue, with laminin levels low, and mainly restricted to blood vessels (Figure 34 A). At 8 hpi, laminin was observed colocalising with *mpx:*GFP and *lyz:H2A*-mCherry in both treatment groups (white arrowheads, Figure 34 B). However, levels of *lyz:H2A*-mCherry appeared lower in SB225002 treated fractures compared to DMSO treated fractures at 8 hpi, with less laminin observed in regions of *lyz:H2A*-mCherry staining (Figure 34 B). Moreover, bright regions of extracellular chromatin, which colocalised with DAPI, could be clearly observed in DMSO treated fractures at 8 hpi, but were less visible in SB225002 treated fractures (yellow arrowheads, Figure 34 B).

Taken together, these results suggest that Cxcr2 inhibition results in a significant reduction in chromatin release post fracture, which may contribute to increased fracture dissociation in SB225002 treated zebrafish.

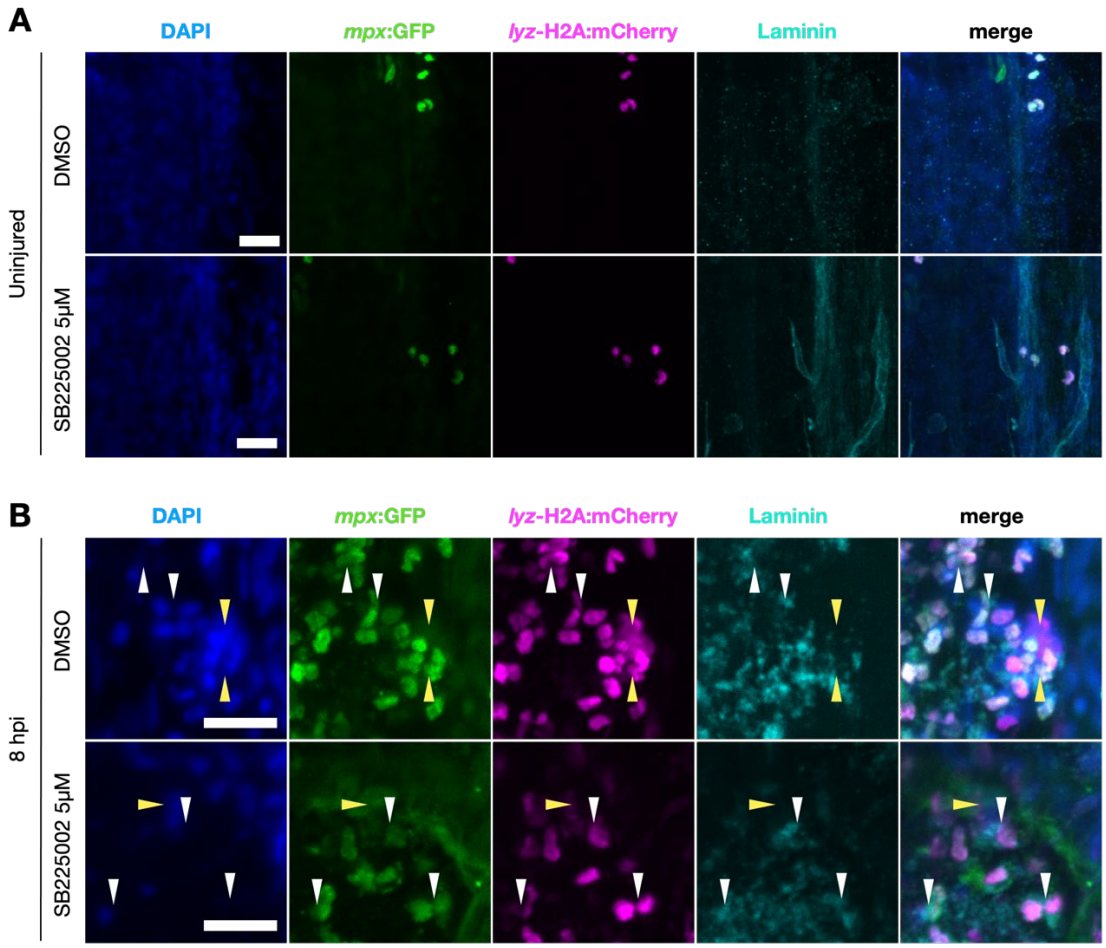

Figure 35. Localization of Neutrophil Chromatin and Laminin May Be Altered by Cxcr2 Inhibition At 8 Hours Post Injury (hpi). *mpx:GFP;lyz-H2A:mcherry zebrafish were treated with 5 μM SB225002, to inhibit Cxcr2, or DMSO, 24 hours prior to injury and then every 24 hours thereafter, as illustrated in Figure 29 A. Fractures were induced in the caudal fins of treated zebrafish, harvested and fixed at 8 hours post injury (hpi). Immunohistochemistry to detect DAPI, mpx:GFP, lyz-H2A:mcherry and laminin was performed.* ***A:*** *Uninjured fin tissue contained few neutrophils with mCherry^{+} punctate (chromatin), and low levels of laminin, mainly in blood vessels. Uninjured DMSO and SB225002 treated fins showed comparable staining.* ***B:*** *In both DMSO and SB225002 treated fractures, levels of mpx:GFP and lyz-H2A:mCherry increase due to neutrophil recruitment 8 hpi. However, levels of lyz-H2A:mCherry are lower in SB225002 treated fractures, appearing more rounded in shape. Yellow arrowheads indicate areas where chromatin morphology became more diffuse or extruded from the cell, sometimes colocalising with laminin, suggestive of NET release. White arrowheads highlight areas of colocalization between mpx:GFP and laminin and lyz-H2A:mcherry. Scale bar = 20 μm. Images representative of N≥7 (uninjured) N=8 (8 hpi) from a single experiment.*

4.3 DISCUSSION

4.3.1 SUMMARY OF RESULTS

Historically, the pro-inflammatory properties of neutrophils in healthy and pathogenic fracture healing have been studied far more rigorously than their potential pro-reparative properties. Although it has been proposed that neutrophils play a role in early fracture stabilisation via the production of emergency ECM in humans (267), this intriguing potential function had not been studied more dynamically *in vivo*. Here, I aimed to establish whether neutrophils contribute directly to fracture stabilisation and early bone repair. Using the induced caudal fin fracture model in zebrafish with transgenically labelled neutrophils, I demonstrated that neutrophils recruited to fracture within the first 8 hpi stain positive for ECM proteins, laminin and fibronectin (Figure 25). These neutrophils also release chromatin within the fracture haematoma, between 4-8 hpi (Figure 26 and Figure 27). Treatment with the Cxcr2 antagonist, SB225002, significantly reduced neutrophil recruitment to larval fin resections (Figure 28), but not to caudal fin fractures in adult zebrafish (Figure 30). However, treatment with SB225002 resulted in a high incidence of fracture dissociation events, a phenomenon by which the fracture fails to repair and the bone distal to the injury site is lost in favour of regeneration (Figure 29). Immunohistochemical analysis revealed that SB225002 treatment does not appear to alter neutrophil morphology but may alter laminin localisation at the fracture site (Figure 31). Interestingly, Cxcr2 inhibition resulted in a significant reduction in chromatin release from neutrophils post fracture (Figure 33). Collectively, these results suggest that neutrophils recruited to fracture support bone repair. Data suggests that neutrophils secrete or remodel the ECM, within the fracture, and that NETs may also support bone repair in a Cxcr2-dependent manner. Further research is required to establish the exact mechanisms by which neutrophils mediate their pro-reparative functions in fracture. However, this work uncovers exciting novel roles for neutrophils in bone repair, which warrant further study.

1.1.2 ECM PROTEINS WITHIN NEUTROPHILS POST FRACTURE: SYNTHESIS OR REMODELLING?

A study of human fracture hematomas by Bastian *et al.*, proposed that neutrophils synthesise a fibronectin rich ECM, which stabilises the bone prior to remineralisation (267). This intriguing conclusion was based on

immunohistochemistry to label insoluble cellular fibronectin and neutrophils in fracture hematomas, which were isolated from patients within 3 days of injury; fibronectin could clearly be observed within neutrophils inside the fracture haematoma, but not within neutrophils isolated from peripheral blood. However, whether these fibronectin^{+} neutrophils are responsible for synthesising fibronectin, or whether they degrade and remodel the ECM was not investigated.

In uninjured zebrafish caudal fin tissue, neutrophils did not stain positive for either laminin, or fibronectin. However, consistent with human fracture hematomas, neutrophils (*anti-mpx:*GFP^{+} cells) recruited to fracture between 4 and 8 hpi, stained positive for laminin and fibronectin (Figure 25). Interestingly, levels of laminin and fibronectin at 24 hpi appeared lower than at earlier time points. Higher levels of staining were observed compared to uninjured bone, in the absence of neutrophil activation and recruitment. This provided further evidence to suggest that neutrophils produce ECM in response to fracture. However, since levels of laminin and fibronectin appear to decrease as the number of neutrophils reduce (24 hpi), it remains plausible that neutrophils recruited to fracture may remodel ECM. Indeed, neutrophil derived proteinases are capable of remodelling a variety of ECM proteins, including laminin and fibronectin (374). Other cells, such as fibroblasts, may be responsible for the rapid production of ECM proteins within the haematoma post fracture, though establishing this requires further investigation (367). Therefore, transcriptomic or proteomic analysis of neutrophils isolated from fractures will help to elucidate whether neutrophils truly synthesise ECM in response to fracture, or whether the fibronectin and laminin contained within them is a result of ECM remodelling.

4.3.2 NEUTROPHILS RELEASE CHROMATIN IN RESPONSE TO FRACTURE IN ZEBRAFISH

NETs provide an important antimicrobial defence mechanism, but have been implicated in dysregulated wound healing and disease (375). However, it has been shown that aggregated NETs can degrade pro-inflammatory chemokines and cytokines in sterile models of inflammation (353). It has also been proposed that NETs associate with ECM proteins, such as fibronectin, to facilitate the migration of leukocytes, platelets and endothelial cells through inflamed tissues (350). Assessment of human hip fractures has shown the presence of NETs for up to 5 days post-injury (376), yet little is known about the role of NETs in fracture repair.

Whilst imaging laminin and fibronectin within fractures during neutrophil recruitment, I observed large, diffuse regions of anti-*mpx:*GFP at 8 hpi, in addition to bright staining within cells (Figure 25). I also demonstrated that neutrophils recruited to zebrafish caudal fin fractures released chromatin within the first 8 hpi, suggesting that neutrophils produce NETs at the fracture site (Figure 26, Figure 27). Neutrophil-derived myeloperoxidase, normally contained within granules, is known to quench GFP signal (377). This may explain why a reduction in *mpx:*GFP intensity was observed at the fracture site after chromatin release, prior to a reduction of *lyz:H2A*-mCherry (Figure 26 A-B). Neutrophil elastase, a major component of NETs, has been shown to promote the differentiation of osteoclasts *in vitro* via the degradation of the osteogenic protein, osteoprotegerin. This suggests that dysregulated or chronic NET production within fractures may impede bone repair. In zebrafish caudal fin fractures, osteoblasts peak in number and begin bone remineralisation at around 4 dpi (2, 147). However, by 48 hpi, levels of extracellular chromatin had decreased, demonstrating that neutrophilic inflammation resolves prior to the osteoblast-mediated repair phase post fracture. This suggests that neutrophil chromatin release during the inflammatory phase promotes healthy fracture repair. Laminin appeared to colocalise with regions of neutrophil-derived chromatin post fracture (Figure 27). Laminin alpha 4 has been shown to mediate pro-osteogenic and pro-angiogenic differentiation within a decalcified bone matrix scaffold (366). Therefore, associations between extracellular chromatin (NETs) and ECM proteins may facilitate fracture stabilisation, or form a scaffold on which cells can regenerate bone (350).

4.3.3 CXCR2 INHIBITION RESULTS IN FRACTURE DISSOCIATION IN ZEBRAFISH

CXCR2 is a conserved chemokine receptor, known to play a major role in neutrophil chemotaxis to sites of inflammation in vertebrates (235, 326). Antagonism of Cxcr2 with the compound SB225002 has been previously shown to reduce neutrophil recruitment to larval wounds (359), an effect which was recapitulated in this study (Figure 28). Therefore, it was surprising that SB225002 treatment did not significantly reduce neutrophil recruitment to caudal fin fractures (Figure 30). In a study of heart regeneration in adult zebrafish, Cxcr2 inhibition resulted in neutrophil retention at the site of cardiac cryoinjury and impaired regeneration of the cardiac tissue (378). This indicates that reduced Cxcr2 mediated chemotaxis may be compensated for by other chemokine receptors, such as Cxcr1, in adult zebrafish (379). This also suggests that Cxcr2 may play an important role in neutrophil behaviour and reverse migration, once recruited to injury.

Although SB225002 treatment did not significantly reduce neutrophil recruitment, unexpectedly, Cxcr2 inhibition resulted in a significantly higher number of fracture dissociation events within 48 hpi, compared to control injuries (Figure 29). This observation was consistent across independent experiments and occurred during the window of neutrophil recruitment to fracture, suggesting that Cxcr2 promotes fracture retention via neutrophils. Fin dissociation has been previously described in a zebrafish caudal fin fracture assay, and was associated with dysregulated neutrophilic inflammation as a result of infection (147). However, since fracture dissociation cannot be studied retrospectively (due to the tissue being lost), it is difficult to identify the underlying cause. However, fracture dissociation in the caudal fin appears to result from a dysregulated inflammatory response to fracture, which may recapitulate the unfavourable inflammatory conditions resulting in non-union bone repair, a major complication of orthopaedic trauma in humans (134). It is also worth noting that bone regeneration proceeded as normal after fracture dissociation, suggesting that zebrafish can overcome Cxcr2 inhibition during fin regeneration via redundancy, or that Cxcr2 is less important in fin regeneration. Immobilisation of injured zebrafish during early fracture repair, via sustained anaesthesia, may help to understand mechanisms of increased fracture dissociation, by preventing loss of the tissue. This may also highlight differing inflammatory profiles underpinning divergence in bone repair versus bone regeneration, indicating how these processes could be improved in humans. Moreover, immobilization allows for sustained, dynamic live-imaging of fracture, allowing for longitudinal analysis of individual cells.

4.3.4 POSSIBLE MECHANISMS OF CXCR2 MEDIATED FRACTURE RETENTION IN ZEBRAFISH

Since treatment with the Cxcr2 antagonist did not significantly decrease neutrophil chemotaxis to injury, fracture dissociation in SB225002 treated zebrafish likely results from a change in neutrophil activity within the fracture. One potential factor underpinning fracture dissociation in SB225002 treated zebrafish could be changes to the ECM, given the proposed role of neutrophils in synthesising an emergency matrix to stabilise fractures (267, 367). No observable difference in the levels or distribution of laminin in response to Cxcr2 inhibition was noted at 8 hpi, in the initial immunostaining experiment using *mpx:*GFP zebrafish (Figure 31 B). However, laminin staining appeared brighter in DMSO treated fractures, compared to SB225002 treated fractures, in the second immunostaining experiment using *mpx:GFP:lyz:H2A-mCherry* zebrafish (Figure 34 B). This highlights the need for unbiased quantitative analysis of laminin staining, to

determine whether Cxcr2 inhibition alters laminin within the fracture site, and whether this is likely to contribute towards increased fracture dissociation. Collectively, these data suggest that alterations to laminin at the fracture site may contribute to fracture dissociation within the first 24 hpi in SB225002 treated zebrafish. However, image processing and quantitative analysis of staining are required to fully determine whether Cxcr2 inhibition alters laminin post fracture. Other methods, such as western blotting or proteomics of neutrophils isolated from fractures, may reveal more about the influence of Cxcr2 inhibition on the neutrophil proteome during early bone repair. Moreover, it remains plausible that variable expression of Cxcr2 by individual neutrophils, or neutrophil subsets, may result in differential effects of SB225002 treatment from cell-to-cell.

Low levels of alcian blue staining at the fracture site in SB225002 and DMSO treated zebrafish indicates that soft callus formation may not be enriched within the first 24 hpi (Figure 32). Indeed, this is consistent with published data of alcian blue staining in zebrafish fractures at 24 hpi, where glycosaminoglycan levels appeared comparable with uninjured bone (147). This suggests that neutrophils recruited to fractures may contribute to remodelling the ECM to favour bone repair, rather than depositing additional ECM. Investigations into the effect of Cxcr2 inhibition on other ECM proteins, such as fibronectin or collagens, are required to truly determine whether alterations to ECM within the fracture are likely to contribute to Cxcr2-dependent fracture dissociation.

In addition to chemotaxis, CXCR2 has been implicated in NETosis (370, 372). Here, I demonstrated that treatment with a Cxcr2 antagonist resulted in a significant reduction in the levels of *lyz:H2A*-mCherry within the fracture, at time points between 2-24 hpi. This suggests that neutrophil chromatin release post fracture is significantly reduced by Cxcr2 inhibition, and that NETs may promote healthy bone repair and fracture retention. Timely resolution of inflammation is crucial for optimal bone repair to proceed post-fracture. Excessive recruitment, activity, or retention of neutrophils within the fracture haematoma is known to slow repair, in human, mammalian and zebrafish models (134, 147). Given that NETs can degrade pro-inflammatory chemokines and cytokines (353, 380), it is possible that chromatin release from neutrophils helps to resolve inflammation at the injury site, allowing repair to proceed. However, given that fractures in SB225002 treated zebrafish often dissociate within the first 24 hpi, when inflammation is peaking, it is unlikely that this is the mechanism underpinning fracture dissociation in this instance. NETs have also been shown to modify the ECM via interactions with fibronectin and laminin *in vivo* (351, 381). Moreover, NETs may support integrin-mediated cell migration within injured tissue by associating with ECM proteins to form a stable substrate on to which cells can adhere (350). Imaging suggests that Cxcr2 inhibition may also

alter ECM at the fracture site (Figure 33). However, further investigation is required to establish whether NETs associate with ECM proteins post fracture, and whether this contributes to Cxcr2-mediated fracture repair. Treating induced caudal fractures with DNAse between 4-8 hpi, to degrade NETs, will help to elucidate whether NETs support fracture retention in zebrafish.

4.3.5 EXTENDED DISCUSSION: CURRENT LIMITATIONS

4.3.5.1 NETOSIS IN ZEBRAFISH

NETs in zebrafish neutrophils was first reported in 2006 by Palić *et al*., who showed that DNA was released from kidney derived neutrophils in response to known chemical and bacterial NET stimuli, and associated with antimicrobial enzymes (364). However, whether these responses represent true NETosis, comparable with the process in mammals, has been debated. Recently, more compelling evidence to suggest that NETosis is a conserved mechanism within the Osteichthyes (bony fish) group has emerged. Isles *et al*., performed the most convincing study of NETs in zebrafish to date, and developed the novel neutrophil-specific chromatin reporter zebrafish line (232), which was further utilised here. In this study, it was shown that pioneer neutrophils recruited to wounds release chromatin to induce neutrophil swarming, and that *lyz:*DsRed^{+} neutrophils isolated from adult zebrafish could release NETs upon stimulation *in vitro*. Moreover, in a fascinating study of lungfish, a critical role for leukocyte extracellular trap formation in epithelial barrier maintenance and bacterial symbiosis during terrestrialization was revealed (382). Therefore, current evidence suggests that NET production in Osteichthyes is as least partially, if not heavily, conserved with mammals (383). Further research into NETosis in teleost models are required to establish the translational potential of studying the role of neutrophil chromatin release in bone repair in these model organisms.

4.3.5.2 IMAGING OF NEUTROPHILS IN ZEBRAFISH

The duration for which live adult zebrafish can be imaged under anaesthesia is improving. Intubation of zebrafish within temperature regulated hydro-chambers mounted to microscopes have allowed for longer time-lapse images of leukocyte responses to wounds; these injuries have been effectively imaged in adult transgenic zebrafish for up to 24 hpi (250). High resolution intravital time-course microscopy of caudal fin fractures in *mpx:GFP;lyz:H2A-mCherry* transgenic zebrafish will create a clearer picture of chromatin

release from neutrophils post fracture. Given that *mpx:*GFP^{+} neutrophils release chromatin within 8 hpi, in the zebrafish caudal fin fracture model, live time-lapse imaging of this event should be possible.

Whilst use of the *mpx:GFP* transgenic line has been instrumental for dynamic imaging of live neutrophils - as a cytosolic fluorescent marker - it may be less appropriate for visualising NET formation in fixed fractures with immunohistochemistry; after cell membrane rupture during chromatin release, GFP will likely diffuse into the extracellular space, before being quenched or degraded. Here, confocal imaging of immunostained fractures showed that diffuse anti-*mpx:*GFP staining could be seen in the same regions as extracellular chromatin (Figure 27), but did not completely colocalise with *H2A*-mCherry. Immunohistochemistry using antibodies to directly detect markers such as neutrophil elastase, and Mpx, alongside the fused *H2A*-mCherry zebrafish reporter line (232), will help to further establish the significance of neutrophil chromatin release in zebrafish caudal fin fracture.

4.3.5.3 UNEXPECTED TOXICITY OF SB225002 TREATMENT IN IMPORTED ZEBRAFISH

Live, time course imaging showed that Cxcr2 inhibition with SB225002 resulted in a significant decrease in neutrophil chromatin release post fracture (Figure 33). Though data derived from this experiment is promising, it must be treated as preliminary, at this time. Initially, as with other experiments, live imaging of fractures was planned through to 48 hpi. However, at around 24 hpi, 3 out of 4 zebrafish in the SB225002 treatment group appeared to be under physical stress (reduced swimming and increased panting). Therefore, the experiment was aborted to minimise unnecessary pain or suffering, and the fish were euthanised. Given that SB225002 treatment had been administered to adult zebrafish throughout the course of fracture repair in at least 5 other, independent experiments, this apparent adverse reaction to SB225002 was unlikely solely due to Cxcr2 inhibition. The zebrafish used in this experiment had been bred by their lab of origin at the University of Sheffield and shipped to the University of Bristol, where they were then raised to adulthood. Imported zebrafish lines are raised within a quarantined aquarium facility, which is independent to the main aquarium. Whilst strict animal husbandry procedures are followed to maintain zebrafish health in this facility, the presence of unfamiliar pathogens in the water is more likely, since lines imported from any external facility are maintained there. Neutrophils provide an essential first line of defence against pathogens, with Cxcr2 playing a major role in their recruitment and function. Therefore, it is possible that Cxcr2 inhibition became toxic, specifically for zebrafish maintained in the quarantine facility. To conclusively determine whether Cxcr2 inhibition reduces chromatin release from neutrophils post

fracture, these experiments must be repeated in a new generation of *mpx:GFP;lyz:H2A-mCherry* zebrafish that have been raised in the main zebrafish facility at the University of Bristol.

4.3.6 CONCLUSIONS AND FUTURE DIRECTIONS

Pathogenic inflammation, caused by neutrophils, is currently a key are of interest for the development of new therapies to treat multiple diseases (384). However, little is known about the pro-reparative properties of neutrophils in bone injury. Here, I used the zebrafish caudal fin fracture model to provide further evidence that neutrophils recruited to fracture contain ECM proteins, laminin and fibronectin. Precisely how neutrophils contribute to ECM synthesis or remodelling at the fracture site remains unclear. However, this interaction may be mediated, in part, by NETs. I demonstrated that neutrophils recruited to fracture release chromatin, likely via NETs, which was observed to colocalise with laminin. Treatment with the Cxcr2 antagonist, SB225002, was associated with increased incidence of fracture dissociation. This data suggests that Cxcr2-mediated chromatin release from neutrophils may support fracture stabilisation, but further investigation is required.

This study highlights intriguing potential non-canonical roles for neutrophils and NETs in fracture healing. Whether neutrophils synthesise or remodel ECM at the fracture site remains unclear; transcriptomics of neutrophils isolated from the injury will reveal whether ECM genes are upregulated by neutrophils in response to fracture. Many questions remain about how Cxcr2 promotes fracture stabilisation in zebrafish. One next step will be to perform intravital time lapse imaging of fractures performed on *mpx:GFP;lyz:H2A-mCherry* zebrafish, to reveal novel insights into neutrophil chromatin dynamics in bone repair. Moreover, immobilisation of SB225002 treated zebrafish with long-term anaesthesia will likely prevent tissue loss due to fracture dissociation, allowing for longer-term imaging of fractures under these conditions; this will shed light on the mechanism underpinning Cxcr2-mediated fracture stabilisation. Finally, degradation of NETs with DNAse post injury will further unravel the role of extracellular chromatin in early fracture stabilisation.

CHAPTER 5: RESULTS SECTION 3

EXPLORING A PRO-OSTEOGENIC ROLE FOR TNF-α IN BONE REGENERATION AND REPAIR

The data described within this chapter is currently unpublished. All data within this chapter was collected, analysed and presented by Lucy McGowan. MIA pipelines were written by Dr Stephen Cross from the Wolfson Bioimaging Facility at the University of Bristol (see section 2.16). Some experiments within this project were impacted by the COVID-19 pandemic (aims 2 and 3), as described in the "COVID Impact Statement" in the preliminary pages of this thesis.

5.1 INTRODUCTION

5.1.1 TNF-α AND TNF RECEPTORS

First discovered in the serum of bacillus Calmette-Guerin infected mice in 1975, tumour necrosis factor alpha (TNF-α) was noted for its necrotic effects on transplanted tumours *in vivo* and on neoplastic cells *in vitro* (385). Though it was first highlighted as an attractive target for cancer therapy, since its discovery, this small secreted protein has been implicated in a wide array of physiological processes and inflammatory diseases (386). Now, TNF-α is known to be one of 19 ligands and 29 receptors within the human TNF superfamily of proteins (387).

Innate immune cells such as monocytes, macrophages and granulocytes are known as the main source of TNF-α (388). However, *TNFα* can also be expressed by MSC-derived cell types under inflammatory conditions (389). TNF-α is initially expressed on the cell surface in a membrane-bound state (mTNF-α), which can undergo proteolytic cleavage by the TNF-α converting enzyme (TACE) and be released as soluble TNF-α (sTNF-α) (Figure 35) (386). TNF-α may bind to its ligand receptors in either the membrane-bound

(local), or soluble state (locally and systemically). There are 2 transmembrane receptors to which TNF-α can bind, with divergent downstream physiological effects: TNF receptor 1 (TNFR1), and TNFR2. TNFR1 is widely expressed by most mammalian cell types, whereas TNFR2 expression is primarily restricted to immune and endothelial cell types (386). Moreover, TNFR1 binds strongly to either sTNF-α or mTNF-α, whereas TNFR2 has been shown to have a far higher affinity for mTNF-α (390).

The intracellular portion of TNFR1 contains a death domain (DD); this domain is responsible for the pleiotropic effects of TNFR1 on cell proliferation and survival in response to TNF-α (391) (Figure 35). Upon engagement with TNF-α, the DD of TNFR1 recruits an adapter molecule called the TNFR1-associated death domain protein (TRADD) (392). TRADD activates the canonical nuclear factor-kappa B (NF-κB) pathway, as well as mitogen-associated protein kinases (MAPKs), such as c-Jun kinase (JNK) (393-395). However, paradoxically, engagement of TNFR1 can also trigger cell apoptosis by activating intracellular caspase cascades (395, 396). TNFR2 also activates the NF-κB pathway upon engagement with TNF-α. However, unlike TNFR1, TNFR2 lacks an intracellular DD, instead transducing intracellular signals via TNFR-associated factors (TRAFs), activating NF-κB non-canonically. This means that TNF-α-TNFR2 signalling promotes cell survival and proliferation and does not trigger apoptosis. Whether TNF-α-TNFR1 signalling causes downstream cell proliferation or apoptosis likely depends on the intracellular protein composition of the target cell; heterogeneity in the concentrations of caspase 3 and 8, as well as their inhibitors, have been shown to regulate cell fate in response to TNFR1 signalling (397). It is plausible that TNF-α-TNFR2 signalling may counteract apoptotic TNF-α-TNFR1 mediated signals by promoting survival, particularly in cells such as macrophages, which express both receptors and proliferate in response to TNF-α (394, 398). It has also been shown that TNF receptors may exist in a soluble state where they act as endogenous inhibitors by competitively binding to TNF-α; this prevents activation of cell membrane-bound TNF receptors and supresses inflammation (399). Collectively, this highlights the complexity and pleiotropic effects of TNF-α mediated cell signalling.

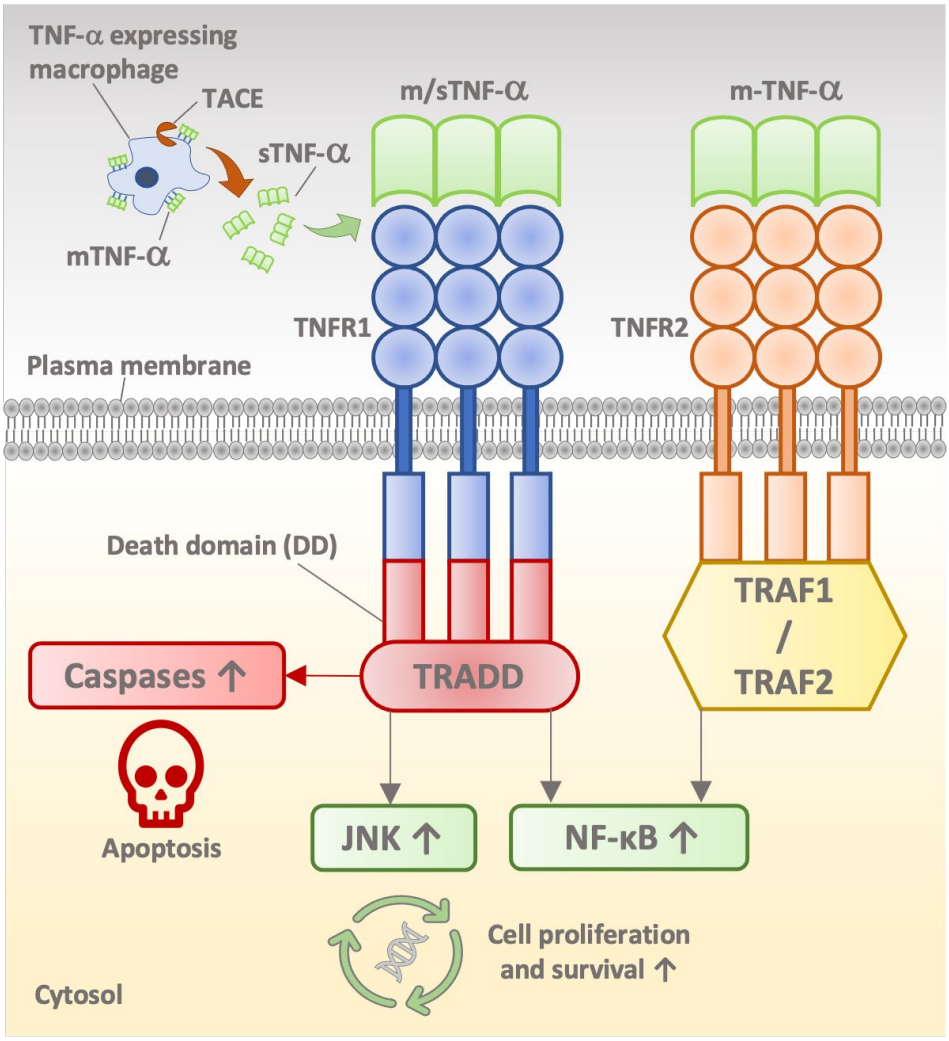

Figure 36. Mechanisms of Tumour Necrosis Factor Alpha (TNF-α) Signalling. *A cell, such as a macrophage, expresses membrane-bound TNF-α (m-TNF-α). m-TNF-α can be cleaved from the cell by the TNF-α converting enzyme TACE and released as soluble TNF-α (s-TNF-α). TNF-α binds to the transmembrane TNF-α receptors (TNFR1 / TNFR2). TNFR1 is expressed by most cell types and binds either m-TNF-α or s-TNF-α,, whereas TNFR2 is restricted to immune and endothelial cells and preferentially binds m-TNF-α. TNFR1 possesses an intracellular death domain (DD), which recruits the TNFR1-associated DD protein, TRADD, upon engagement with s-TNF-α or m-TNF-α.. This can trigger caspase cascades leading to cell apoptosis. Alternatively, TRADD can activate the canonical nuclear factor-kappa B (NF-κB) pathway and c-Jun kinase (JNK) to promote cell proliferation and survival. TNFR2 binds preferentially to m-TNF-α and lacks an intracellular DD, instead recruiting TNFR-associated factors 1 and 2 (TRAF1/2). TRAF1 and 2 activate NF-κB non-canonically to promote cell proliferation and survival.*

5.1.2 TNF-α IN HEALTH AND DISEASE

Though it was first acknowledged for its ability to kill tumour cells (385), TNF-α is now recognised as a major pro-inflammatory cytokine, with central roles in regulating immunity in healthy and diseased states. TNF-α was first linked to immunity against listeriosis over 30 years ago (400). Upon infection with a pathogen, TNF-α is produced to activate immune cells and facilitate microbial clearance (401). Macrophages become activated via the classical pathway, and polarise to a pro-inflammatory state whereby they express cytokines, including TNF-α, to drive inflammation; these are termed "M1" macrophages (402). Mice deficient in TNF display defective early innate immune responses and are susceptible to yeast infection, yet they also develop lethal hyperinflammation in response to *Corynebacterium parvum*. This suggests that TNF-α has roles in balancing late-stage inflammation, as well as promoting the initial inflammatory response to pathogens (403). Heterozygous *Tnfα*$^{+/-}$ mice show increased susceptibility to yeast infection, demonstrating haploinsufficiency of the *Tnfα* gene (403). Mice lacking the *Tnfα*, *Tnfr1*, or *Tnfr2* genes succumb to lethal bacterial infection, yet are also resistant to lethal lipopolysaccharide (LPS) induced hyperinflammation and tissue damage (403-406). This highlights the negative impact of TNF-α overactivation.

After tissue injury, M1 macrophages are initially required to trigger inflammatory processes in the damaged tissue. During wound repair, *tnfα*$^{+}$ M1 macrophages associate with sprouting blood vessels and drive angiogenesis via vascular endothelial growth factor (VEGF) signalling (240). Moreover, TNF-α inhibition during early wound repair results in delayed healing, whereas stimulation with TNF-α accelerates this process (407). However, alternatively activated macrophages (M2), which down regulate TNF-α and express anti-inflammatory cytokines, are required to resolve inflammation and promote healthy tissue repair (402, 408). Timely attenuation of the pro-inflammatory injury response and reduction in *tnfα* expression by macrophages has been associated with improved scar resolution during cardiac regeneration (238). Moreover, dynamic control of macrophage activation states is essential to promote healthy wound repair; excessive or prolonged Tnf-α activation has been associated with reduced angiogenesis and increased tissue fibrosis (240, 409).

Given its dominant role in orchestrating inflammation, it is unsurprising that dysregulated TNF-α signalling has been implicated in a wide array of pathologies including autoimmune disease, cancer, allergy and chronic wounds (386, 410-413). Aberrant overexpression of *Tnf*-α by intestinal epithelial cells results in chronic inflammation of the gut and drives Crohn's-like pathology (414, 415). As such, pharmacological

modulation of TNF-α has been extensively researched for the treatment of inflammatory diseases, with 5 TNF-α biologic inhibitors currently clinically approved for use in humans in the UK (416). Four of these inhibitors are monoclonal antibodies (adalimumab, certolizumab, golimumab, and infliximab), and one (etanercept) contains the extracellular domain of TNFR2 linked to the Fc portion of a human IgG1; all 5 inhibitors bind and inhibit TNF-α with high affinity and specificity (416, 417).

TNF-α inhibitors offer an effective treatment option for people suffering from autoimmune diseases, such as rheumatoid arthritis and Crohn's disease. However, given the central and pleiotropic roles of TNF-α in controlling inflammation, TNF-α targeting drugs are likely to have broad implications on a variety of immune defence mechanisms and injury responses. Indeed, treatment with several different human-approved TNF-α targeting drugs has been shown to increase susceptibility to latent tuberculosis infection, by supressing phagosome formation in macrophages (418, 419). Treatment with TNF-α targeting therapies has also been associated with increased cancer risk in some studies, though this purported association is debated (420, 421). It is also known that TNFR2 is preferentially expressed by regulatory immune cells, meaning TNF-α-TNFR2 signalling may actually support the expansion of these immunosuppressive cell populations (411). Small molecules which specifically disrupt TNF-α-TNFR1 binding are being investigated (422); such targeted inhibition may help to reduce side effects resulting from global TNF-α inhibition and increase the proportion of patients eligible for TNF-α-targeting therapy.

Like all tissues in the body, bone is influenced by TNF signalling (423). Healthy bone remodelling during homeostasis is regulated in part by TNF-α, which simulates bone resorption via osteoclasts (423). However, this must be balanced, as TNF-α is known to drive inflammation and pathological bone loss in rheumatoid arthritis (413). Moreover, paradoxical effects of TNF-α on osteoblasts have been reported (38), yet are poorly understood. Given the increasingly widespread use of TNF-α inhibitors, the role of TNF-α in bone requires further characterisation.

5.1.3 THE PLEIOTROPIC EFFECTS OF TNF-α ON BONE

TNF-α has been noted for its pleiotropic effects on various cell types under different physiological conditions (424); non-more so than for its effect on bone (38). Bone is a highly dynamic tissue, which constantly undergoes homeostatic remodelling, as well as responding to and repairing damage. Upregulation of TNF-α alone is not sufficient to drive bone resorption; TNF-α is known to stimulate

osteoclastogenesis via synergy with Receptor activator of NF-κB ligand (RANK-L) (41, 423), and by stimulating the release of osteoclast precursor cells from the bone marrow (425, 426). Increased TNF-α levels also promote the expression of RANK by macrophages, polarising them towards an osteoclastogenic phenotype (43, 133). Moreover, TNF-α can increase the production of RANK-L by stromal and immune cells, further driving bone catabolic processes (427). In a medaka model of RANK-L induced osteoporosis, TNF-α was found to be responsible for the recruitment of macrophages which differentiate into osteoclasts (428). Anti-TNF-α therapies have been shown to decrease levels of soluble RANK-L, in rheumatoid arthritis and ankylosing spondylitis patients (429). This resulted in reduced pathological bone loss and stabilisation of BMD at multiple sites. Moreover, in psoriatic arthritis patients treated with etanercept, TNF-α inhibition has been shown to significantly decrease numbers of osteoclast precursor cells and reduce bone resorption (430). These human studies highlight the stimulatory effect of TNF-α on bone resorption *in vivo*.

Under healthy, homeostatic conditions, bone turnover is a self-regulated process, whereby osteoblasts express genes to promote osteoclast activity, and vice versa (6). In addition to promoting bone resorption, TNF-α has also been shown to negatively regulate osteoblast differentiation and activity via activation of the NF-κB pathway (431, 432). TNF-α, along with other proinflammatory cytokines such as interleukin-6, increases levels of osteoinhibitory sclerostin (SOST) and Dickkopf-related protein 1 (DKK-1) (38). Production of these inflammatory cytokines by macrophages has been shown to upregulate SOST in both osteoprogenitor and osteoblast cells; this leads to the autocrine suppression of the canonical Wnt and Bone morphogenic protein (BMP) pathways, and down regulation of Runx2 and osteocalcin (433).

Paradoxically, numerous studies have found that TNF-α stimulates osteogenic differentiation, *in vitro* and *in vivo*. Low concentrations of TNF-α have been shown to stimulate the expression of *Osx*, *Runx2* and *Alp* in mesenchymal stem cells and promote osteogenic differentiation (434, 435). TNF-α has also been shown to increase the expression of alkaline phosphatase (ALP) by stromal cells *in vitro* (432). In rheumatoid arthritis patients with high levels of TNF-α, expression of the anti-resorptive protein osteoprotegerin (OPG) by synovial fibroblasts has been shown to be significantly increased compared to non-inflammatory controls (436). Interestingly, pro-osteogenic effects of TNF-α have been linked to Wnt signalling; TNF-α increases the expression of the non-canonical Wnt ligand, Wnt5a, in MSCs, which increases levels of tissue non-specific alkalise phosphatase (TNAP) and matrix mineralisation (437). This study suggests that osteoblast activity may be stimulated in an autocrine manner via the canonical Wnt pathway, in response to TNF-α.

As described in Section 5.1.2, TNF-targeting therapies are increasingly used to treat chronic inflammatory diseases. One study of rheumatoid arthritis patients demonstrated a beneficial effect of combined etanercept and infliximab treatment, alongside prednisolone and methotrexate, on lumbar spine BMD, compared to those without anti-TNF-α therapy (438). More recently, another study of rheumatoid arthritis patients treated with anti-TNF-α therapies demonstrated reduced bone loss resulting from a decrease in osteoclast precursors, regardless of clinical response at inflamed joints (439). TNF-α inhibition has been shown to increase spine BMD, whilst worsening radiographic progression of disease in patients with ankylosing spondylitis, indicating that anti-TNF-dependent changes to bone metabolism (440). However, despite improving lumbar spine BMD, treatment of chronic inflammatory diseases with anti-TNF therapy does not protect against the incidence of fracture (441, 442). In a genetic mouse model of lupus, etanercept was capable of reducing levels of pro-inflammatory cytokines in the serum, whilst also reducing TNF-α mediated mandibular bone loss (443). However, in this study, etanercept increased trabecular but not cortical bone volume in WT mice, suggesting that TNF-α may exert pleiotropic effects on different parts of the skeleton. A three year study of rheumatoid arthritis patients treated with a range of biologic therapies, including anti-TNF-α biologics, showed a protective effect of biologics against osteoporosis, compared to conventional antirheumatic drugs (444). However, studies investigating the long-term effects of anti-TNF therapy on bone are lacking, and pleiotropic effects of TNF-α in fracture repair have been reported.

5.1.4 TNF-α IN BONE REPAIR

Fracture repair requires an inflammatory phase, followed by an increase in osteoblast activity to remineralise the damaged bone (121). As such, the roles of TNF-α in bone repair and regeneration are unclear. Hyper inflammatory conditions negatively impact bone repair mechanisms, by inhibiting osteoblast differentiation and activity (134). Chronic inflammation and high levels of TNF-α in a murine model of rheumatoid arthritis causes impaired fracture healing, which can be rescued by TNF-α inhibition (445). However, TNFR signalling increases the production of angiogenic factors and matrix metalloproteinases (MMPs) by chondrocytes post fracture, which are essential for endochondral bone repair (446). Low concentrations of TNF-α have been shown to augment the recruitment and differentiation of nearby muscle derived stromal cells into osteoblasts with high ALP activity (447). Moreover, low-dose treatment with recombinant TNF-α (r-TNF-α) has been shown to promote efficient fracture repair in healthy and osteoporotic mice (447); this effect was only observed when r-TNF-α was

administered locally, at the fracture site, and within 24 hours of injury (448). A recent study showed a significant association between reduced levels of TNF-α, within hours of fracture, with poorer bone healing outcome and incomplete callus formation in children (449). Collectively, these studies highlight the dose-dependent and spatiotemporal nature of the pleiotropic effects of TNF-α on bone repair. The sensitivity or response of osteoblast lineage cells to TNF-α is likely dependent on the physiological environment and differentiation state of the target cell. Whether TNF-α acts as a pro-osteogenic signal in bone repair remains unclear. Models which allow for live imaging of the spatiotemporal dynamics of *TNF-α,* as well as pharmacological and genetic manipulation of *TNF-α,* will help to further elucidate the net contribution of this pleiotropic cytokine on bone repair.

5.1.5 ZEBRAFISH AS A MODEL FOR STUDYING THE ROLE OF TNF-α ON BONE REPAIR AND REGENERATION

Given their comparable skeletal physiology to humans, ease of use for live imaging adult bone and amenability to pharmacological and genetic manipulation, zebrafish could provide an excellent model for further characterising the paradoxical effects of TNF-α on bone (1). The TNF superfamily of proteins is well conserved in fish; zebrafish possess gene homologs for key ligands such as *tnfα, tace*, *trail* and *rank-l,* as well as receptors *tnfr1* (*tnfrsf1a*) and *tnfr2* (*tnfrsf1b*) (450). Both human and zebrafish genes encoding TNF-α are comprised of 4 exons, with around 80% of the mature RNA encoded by the fourth exon (401, 450). The translated zebrafish Tnf-α protein shares only 30% sequence similarity with humans, forming a trimer which is unique in structure from mammalian TNF-α (451). However, the location of the TNFR1 binding site in zebrafish Tnf-α is conserved, associating with human TNFR1 via the same residues (451). Tnf-α is also functionally comparable to the human homolog, with known roles in immunity, inflammation, facilitating angiogenesis and governing effective tissue repair and regeneration (238, 240, 272, 275, 452).

A number of useful zebrafish lines are available for studying the relationship between Tnf-α and bone. The *tnfα:GFP* transgenic line, often used in combination with *mpeg1:mCherry* line (immune cells), allows for the dynamic visualisation of *tnfα in vivo* (Table 4, (245, 272)). Moreover, the *osx:mCherry-ntr* zebrafish line allows for controlled ablation of osteoblasts via the addition of a pro-drug to trigger nitroreductase-mediated apoptosis (Table 4, (212)). Osteoblast apoptosis via laser ablation is known to trigger the recruitment of pro-inflammatory macrophages which support larval bone regeneration (234). Therefore,

genetic ablation of osteoblasts using this line may be used to investigate the effect of Tnf-α on bone regeneration. Recently, Keatinge *et al*., generated a stable *tnfα* mutant via CRISPR, which lacks the functional Tnf-α protein (274). This line can be used to study osteoblast activity and bone repair dynamically, in the absence of Tnf-α.

The dynamic expression of *tnfα* by pro-inflammatory macrophages is known to support bone (operculum) and fin regeneration in larval zebrafish (234, 453); however, the role of Tnf-α in adult zebrafish bone repair and regeneration has not been studied. Understanding the basic biology of Tnf-α signalling in bone repair may have implications for the increasing number of patients receiving TNF targeting therapies (416). Moreover, this may reveal clinical applications for the use of TNF therapeutics to improve fracture healing.

Therefore, in this chapter, I aimed to:

1. Define the spatiotemporal dynamics of *tnfα* expression in fractured or regenerating bone in the zebrafish caudal fin.
2. Characterise the source and recipient cells of Tnf-α in bone repair and regeneration.
3. Investigate the effects of pharmacological and genetic suppression of *tnfα* on bone repair and regeneration.
4. Explore the suitability of *ex vivo* zebrafish scale culture as a model for studying the effect of Tnf-α on osteoblasts.

5.2 RESULTS: TNF-α IN BONE REGENERATION AND REPAIR

5.2.1 *TNFα IS* EXPRESSED BY BONE DURING FRACTURE REPAIR

Tnf-α is a major pro-inflammatory cytokine which has poorly characterised, pleiotropic effects on bone (38). The role of Tnf-α in adult bone repair in zebrafish has not been studied. Therefore, I first sought to characterise the expression of *tnfα* post-fracture in the zebrafish caudal fin. Fractures were induce in the caudal fins of adult *tnfα:GFP;mpeg1:mCherry* zebrafish (Table 4 (245, 272)); this line is commonly used to stratify M1 and M2 populations of macrophages, based on the expression of *tnfα* (238, 240). However, in adult zebrafish, *mpeg1* may also be expressed by other cell types, such as B cells (249), lymphocytes (248) and even macrophage-derived osteoclasts (2, 428). Fractures were live imaged between 0-7 days post injury (dpi) and representative images shown in Figure 36 A. Immediately after injury (0 dpi), no *mpeg1*$^{+}$ cells are present at the fracture site, with few *mpeg1*$^{+}$ cells in the surrounding tissue expressing *tnfα*. At 1 dpi, *mpeg1*$^{+}$ cells, likely macrophages, have infiltrated the fracture site; expression of *tnfα* is restricted to *mpeg1*$^{+}$ cells in and around the fracture (white arrowheads). Strikingly, at 2 dpi, *tnfα* is expressed at high levels in the bone tissue, directly adjacent to the fracture site (yellow arrowheads), whilst high numbers of *tnfα*$^{+}$*:mpeg*$^{+}$ immune cells remain at, or around, the fracture site (white arrowheads). Between 4-7 dpi, levels of *tnfα:*GFP in both bone and *mpeg1*-expressing cells, decreases. Levels of *tnfα:*GFP at the injury site were quantified relative to uninjured bone in the same fin (intensity ratio) and analysed (Figure 36 B). Significantly higher levels of *tnfα:*GFP were measured at 1 and 2 dpi, compared to 0 dpi. Higher levels of *tnfα:*GFP correspond to the time points where not only inflammatory immune cells are recruited to the fracture (Section 3.2.7), but also where cells within the inured bone itself upregulate *tnfα* expression (Figure 36 A, 2 dpi).

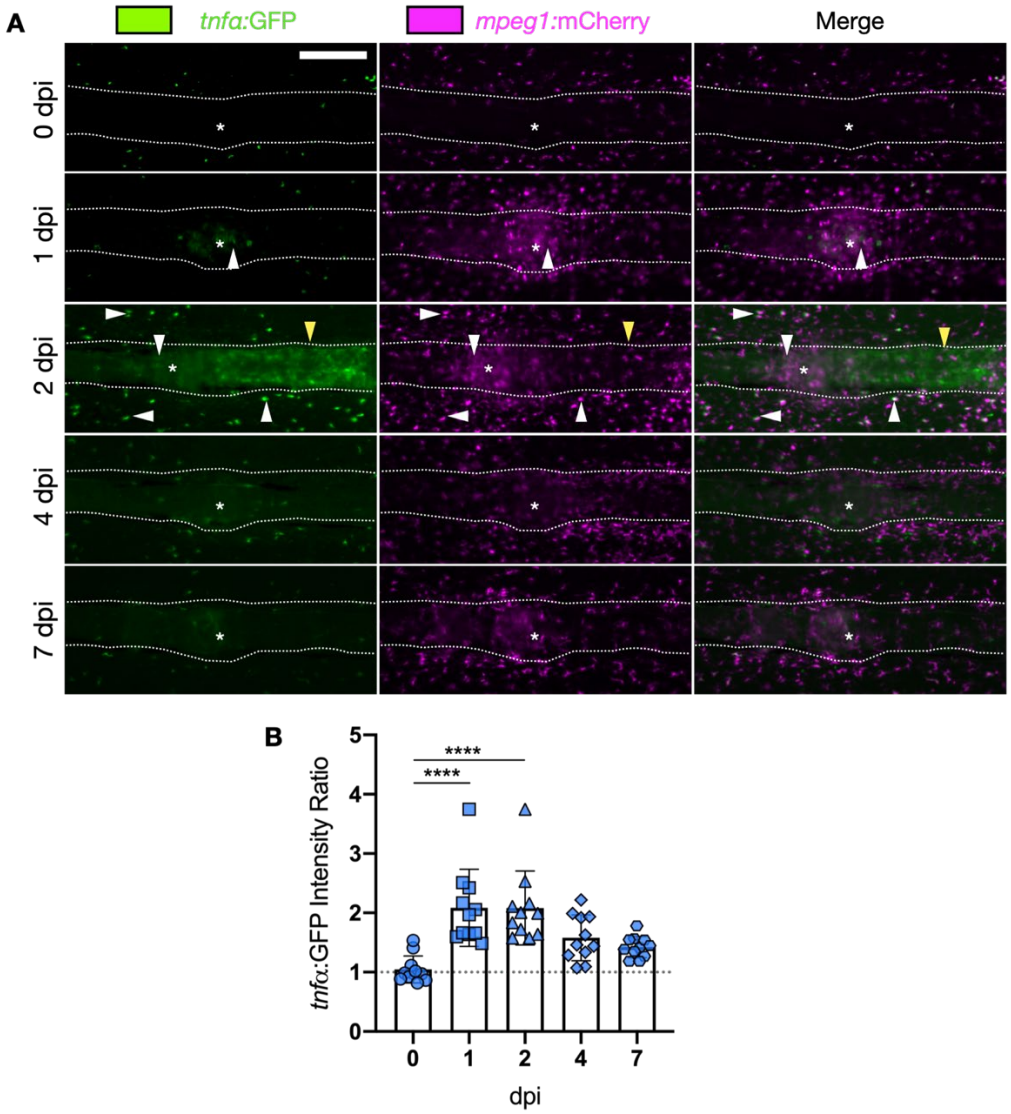

Figure 37. tnfα is Expressed by Bone Post Fracture in Zebrafish. *The caudal fins of adult tnfα:GFP; mpeg1:mCherry zebrafish were fractured and imaged between 0 – 7 days post-injury (dpi).* ***A:*** *At 0 dpi, low numbers of mpeg1⁺ immune cells are observed around the bone in the caudal fin; no tnfα:GFP is observed in the bone, with few mpeg1⁺· cells co-expressing tnfα:GFP (white arrowheads). Upon injury mpeg1⁺ immune cells are recruited to the fracture by 1 dpi. At 2 dpi, pro-inflammatory mpeg1⁺ tnfα⁺ immune cells remain high in number (white arrowheads). However, bone distal to the fracture site also expresses tnf-α:GFP at 2 dpi (yellow arrowhead). Expression of tnfα:GFP in both bone and mpeg1⁺ immune cells is reduced by 4 dpi. Dotted line = bone outline, asterisk (*) = centre of fracture, scale bar = 200 μm.* ***B:*** *Levels of tnfα:GFP were measured, relative to uninjured bone in the same fin (intensity ratio). A significant increase in the intensity ratio of tnfα:GFP at both 1 and 2 dpi were measured compared to 0 dpi. N = 11, points represent mean (± SD). **** = p < 0.001.*

5.2.2 *TNFα* EXPRESSION PATTERNS BONE REGENERATION POST AMPUTATION IN THE ADULT ZEBRAFISH CAUDAL FIN

In addition to fracture repair (2, 147), zebrafish are capable of complete bone regeneration after fin amputation in just 2 weeks (1). However, the proliferation and differentiation of *osx*$^{+}$ osteoblasts is common to both processes in zebrafish, with bone tissue adjacent to fractures expressing blastema markers (197). Given that *tnfα* is expressed by bone post-fracture (Figure 36), I next assessed *tnfα* expression within the blastema of regenerating zebrafish caudal fins. Fins were amputated from adult transgenic zebrafish expressing either *tnfα:GFP;osx:mCherry*, or *tnfα:GFP* alone (Table 4, Figure 37). Single transgenic *tnfα:GFP* zebrafish were stained in Alizarin red, prior to injury and each imaging time point, to label mineralised bone. Regenerating fins were imaged at regular time points between 0-14 days post amputation (dpa) (Figure 37). At 0 dpa, *tnfα:*GFP levels in the fin appear low, restricted to few immune cells (GFP^{+} punctae) in the ontogenetic tissue (Figure 37 A & B). From just 2-6 dpa, high levels of *tnfα:*GFP can be observed at the distal end of the blastema, ahead of both osteoblasts (Figure 37 A), and mineralised bone (Figure 37 B), in the blastema. Some colocalization between *osx*:mCherry and *tnfα*:GFP is observed at the boundary between the two populations of cells, at 4 and 6 dpa (Figure 37 A). By 10 dpa, levels of *tnfα*:GFP reduced, with few cells in and around the regenerating bone expressing *tnfα*. Levels of *tnfα:*GFP in regenerating bone within the blastema were quantified relative to uninjured bone in the same fin (intensity ratio) and analysed (Figure 37 C). Significantly higher levels of *tnfα:*GFP were measured at 2 and 4 dpa, but not 6 dpa, compared to uninjured bone (Figure 37 C). Collectively, this suggests that Tnf-α has a pro-osteogenic role in both early caudal fin fracture repair (Figure 36), and early bone regeneration post-amputation (Figure 37), in zebrafish. This also suggests that *tnfα* may be expressed by differentiating osteoprogenitor cells during early fin regeneration, to promote osteogenic differentiation. Given the higher numbers of *tnfα* expressing cells in regenerating bone tissue, proceeding experiments focussed primarily on *tnfα* in regenerating bone. Regenerating tissue would allow for higher yields of *tnfα:GFP*$^{+}$ cells, from fewer animals, for more in-depth analysis of the effect of Tnf-α in osteoblast differentiation.

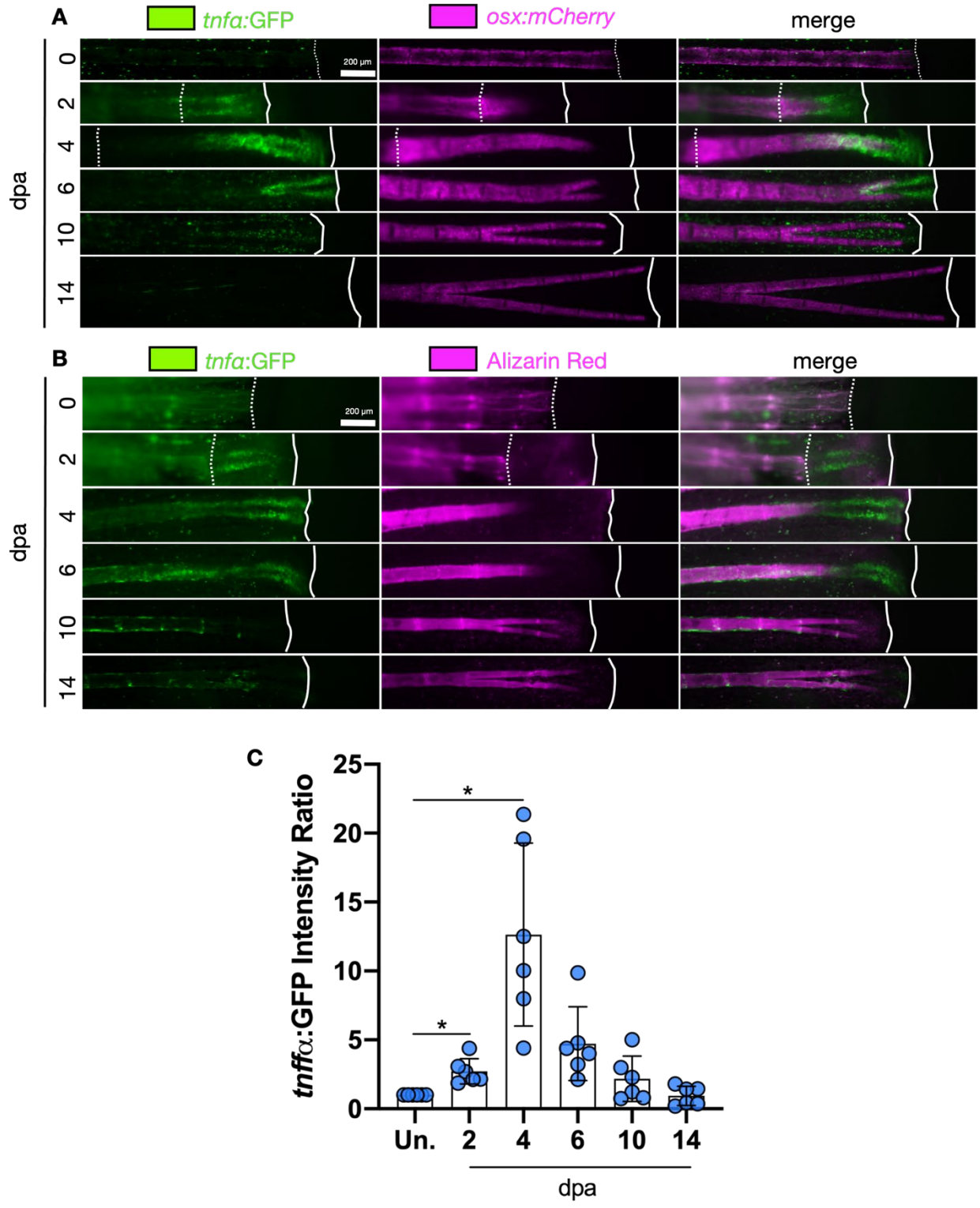

Figure 38. tnfα Expression Patterns Bone Regeneration in The Adult Zebrafish Caudal Fin Post Amputation. A: The caudal fins of adult tnfα:GFP; osx:mCherry zebrafish were amputated and imaged

between 0–14 days post-amputation (dpa). As bone regeneration commences, the tnfα:GFP can be observed distal to the amputation site and osx:mCherry between 2-6 dpa, appearing brightest at 4 dpa. By 10 dpa, few tnfα:GFP⁺ punctae can be observed around the distal end of the regenerating bone, reducing completely by 14 dpa. ***B:*** *Adult tnfα:GFP zebrafish were live stained with Alizarin red to label calcified bone, before their caudal fins were amputated and imaged between 0-14 dpa. Zebrafish were restained in Alizarin red prior to each imaging point to label any newly calcified bone. High levels of tnfα:GFP are observed distal to the amputation site, and distal to calcified bone in the regenerating fin, between 2-6 dpa.* ***A-B:*** *Dotted line = amputation site, solid line = edge of regenerating blastema, scale bar = 200 μm.* ***C:*** *Levels of tnfa:GFP in the regenerating blastema were measured, relative to uninjured bone in the same fin (intensity ratio). A significant increase in the intensity ratio of tnfα:GFP at both 2 and 4 dpa were detected compared to uninjured fins. N = 6. points represent mean (± SD), * = p < 0.05.*

5.2.3 *TNFα, RUNX2A AND TNFRSF1B* ARE EXPRESSED DURING OSTEOGENESIS IN THE REGENERATING ZEBRAFISH FIN

Since the expression of *tnfα* patterns bone regeneration in the zebrafish caudal fin, I next performed combined whole mount immunohistochemistry and *in situ* hybridisation on fixed uninjured and regenerating fins (at 2, 4 and 6 dpa), to visualise the expression of *tnfα:GFP* relative to *osx*⁺ osteoblasts and *runx2a* (Figure 38). Runx2 is a transcription factor, expressed by immature differentiating osteoblasts (193). Whole-mount *in situ* hybridisation was used to detect *runx2a* as GFP and mCherry transgenics (*osx* and *tnfα*) were already in use, and antibodies for Runx2 did not work for wholemount immunohistochemistry. As expected, levels of *tnfα*:GFP and *runx2a* are low in uninjured bone, with homeostatic expression of *osx*:mCherry by osteoblasts (Figure 38 A). However, at 2 dpa, the number of *tnfα*:GFP⁺ cells within the blastema increases, and increased levels of *osx:*mCherry and *tnfα*:GFP can be observed within some osteoblasts along the edge of the amputation site (yellow arrowheads, Figure 38). By 4 dpa, many bright, *tnfα*:GFP⁺ cells are visible within the regenerating bone; a number of these cells also strongly express *osx* (yellow arrowheads, Figure 38 A*). Levels of *runx2a* are also high within this region at 4 dpa, compared to uninjured bone, but are highest in the areas where lower levels *osx:*mCherry and *tnfα*:GFP can be observed. This suggests that *tnfα* is expressed as *runx2a*⁺ osteoblast precursor cells mature into *osx*⁺ osteoblasts. By 6 dpa, some GFP⁺ osteoblasts remain (yellow arrowheads). However, levels of *tnfα*:GFP throughout the

regenerating bone had reduced, whilst levels of *osx*:mCherry and *runx2a* remained high. The Pearson's coefficient was quantified as a measure of the colocalization between *tnf*:GFP and *osx*:mCherry in uninjured and regenerating fins (Figure 38 B), where 1 represents perfect colocalization, and 0 represents stochastic overlap between channels. High variability between replicates was observed for uninjured fins, and regenerating fins, at 6 dpa. The mean Pearson's coefficient for *tnfα*:GFP and *osx*:mCherry increased at 2, 4 and 6 dpa, compared to uninjured bone. However, this increase was only statistically significant at 4 dpa (Figure 38 B).

TNF-α signals via two major receptors (TNFR1 and TNFR2), with pleiotropic downstream effects (Figure 35) (387). Both of these receptors are conserved in zebrafish (450); Tnfr2, the Tnf-α receptor associated with cell proliferation and survival, is encoded by *tnfrsf1b* (454, 455). Therefore, further whole mount immunohistochemistry and *in situ* hybridisation was performed on fixed uninjured and regenerating fins (at 2 and 4 dpa), to visualise the expression of *tnfα:GFP* relative to *osx*$^{+}$ osteoblasts and *tnfrsf1b* (Figure 39). In uninjured bone, low levels of *tnfα*:GFP and *tnfrsf1b* are observed, with low levels of *osx*:mCherry present in osteoblasts. Consistent with previous immunostaining data (Figure 38), *tnfα*:GFP is present within some *osx*:mCherry^{+} osteoblasts (yellow arrowheads, Figure 39), at 2 and 4 dpa, as well as some *osx*:mCherry^{-} cells. Some of these *tnfα*:GFP^{+} only cells are likely immune cells, due to their morphology (dotted box, Figure 39). However, most appear round and morphologically similar to osteoblast precursors in regenerating bone. Interestingly, increased expression of *tnfrsf1b* can be observed in dense areas of *osx*:mCherry^{+} osteoblasts in the regenerating bone, at both 2 and 4 dpa (Figure 39). This suggests that Tnf-α may promote osteogenic differentiation via Tnfr2 in regenerating bone.

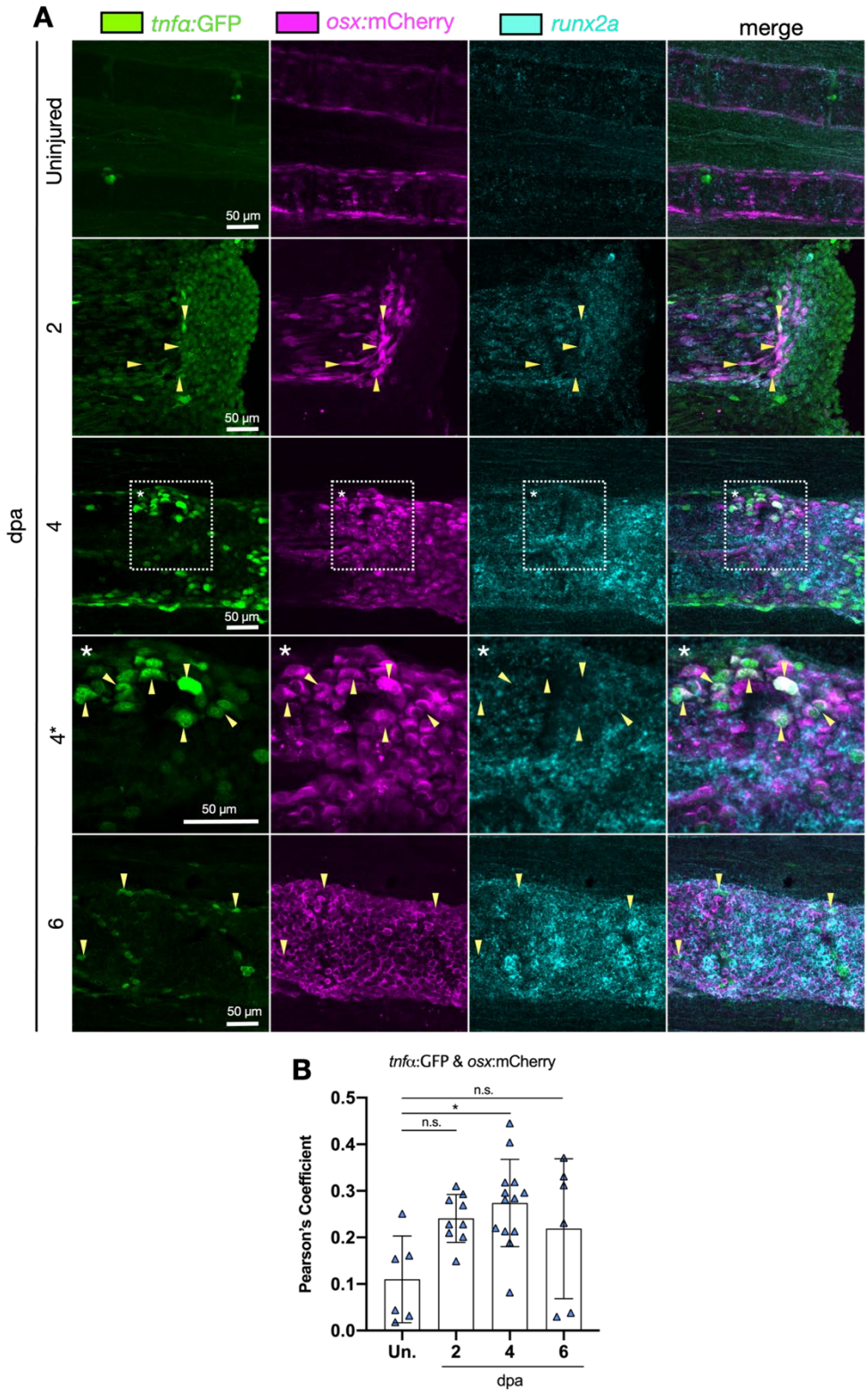

Figure 39. Osteoblasts Co-Express tnfα:GFP and osx:mCherry in the Regenerating Fin. *The caudal fins of adult tnfα:GFP; osx:mCherry zebrafish were amputated. Between 2 – 6 days post-amputation*

(dpa), regenerating fins were re-amputated and fixed. Whole mount in situ hybridisation to detect runx2a expression, and immunohistochemistry to detect tnfα:GFP and osx:mCherry, were performed. ***A:*** *In uninjured bone, the presence of tnfα:GFP and runx2a are almost undetectable, whilst homeostatic levels of osx:mCherry^{+} in osteoblasts are observed. At 2 dpa, runx2a expression increases and increased levels of tnfα:GFP are observed in the blastema. Bright osx:mCherry^{+} osteoblasts begin to populate the blastema, adjacent to the amputations site; some of these osteoblasts express tnfα:GFP (yellow arrowheads). By 4 dpa, a large increase in runx2a expression, tnfa:GFP and osx:mCherry can be observed in the regenerating fin, with some osx:mCherry^{+} osteoblasts co-expressing tnfα:GFP (yellow arrowheads). At 6 dpa, expression of runx2a and osx:mCherry remain high, as bone regenerates; expression of tnfα:GFP has reduced, with few cells within the bone still staining positive.* ***B:*** *The Pearson's coefficient was calculated as a measure of colocalization between tnfα:GFP and osx:mCherry for each time point. A significant increase in the Pearson's coefficient was observed at 4 dpa, compared to uninjured bone tissue, but not any other time point. N≥6, points represent mean (± SD), n.s = no significant difference, * = p < 0.05.*

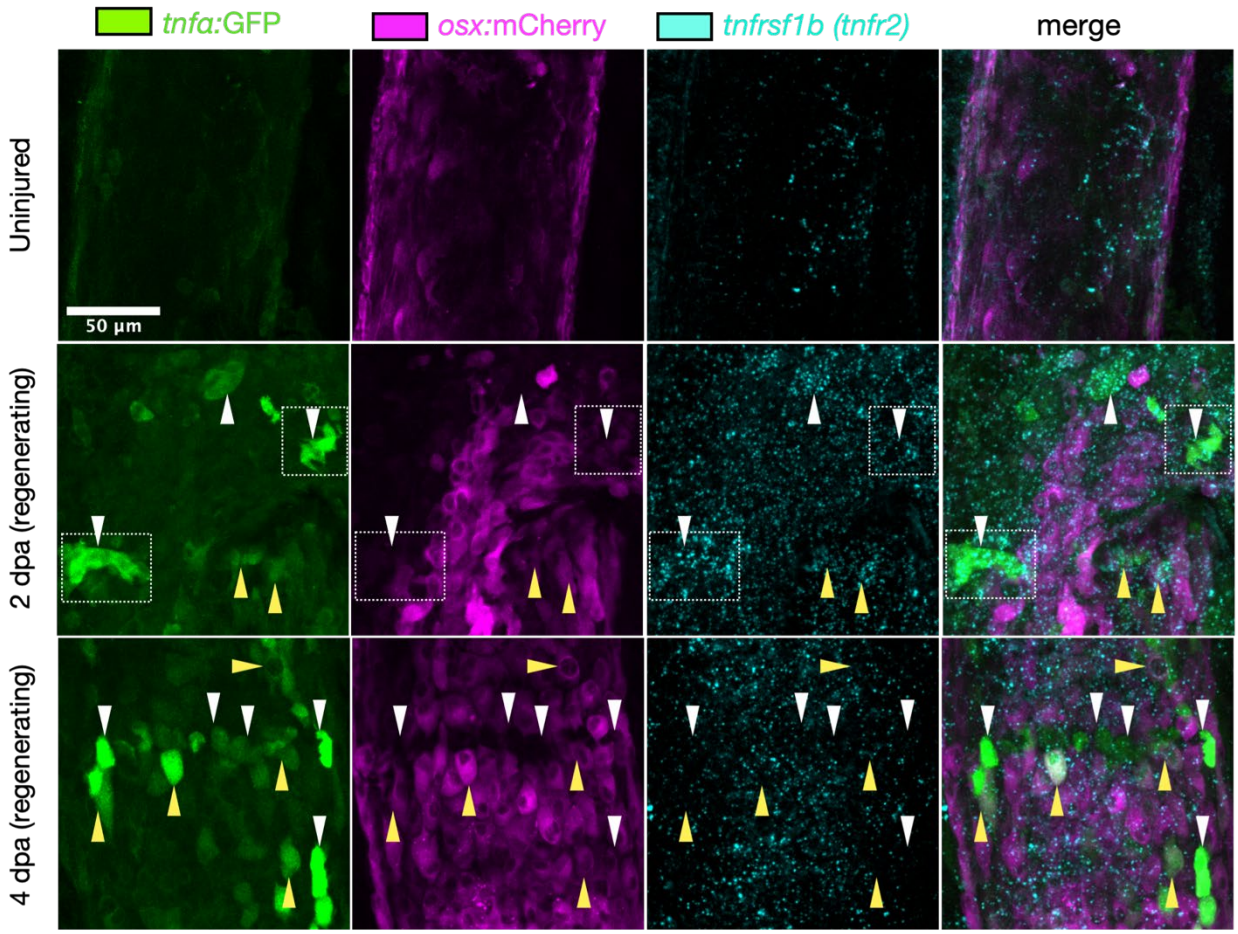

Figure 40. Expression of tnfrsf1b (tnfr2) Increases Alongside tnfα: GFP Levels in Regenerating Bone Within the Zebrafish Fin. *The caudal fins of adult tnfα:GFP; osx:mCherry zebrafish were amputated. Between 2 – 4 days post-amputation (dpa), regenerating fins were re-amputated and fixed. Whole mount in situ hybridisation to detect tnfrsf1b (tnfr2) expression, and immunohistochemistry to detect tnfα:GFP and osx:mCherry, were performed. In uninjured bone, the presence of tnfα:GFP is almost undetectable, levels of tnfrsf1b are low and homeostatic levels of osx:mCherry⁺ in osteoblasts are observed. At 2 dpa, tnfrsf1b expression increases as levels of tnfα:GFP increase in the blastema. osx:mCherry⁺ cells (osteoblasts) begin to populate the blastema, adjacent to the amputations site; tnfα:GFP is expressed by some osteoblasts (white arrowheads), but is more bright in osx:mCherry⁻ cell types (yellow arrowheads). At 4 dpa, a tnfrsf1b expression remains high compared to uninjured bone. tnfα:GFP and osx:mCherry can be observed in the regenerating fin, with more osx:mCherry⁺ osteoblasts co-expressing tnfα:GFP compared to 2 dpa (white arrowheads). However, bright tnfα:GFP cells, negative for osx:mCherry, are also present (yellow arrowheads), some of which appear morphologically to be immune cells (dotted boxes).*

Collectively, these experiments suggest that *tnfα* may be expressed by osteoblast precursors, in the zebrafish blastema. Moreover, this suggests that Tnf-α may promote the proliferation and differentiation of osteoblasts in regenerating bone. The expression of *tnfrsf1b* in the regenerating bone suggests that Tnf-α expressed by osteoblast lineage cells in the regenerating fin acts in an autocrine or paracrine manner to regulate osteoblast proliferation and differentiation. Further transcriptomic characterisation of *tnfα*-expressing and Tnf-α responding cells within the early blastema is required to further elucidate the molecular pathways underpinning the role of Tnf-α patterning in osteoblast differentiation and bone regeneration.

5.2.4 FLUORESCENCE ACTIVATED CELL SORTING (FACS) FOR ISOLATION OF *TNFα* EXPRESSING CELLS FROM REGENERATING FINS

Heterogenous populations of *tnfα*-expressing and Tnf-α responsive cells are present in regenerating bone (Figure 38, Figure 39); the roles of these in bone regeneration are likely to vary dynamically depending on the cell type, the number of days post-amputation and the position of the cells in the blastema. Further characterisation of these GFP$^+$, *osx*:mCherry$^+$ and double positive cell populations via transcriptomic analyses, such as RNA sequencing (RNA-seq) or single cell RNA-seq (scRNA-seq), will help to discern the key pathways in regenerating osteoblasts which are influenced by Tnf-α signalling, and whether this signalling occurs in an autocrine or paracrine manner. Thus, I next performed FACS on cells dissociated from the uninjured and regenerating fins of *tnfα:GFP; osx:mCherry* zebrafish (Table 4, Figure 40), with the aim to isolate high-quality RNA from each population for transcriptomic analyses. Figure 40 A-C shows representative contour plots of discrete cell populations within the uninjured fin (A) or blastema at 4 (B) or 6 (C) dpa. Cells were gated as either double negative (grey), *tnfα*:GFP$^+$ (green), *osx*:mCherry$^+$ (magenta) or double positive (orange), expressing both *tnfα*:GFP and *osx*:mCherry. Each population of cells was quantified as a percentage of the total number of live cells (Figure 40 D-F). A high proportion of the total number of live cells were double negative, for each condition. The mean proportion of *osx*:mCherry$^+$ cells increased in the blastema at 4 and 6 dpa, compared to uninjured bone, though not significantly (Figure 40 D). As expected, the proportion of *tnfα*:GFP$^+$ cells in uninjured fins were consistently low; the proportion of *tnf*:α:GFP$^+$ cells increased significantly at both 4 and 6 dpa (Figure 40 E). However, the proportion of cells within this population showed high variability between replicates at 4 dpa. Surprisingly, though the mean proportion of double positive cells was higher in regenerating fins at both 4 and 6 dpa, there was no

significant increase compared to uninjured fins (Figure 40 F). However, the proportion of double positive cells was consistently higher at 4 dpa, with little variability between replicates, whereas this was far more variable in uninjured and regenerating fins at 6 dpa (Figure 40 F). Cells were sorted directly into RNA isolation buffer, and a number of different RNA extraction and clean up methods applied. However, the isolation of sufficient high quality RNA could not be achieved from these sorts (data not shown).

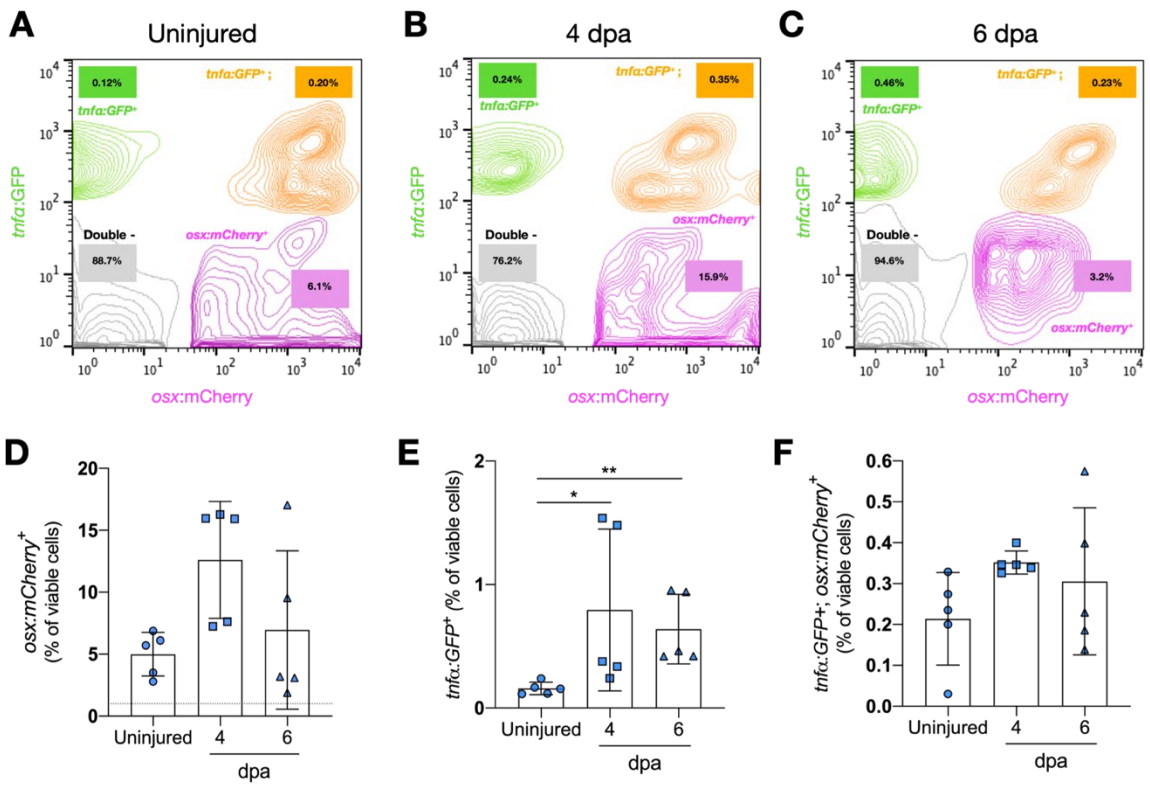

Figure 41. Fluorescence Activated Cell Sorting (FACS) of Uninjured and Regenerating Fin Tissue Shows Small Population of tnfα:GFP and osx:mCherry Double⁺ Cells. Uninjured and regenerating fins were harvested from tnfα:GFP; osx:mCherry, and cells dissociated for FACS. **A-C:** Plots of cells from uninjured (A) and injured caudal fins at 4 (B) and 6 (C) days post amputation (4 dpa) show a population of osx:mCherry⁺ cells, with varying intensities of mCherry. Small populations of tnfα:GFP⁺ and double⁺ cells are also observed in the uninjured transgenic. The majority of cells within the fin are double-. **B:** At 4 days post amputation (4 dpa), as bone regeneration progresses an increase in the populations of osx:mCherry⁺, tnfα:GFP⁺ and double+ cells is observed. **C:** At 6 dpa, all 3 populations are observed, but the proportion of osx:mCherry⁺ and double+ cells appears to decrease again. **D-F:** Quantification of the populations of osx:mCherry⁺ (D), tnfα:GFP+ (E) and double+ (F) cells in uninjured and injured (4 and 6 dpa) fins are plotted as a proportion of the total number of viable cells. **D:** An Increase in the mean proportion of osx:mcherry⁺ cells can be observed at 4 and 6 dpa, compared to uninjured fin, however, there is no statistically significant difference. **E:** A significant increase in the proportion of tnfα:GFP+ cells are observed at 4 and 6 dpa, compared to uninjured fins. **F:** A slight increase in the mean proportion of double⁺ cells are observed at 4 and 6 dpa, compared to uninjured fin, however, there is no statistically significant difference. * = $p < 0.05$, ** = $p < 0.01$, $N = 5$, points represent mean (± SD).

5.2.5 PARTIAL INHIBITION OF *TNFα* EXPRESSION SHOWS VARIABLE EFFECTS ON BONE REGENERATION

Given that *tnfα* expression patterns bone regeneration in the zebrafish blastema, I next sought to determine the effect of Tnf-α inhibition on this process. The compound pomalidomide, an analog of thalidomide, is a potent and non-teratogenic inhibitor of TNF-α production, proven effective in larval and embryonic zebrafish (258, 275, 456). Current evidence suggests that pomalidomide represses the translation TNF-α mRNA into protein by binding to the 3' untranslated region of TNF-α mRNA, leading to transcript degradation (457). Therefore, *tnfα:GFP; osx:mCherry* zebrafish were treated with either 200 μM pomalidomide or an equivalent volume of DMSO for 24 hours prior to fin amputation. Treatment was continued for 14 days post amputation and refreshed daily. Fins were live imaged at regular time points post amputation, to study the effect of Tnf-α inhibition on osteoblasts and bone regeneration in the blastema (Figure 41 and Figure 42).

Representative images of regenerating lepidotrichia (bone rays) from DMSO treated and pomalidomide treated (Pom) zebrafish between 0-14 dpa are shown (Figure 41 A). Due to variable effects of pomalidomide treatment, images from two pomalidomide treated zebrafish are shown. In DMSO treated zebrafish, the normal expression of *tnfα*:GFP and *osx*:mCherry can be observed throughout (as previously described, Figure 37), with *tnfα*:GFP expressed during early bone regeneration. Most pomalidomide treated zebrafish displayed normal bone regeneration (3 / 4), comparable to DMSO treated zebrafish (Pom 1, Figure 41 A). However, one pomalidomide treated zebrafish (Pom 2) showed a visible reduction in the levels of *tnfα*:GFP at the distal end of the blastema. Interestingly, in regions where *tnfα*:GFP levels appeared lower, osteoblasts did not populate the blastema and bone failed to regenerate (Pom 2, Figure 41 A). Levels of *tnfα*:GFP and *osx*:mCherry were quantified in the middle (mid) and lateral regions of the blastema (Figure 41 B-C). The fluorescence intensities of *tnfα*:GFP and *osx*:mCherry were measured in each region, relative to the fluorescence intensity in uninjured tissue in the same fin (intensity ratio) (Figure 41 D-G). The mean intensity ratios of *tnfα*:GFP in Pom treated zebrafish appear lower between 2-6 dpa, compared to the DMSO group; *tnfα*:GFP levels were significantly lower in Pom treated fish at 2 (lateral) and 6 (mid) dpa, compared to the DMSO group (Figure 41 D-E). This suggests that 200 μM pomalidomide treatment partially inhibits Tnf-α production during bone regeneration. Mean intensity ratios of *osx*:mCherry in Pom treated zebrafish appear lower between 4-10 dpa, compared to the DMSO group; however, no significant difference in *osx*:mCherry intensity ratios were detected at any time point, suggesting that partial inhibition

of Tnf-α with 200 μM pomalidomide is insufficient to induce gross changes to osteoblasts during zebrafish fin regeneration.

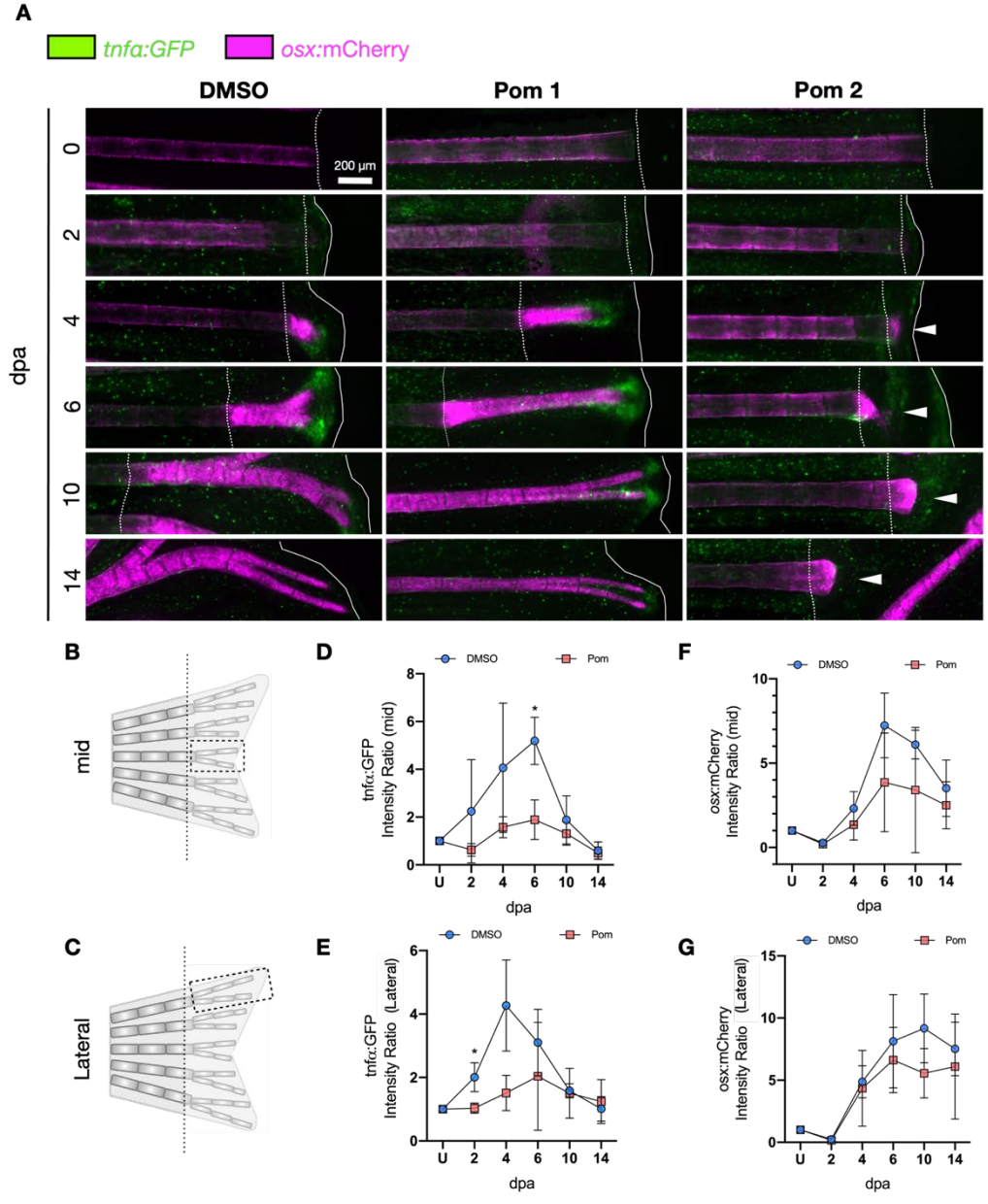

Figure 42. Pomalidomide Treatment Results in Varied Effects On Bone Regeneration in the Adult Caudal Fin. *tnfα:GFP; osx:mCherry zebrafish began treatment via immersion with 200 μM pomalidomide (Pom), or an equivalent volume of DMSO, from 24 hours prior to caudal fin amputation. Uninjured (U) caudal fins were imaged prior to amputation. Regenerating caudal fins were then imaged between 0-14 days post amputation (dpa). Drug treatments were refreshed every 24 hours throughout the*

time course. ***A:*** *Representative images of lepidotrichia (bone rays) from DMSO and Pom treated zebrafish during fin regeneration are shown. Images from 2 separate Pom treated fish are shown due to variability between individuals. Expression of tnfα can be observed distally to the expression of osx by osteoblasts in the regenerating fin, in DMSO and most Pom treated fish (Pom 1). However, in one Pom treated zebrafish (Pom 2), there was a visible reduction in the levels of tnfα:GFP in the regenerating fin, where bone regeneration did not proceed as normal; in these regions, levels of osx:mCherry remained low and osteoblasts did not form a new bone ray (arrowheads).* ***B-C:*** *Schematics of caudal fins showing amputation point (dotted line) mid (B) and lateral (C) regions where osx:mCherry and tnfα:GFP levels were quantified in the regenerating fin (dotted box).* ***D-G:*** *The fluorescence intensities of tnfα:GFP (D-E) and osx:mCherry (F-G) were measured in the mid (D & F) and lateral (E & G) regions of the regenerating fin, relative to the fluorescence intensity in uninjured tissue in the same fin (intensity ratio).* ***D-E:*** *Mean intensity ratios of tnfα:GFP in Pom treated zebrafish appear lower between 2-6 dpa, compared to the DMSO group; tnfα:GFP levels were significantly lower in Pom treated fish at 2 (lateral) and 6 (mid) dpa, compared to the DMSO group.* ***F-G:*** *Mean intensity ratios of osx:mCherry in Pom treated zebrafish appear lower between 4-10 dpa, compared to the DMSO group; however, no significant difference in osx:mCherry intensity ratio was detected at any time point. * = $p < 0.05$, N = 4 per treatment group, points represent mean (± SD).*

The effect of pomalidomide treatment on total fin tissue regeneration was also measured, as dynamic production of Tnf-α is known to control fin regeneration in larval zebrafish (275). Representative images of whole regenerating fins from DMSO treated and pomalidomide treated (Pom 1 and 2) zebrafish between 0-14 dpa are shown (Figure 42 A). In pomalidomide treated zebrafish, whole fin tissue regeneration appeared comparable to DMSO treated zebrafish. However, failure to regrow several lepidotrichia, in regions where *tnfα:*GFP levels were reduced, can be observed in one individual (Pom 2, white arrowheads, Figure 42 A-B). Other lepidotrichia in the fin did regenerate (Pom 2, yellow arrowheads, Figure 42 A-B). However, these bones grew aberrantly, extending laterally, instead of distally. The osteoblasts within these aberrant regenerating lepidotrichia extended towards areas with high levels of *tnfα:*GFP in the distal end of the blastema throughout regeneration (Figure 42 B). Total fin tissue regeneration was quantified in two ways: the total area of regenerated fin tissue was quantified as a proportion of the pre-amputated tissue area (% area regeneration, Figure 42 B) and the length of regenerated fin tissue was measured along the dorsal periphery of the fin and quantified as a proportion of the pre-amputated length (% length regeneration Figure 42 C). No difference in total fin regeneration (% area or length) was observed as a result of pomalidomide treatment at any time point post amputation (Figure 42 B-C).

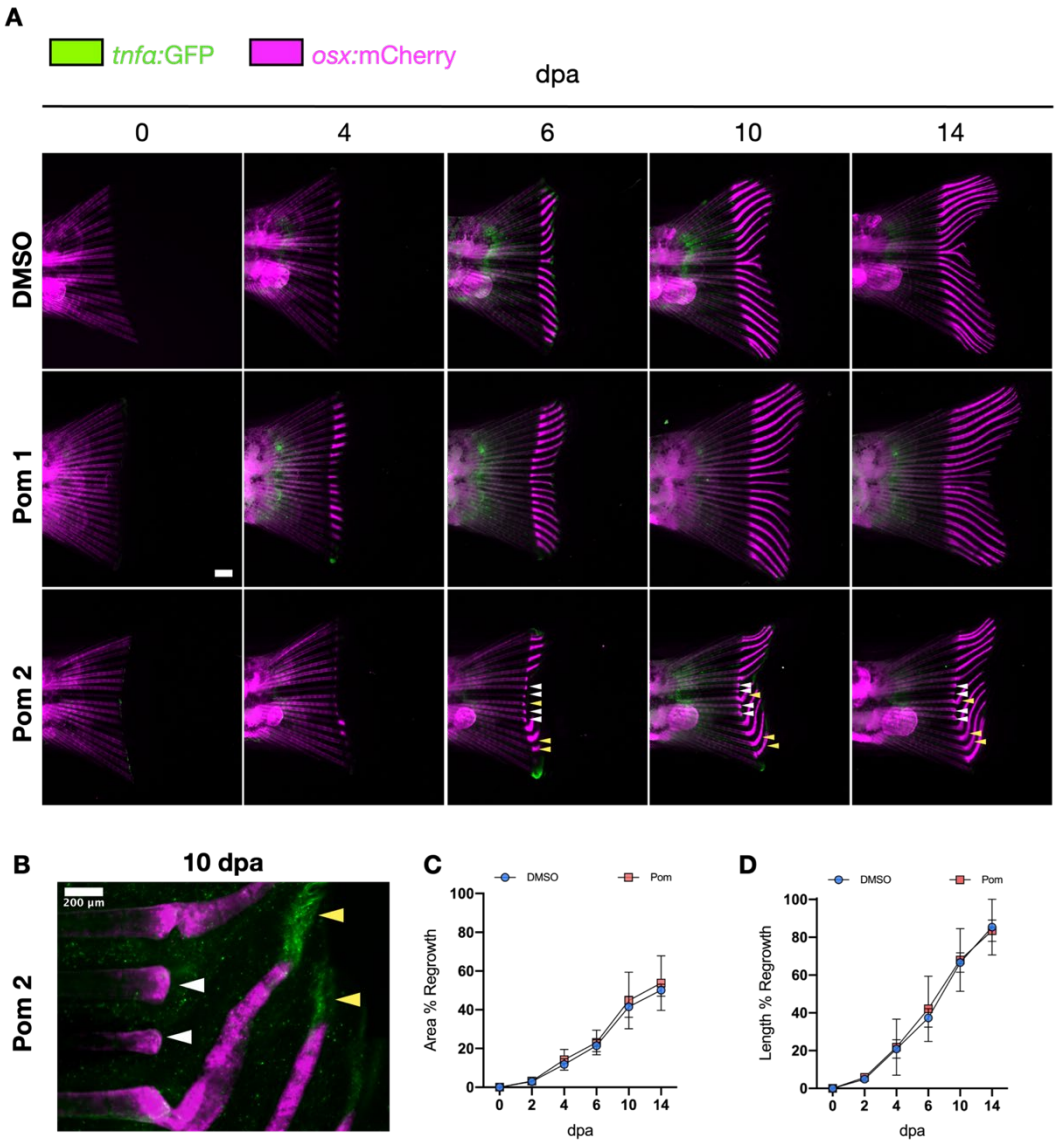

Figure 43. Pomalidomide Treatment Does Not Significantly Affect Total Fin Tissue Regeneration in Adult Zebrafish. *tnfα:GFP; osx:mCherry zebrafish began treatment via immersion with 200 μM pomalidomide (Pom), or an equivalent volume of DMSO, from 24 hours prior to caudal fin amputation. Regenerating caudal fins were imaged between 0-14 days post amputation (dpa). Drug treatments were refreshed every 24 hours throughout the time course.* ***A:*** *Representative images of whole fins of DMSO and Pom treated zebrafish during fin regeneration are shown. Images from 2 separate Pom treated fish are shown due to variability between individuals. In DMSO and most Pom treated zebrafish (Pom 1), fin regeneration proceeds normally, with bright osx:mCherry⁺ lepidotrichia (bone rays) evenly distributed across the new fin tissue. However, in one Pom treated zebrafish (Pom 2), failure to regenerate several lepidotrichia can be observed between 4-14 dpa (white arrowheads), in*

regions where tnfα:GFP levels appeared low at 4 dpa, compared to DMSO and Pom 2. Other lepidotrichia in Pom 2 were malformed during regeneration (yellow arrowheads). Scale bar = 1 mm. ***B:*** *Higher magnification image of Pom 2 at 20 dpa showing lepidotrichia which have failed to regenerate (white arrowheads) and aberrant bone regeneration (yellow arrowheads), in which lepidotrichia extend towards high levels of tnfα:GFP in the blastema.* ***C:*** *The total area of regenerated fin tissue was measured and plotted as a proportion of the pre-amputated area (percentage regrowth).* ***D:*** *The length of regenerated fin tissue was measured along the dorsal periphery of the fin and plotted as a proportion of the pre-amputated length (percentage regrowth). B-C: No significant difference in regrowth was measured at any time point post amputation between Pom and DMSO treated zebrafish. N = 4 per treatment group, points represent mean (± SD).*

Treatment of zebrafish with pomalidomide (200 μM) prior to, and throughout, fin regeneration resulted in partial inhibition of Tnf-α, but did not significantly reduce *osx:mCherry* expression, or affect total fin regeneration (Figure 41 and Figure 42). However, visibly reduced *tnfα*:GFP levels in the blastema corresponded with failure of bone regeneration (Pom 2, Figure 41 A and Figure 42 B). Aberrant patterning of bone in Pom 2 further suggests that cells expressing *tnfα*:GFP pattern bone regeneration or differentiate into osteoblasts in the blastema. Collectively, this suggests that reduced expression of *tnfα* in the blastema may result in failure of osteoblasts to regenerate bone. More effective inhibition of Tnf-α via stronger pomalidomide dosage, alternative Tnf-α targeting drugs or genetic approaches could better elucidate the osteogenic influence of Tnf-α during bone regeneration and repair.

5.2.6 STABLE HETEROZYGOUS MUTATION OF *TNFα* HAS NO EFFECT ON BONE REMINERALISATION DURING FIN REGENERATION OF FRACTURE REPAIR

Although partial inhibition of Tnf-α had no significant effect on bone regeneration, anecdotal evidence from one pomalidomide-treated fish suggests that reduced or ectopic expression of *tnfα* perturbs normal bone regeneration (Pom 2, Figure 41 and Figure 42). Genetic approaches, such as CRISPR, could disrupt levels of Tnf-α with higher efficacy and specificity than pharmacological approaches. F0 generations of CRISPR-Cas9 injected embryos display genetic mosaicism of the targeted gene; F0 mosaic zebrafish can be used to rapidly screen for phenotypes due to mutant mRNA expression in some cells, and functional knockdown of wild type (WT) mRNA across the tissue (217, 255, 274). Initially, a range of guide RNAs (gRNAs) targeting exons 1 and 4 of *tnfα* were designed and tested, with the aim to create a mosaic F0 generation using CRISPR-Cas9 mutagenesis. Only one of the gRNAs resulted in mutagenesis, with low efficiency unsuitable for CRISPR knockdown experiments (25%) (Appendix 2). However, concurrently, a stable CRISPR-Cas9 *tnfα* mutant zebrafish line displaying functional loss of Tnf-α became available (274). Therefore, I next sought to establish whether functional loss of Tnf-α, in *tnfα* mutant zebrafish, would affect bone regeneration and repair post injury.

WT and heterozygous *tnfα*$^{+/-}$ zebrafish were live stained in Alizarin red to label calcified bone prior to injury. Uninjured bone in *tnfα*$^{+/-}$ zebrafish appeared morphologically comparable to WT siblings (Figure 43 A). Either amputation or induced fracture injuries were then performed on the caudal fins of WT and *tnfα*$^{+/-}$ zebrafish (Figure 43 and Figure 44, respectively). Zebrafish were live stained in calcein green to label newly formed bone matrix, prior to imaging of the regenerating or fractured bone post injury.

Representative images of uninjured and regenerating (0-14 dpa) lepidotrichia in the caudal fins of WT and heterozygous *tnfα* mutant zebrafish are shown (Figure 43 A). Regenerated mineralised bone matrix is observed in the blastema at around 6 dpa, in both WT and *tnfα*$^{+/-}$ zebrafish. Regeneration of lepidotrichia appears comparable between WT and *tnfα*$^{+/-}$ zebrafish throughout. Mineralised bone in the regenerating fin was quantified by measuring the calcein intensity within lepidotrichia in the middle (mid) and lateral regions of the blastema relative to uninjured bone in the same fin (intensity ratio), as previously described (Figure 43 B-C). At 6 dpa, a higher mean calcein intensity ratio (mid region) was observed in WT zebrafish, compared to *tnfα*$^{+/-}$ zebrafish (Figure 43 B). However, no significant difference in calcein intensity ratios of *tnfα*$^{+/-}$ zebrafish was detected when compared to WT zebrafish, at any time point post amputation, in either region of the blastema (Figure 43 B-C). Moreover, total fin tissue regeneration was measured as previously

described (Section 5.2.5, Figure 42). WT and *tnfα*$^{+/-}$ zebrafish showed no significant difference in total fin regeneration, displaying almost identical percentage areas for fin total regrowth at each time point post amputation (Figure 43 D).

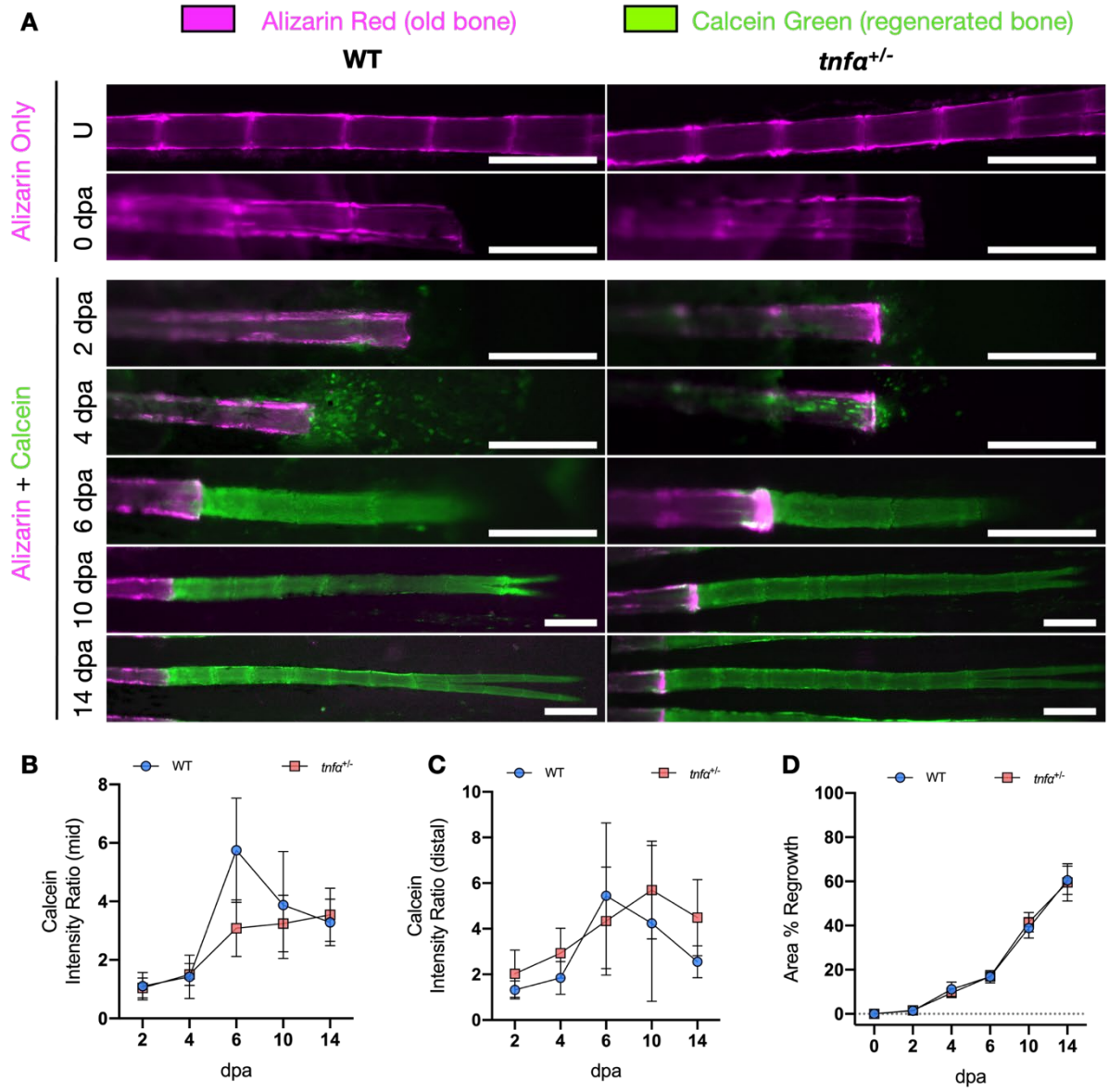

Figure 44. No Effect on Bone Regeneration Is Observed Post Amputation in the Fins of Heterozygous tnfα Mutant Zebrafish. *Uninjured (U) adult wild type (WT) and tnfα*$^{+/-}$ *(heterozygous) zebrafish were live stained in Alizarin red to label calcified bone and their caudal fins imaged, prior to amputation. Fins were re-imaged between 0-14 days post amputation (dpa). Prior to re-imaging, zebrafish were live stained in calcein green to label newly formed bone matrix in the regenerating fin.* ***A:*** *Representative images of bone regeneration in the caudal fin between 0-14 dpa are shown. In both*

WT and heterozygous zebrafish, newly formed bone matrix in the regenerating lepidotrichia (bone rays) can be clearly observed from 6 dpa. Heterozygotes appear to show no difference in bone regeneration compared to WT. Scale bar = 200 μm. ***B-C:*** *The fluorescence intensity of calcein in the mid region (B) and the lateral region (C) was calculated relative to calcein intensity in the uninjured fin (intensity ratio) and plotted as mean (± SD). Mean calcein intensity ratio appeared lower between 6-10 days in tnfα$^{+/-}$ fins compared to WT in the mid region (B), however, no significant differences in the calcein intensity ratios of heterozygotes were detected in either region, compared to WT (B & C).* ***D:*** *The total area of regenerated fin tissue was measured and plotted as a proportion of the pre-amputated area (percentage regrowth, mean (± SD)). No significant difference in regrowth was measured at any time point post amputation between WT and tnfα$^{+/-}$ zebrafish. N = 4 per group.*

Similarly, bone remineralisation during fracture repair was comparable between WT and *tnfα*$^{+/-}$ zebrafish. Representative images of fractured bone within the caudal fins of WT and *tnfα*$^{+/-}$ zebrafish at various time points throughout callus formation are shown (Figure 44 A). No difference in calcein deposition at the fracture site can be observed between WT and *tnfα*$^{+/-}$ fractures at any time point post injury. Bone mineralisation during bone repair was quantified by measuring the calcein intensity within the fractured region relative to the calcein intensity of uninjured bone in the same fin (intensity ratio). When compared to fractures in WT siblings, *tnfα*$^{+/-}$ zebrafish displayed no significant difference in the calcein intensity ratio at any time point post injury (Figure 44 B).

Collectively, this demonstrates that bone remineralisation is not affected in heterozygous *tnfα* mutant zebrafish, during either fin regeneration or fracture repair. Studies using homozygous (*tnfα*$^{-/-}$) zebrafish are now required to determine whether complete loss of Tnf-α affects osteoblasts during bone regeneration and repair.

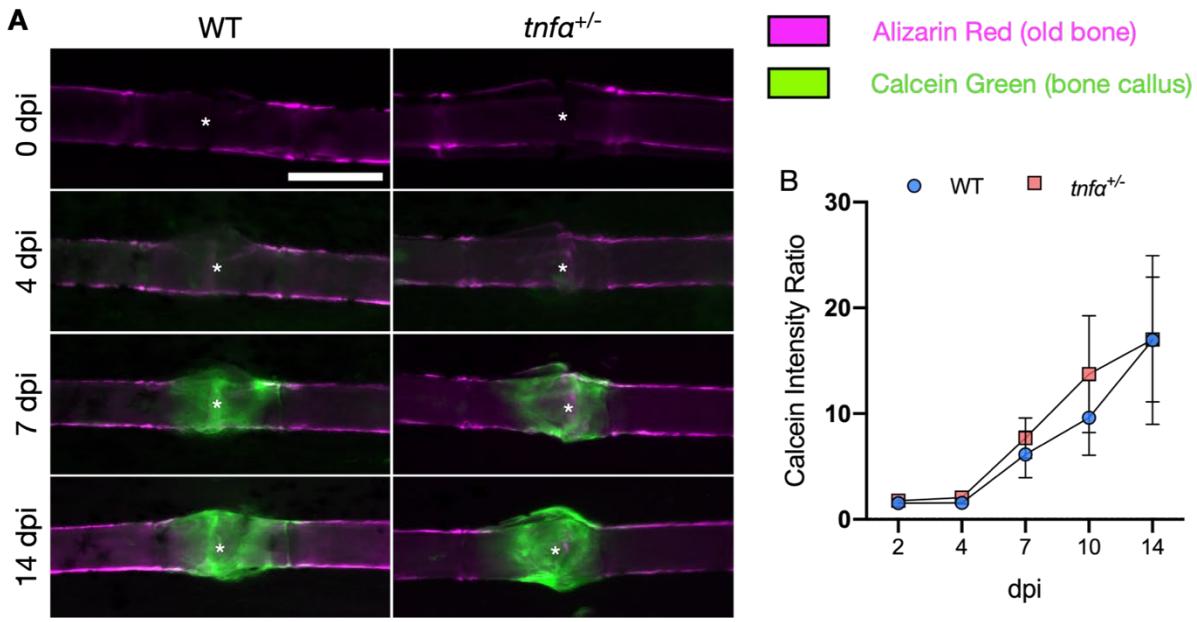

Figure 45. No Effect on Bone Repair Is Observed Post Fracture in the Fins of Heterozygous tnfα Mutant Zebrafish. *Uninjured adult wild type (WT) and tnfα$^{+/-}$ (heterozygous) zebrafish were live stained in Alizarin red to label calcified bone in, before fractures were induced in the caudal fins. Fins were re-imaged between 0-14 days post injnury (dpi). Prior to re-imaging, zebrafish were live stained in calcein green to label newly formed bone matrix at the fracture site.* ***A:*** *Representative images of fractures in the caudal fins of WT and tnfα$^{+/-}$ zebrafish are shown between 0-14 dpa. Heterozygotes appear to show no difference in bone remineralisation post fracture, compared to WT zebrafish. Asterik = centre of fracture, scale bar = 200 μm.* ***B:*** *Calcein fluorescence intensity at the fracture site was measured relative to uninjured bone in the same fin (intensity ratio), as a proxy for bone remineralisation post fracture. Fractures from heterozygotes showed significant difference in the calcein intensity ratio compared to WT fractures at any time point post injury. Plot displays mean (± SD), N = 4.*

5.2.7 ADDITION OF RECOMBINANT TNF-α TO OSTEOGENIC MEDIA HAS NO EFFECT ON OSTEOBLAST ACTIVITY IN AN *EX VIVO* ZEBRAFISH SCALE CULTURE SYSTEM

Inflammatory cells, such as macrophages, are known to play a key role in directing zebrafish fin regeneration (131). Tnf-α is a major proinflammatory cytokine, which is upregulated by macrophages in response to osteoblast apoptosis and influences the inflammatory response during regeneration (234, 453). However, excessive inflammation during bone repair is known to negatively affect osteoblasts and bone mineralisation (134, 147). Immune and skeletal systems are in intrinsically linked via complex and dynamic signalling interactions. Zebrafish are excellent models for studying the whole-organism effects of pharmacological compounds and mutations, that cannot always be accurately modelled *in vitro*. However, *in vivo*, it is difficult to discern the influence of Tnf-α on osteoblasts in isolation from the immune system.

The zebrafish elasmoid scale is a living tissue, populated with osteoblasts and osteoclasts which maintain a sheet of calcified dermal bone (458). Similarly, to fins, zebrafish scales can completely regenerate via the upregulation of osteogenic genes such as *osx* and *spp1* (osteopontin) (280). Crucially, ontogenetic and regenerating zebrafish scales can be cultured *ex vivo*, in isolation from the influence of systemic osteomodulatory factors or recruited immune cells (195, 458).

Therefore, I next investigated whether addition of zebrafish recombinant Tnf-α (r-Tnf-α) to osteogenic medium influenced *osx* expression and ALP activity of osteoblasts in ontogenetic and regenerating scales cultured *ex vivo*. Scales were plucked from *osx*:*mCherry* zebrafish and left to regenerate for 9 days (Figure 45 A). Ontogenetic and regenerating scales were then harvested from the same fish and cultured in either normal osteogenic culture medium, or osteogenic culture medium supplemented with 10 ng ml^{-1} of r-Tnfα, for 4 days in an Incucyte® (Figure 45 B). Bright field and mCherry images of scales were acquired every 4 hours within each well to assess expression of *osx* (Figure 45 C). Interestingly, expression of *osx:mCherry* appeared almost non-existent in ontogenetic scales supplemented with r-Tnf-α, whereas ontogenetic scales cultured in unsupplemented osteogenic medium displayed expected levels of *osx*:mCherry. This effect was not observed in regenerating scales, with *osx:mCherry* expression high throughout under both conditions. This preliminary finding suggests that Tnf-α may negatively affect *osx* expression by mature osteoblasts in ontogenetic scales, but not regenerating osteoblasts. Modular Image Analysis (MIA) can be used to automatically detect scales within each well and outline areas expressing *osx:mCherry* based on a defined fluorescence threshold (287). However, due to scale movement around the culture well, artefacts in some images, and issues with reproducible analysis automation, this data could not be analysed.

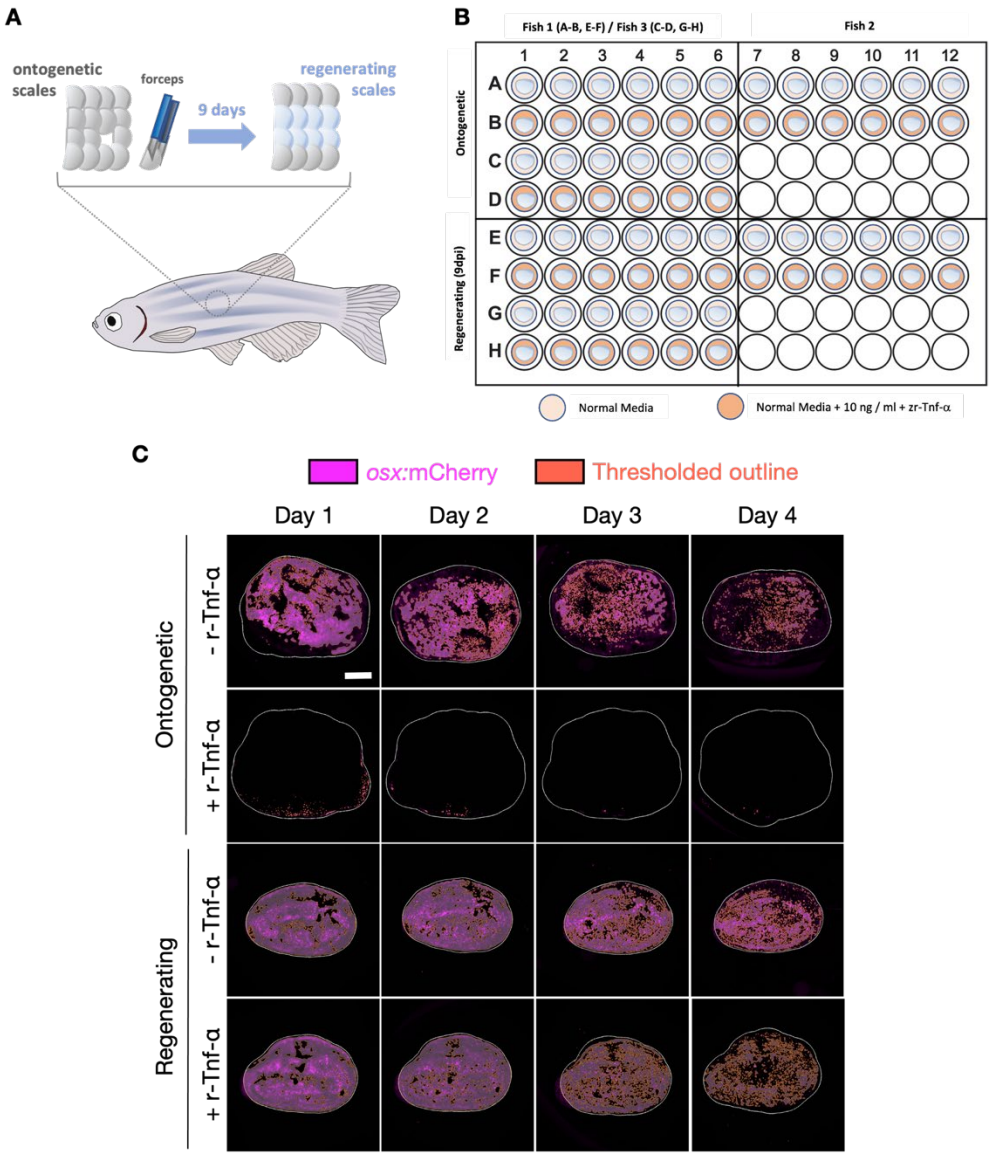

Figure 46. Ex Vivo Zebrafish Scale Culture as A Model to Understand the Influence of Tnf-α on Osteoblasts in Isolation from The Immune System. A: *Scales were plucked from the left flank of osx:mCherry zebrafish and left to regenerate. Regenerating scales were harvested from the left flank 9 days post removal, and ontogenetic scales were harvested from the right flank.* ***B:*** *Scales were cultured individually in the well of a 96-well plate, in either standard osteogenic media, or osteogenic media supplemented with 10 ng ml^{-1} zebrafish recombinant Tnf-α (r-Tnf-α). Cultures were performed for 4 days in an IncuCyte®. Brightfield and mCherry IncuCyte® images of each well were acquired every 4 hours, and culture media were refreshed daily.* ***C:*** *Representative images of osx:mCherry are shown for each scale type (ontogenetic / regenerating) and culture condition (± r-Tnf-α) throughout. These images have been processed by a modular image analysis (MIA) pipeline developed by Dr*

Stephen Cross at the University of Bristol (285). White outlines depict the outline of the scale, with red outlines depicting regions of the scale where mCherry fluorescence was detected and measured by MIA, at a defined threshold. From this, the mean fluorescence and scale coverage of osx:mCherry can be calculated for each scale. Interestingly, ontogenetic scales cultured in r-Tnf-α supplemented media showed very low levels of osx:mCherry expression, throughout, yet regenerating scales cultured in r-Tnf-α supplemented media retained high levels of osx:mCherry expression until day 4. Scale bar = 500 μm.

After 4 days of culture in either condition, ALP staining was performed on scales to assess osteoblast activity. Representative images of ontogenetic and regenerating scales cultured under each condition are shown (Figure 46 A). ALP activity was quantified in an automated manner using MIA (287). MIA measured the % area of each scale stained positive for ALP (Figure 46 B), the actual area of scale stained positive for ALP (Figure 46 C) and the mean intensity of ALP staining (Figure 46 D). Addition of r-Tnf-α to osteogenic media had no significant effect on ALP coverage, or intensity, in either ontogenetic or regenerating fins. With further optimisation, *ex vivo* zebrafish scale culture may provide an effective platform to further elucidate the pleiotropic effects of Tnf-α on osteoblasts.

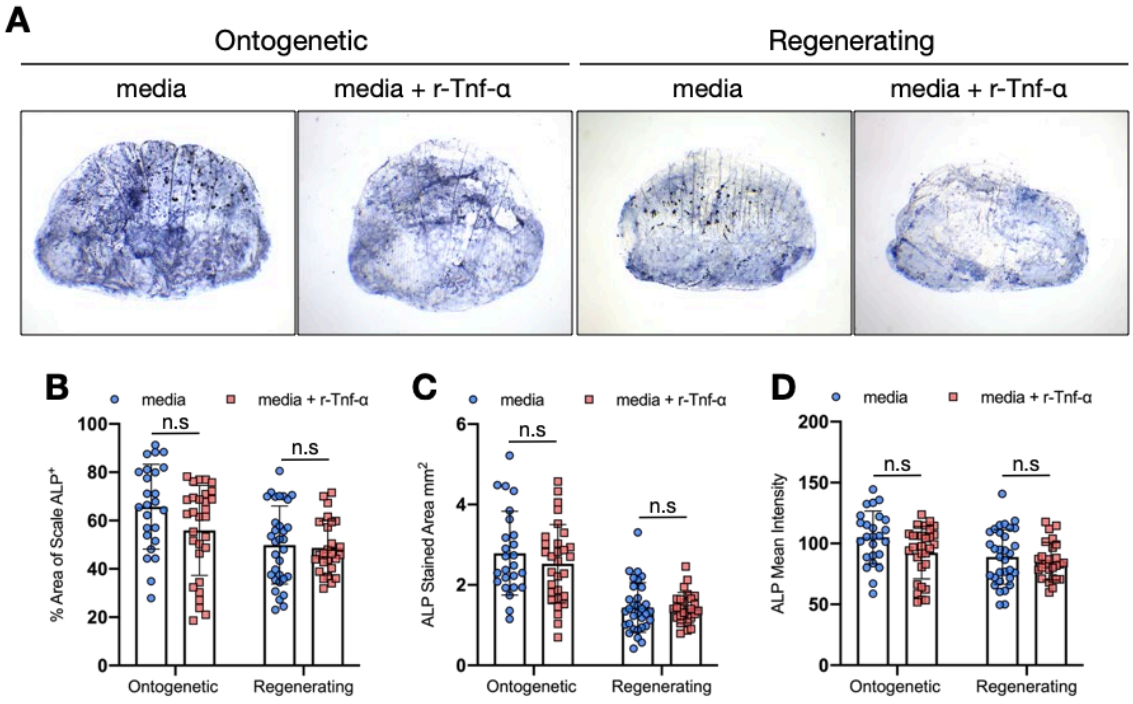

Figure 47. Addition of Recombinant Tnf-α To Osteogenic Media Has No Effect on Osteoblast Activity in Either Ontogenetic or Regenerating Zebrafish Scales in an ex vivo Culture System. A: *Representative images of ALP stained ontogenetic and regenerating scales cultured in either standard media, or media supplemented with r-Tnf-α, are shown.* ***B-D:*** *ALP staining was quantified 3 ways: percentage area of scale stained with ALP (B), actual area of scale stained with ALP (C) and mean intensity of ALP (D) staining across the scale. Bars in plots represent mean (± SD). No significant difference in ALP⁺ area or intensity was detected in either ontogenetic or regenerating scales, as a result of supplementation with r-Tnf-α. n.s. = no significant difference, N ≥ 26.*

5.3 DISCUSSION

5.3.1 SUMMARY OF RESULTS

The pleiotropic effects of TNF-α on bone homeostasis and repair are poorly understood (38). Here, I used zebrafish to investigate the role of Tnf-α throughout fracture repair and bone regeneration dynamically. Expression of *tnfα* was upregulated during both early fracture repair (Figure 36) and early bone regeneration in the blastema (Figure 37). Interestingly, *tnfα* expression appeared to pattern bone regeneration and was expressed by some osteoblasts whilst high levels of *runx2a* and *tnfrsf1b* were expressed in the blastema (Figure 38 and Figure 39); this suggests that osteoblast precursors or differentiating osteoblasts express *tnfα*, and that Tnf-α plays a pro-osteogenic role in bone regeneration. FACS indicate that discrete populations of *tnfα*:GFP^{+}, *osx*:mCherry^{+} and double^{+} cells are present in the zebrafish caudal fin, which respond dynamically to amputation. Partial inhibition of Tnf-α using pomalidomide resulted in variable effects on bone regeneration; most pomalidomide treated fish displayed normal bone regeneration. However, in one individual, reduced or ectopic *tnfα* expression in the blastema resulted in failed or aberrant lepidotrichia formation in the regenerating fin, respectively (Figure 41 and Figure 42). Heterozygous mutation of *tnfα* in zebrafish had no effect on lepidotrichia morphology during homeostasis, bone regeneration or repair, suggesting a lack of haploinsufficiency in zebrafish *tnfα* mutants (Figure 43 and Figure 44). Finally, I introduced *ex vivo* zebrafish scale culture, as a tool for further elucidating the effect of Tnf-α on osteoblasts, in isolation from systemic influences of the immune system (Figure 45 and Figure 46).

5.3.2 EVIDENCE FOR A PRO-OSTEOGENIC EFFECT OF TNF-α IN BONE REPAIR AND REGENERATION

Classically, TNF-α has been described as a promoter of osteoclast differentiation and bone resorption (426, 427, 429). TNF-α reduces the expression of collagens and the osteoblast differentiation marker, RUNX2, in human MSCs and is associated with pathological bone loss in rheumatic diseases (429, 459). Moreover, hyperinflammation is associated with poor bone repair (134). However, a growing body of scientific literature suggests that TNF-α acts to promote efficient bone repair post fracture, in both humans and mice

(38, 448, 449). Here, I demonstrated that *tnfα* is expressed by bone during early fracture repair and fin regeneration. The expression of *tnfα:GFP* within pools of differentiating osteoblasts in the blastema, strongly suggests a pro-osteogenic role for Tnf-α in these processes. Therefore, I explored whether pharmacological or genetic perturbation of Tnf-α would disrupt osteoblast differentiation.

Pomalidomide has been used as an immersion-delivered, non-teratogenic and potent inhibitor of Tnf-α production in larval zebrafish studies (258, 275). Despite using a concentration comparable with those which elicited effective Tnf-α inhibition in larval studies, only partial inhibition of *tnfα:GFP* resulted from 200 μM pomalidomide treatment in adult zebrafish (Figure 41). Higher dosage of pomalidomide may be required. Pentoxifylline is an alternative Tnf-α inhibiting compound which had been effectively used to reduce *tnfα* expression in larval zebrafish (453). However, this compound is not well tolerated by adult zebrafish (data not shown). Though statistical analysis detected only partial inhibition of *tnfα* by pomalidomide in this experiment, a reduction in mean *tnfα*:GFP and *osx*:mCherry levels in pomalidomide treated animals can be observed through regeneration, relative to the DMSO group. This, along with Priori power calculations, suggests that a larger sample size is required to determine whether pomalidomide is effective at inhibiting *tnfα* and *osx* expression during zebrafish fin regeneration.

Partial inhibition of *tnfα* expression using 200 μM pomalidomide resulted in no significant effect on *osx* expression by osteoblasts in the regenerating fin. However, one pomalidomide-treated zebrafish displayed aberrant bone regeneration. During normal fin regeneration, *tnfα* is expressed in the blastema, distal to the bone amputation site and any calcified regenerate (Figure 37). Intriguingly, *osx*:mCherry^{+} cells did not differentiate and regenerate lepidotrichia in areas of the blastema where *tnfα*:GFP levels were visibly low from 2-4 dpa, immediately distal to the amputation site (Figure 41 and Figure 42). Moreover, ectopic *tnfα:GFP* expression in the blastema resulted in aberrant direction of osteoblast migration during bone regeneration, towards the area of *tnfα*:GFP^{+} cells (Figure 42). This supports the hypothesis that Tnf-α supports osteoblast proliferation, migration and differentiation during bone regeneration. However, more concrete evidence of this relationship is required. Dysregulated bone formation in this individual animal may have resulted from infection or injury post-amputation in the tank. However, this seems unlikely given that fish were housed individually post-injury and the non-skeletal fin tissue regenerated normally, and only bone regeneration was affected by aberrant *tnfα* expression. Alternatively, this phenotype may be the result of an unknown background mutation in the animal. Therefore, repeat experiments with increased sample sizes are required to better determine the effect of pomalidomide on bone regeneration.

Bone regeneration and repair was also studied in a stable *tnfα* mutant line of zebrafish displaying functional loss of the Tnf-α protein (274). Unfortunately, only heterozygous animals were available during this study, due to difficulties with breeding and import of the line (see COVID impact statement). Indeed, experiments using homozygous (*tnfα*$^{-/-}$) mutants would be preferable to using heterozygous mutants, provided that they survive well to adulthood. However, heterozygous mutation of *Tnfα* in mice results in reduced Tnf-α production in response to LPS compared to WT. Moreover, *Tnfα*$^{+/-}$ mice do not mirror the phenotype of *Tnfα*$^{+/+}$ littermates, showing increased susceptibility to infection, increased sensitivity to LPS-mediated toxicity and delayed resolution of inflammation (403). This suggests that there is a degree of haploinsufficiency in the *Tnfα* gene, and that the pleiotropic effects of TNF-α are dose-dependent. However, uninjured bone in adult heterozygous *tnfα* zebrafish appeared morphologically comparable to WT siblings. Moreover, *tnfα*$^{+/-}$ zebrafish displayed no difference in either bone remineralisation post fracture, or bone and fin regeneration post amputation. Expression of WT *tnfα* mRNA levels in *tnfα*$^{+/-}$ zebrafish was not measured here. Quantification of *tnfα* expression within WT and *tnfα*$^{+/-}$ zebrafish will better determine whether Tnf-α production is affected in heterozygous mutants. However, given that there was no effect on bone repair or regeneration, it is unlikely that any effect on *tnfα* expression in *tnfα*$^{+/-}$ zebrafish is sufficient to induce changes to osteogenesis or tissue regeneration post injury. Further studies using homozygous *tnfα*$^{-/-}$ zebrafish are required to characterise the effect that loss of Tnf-α has on osteoblast differentiation in bone repair and regeneration. It is currently unclear whether *tnfa*$^{-/-}$ zebrafish survive to adulthood. Though stable homozygous *tnfα* mutant zebrafish have been used in larval injury studies, to date, no published study has investigated the effect of homozygous mutation in *tnfα* in any context. If bone regeneration or fracture experiments cannot be performed on adult *tnfa*$^{-/-}$ zebrafish, dual genetic and pharmacological suppression of Tnf-α via pomalidomide treatment in heterozygous *tnfα* mutants may provide more effective inhibition of Tnf-α in bone regeneration and repair.

5.3.3 EXPLORING THE IDENTITY OF *TNF-α* EXPRESSING CELLS IN BONE REPAIR AND REGENERATION

In this study, I demonstrated that *tnfα* is expressed during bone repair and regeneration in zebrafish. Expression of *tnfα* was observed distal to the fracture site in repairing lepidotrichia. Similarly, *tnfα:GFP* was strongly expressed in the blastema, distal to regenerating lepidotrichia, patterning bone regeneration. It is known that osteoblast progenitor cells (OPCs) migrate from the intersegmental regions of uninjured

lepidotrichia into the blastema, undergo *de novo* differentiation into mature *osx*-expressing osteoblasts and secrete bone matrix (212, 460). However, it is also known that mature osteoblasts undergo dedifferentiation, proliferate and migrate into the blastema, where they redifferentiate and facilitate bone regeneration (199, 461). Osteoblast dedifferentiation is not specific to zebrafish fin regeneration; this also occurs during repair of skull and fin fractures (198). It is unknown whether *de novo* dedifferentiation of osteoblasts contributes to fracture repair in zebrafish (1).

TNF-α is known to activate the NF-κB pathway both canonically, via TNFR1, and non-canonically, via TNFR2 (393, 394). Signalling of TNF-α via TNFR1 may trigger cell apoptosis, whereas signalling via TNFR2 promotes cell proliferation and survival, especially when expressed by cells under oxidative stress during inflammation (394, 455). NF-κB activity can induce the expression of anti-apoptotic factors, adhesion molecules, as well as increasing the expression of TNF-α and other pro-inflammatory cytokines in the target cell (462). Here, increased expression of *tnfrsf1b* (encoding Tnfr2 in zebrafish) was observed in regenerating bone between 2-4 dpa (Figure 39), as osteoblast differentiation is occurring (Figure 38), (212)). Recently, NF-κB has been shown to negatively regulate osteoblast dedifferentiation during fin regeneration in a cell autonomous manner, without reducing osteoblast proliferation (463). This suggests that *tnfα* expression by osteoblast precursors within the blastema could act as a molecular brake, by activating NF-κB in an autocrine or paracrine manner. This would act to suppress the dedifferentiation of osteoblasts in the blastema and promote the differentiation of mature osteoblasts. Alternatively, NF-κB may induce the expression of *tnfα* in dedifferentiated osteoblasts and amplify NF-κB signalling to supress dedifferentiation in a cell autonomous manner.

Imaging of regenerating *tnfα:GFP; osx:mCherry* fins expressing the pre-osteoblast marker, *runx2a*, suggests that *tnfα*:GFP^{+} cells within regenerating bone between 2-6 dpa represent pools of OPCs undergoing *de novo* osteoblast differentiation. At 2 dpa, mCherry^{+} intensity increases in *osx*$^{+}$ cells, which express *tnfα,* adopt an elongated morphology, and appear to migrate towards the blastema (Figure 38). Moreover, confocal imaging shows high expression of *tnfα:GFP* by differentiating osteoblasts at 4 dpa, but reduced expression of *tnfα:GFP* as osteoblasts mature within the regenerating bone. These observations are comparable with the migration of *mmp9*$^{+}$ OPCs into the blastema and their differentiation into osteoblasts during fin regeneration, that was previously described by Ando *et* al., (460). OPCs have also been shown to maintain osteoblast populations during normal bone homeostasis (460). Given that *tnfα:GFP* does not appear to be expressed in uninjured adult bone, this suggests that *tnfα* may be specifically upregulated by OPCs during bone regeneration and repair.

Both dedifferentiated osteoblasts and *de novo* differentiation from OPCs contribute to bone regeneration in the zebrafish caudal fin (1). Therefore, further investigation into the origin, identity, and expression profiles of *tnfα*$^{+}$ cells in regenerating bone are required. This will help to reveal more about the pleiotropic effects of TNF-α on osteoblasts and contribute to the understanding of the role of this cytokine in regulating human skeletal biology.

5.3.4 INDIRECT MECHANISMS WHICH MAY UNDERPIN OSTEOGENIC EFFECTS OF TNF-α

Bone repair and regeneration are highly dynamic processes, involving complex interactions between multiple cell types to restore tissue homeostasis. Therefore, it is plausible that Tnf-α modulates osteoblasts in an indirect manner, via the regulation of interconnected processes in other cell types such as macrophages, fibroblasts or endothelial cells. Here, I will explore how these cell types and signalling networks may intersect with the osteogenic properties of TNF-α during bone regeneration and repair.

5.3.4.1 MACROPHAGES

Macrophages are known to be required for proper blastema formation and regeneration of fin tissue in zebrafish. Genetic ablation of macrophages (*mpeg1*$^{+}$ cells) results in impaired fin regeneration and bone patterning (131). However, given evidence that *mpeg1* is also expressed by macrophage-derived osteoclasts in teleosts, the bone patterning phenotype in *mpeg1*$^{+}$ cell-ablated animals may result from altered bone resorption (2, 428). Nonetheless, the dynamic expression of *tnfα* by macrophages has been shown to promote axonal bridging during spinal cord regeneration in zebrafish larvae, suggesting that M1 macrophages may also promote bone regeneration (275). Glucocorticoid treatment of adult zebrafish results in depletion of myeloid progenitors and macrophages, which is correlated with inhibitory effects on osteoblast differentiation and bone regeneration (111). However, early osteoblast dedifferentiation during fin regeneration is not perturbed by clodronate-mediated macrophage ablation (463). This suggests that glucocorticoids mediate their bone suppressive effects on osteoblasts directly, independently of macrophages.

Less is known about the role of macrophages in zebrafish fractures. Cells expressing *mpeg1*, which includes macrophages, other immune cells and potentially osteoclasts, respond to caudal fin fracture in a biphasic

manner (2). The initial wave of *mpeg1*-expressing cells arrives at the fracture site within 48 hours of the injury, coinciding with TRAP production, during the inflammatory phase of repair (2, 147). Here, I showed that, inflammatory *mpeg1*$^{+}$ cells responding to fracture express *tnfα*, in addition to bone distal to the injury site, (Figure 36). The recruitment of inflammatory *mpeg1*$^{+}$ cells preceded the expression of *tnfα* by injured bone, suggesting that these cells may influence downstream bone repair via Tnf-α. Alendronate is a bisphosphonate used to suppress osteoclasts, but can also cause macrophage apoptosis (464). Alendronate treatment has been shown to cause reduced resorption of damaged bone and impaired callus formation post fracture in zebrafish (147). Since the recruitment of pro-inflammatory *mpeg1*$^{+}$ cells coincides with early TRAP synthesis and bone resorption post fracture (2, 147), this implies that the differentiation of *mpeg1* cells into bone resorptive osteoclasts may be impaired by alendronate treatment (428). Given that osteoblast and osteoclast differentiation are intimately linked, this may result in downstream effects on osteoblasts and bone repair. Therefore, it is plausible that *tnfα* expression in pro-inflammatory macrophages may influence osteoblast activity during bone repair, via osteoclastogenesis.

5.3.4.2 FIBROBLASTS

Mesenchymal connective tissue in the zebrafish fin is formed and maintained by fibroblasts, which are dispersed throughout the interray tissue and between lepidotrichia hemirays (intraray fibroblasts) (465). This connective tissue supports a network of nerves, blood vessels, pigment cells and bone throughout the fin. Fibroblasts were not investigated during this study. However, after amputation, intraray fibroblasts from lepidotrichia are known to migrate into the distal portion of the blastema, along with dedifferentiated osteoblasts, to support fin regeneration (199). Moreover, Fibroblast Growth Factor (FGF) is required for blastema formation and the proliferation of dedifferentiated osteoblasts (199, 466). It has also been suggested that fibroblasts within the blastema may be capable of transdifferentiation into osteoblasts, though concrete evidence for this is lacking (212). Interestingly, TNF-α has been shown to induce the expression of OPG in human synovial fibroblasts to promote osteoblast activity (436). However, it has been shown that loss of intersegmental derived fibroblasts via mutation of *tph1b* (tryptophan 5-monooxygenase) has no effect on osteoblast differentiation during fin regeneration (467). Under inflammatory conditions, TNF-α is known to upregulate production of Fibroblast Activating Protein (FAP) by stromal fibroblasts, which has recently been identified as a suppressor of osteogenic differentiation in mice and zebrafish (468, 469). FAP promotes osteoclastagenesis via NF-κB activation in macrophages, whilst supressing canonical Wnt activity in osteoblasts. However, it was also shown that osteolectin, an endogenous inhibitor of FAP, promotes ossification during zebrafish development (468). This suggests that endogenous regulation of fibroblast-derived growth factors may also support osteoblast activity during bone repair and regeneration.

5.3.4.3 ANGIOGENESIS

Zebrafish fins are heavily vascularised, containing a dense network of interconnected blood vessels; arteries carrying oxygenated blood distally are encased between the hemirays of lepidotrichia, whilst veins are dispersed throughout the interray tissue (465). Perhaps unsurprisingly, the patterning of revascularisation closely mirrors that of bone remineralisation in the blastema, with high expression of the endothelial marker, *tik* (tyrosine endothelial kinase), patterning lepidotrichia regeneration (470). Potent inhibition of VEGF receptor signalling via treatment with PTK787 completely supresses neovascularisation of the blastema and results in stunted fin regeneration by 7 dpa (470). Moreover, though treatment with this inhibitor does not completely prevent blastema formation and fin tissue growth, osteoblast infiltration of the avascular regenerate is limited to within 1mm of the amputation plane (471). Direct interactions between *tnfα*$^{+}$ macrophages and lesioned blood vessels are known to support vessel sprouting during

zebrafish wound healing via the production of Vegfa, which is recapitulated in mouse models and human cell culture (240). Therefore, it is also plausible that the expression of *tnfα* during early fin regeneration stimulates osteoblast proliferation and differentiation indirectly by promoting angiogenesis in the blastema.

5.3.4.4 CELL METABOLISM

Bone regeneration and angiogenesis are tightly coupled processes during fin regeneration, with osteoblasts unable to populate avascular blastema tissue (471, 472). Poor vascularisation or vascular obstruction results in ischemia, causing hypoxic conditions in downstream tissues. Osteogenesis carries a high metabolic demand, with ischemia thought to skew the differentiation of MSCs towards a less metabolically active chondrogenic fate (136). Hypoxia induces apoptosis of osteoblasts in culture. However, upregulation of hypoxia inducible factor 1 alpha (HIF-1α) by these cells protects against hypoxia-induced osteoblast apoptosis (473). Moreover, HIF-1α induces the production of VEGF in osteoblasts to stimulate angiogenesis (474). During osteogenesis, the differentiation of OPCs into osteoblasts is highly dependent on energy derived from glycolytic metabolism. The expression of HIF-1α by OPCs promotes a switch to glycolysis via the upregulation of glycolytic enzymes, including pyruvate dehydrogenase kinase 1 (PDK1) (475). Induced hypoxia, or pharmacological overstimulation of Hif1-α, throughout zebrafish fin regeneration results in perturbed angiogenesis, failure of vessel maturation and reduced bone regeneration in the blastema (476). However, in normal fin regeneration, extreme hypoxia is likely limited to the avascular distal portion of the blastema, not within the revascularized regions of the regenerate where *osx*$^{+}$ cells reside (Figure 37). Intriguingly, upregulation of HIF-1α in response to hypoxia has been shown to induce the production of TNF-α by osteoblasts, suggesting that hypoxia may regulate *tnfα* expression by osteoblast precursors during fin regeneration in zebrafish.

Another key nutrient recycling process is autophagy, whereby an autophagosome forms around damaged proteins or organelles and is targeted for lysosomal degradation. Autophagy is upregulated in response to cellular metabolic stress elicited by inflammation or injury, including post fracture in zebrafish (477). TNF-α induces both increased autophagy and apoptosis in osteoblasts in a dose-dependent manner. However, upregulation of autophagy protects these osteoblasts from the apoptotic effects of TNF-α (478). Moreover, it was recently demonstrated that reduced ion transport and lysosomal acidification promote glucocorticoid-mediated suppression of bone regeneration in the zebrafish caudal fin (479). Collectively, this further suggests that Tnf-α may regulate metabolic processes in osteoblast progenitors during early fin

regeneration. Furthermore, it suggests that cellular metabolic switches may confer resilience to TNF-α-mediated apoptosis and account for the pleiotropic effects of this cytokine on cell survival and death.

5.3.4.5 WNT SIGNALLING

Wnt signalling pathways are activated after bone injury and are required for osteoblast proliferation and differentiation (16, 289). Dysregulated Wnt signalling is known to negatively affect these processes (2, 313). In fin regeneration, canonical Wnt signalling is upregulated in the distal most end of the blastema; this promotes stemness and facilitates the proliferation and differentiation of progenitor cells in more proximal regions of the regenerating tissue (480). Importantly, inhibition of canonical Wnt signalling via overexpression of Dkk1, or deletion of Tcf, results in impaired blastema formation and failure to regenerate fin tissue (481). This demonstrates that canonical Wnt signalling is critical for fin regeneration. However, autocrine down regulation of canonical Wnt signalling via the BMP pathway is required for the differentiation of *runx2*$^{+}$ osteoprogenitors into *osx*$^{+}$ osteoblasts (482). Interestingly, synergistic expression of *HIF1α* and *OSX* has been shown to supress canonical Wnt activity, possibly to promote differentiation into mature osteoblasts (483). Non-canonical Wnt signalling is also known to negatively regulate β-catenin in differentiating cells within the regenerating fin; *wnt5a* is known to be upregulated in more proximal regions of the day 3 blastema, compared to canonical Wnt ligands (481). I observed *tnfα*:GFP in comparable regions of the blastema to previously reported *wnt5a* expression, coinciding with osteoblast differentiation from 2-4 dpa (Figure 37) (481). Interestingly, TNF-α has been shown to induce osteoblast differentiation and activity via autocrine WNT5A signalling in human MSCs. Collectively, this suggests that TNF-α may promote osteoblast differentiation during bone regeneration and repair via modulation of Wnt signalling pathways.

5.3.5 ALTERNATIVE METHODS FOR MODELLING THE OSTEOGENIC POTENTIAL OF TNF-α IN ZEBRAFISH

Here, I provided evidence supporting a pro-osteogenic role for Tnf-α in osteoblast differentiation during bone repair and regeneration in zebrafish. Imaging suggests that differentiating osteoblasts within the blastema express *tnfa* and *runx2a*, before expressing the osteoblast marker *osx*. Reduced *tnfα* expression in the blastema of one pomalidomide-treated zebrafish suggests that perturbing Tnf-α production by these progenitor cells may cause dysregulated osteoblast proliferation and differentiation (Figure 41 and Figure

42). However, more definitive studies are required to fully establish the identity of the *tnfα* expressing cells and the influence that Tnf-α has on osteoblasts in bone regenerative scenarios. Here, I will explore methods which could help to address these outstanding questions.

5.3.5.1 FACS AND TRANSCRIPTOMICS

FACS can be used to isolate discrete populations of cells expressing a fluorescent protein under a gene of interest, for further transcriptomic or proteomic profiling. I demonstrated that FACS could be applied to cells dissociated from uninjured and regenerating (4 and 6 dpa) fins from *tnfα:GFP;osx:mCherry* fish (Figure 40). However, populations of live cells contained a high proportion of double negative or background events, meaning relatively few cells of interest (GFP^+, $mCherry^+$ and double positive) were isolated. Moreover, the total number of cells isolated for each population varied between experiments. Despite this, RNA isolation was attempted via two separate methods: the Qiagen RNAeasy Mini Kit and the phenol-chloroform method using TRIzol-LS. Both methods are used to isolate RNA from zebrafish FACS populations for transcriptomic analysis (220, 484). In both scenarios, unviable yields or quality of RNA were isolated from sorted populations (data not shown). In one instance, RNA isolation (TRIzol-LS) was performed on unsorted cells from regenerating fins in parallel with RNA isolation from sorted cells; here, unsorted cells yielded a high concentration and quality of RNA, but FACS derived cells did not (data not shown).

Collectively, this suggests that the proportion of cells within each population vary by experiment, suggesting a higher number of replicates are required. Moreover, relatively low numbers of fluorescent cells observed during FACS, suggests that other methods of fin tissue dissociation may increase cell yield for each population. Finally, RNA isolation from sorted cells requires further optimisation before transcriptomic analyses can be performed; poor RNA yield and quality from FACS-derived cells compared to unsorted cells suggests that FACS induces cellular stress which may promote RNA decay (485). Further optimisation of FACS and RNA isolation of $tnf\alpha^+$ cells within regenerating fins will allow for transcriptomic cell profiling and help to elucidate the effect of *tnfα* in the osteogenic response to skeletal injury.

5.3.5.2 *EX VIVO* ZEBRAFISH SCALE CULTURE

Skeletal and immune cell activity is intimately linked via inflammation; TNF-α is known to regulate osteogenesis pleiotropically, eliciting varied effects on different cell types (38, 300). As a result, it is hard to disentangle the effects of Tnf-α on osteogenesis from those on the immune system, and vice versa. In 2012, zebrafish scales were shown to retain bone synthesising osteoblasts and bone resorptive osteoclasts *ex*

vivo, which remained viable for up to 4 days in culture (458). Since then, relatively few studies have utilised this system, yet it holds remarkable potential for screening the osteomodulatory properties of specific proteins and compounds (195, 219, 280). Here, I introduced *ex vivo* culture of ontogenetic and regenerating zebrafish elasmoid scales as a method for studying the effect of r-Tnf-α on osteoblast gene expression (*osx:mCherry*) and activity (ALP), in isolation from the immune system.

The addition of r-Tnf-α to osteogenic media had no effect on ALP activity in either ontogenetic or regenerating scales (Figure 46). Fluorescent images (mCherry) were also acquired every 4 hours for the duration of culture, using an IncuCyte® (Figure 45). Automated analysis of *osx:mCherry* expression in scales using MIA is required due to the high-throughput nature of the 4 day assay (96-well plate) (287). However, this analysis pipeline could not be automated for reproducibility between wells. Mainly because scales move within the well, meaning accuracy of automated scale detection can vary between frames. Moreover, daily media changes further exacerbate scale movement, sometimes resulting inadvertent scale destruction or removal from the well. Occasionally, artefacts in the image (reflections or bubbles in media) interfere with analysis automation. Therefore, IncuCyte® plate setup requires further optimisation to prevent scale movement and reduce image artefacts. One approach could include the addition of Cell-Tak™ tissue adhesive to the 96-well plates (Sigma), to promote adhesion of the scale to the plastic beneath. Despite this, qualitative interpretation of *osx* expression throughout *ex vivo* scale culture suggests that r-Tnf-α may promote osteoblast depletion in ontogenetic, but not regenerating scales; observationally, ontogenetic scales supplemented with r-Tnf-α displayed drastically reduced levels of *osx*:mCherry compared to regenerating scales, or non-supplemented scales in any state (Figure 45). This suggests that osteoblasts within regenerating tissues may possess unique resilience to r-Tnf-α mediated apoptosis. However, further studies employing apoptosis markers such as caspase-3 or Terminal deoxynucleotidyl transferase dUTP nick end labelling (TUNEL), in conjunction with anti-osteoblast staining, in ontogenetic and regenerating scales are required.

In summary, *ex vivo* zebrafish scale culture may represent a useful method for deciphering the pleiotropic effects of Tnf-α on osteoblasts. Moreover, given the dose-dependent nature of the osteogenic versus apoptotic effects of r-TNF-α *in vivo* and *in vitro* (434, 448), this system may help to define biologically relevant concentrations of Tnf-α for assays *in vivo*. Future experiments could use implantation of r-Tnf-α soaked microbeads into fractures, or in the blastema during early regeneration (486). This experiment may help to elucidate whether exogenous Tnf-α can promote osteogenesis (and at which concentrations), or whether expression of *tnfα* facilitates osteoblast differentiation in a cell autonomous or autocrine manner.

5.3.5.3 STUDYING THE ROLE OF *TNF-α* IN LARVAL ZEBRAFISH BONE REGENERATION

Zebrafish bone development commences at around 3 days post fertilisation (dpf). One of the first skeletal elements formed is the operculum, a layer of dermal bone which eventually covers the gills of the fish (1). Studying zebrafish larvae could reveal whether Tnf-α promotes osteogenesis during bone development, or whether the expression of *tnfα* is unique to regenerating osteoblasts. Nitroreductase-mediated ablation of osteoblasts in the developing operculum can be easily induced via the addition of a pro drug, nifurpirinol (NFP), to *osx*:*mCherry-ntr* zebrafish larvae (212, 487). Preliminary data shows ontogenetic (DMSO treated) and regenerating (NFP ablated) opercula between 3-5 dpf (Appendix 3). These images suggest that *tnfα* is not expressed by osteoblasts or their precursors in either normal operculum development, or regeneration of the operculum post-ablation. Instead, *tnfα* expression in that region was restricted to what morphologically appeared to be the developing gills (DMSO and NFP), or pro inflammatory macrophages containing mCherry from apoptotic osteoblasts (NFP only). (488). This suggests that larval zebrafish may not provide a suitable model for studying the pleiotropic effects of Tnf-α on osteoblasts.

5.3.6 CONCLUSIONS AND FUTURE DIRECTIONS

The modulation of TNF-α has become an attractive target for the treatment of a myriad of pathologies, from neurological degeneration to cancer. Moreover, use of clinically approved TNF-α inhibiting drugs for effective treatment of autoimmune diseases is becoming more widespread. Despite this, the pleiotropic effects of TNF-α on osteoblasts in homeostasis and repair are poorly understood. Here, I demonstrated the utility of the adult zebrafish caudal fin fracture and regeneration models for characterising the effect of Tnf-α on osteoblast differentiation. Pools of differentiating osteoblast precursors strongly express *tnfα* in the blastema. Moreover, dysregulated *tnfα* expression in these cells correlated with failed or ectopic bone growth during regeneration, in a pomalidomide-treated zebrafish. Future experiments should focus on studying the influence of effective Tnf-α suppression on differentiating osteoblasts, identifying the transcriptomic profile of *tnfα*$^{+}$ cells in regenerating lepidotrichia and exploring the dose-dependent relationship between Tnf-α and osteogenesis. Further studies should also explore the indirect mechanisms by which Tnf-α may modulate osteoblasts, as discussed in section 5.3.4.

CHAPTER 6: FINAL DISCUSSION

6.1 SUMMARY OF RESULTS AND FUTURE PLANS

6.1.1 FINAL OVERVIEW

Osteoporosis is a great source of morbidity and debilitation for the ageing population (64). The increasing prevalence of osteoporosis and fragility fractures means the demand for osteoanabolic therapies has never been higher. Zebrafish are an excellent model for studying aberrant human bone pathologies due to strong conservation of disease-associated genes and comparable skeletal physiology throughout life (195, 489). Here, I demonstrated the utility of the zebrafish caudal fin fracture and regeneration injury assays to study bone physiology dynamically. Collectively, these data highlight the need for highly coordinated spatiotemporal regulation of different cell types and processes to achieve optimal bone repair. I have demonstrated that small perturbations to the cellular and molecular mechanisms underpinning adult osteogenesis can have significant impacts on bone repair and regeneration. Whilst fracture repair is typically presented as a process comprised of three phases (inflammation, repair and remodelling), these phases overlap and interact in space and time, as illustrated in Figure 47. Therefore, when studying factors which may underpin optimal fracture repair, their impact on each of these phases should be considered.

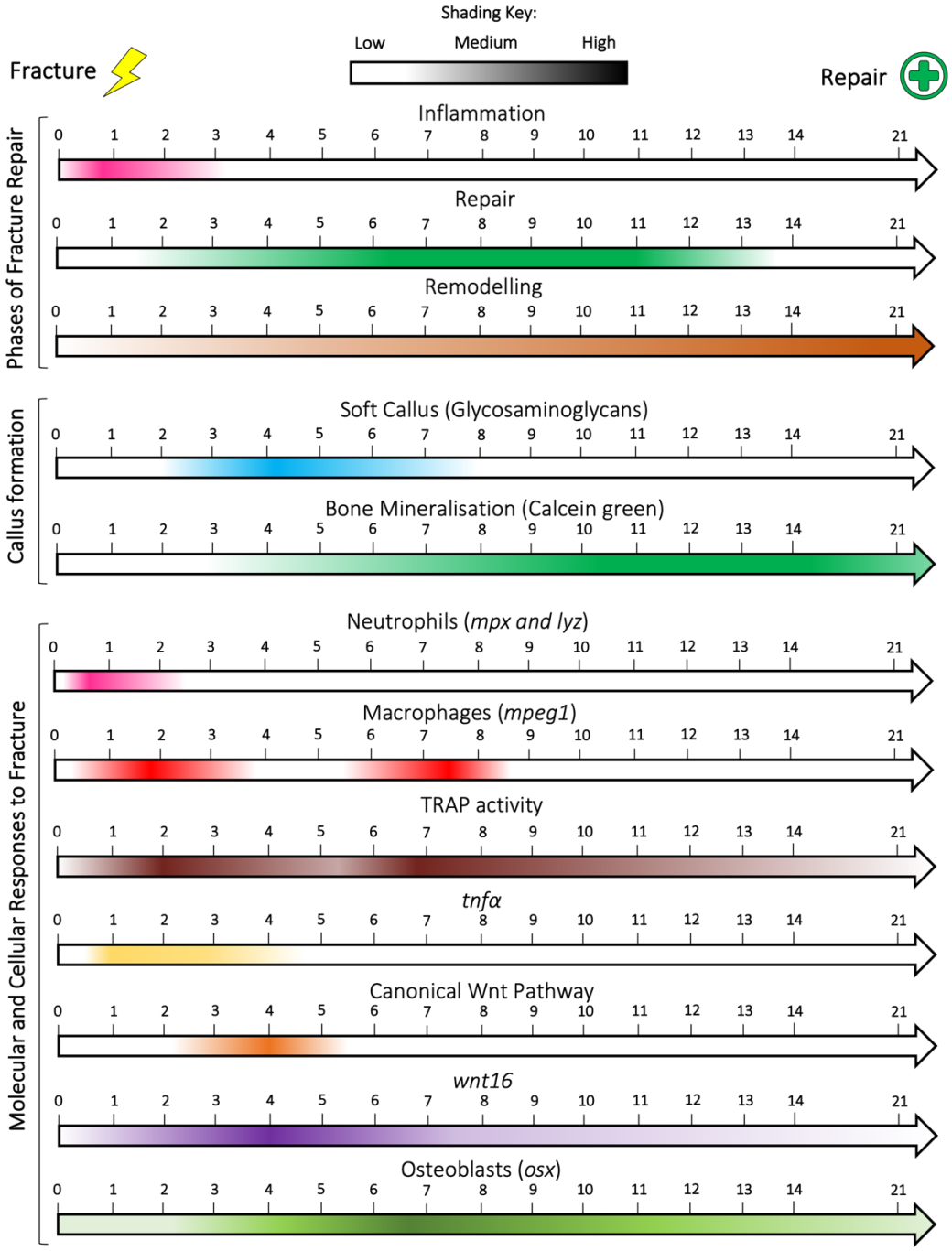

Figure 48. A Timeline of the Cellular and Molecular Events Underpinning Fracture Repair in the Zebrafish Caudal Fin. *Numbers above arrows represent number of days post injury (dpi), with the fracture occurring at 0 hpi and complete bone repair and remodelling being achieved around 21 dpi. Remodelling may continue after 21 dpi. Shading represents levels of activity from various cellular and molecular factors underpinning fracture repair. Evidence for this illustration is based on data from this thesis and from a previous zebrafish fracture repair study by Tomecka et al., 2019 (147).*

6.1.2 WNT16 IN FRACTURE REPAIR

First, I investigated how loss of Wnt16 affected fracture susceptibility and bone repair in zebrafish. In mice and humans, mutations in *WNT16* have been associated with low BMD, reduced cortical bone thickness and decreased bone strength, indicative of osteoporosis (263, 490). However, little was known about the role of Wnt16 in fracture repair. I demonstrated that Wnt16 protects against an osteoporosis-like phenotype in zebrafish; *wnt16*$^{-/-}$ mutant zebrafish displayed reduced TMD and increased fracture susceptibility within caudal fin lepidotrichia at a young age. I provided the first evidence to show that Wnt16 not only protects against fracture but also supports optimal fracture repair. Loss of Wnt16 resulted in precocious activation of the canonical Wnt signalling pathway, delayed upregulation of *osx* and delayed callus formation post-fracture. Visualisation of *wnt16* expression indicated that *wnt16* promotes efficient osteoblast differentiation by modulating canonical Wnt activity during the osteogenic stages of bone repair. Agonists of Wnt16, or suppression of precocious canonical Wnt pathway activity, may be targets of interest for promoting efficient osteogenesis.

Outstanding questions around the role of Wnt16 in bone repair remain. Given that *wnt16* mutants displayed dysregulated activation of the canonical Wnt signalling pathway post fracture, future studies should aim to explore how the expression of other canonical and non-canonical Wnt ligands are affected by loss of Wnt16. This may reveal the mechanism by which Wnt16 regulates canonical Wnt activity during bone repair. Moreover, this may reveal further targets which regulate osteogenesis. WNT16 has also been shown to negatively regulate osteoclastogenesis (264, 305). Given that differences in TRAP staining were observed in *wnt16* mutants post fracture, the role of Wnt16 in regulating bone resorption during early fracture repair warrants further investigation. Performing *in situ* hybridization for the osteoclast marker, *ctsk*, would further help to define the relationship between Wnt16 and osteoclast differentiation. Moreover, since TRAP activity coincided with the recruitment of *mpeg1*$^{+}$ cells to fracture, it would be interesting to explore the relationship between the recruitment of *mpeg1*$^{+}$ cells and osteoclastogenesis post fracture in zebrafish, and whether Wnt16 plays a role in this.

6.1.3 NEUTROPHILS IN BONE REPAIR

I next investigated a potential pro-reparative role for neutrophils in the early stages of fracture repair. In mammals, neutrophils are rapidly recruited to bone post-fracture, releasing pro-inflammatory cytokines

and performing microbial clearance (268). Though excessive or prolonged neutrophil activity is known to perturb bone repair, it has also been suggested that ECM production by neutrophils contributes to bone stabilisation post-fracture (134, 267). However, this potential pro-reparative function of neutrophils in bone repair was poorly defined. By imaging fractures dynamically in live zebrafish, and at fixed time points post-injury, I demonstrated that neutrophils are rapidly recruited to fractures within the first 4-8 hours post injury (hpi), contain the ECM proteins laminin and fibronectin and release chromatin. I also demonstrated that pharmacological inhibition of the neutrophil chemokine receptor, Cxcr2, does not significantly reduce neutrophil recruitment to fracture. However, Cxcr2 inhibition resulted in reduced neutrophil chromatin release post fracture and a significantly higher incidence of fracture dissociation events within the first 48 hpi. Data suggests that Cxcr2 supports early bone repair, potentially by mediating (NETosis-like) neutrophil chromatin release and ECM localisation within the fracture haematoma. Though further investigation is required, these results support the intriguing idea that neutrophils may help to stabilise fractured bone in a Cxcr2-dependent manner, potentially via chromatin release (NETs) and by contributing to ECM remodelling.

In the short term, I will repeat the fracture assays with SB225002 in *mpx*:*GFP*; *lyz:H2A-mCherry* zebrafish to ensure whether the CXCR2-dependent reduction of H2A-mCherry signal at the fracture site is reproducible. Moreover, I will live image the neutrophil response to fracture in DMSO and SB225002 treated fractures in *mpx*:*GFP*; *lyz:H2A-mCherry* under sustained anaesthesia, with the aim to capture H2A-mCherry release from neutrophils dynamically. This will also allow me to examine the effect of CXCR2 inhibition on neutrophil behaviour post fracture in more detail. I also will repeat these experiments using an alternative CXCR2 inhibitor, such as AZD5069, to determine whether fin dissociation in SB225002 treated animals is due to CXCR2-mediated effects on neutrophils, or off-target effects of the inhibitor (491). I will also seek to use published techniques to inhibit NET formation (gasdermin or neutrophil elastase inhibition) or degrade NETs (DNAse treatment) post fracture to determine whether fracture dissociation is likely due to reduced neutrophil recruitment, or due to reduced NET production in SB225002 treated animals (232, 382). In the longer term, I plan to explore the influence of ageing the neutrophilic response to fracture repair, as later described in section 6.2.1.

6.1.4 TNFα IN BONE REPAIR AND REGENERATION

Finally, I explored the pleiotropic effects of Tnf-α on bone. Both classical (anti-osteogenic) and paradoxical (pro-osteogenic) effects of TNF-α on osteoblast differentiation and activity have been described (38). In some instances, TNF-α is known to promote osteoblast apoptosis and bone resorption, whereas in others, it is known to promote osteoblast differentiation and augment fracture healing (42, 426, 437, 448, 478). Therefore, I sought to better characterise the pro-osteogenic influence of Tnf-α during bone repair and regeneration in zebrafish. By monitoring the spatiotemporal expression of *tnfα* in a fluorescent transgenic reporter line, I demonstrated that *tnfα* is strongly expressed by bone directly adjacent (distally) to fractured lepidotrichia and also patterns bone regeneration post-amputation in the caudal fin. Confocal imaging demonstrated that *tnfα* was strongly expressed by some differentiating osteoblasts, and potentially by osteoblast precursor cells, during osteogenesis post-amputation. Partial inhibition of Tnf-α resulted in varied effects on bone regeneration, though anecdotal evidence from one animal in which *tnfα* expression was perturbed suggests that Tnf-α is required for the regeneration of bone (lepidotrichia). Heterozygous *tnfα* mutants showed no significant difference in either callus formation post-fracture, or bone regeneration post-amputation, in the caudal fin, suggesting a lack of haploinsufficiency in the *tnfα* gene. I also introduced *ex vivo* scale culture as a potential method for studying the dose-dependent effect of Tnf-α on osteoblasts, in isolation from the immune system. Further experiments and optimisation of assays are required. However, these results suggest that expression of *tnfα* supports osteoblast differentiation during adult bone repair and regeneration.

In the short term, it must be first be established whether homozygous *tnfα* mutant zebrafish survive to adulthood, and whether they have altered skeletal development compared to WT (vial Alizarin Red staining or μ-CT). Provided healthy homozygous adults are available, I will establish whether osterix expression (via *osx*:mCherry) and bone mineralisation (via Alizarin Red staining) are affected by loss of Tnf-α during fracture repair and regeneration. Given that Tnf-α also plays a key role in orchestrating the recruitment and activity of immune cells to injury, as well as angiogenesis, these processes should also be monitored for differences in *tnfα*$^{-/-}$ zebrafish in future studies (240, 453). Given the apparent dose-depended effect of TNF-α on osteoblasts, a range of physiologically relevant concentrations of r-Tnf-α should be established using larval or *ex vivo* assays (434, 448). Once established, these concentrations can be applied *in vivo* during bone regeneration (via r-Tnf-α soaked bead implantation) or in further scale culture studies to characterise the pleiotropic effects of Tnf-α on osteoblasts. I also demonstrated that *tnfα* is co-expressed by some

osteoblasts during caudal fin lepidotrichia regeneration. However, a complete picture of which skeletal cells express and respond to *tnfα* during adult osteogenesis is missing. It will be crucial to further optimise FACS and RNA isolation from *tnfα*:GFP^{+} and *osx*:mCherry^{+} from regenerating fins to perform transcriptomic analyses of these cell populations. Finally, cell proliferation (PCNA) and apoptosis marker (TUNEL or caspase 3) staining should be incorporated into future experiments to determine whether *tnfα* expression by skeletal cells has a proliferative or pro-apoptotic effect.

6.2 FUTURE PERSPECTIVES

6.2.1 STUDYING THE EFFECTS OF AGEING ON FRACTURE REPAIR IN ZEBRAFISH

Increasing age is strongly correlated with the onset of osteoporosis; 1 in 3 women and 1 in 5 men over 50 experience osteoporotic fracture in their lifetime (67). Recently, interest in the role of inflammaging in skeletal health and fracture repair has emerged. Interestingly, high peripheral blood neutrophil counts are associated with decreasing BMD in ageing populations, more severe fracture trauma and increased mortality in elderly hip fracture patients (342-345). The pathological effects of dysregulated inflammation are well established, yet I and others have demonstrated a potential pro-reparative role for neutrophils in bone repair (267). Whilst markers of systemic inflammation increase in older people, the responsiveness of neutrophils decline with age (77, 492). Furthermore, a relationship between age-related inflammation and the dysfunction of skeletal progenitor cells was recently demonstrated in mice and humans, resulting in reduced osteoblast activity and a decline in trabecular bone health (493). Interestingly, this effect could be reversed by treatment with non-steroidal anti-inflammatories. Given that local and systemic inflammation can trigger osteoclastogenesis, inflammaging may underpin increased bone resorption leading to osteoporosis (41, 42, 494). I demonstrated that bone calluses resulting from spontaneous fractures accumulate with age in zebrafish. Moreover, it has recently been shown that zebrafish vertebrae display osteoporotic changes as they age, as well as intervertebral disc degeneration (224, 227). This demonstrates that age-related bone degeneration can be modelled in zebrafish. Due to the ease and low cost of long-term maintenance of zebrafish in high numbers (relative to rodents), zebrafish present a practical and efficient model for studying the influence of inflammaging on bone. Future zebrafish studies should seek to examine the relationship between immune dysregulation, ageing and bone maintenance and repair. This will reveal novel insights into the effect of ageing on bone physiology.

Indeed, I plan to compare fracture repair in young (under 1 yo) and aged (over 2 yo) adult zebrafish, with a focus on immune regulation in this process. I will isolate protein from uninjured or fractured bone tissue in young and aged zebrafish at time points relevant to neutrophil recruitment for proteomic analysis. This will reveal novel insights about the role of neutrophils in fracture stabilisation and matrix production or remodelling post fracture, whilst also revealing whether ageing affects osteoimmunology during homeostasis and bone repair. These experiments may highlight novel functions of neutrophils in bone for further exploration.

6.2.2 SEX DIFFERENCES IN ZEBRAFISH MAY AFFECT BONE PHYSIOLOGY

It is well established that sex differences in bone turnover exist, particularly in ageing populations (Section 1.1.1.9). This is due to the role that oestrogen ("female" sex hormone) and androgens ("male" sex hormones) play in skeletal maintenance (84). Whilst oestrogen plays an important role in the normal physiology of both men and women, women experience a rapid decline in oestrogen levels throughout perimenopause that causes a reprogramming in skeletal physiology. This leads to increased osteoblast apoptosis and increased osteoclastogenesis, causing a decline in BMD (85, 87). Therefore, osteoporosis is highly prevalent in postmenopausal women (69). The effects of oestrogen deficiency have been successfully modelled in mice, both genetically, and via ovariectomy (82, 283, 490). These studies have revealed insights into the role of oestrogen signalling in the development of osteoporosis (83).

Sex differences are not typically accounted for in zebrafish bone studies. Sex determination is polygenic and highly plastic in teleosts; gonadal development depends on a variety of environmental and genetic factors (495). Zebrafish are classed as juvenile hermaphrodites, meaning they develop ovary-like undifferentiated gonads, which may differentiate into ovaries, or testis, as the fish matures (496). This means that sex is not determined throughout early and juvenile skeletal development in zebrafish. Despite this, oestrogen-mediated effects on skeletal gene expression, including *opg* and *rankl*, have been demonstrated throughout craniofacial development in zebrafish (497). Moreover, disruption of oestrogen-related receptor alpha (*esrra*) in zebrafish larvae impairs chondrocyte differentiation by reducing the expression of *sox9*, *col2a1* and *col10a1* (498). Functional knockout of oestrogen receptor alpha (*esr1*) has been shown to cause premature ovarian failure in zebrafish, suggesting that oestrogens influence ageing, similarly to humans (499). Remarkably, female-to-male sex change can be induced in adult zebrafish via treatment with an aromatase inhibitor (ingested or injected), resulting in the formation of a functional

testis-like tissue which generates fertile sperm (500, 501). This suggests that the physiological effects of oestrogen on the mature zebrafish skeleton may differ from humans or vary dynamically throughout life in response to environmental stimuli. Transgenic zebrafish lines which allow the visualisation of oestrogen receptor expression and activation are available, largely due to the use of zebrafish as a model for studying the physiological effects of exogenous oestrogen-mimicking chemicals in the environment (502, 503). These lines may be used to reveal more about the role of oestrogen signalling in bone homeostasis, repair and ageing in zebrafish. To date, few studies have characterised sex differences in skeletal ageing in zebrafish. One study demonstrated that 9 month-old female zebrafish exhibit higher trabecular volume compared to males, but that this difference is lost as the females age (227). Moreover, 1 year old male zebrafish displayed higher vertebral tissue space, analogous to the bone marrow space in human vertebrae, compared to female fish of the same age. Currently, preliminary data from the Hammond lab suggests that zebrafish scale regeneration becomes dysregulated with age, and that aged females display more severe scale regeneration phenotypes compared to aged males (Unpublished data generated by Qiao Tong). Collectively, this suggests that sex may influence age-related bone deterioration in zebrafish. Given the importance of oestrogen in bone, future studies of skeletal biology in zebrafish should seek to monitor sex differences in experiments, particularly where ageing is a factor. This will help to ensure that results are not confounded by potential differences in the physiology of male and female animals, improving the translational impact of zebrafish as a model for bone pathologies.

6.2.3 INTEGRATED EPIDEMIOLOGICAL AND ZEBRAFISH STUDIES

In recent years, advances in high-throughput gene sequencing technologies and large-scale genetic epidemiological studies have propelled our understanding of healthy bone physiology and skeletal pathologies (163). However, these genetic candidates require functional validation in laboratory models to determine the mechanistic impact of gene disruption on osteometabolic processes. This is required to determine whether affected pathways are likely to be of therapeutic interest, and to evaluate the potential off-target effects of signal disruption within these pathways *in vivo*. Crispant zebrafish are increasingly being used as a model for rapid high-throughput phenotyping of GWAS-derived genes associated with aberrant skeletal phenotypes and disease, whilst stable mutagenesis of priority genes allows for clinically relevant study of bone (217, 255, 489). Future studies should aim to align human epidemiological analysis with functional validation experiments in zebrafish, via multi-disciplinary collaboration. Recently, a single

interdisciplinary study identified a rare mutation in *SMAD9* via genetic analysis of a pedigree with unexplained HBM, before using follow-up *in vivo* experiments to demonstrate that the Smad9 protein can be detected during skeletal development in zebrafish larvae, and that *Smad9* is also expressed by cortical bone osteocytes in mice (161). This study highlighted the potential of SMAD9 as a novel osteoanabolic target for osteoporosis. A follow-up study in zebrafish larvae revealed that Smad9 labels proliferating osteochondral precursor cells during skeletal development and regeneration, and that Smad9 expression is altered by osteomodulatory compounds (487). These studies demonstrate how triangulation of results derived from human epidemiological, murine and zebrafish studies can elevate the clinical relevance of bone research. Integrative approaches such as this will ensure that studies yield translational results and accelerate the discovery of novel therapies for the treatment of bone pathologies.

6.3 CONCLUSION

Over the past two decades zebrafish have been used to unravel the secrets of bone development and regeneration. Here, I demonstrated that zebrafish bone injury assays (caudal fin fracture and regeneration) can be used to investigate genetic and immunological factors underpinning optimal fracture repair, which can reveal new insights into the aetiology of osteoporosis and non-union fractures. Fracture repair is an elaborate form of adult osteogenesis, with the cellular and molecular responses to bone damage requiring tight spatiotemporal coordination. I highlighted that the phases of fracture repair are interconnected, elaborate and highly sensitive to subtle perturbations. Moving to the future, zebrafish assays (*in vivo* and *ex vivo*) will continue to present an exciting platform to rapidly discover or validate novel osteoanabolic pathways, which could be translated back into the clinic as therapies to improve patients' lives.

APPENDICES

APPENDIX 1

Modular image analysis workflow (.mia) and classifier model (.model) files used for automated image analysis can be accessed via the relevant links below. The Modular Image Analysis plugin can be accessed as described in the Materials and Methods section (Chapter 2). All MIA workflows were written and developed by Dr Stephen Cross in the Wolfson Bioimaging facility at the University of Bristol. Parameters for each analysis (e.g., threshold values, cell area limits) should be adjusted for every new analysis on a test-set of images to ensure compatibility for analysis and optimised results.

MIA for immune cells distance to fracture counts:

https://drive.google.com/drive/folders/1oCSUAMiqOcJPOuQakyg7i6l0ldbxVE1X?usp=sharing

MIA for ALP analysis of scales:

https://drive.google.com/drive/folders/1dBPQYKRAUq9C9pFBcB04QHoBW7e-Lgd_?usp=sharing

MIA for automated analysis of *osx*:mCherry on Incucyte-imaged scales:

https://drive.google.com/drive/folders/1aUsnvSlIICkJTBEBtmWl25XlTWqqQMk_?usp=sharing

APPENDIX 2

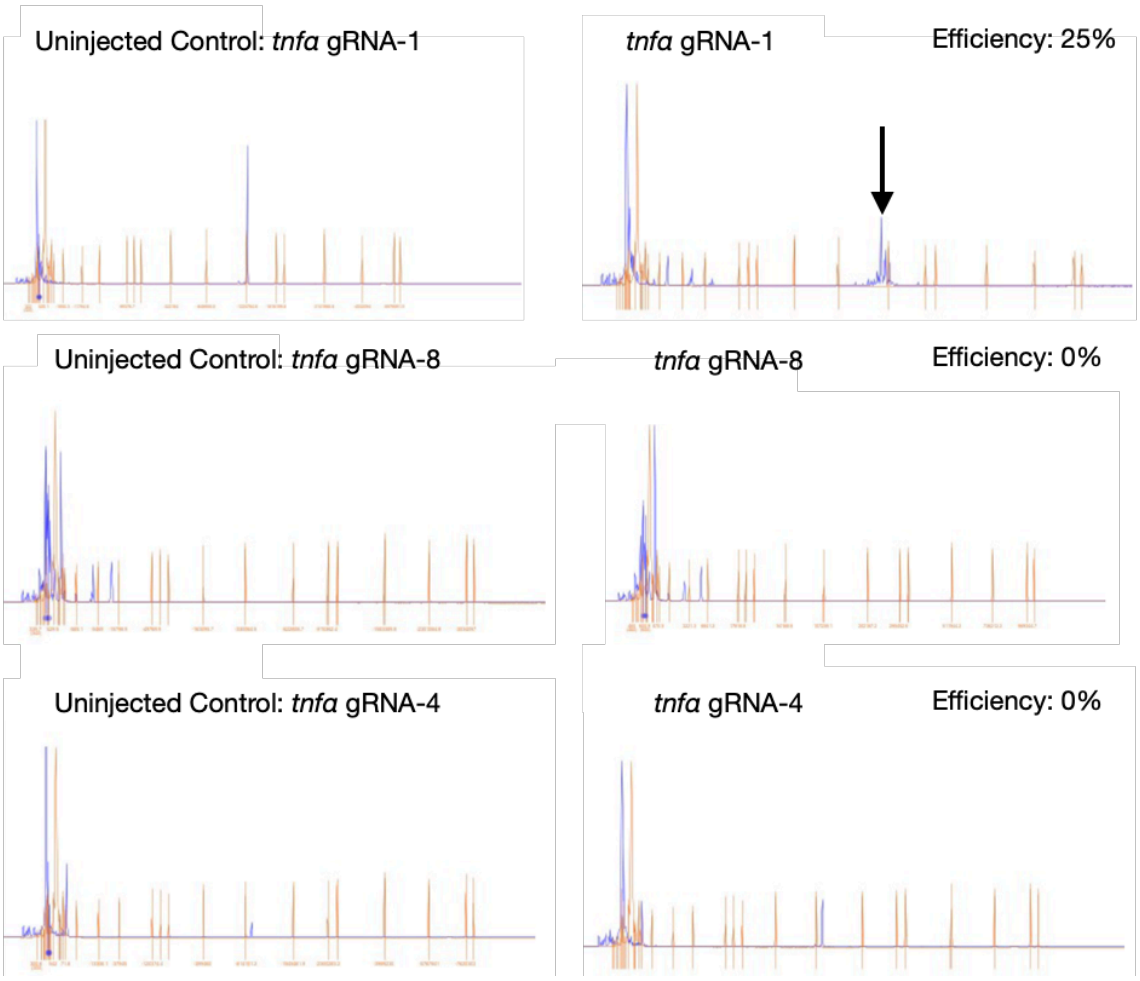

Appendix 2. Fragment Analysis of tnfα Amplicons from F0 Embryos Targeted with CRISPR-Cas-9 Mutagenesis. *Three guide RNAs (gRNAs) targeting either exons 1 (gRNA-8 and gRNA-4) or 4 (gRNA-1) of tnfα were designed and tested, with the aim to create a mosaic F0 generation using CRISPR-Cas9 mutagenesis. Only gRNA-1 resulted in mutagenesis (arrowhead highlighting multiple fragments), with low efficiency (25%), unsuitable for CRISPR knockdown experiments (>90% efficiency required). gRNA-8 showed no peaks in either control or injected samples, suggesting PCR product was poor quality or concentration. gRNA-4 showed lo height, single peaks; low height of peak suggests concentration of PCR product was too low, but the presence of single peaks suggest a lack of mutagenesis using this gRNA. Exon 1 of tnfα is relatively short compared to exon 4. Collectively, this suggests that multiple gRNAs targeting exon 4 will be more appropriate for CRISPR-Cas9 mediated mutagenesis of tnfα. Plots visualised in Geneious software.*

APPENDIX 3

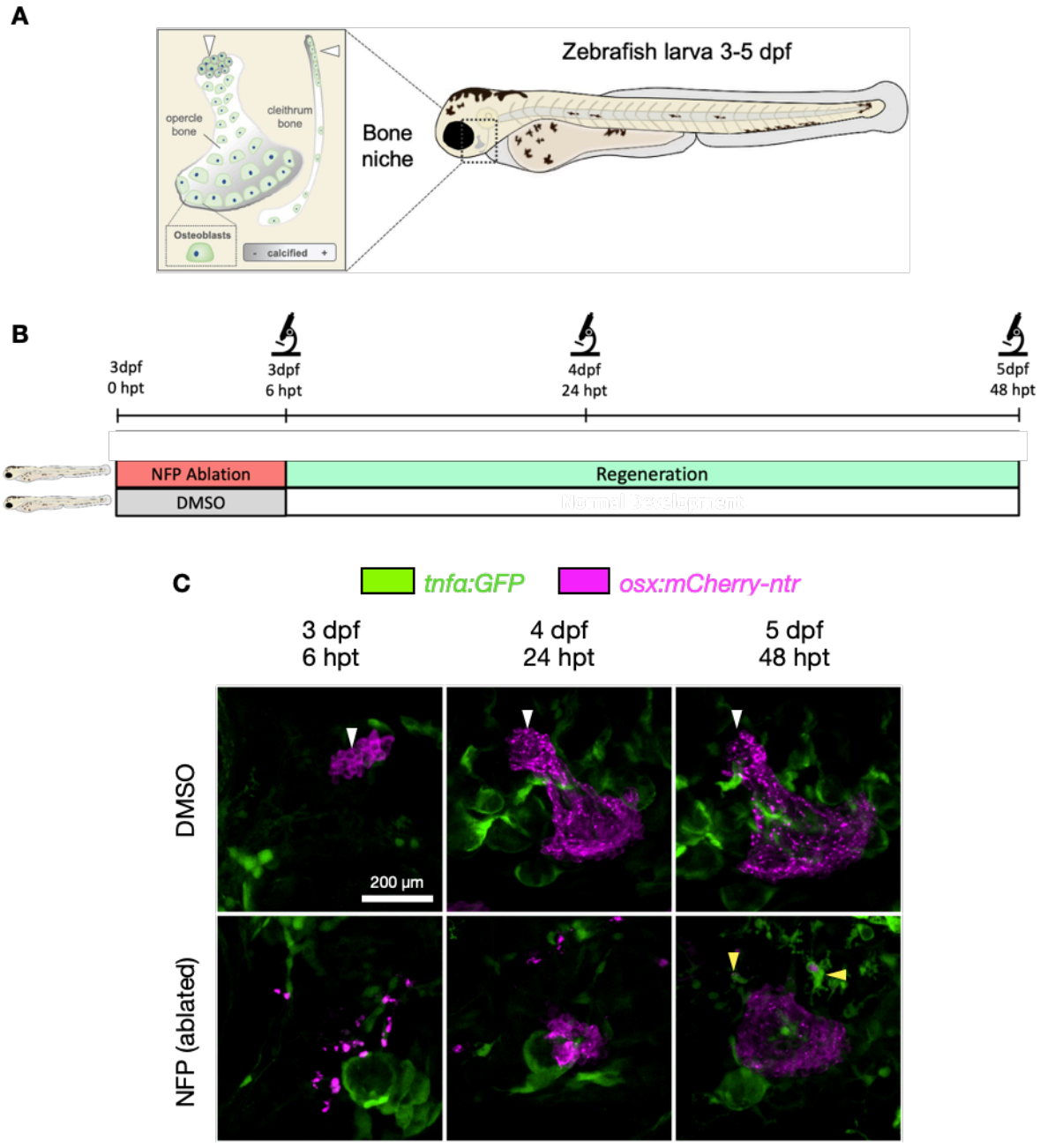

Appendix 3. tnfα Does Not Appear To Be Expressed By osx:mCherry⁺ Osteoblasts In Either The Developing Or Regenerating Operculum In Zebrafish Larvae. A: between 3-5 days post fertilisation (dpf), the first mineralised bones begin to develop in zebrafish. The operculum and cleithrum, external sheets of dermal bone, are formed from small pockets of cells (white arrowheads), which differentiate into osteoblasts and produce bone matrix. B: Schematic showing ablation model in larval

osx:mCherry-ntr zebrafish. Larval zebrafish are incubated in either DMSO (control), or a pro-drug, nifurpirinol (NFP) for 6 hours at 3 dpf; NFP is reduced by the nitroreductase (ntr) enzyme, expressed under the control of the osx promoter, causing osteoblast apoptosis and ablation. Larval zebrafish are imaged between 6 and 24 hours post-treatment (hpt). Regeneration of the operculum (NFP) or normal operculum development (DMSO) can be observed. C: Representative maximum projection images of the normal developing operculum (DMSO treated) and the regenerating operculum post-ablation (NFP). Regions of tnfα:GFP can be observed in DMSO and NFP treated larvae, but do not colocalise with regions of osx:mCherry in the operculum. These tnfα:GFP^{+} regions are likely the developing gills, due to the morphology and location of the GFP. However, in NFP treated larvae, some tnfα:GFP^{+} immune cells can be seen containing mCherry, as they clear the apoptotic cells (yellow arrowheads).

BIBLIOGRAPHY

1. Dietrich K, Fiedler IAK, Kurzyukova A, Lopez-Delgado AC, McGowan LM, Geurtzen K, et al. Skeletal Biology and Disease Modeling in Zebrafish. Journal of Bone and Mineral Research. 2021;36(3):436-58.
2. McGowan LM, Kague E, Vorster A, Newham E, Cross S, Hammond CL. Wnt16 Elicits a Protective Effect Against Fractures and Supports Bone Repair in Zebrafish. JBMR Plus. 2021;5(3):e10461.
3. Su N, Yang J, Xie YL, Du XL, Chen HG, Zhou H, et al. Bone function, dysfunction and its role in diseases including critical illness. International Journal of Biological Sciences. 2019;15(4):776-87.
4. Drake MT, Clarke BL, Lewiecki EM. The Pathophysiology and Treatment of Osteoporosis. Clinical Therapeutics. 2015;37(8):1837-50.
5. Sinder BP, Pettit AR, McCauley LK. Macrophages: Their Emerging Roles in Bone. Journal of Bone and Mineral Research. 2015;30(12):2140-9.
6. Raggatt LJ, Partridge NC. Cellular and Molecular Mechanisms of Bone Remodeling. Journal of Biological Chemistry. 2010;285(33):25103-8.
7. Chen D, Shen J, Zhao WW, Wang TY, Han L, Hamilton JL, et al. Osteoarthritis: toward a comprehensive understanding of pathological mechanism. Bone Research. 2017;5.
8. Akkiraju H, Nohe A. Role of Chondrocytes in Cartilage Formation, Progression of Osteoarthritis and Cartilage Regeneration. Journal of Developmental Biology. 2015;3(4):177-92.
9. Lawrence EA, Kague E, Aggleton JA, Harniman RL, Roddy KA, Hammond CL. The mechanical impact of col11a2 loss on joints; col11a2 mutant zebrafish show changes to joint development and function, which leads to early-onset osteoarthritis. Philosophical Transactions of the Royal Society B-Biological Sciences. 2018;373(1759).
10. Li JM, Dong SW. The Signaling Pathways Involved in Chondrocyte Differentiation and Hypertrophic Differentiation. Stem Cells International. 2016;2016.
11. Chen H, Tan XN, Hu S, Liu RQ, Peng LH, Li YM, et al. Molecular Mechanisms of Chondrocyte Proliferation and Differentiation. Frontiers in Cell and Developmental Biology. 2021;9.
12. Stegen S, Rinaldi G, Loopmans S, Stockmans I, Moermans K, Thienpont B, et al. Glutamine Metabolism Controls Chondrocyte Identity and Function. Developmental Cell. 2020;53(5):530-+.
13. Rutkovskiy A, Stenslokken KO, Vaage IJ. Osteoblast Differentiation at a Glance. Medical Science Monitor Basic Research. 2016;22:95-106.
14. Debiais-Thibaud M, Simion P, Venteo S, Munoz D, Marcellini S, Mazan S, et al. Skeletal Mineralization in Association with Type X Collagen Expression Is an Ancestral Feature for Jawed Vertebrates. Molecular Biology and Evolution. 2019;36(10):2265-76.
15. Eames BF, Amores A, Yan YL, Postlethwait JH. Evolution of the osteoblast: skeletogenesis in gar and zebrafish. Bmc Evolutionary Biology. 2012;12.
16. Felber K, Elks PM, Lecca M, Roehl HH. Expression of osterix Is Regulated by FGF and Wnt/beta-Catenin Signalling during Osteoblast Differentiation. Plos One. 2015;10(12).
17. Komori T. Regulation of Proliferation, Differentiation and Functions of Osteoblasts by Runx2. International Journal of Molecular Sciences. 2019;20(7):11.
18. Reinhold MI, Naski MC. Direct interactions of Runx2 and canonical Wnt signaling induce FGF18. Journal of Biological Chemistry. 2007;282(6):3653-63.
19. Komori T, Yagi H, Nomura S, Yamaguchi A, Sasaki K, Deguchi K, et al. Targeted disruption of Cbfa1 results in a complete lack of bone formation owing to maturational arrest of osteoblasts. Cell. 1997;89(5):755-64.
20. Carvalho MS, Cabral JMS, da Silva CL, Vashishth D. Synergistic effect of extracellularly supplemented osteopontin and osteocalcin on stem cell proliferation, osteogenic differentiation, and angiogenic properties. Journal of Cellular Biochemistry. 2019;120(4):6555-69.
21. Creecy A, Damrath JG, Wallace JM. Control of Bone Matrix Properties by Osteocytes. Frontiers in Endocrinology. 2021;11.
22. Bonewald LF. The Amazing Osteocyte. Journal of Bone and Mineral Research. 2011;26(2):229-38.

23. Cawley KM, Bustamante-Gomez NC, Guha AG, MacLeod RS, Xiong JH, Gubrij I, et al. Local Production of Osteoprotegerin by Osteoblasts Suppresses Bone Resorption. Cell Reports. 2020;32(10).
24. Capulli M, Paone R, Rucci N. Osteoblast and osteocyte: Games without frontiers. Archives of Biochemistry and Biophysics. 2014;561:3-12.
25. McDonald MM, Kim AS, Mulholland BS, Rauner M. New Insights Into Osteoclast Biology. Jbmr Plus. 2021;5(9).
26. Jacome-Galarza CE, Percin GI, Muller JT, Mass E, Lazarov T, Eitler J, et al. Developmental origin, functional maintenance and genetic rescue of osteoclasts. Nature. 2019;568(7753):541-+.
27. Kukita T, Wada N, Kukita A, Kakimoto T, Sandra F, Toh K, et al. RANKL-induced DC-STAMP is essential for osteoclastogenesis. Journal of Experimental Medicine. 2004;200(7):941-6.
28. Ikeda K, Takeshita S. The role of osteoclast differentiation and function in skeletal homeostasis. Journal of Biochemistry. 2016;159(1):1-8.
29. Yagi M, Miyamoto T, Sawatani Y, Iwamoto K, Hosogane N, Fujita N, et al. DC-STAMP is essential for cell-cell fusion in osteoclasts and foreign body giant cells. Journal of Experimental Medicine. 2005;202(3):345-51.
30. Tsukasaki M, Huynh NCN, Okamoto K, Muro R, Terashima A, Kurikawa Y, et al. Stepwise cell fate decision pathways during osteoclastogenesis at single-cell resolution. Nature Metabolism. 2020;2(12).
31. Teitelbaum SL, Ross FP. Genetic regulation of osteoclast development and function. Nature Reviews Genetics. 2003;4(8):638-49.
32. Goto T, Yamaza T, Tanaka T. Cathepsins in the osteoclast. Journal of Electron Microscopy. 2003;52(6):551-8.
33. Merrild DMH, Pirapaharan DC, Andreasen CM, Kjaersgaard-Andersen P, Moller AMJ, Ding M, et al. Pit- and trench-forming osteoclasts: a distinction that matters. Bone Research. 2015;3.
34. McDonald MM, Khoo WH, Ng PY, Xiao Y, Zamerli J, Thatcher P, et al. Osteoclasts recycle via osteomorphs during RANKL-stimulated bone resorption. Cell. 2021;184(5):1330-+.
35. Pereira M, Petretto E, Gordon S, Bassett JHD, Williams GR, Behmoaras J. Common signalling pathways in macrophage and osteoclast multinucleation. Journal of Cell Science. 2018;131(11).
36. Tsukasaki M, Takayanagi H. Osteoimmunology: evolving concepts in bone-immune interactions in health and disease. Nature Reviews Immunology2019. p. https://doi.org/10.1038/s41577-019-0178-8.
37. Anderson JM. Multinucleated giant cells. Current Opinion in Hematology. 2000;7(1):40-7.
38. Osta B, Benedetti G, Miossec P. Classical and paradoxical effects of TNF-alpha on bone homeostasis. Frontiers in Immunology. 2014;5.
39. Guder C, Gravius S, Burger C, Wirtz DC, Schildberg FA. Osteoimmunology: A Current Update of the Interplay Between Bone and the Immune System. Frontiers in Immunology. 2020;11.
40. Hu XL, Sun YC, Xu WH, Lin T, Zeng H. Expression of RANKL by peripheral neutrophils and its association with bone mineral density in COPD. Respirology. 2017;22(1):126-32.
41. Lam J, Takeshita S, Barker JE, Kanagawa O, Ross FP, Teitelbaum SL. TNF-alpha induces osteoclastogenesis by direct stimulation of macrophages exposed to permissive levels of RANK ligand. Journal of Clinical Investigation. 2000;106(12):1481-8.
42. Marahleh A, Kitaura H, Ohori F, Kishikawa A, Ogawa S, Shen WR, et al. TNF-alpha Directly Enhances Osteocyte RANKL Expression and Promotes Osteoclast Formation. Journal of Bone and Mineral Research. 2019;34:238-.
43. Batoon L, Millard SM, Raggatt LJ, Pettit AR. Osteomacs and Bone Regeneration. Current Osteoporosis Reports. 2017;15(4):385-95.
44. Chang MK, Raggatt LJ, Alexander KA, Kuliwaba JS, Fazzalari NL, Schroder K, et al. Osteal tissue macrophages are intercalated throughout human and mouse bone lining tissues and regulate osteoblast function in vitro and in vivo. Journal of Immunology. 2008;181(2):1232-44.

45. Bozec A, Soulat D. Latest perspectives on macrophages in bone homeostasis. Pflugers Archiv-European Journal of Physiology. 2017;469(3-4):517-25.
46. Papadaki HA, Margioris AN, Miliaki M, Steriopoulos C, Valatas W, Eliopoulos GD. Chronic idiopathic neutropenia of adults is associated with decreased bone mineral density and alterations in bone turnover biochemical markers. European Journal of Haematology. 1999;62(5):311-6.
47. Olsen BR, Reginato AM, Wang WF. Bone development. Annual Review of Cell and Developmental Biology. 2000;16:191-220.
48. Wagner EF, Karsenty G. Genetic control of skeletal development. Current Opinion in Genetics & Development. 2001;11(5):527-32.
49. Galea GL, Zein MR, Allen S, Francis-West P. Making and shaping endochondral and intramembranous bones. Developmental Dynamics. 2021;250(3):414-49.
50. Mackie EJ, Ahmed YA, Tatarczuch L, Chen KS, Mirams M. Endochondral ossification: How cartilage is converted into bone in the developing skeleton. International Journal of Biochemistry & Cell Biology. 2008;40(1):46-62.
51. Roy ME, Rho JY, Tsui TY, Evans ND, Pharr GM. Mechanical and morphological variation of the human lumbar vertebral cortical and trabecular bone. Journal of Biomedical Materials Research. 1999;44(2):191-7.
52. Giffin JL, Gaitor D, Franz-Odendaal TA. The Forgotten Skeletogenic Condensations: A Comparison of Early Skeletal Development Amongst Vertebrates. Journal of Developmental Biology. 2019;7(1).
53. Maes C. Role and Regulation of Vascularization Processes in Endochondral Bones. Calcified Tissue International. 2013;92(4):307-23.
54. Mackie EJ, Tatarczuch L, Mirams M. The skeleton: a multi-functional complex organ. The growth plate chondrocyte and endochondral ossification. Journal of Endocrinology. 2011;211(2):109-21.
55. Teng CS, Cavin L, Maxson REJ, Sanchez-Villagra MR, Crump JG. Resolving homology in the face of shifting germ layer origins: Lessons from a major skull vault boundary. Elife. 2019;8.
56. Carter DR, Mikic B, Padian K. Epigenetic mechanical factors in the evolution of long bone epiphyses. Zoological Journal of the Linnean Society. 1998;123(2):163-78.
57. Li XH, Han L, Nookaew I, Mannen E, Silva MJ, Almeida M, et al. Stimulation of Piezo1 by mechanical signals promotes bone anabolism. Elife. 2019;8.
58. Qin L, Liu W, Cao HL, Xiao GZ. Molecular mechanosensors in osteocytes. Bone Research. 2020;8(1).
59. Kenkre JS, Bassett JHD. The bone remodelling cycle. Annals of Clinical Biochemistry. 2018;55(3):308-27.
60. Martin TJ. Bone Biology and Anabolic Therapies for Bone: Current Status and Future Prospects. J Bone Metab. 2014;21(1):8-20.
61. Abdelgawad ME, Delaisse JM, Hinge M, Jensen PR, Alnaimi RW, Rolighed L, et al. Early reversal cells in adult human bone remodeling: osteoblastic nature, catabolic functions and interactions with osteoclasts. Histochemistry and Cell Biology. 2016;145(6):603-15.
62. Delaisse J-M. The reversal phase of the bone-remodeling cycle: cellular prerequisites for coupling resorption and formation. BoneKEy reports. 2014;3:561-.
63. Johnell O, Kanis JA, Oden A, Johansson H, De Laet C, Delmas P, et al. Predictive value of BMD for hip and other fractures. Journal of Bone and Mineral Research. 2005;20(7):1185-94.
64. NICE. NICEimpact: falls and fragility fractures. National Institute for Health and Care Excellence; 2018.
65. Al Anouti F, Taha Z, Shamim S, Khalaf K, Al Kaabi L, Alsafar H. An insight into the paradigms of osteoporosis: From genetics to biomechanics. Bone Reports. 2019;11.
66. National Osteoporosis Society. NHS RightCare scenario:The variation between sub-optimal and optimal pathways. 2017.

67. Sozen T, Ozisik L, Basaran NC. An overview and management of osteoporosis. European Journal of Rheumatology. 2017;4(1):46-56.
68. Al-Sari UA, Tobias J, Clark E. Health-related quality of life in older people with osteoporotic vertebral fractures: a systematic review and meta-analysis. Osteoporosis International. 2016;27(10):2891-900.
69. Demontiero O, Vidal C, Duque G. Aging and bone loss: new insights for the clinician. Therapeutic advances in musculoskeletal disease. 2012;4(2):61-76.
70. Chen HY, Zhou XR, Fujita H, Onozuka M, Kubo KY. Age-Related Changes in Trabecular and Cortical Bone Microstructure. International Journal of Endocrinology. 2013;2013.
71. Chen H, Shoumura S, Emura S, Bunai Y. Regional variations of vertebral trabecular bone microstructure with age and gender. Osteoporosis International. 2008;19(10):1473-83.
72. Chappard C, Bensalah S, Olivier C, Gouttenoire PJ, Marchadier A, Benhamou C, et al. 3D characterization of pores in the cortical bone of human femur in the elderly at different locations as determined by synchrotron micro-computed tomography images. Osteoporosis International. 2013;24(3):1023-33.
73. Chen H, Zhou X, Shoumura S, Emura S, Bunai Y. Age- and gender-dependent changes in three-dimensional microstructure of cortical and trabecular bone at the human femoral neck. Osteoporosis International. 2010;21(4):627-36.
74. Piemontese M, Almeida M, Robling AG, Kim HN, Xiong J, Thostenson JD, et al. Old age causes de novo intracortical bone remodeling and porosity in mice. Jci Insight. 2017;2(17).
75. Rosen CJ, Bouxsein ML. Mechanisms of disease: is osteoporosis the obesity of bone? Nature Clinical Practice Rheumatology. 2006;2(1):35-43.
76. Hou J, He C, He WZ, Yang M, Luo XH, Li CJ. Obesity and Bone Health: A Complex Link. Frontiers in Cell and Developmental Biology. 2020;8.
77. Lencel P, Magne D. Inflammaging: The driving force in osteoporosis? Medical Hypotheses. 2011;76(3):317-21.
78. Franceschi C, Garagnani P, Parini P, Giuliani C, Santoro A. Inflammaging: a new immune-metabolic viewpoint for age-related diseases. Nature Reviews Endocrinology. 2018;14(10):576-90.
79. Solana R, Pawelec G, Tarazona R. Aging and innate immunity. Immunity. 2006;24(5):491-4.
80. Saxena Y, Routh S, Mukhopadhaya A. Immunoporosis: Role of Innate Immune Cells in Osteoporosis. Frontiers in Immunology. 2021;12.
81. Khosla S, Oursler MJ, Monroe DG. Estrogen and the skeleton. Trends in Endocrinology and Metabolism. 2012;23(11):576-81.
82. Martin-Millan M, Almeida M, Ambrogini E, Han L, Zhao H, Weinstein RS, et al. The Estrogen Receptor-α in Osteoclasts Mediates the Protective Effects of Estrogens on Cancellous But Not Cortical Bone. Molecular Endocrinology. 2010;24(2):323-34.
83. Almeida M, Laurent MR, Dubois V, Claessens F, O'Brien CA, Bouillon R, et al. Estrogens and Androgens in Skeletal Physiology and Pathophysiology. Physiological Reviews. 2017;97(1):135-87.
84. Manolagas SC, O'Brien CA, Almeida M. The role of estrogen and androgen receptors in bone health and disease. Nature Reviews Endocrinology. 2013;9(12):699-712.
85. Bradford PG, Gerace KV, Roland RL, Chrzan BG. Estrogen regulation of apoptosis in osteoblasts. Physiology & Behavior. 2010;99(2):181-5.
86. Almeida M, Iyer S, Martin-Millan M, Bartell SM, Han L, Ambrogini E, et al. Estrogen receptor-alpha signaling in osteoblast progenitors stimulates cortical bone accrual. Journal of Clinical Investigation. 2013;123(1):394-404.
87. Bord S, Ireland DC, Beavan SR, Compston JE. The effects of estrogen on osteoprotegerin, RANKL, and estrogen receptor expression in human osteoblasts. Bone. 2003;32(2):136-41.
88. Dalal PK, Agarwal M. Postmenopausal syndrome. Indian Journal of Psychiatry. 2015;57:S222-S32.

89. Salari N, Ghasemi H, Mohammadi L, Behzadi MH, Rabieenia E, Shohaimi S, et al. The global prevalence of osteoporosis in the world: a comprehensive systematic review and meta-analysis. Journal of Orthopaedic Surgery and Research. 2021;16(1).
90. Ralston SH, Uitterlinden AG. Genetics of Osteoporosis. Endocrine Reviews. 2010;31(5):629-62.
91. Sabir AH, Cole T. The evolving therapeutic landscape of genetic skeletal disorders. Orphanet Journal of Rare Diseases. 2019;14(1).
92. Marini JC, Forlino A, Bachinger HP, Bishop NJ, Byers PH, De Paepe A, et al. Osteogenesis imperfecta. Nature Reviews Disease Primers. 2017;3.
93. Nijhuis WH, Eastwood DM, Allgrove J, Hvid I, Weinans HH, Bank RA, et al. Current concepts in osteogenesis imperfecta: bone structure, biomechanics and medical management. Journal of Childrens Orthopaedics. 2019;13(1):1-11.
94. Fiedler IAK, Schmidt FN, Wolfel EM, Plumeyer C, Milovanovic P, Gioia R, et al. Severely Impaired Bone Material Quality in Chihuahua Zebrafish Resembles Classical Dominant Human Osteogenesis Imperfecta. Journal of Bone and Mineral Research. 2018;33(8):1489-99.
95. Caparrós-Martín JA, Víctor Martínez-Glez V, Valencia M, Aglan M, Tenorio Ja, Temtamy S, et al. Osteogenesis Imperfecta: A Translational Approach to Brittle Bone Disease. Chapter 19 - BMP1 Mutations in Autosomal Recessive Osteogenesis Imperfecta.: Academic Press; 2014.
96. Sangsin A, Kuptanon C, Srichomthong C, Pongpanich M, Suphapeetiporn K, Shotelersuk V. Two novel compound heterozygous BMP1 mutations in a patient with osteogenesis imperfecta: a case report. Bmc Medical Genetics. 2017;18.
97. Xu XJ, Lv F, Song YW, Li LJ, Asan, Wei XX, et al. Novel mutations in BMP1 induce a rare type of osteogenesis imperfecta. Clinica Chimica Acta. 2019;489:21-8.
98. Puig-Hervas MT, Temtamy S, Aglan M, Valencia M, Martinez-Glez V, Ballesta-Martinez MJ, et al. Mutations in PLOD2 Cause Autosomal-Recessive Connective Tissue Disorders Within the Bruck Syndrome-Osteogenesis Imperfecta Phenotypic Spectrum. Human Mutation. 2012;33(10):1444-9.
99. Fiscaletti M, Biggin A, Bennetts B, Wong K, Briody J, Pacey V, et al. Novel variant in Sp7/Osx associated with recessive osteogenesis imperfecta with bone fragility and hearing impairment. Bone. 2018;110:66-75.
100. Lapunzina P, Aglan M, Temtamy S, Caparros-Martin JA, Valencia M, Leton R, et al. Identification of a Frameshift Mutation in Osterix in a Patient with Recessive Osteogenesis Imperfecta. American Journal of Human Genetics. 2010;87(1):110-4.
101. Streeten EA, McBride D, Puffenberger E, Hoffman ME, Pollin TI, Donnelly P, et al. Osteoporosis-pseudoglioma syndrome: Description of 9 new cases and beneficial response to bisphosphonates. Bone. 2008;43(3):584-90.
102. Balemans W, Devogelaer JP, Cleiren E, Piters E, Caussin E, Van Hul W. Novel LRP5 missense mutation in a patient with a high bone mass phenotype results in decreased DKK1-mediated inhibition of Wnt signaling. Journal of Bone and Mineral Research. 2007;22(5):708-16.
103. Morris JA, Kemp JP, Youlten SE, Laurent L, Logan JG, Chai RC, et al. An atlas of genetic influences on osteoporosis in humans and mice. Nature Genetics. 2019.
104. Kemp JP, Morris JA, Medina-Gomez C, Forgetta V, Warrington NM, Youlten SE, et al. Identification of 153 new loci associated with heel bone mineral density and functional involvement of GPC6 in osteoporosis. Nature Genetics. 2017;49(10):1468-+.
105. Xu F, Li WH, Yang X, Na LX, Chen LJ, Liu GB. The Roles of Epigenetics Regulation in Bone Metabolism and Osteoporosis. Frontiers in Cell and Developmental Biology. 2021;8.
106. Delgado-Calle J, Fernandez AF, Sainz J, Zarrabeitia MT, Sanudo C, Garcia-Renedo R, et al. Genome-wide profiling of bone reveals differentially methylated regions in osteoporosis and osteoarthritis. Arthritis and Rheumatism. 2013;65(1):197-205.

107. Chotiyarnwong P, McCloskey EV. Pathogenesis of glucocorticoid-induced osteoporosis and options for treatment. Nature Reviews Endocrinology. 2020;16(8):437-47.
108. Weinstein RS, Jilka RL, Parfitt AM, Manolagas SC. Inhibition of osteoblastogenesis and promotion of apoptosis of osteoblasts and osteocytes by glucocorticoids - Potential mechanisms of their deleterious effects on bone. Journal of Clinical Investigation. 1998;102(2):274-82.
109. Cooper MS. Glucocorticoids in bone and joint disease: the good, the bad and the uncertain. Clinical Medicine. 2012;12(3):261-5.
110. Liu YZ, Akhter MP, Gao X, Wang XY, Wang XB, Zhao G, et al. Glucocorticod-induced delayed fracture healing and impaired bone biomechanical properties in mice. Clinical Interventions in Aging. 2018;13:1465-74.
111. Geurtzen K, Vernet A, Freidin A, Rauner M, Hofbauer LC, Schneider JE, et al. Immune Suppressive and Bone Inhibitory Effects of Prednisolone in Growing and Regenerating Zebrafish Tissues. Journal of Bone and Mineral Research. 2017;32(12):2476-88.
112. Kanis JA, The WHO Study Group. Assessment of fracture risk and its application to screening for postmenopausal osteoporosis: Synopsis of a WHO report. Osteoporosis International. 1994;4(6):368-81.
113. Aggarwal V, Maslen C, Abel RL, Bhattacharya P, Bromiley PA, Clark EM, et al. Opportunistic diagnosis of osteoporosis, fragile bone strength and vertebral fractures from routine CT scans; a review of approved technology systems and pathways to implementation. Therapeutic Advances in Musculoskeletal Disease. 2021;13.
114. Gao YG, Patil S, Jia JX. The Development of Molecular Biology of Osteoporosis. International Journal of Molecular Sciences. 2021;22(15).
115. Kennel KA, Drake MT. Adverse Effects of Bisphosphonates: Implications for Osteoporosis Management. Mayo Clinic Proceedings. 2009;84(7):632-8.
116. Hassan N, Gregson CL, Tobias JH. Anabolic treatments for osteoporosis in postmenopausal women. Faculty reviews. 2021;10:44-.
117. Kobayakawa T, Miyazaki A, Saito M, Suzuki T, Takahashi J, Nakamura Y. Denosumab versus romosozumab for postmenopausal osteoporosis treatment. Scientific Reports. 2021;11(1).
118. Prather C, Adams E, Zentgraf W. Romosozumab: A first-in-class scierostin inhibitor for osteoprosis. American Journal of Health-System Pharmacy. 2020;77(23):1949-56.
119. O'Hara NN, Isaac M, Slobogean GP, Klazinga NS. The socioeconomic impact of orthopaedic trauma: A systematic review and meta-analysis. Plos One. 2020;15(1).
120. Tomlinson RE, Silva MJ. Skeletal Blood Flow in Bone Repair and Maintenance. Bone Research. 2013;1:311-22.
121. Marsell R, Einhorn TA. The biology of fracture healing. Injury-International Journal of the Care of the Injured. 2011;42(6):551-5.
122. Bahney CS, Zondervan RL, Allison P, Theologis A, Ashley JW, Ahn J, et al. Cellular biology of fracture healing. Journal of Orthopaedic Research. 2019;37(1):35-50.
123. Huber-Lang M, Kovtun A, Ignatius A. The role of complement in trauma and fracture healing. Seminars in Immunology. 2013;25(1):73-8.
124. Kolar P, Gaber T, Perka C, Duda GN, Buttgereit F. Human Early Fracture Hematoma Is Characterized by Inflammation and Hypoxia. Clinical Orthopaedics and Related Research. 2011;469(11):3118-26.
125. Echeverri LF, Herrero MA, Lopez JM, Oleaga G. Early Stages of Bone Fracture Healing: Formation of a Fibrin-Collagen Scaffold in the Fracture Hematoma. Bulletin of Mathematical Biology. 2015;77(1):156-83.
126. Depypere M, Morgenstern M, Kuehl R, Senneville E, Moriarty TF, Obremskey WT, et al. Pathogenesis and management of fracture-related infection. Clinical Microbiology and Infection. 2020;26(5):572-8.
127. Kovtun A, Messerer DAC, Scharffetter-Kochanek K, Huber-Lang M, Ignatius A. Neutrophils in Tissue Trauma of the Skin, Bone, and Lung: Two Sides of the Same Coin. Journal of Immunology Research. 2018.

128. Chung R, Cool JC, Scherer MA, Foster BK, Xian CJ. Roles of neutrophil-mediated inflammatory response in the bony repair of injured growth plate cartilage in young rats. Journal of Leukocyte Biology. 2006;80(6):1272-80.
129. Xing ZQ, Lu CY, Hu D, Yu YY, Wang XD, Colnot C, et al. Multiple roles for CCR2 during fracture healing. Disease Models & Mechanisms. 2010;3(7-8):451-8.
130. Raggatt LJ, Wullschleger ME, Alexander KA, Wu ACK, Millard SM, Kaur S, et al. Fracture Healing via Periosteal Callus Formation Requires Macrophages for Both Initiation and Progression of Early Endochondral Ossification. American Journal of Pathology. 2014;184(12):3192-204.
131. Petrie TA, Strand NS, Tsung-Yang C, Rabinowitz JS, Moon RT. Macrophages modulate adult zebrafish tail fin regeneration. Development. 2014;141(13):2581-91.
132. Wu AC, Raggatt LJ, Alexander KA, Pettit AR. Unraveling macrophage contributions to bone repair. BoneKEy reports. 2013;2:373-.
133. Lampiasi N, Russo R, Zito F. The Alternative Faces of Macrophage Generate Osteoclasts. Biomed Research International. 2016.
134. Claes L, Recknagel S, Ignatius A. Fracture healing under healthy and inflammatory conditions. Nature Reviews Rheumatology. 2012;8(3):133-43.
135. Chen WT, Han DC, Zhang PX, Han N, Kou YH, Yin XF, et al. A special healing pattern in stable metaphyseal fractures. Acta Orthopaedica. 2015;86(2):238-42.
136. Miclau KR, Brazina SA, Bahney CS, Hankenson KD, Hunt TK, Marcucio RS, et al. Stimulating Fracture Healing in Ischemic Environments: Does Oxygen Direct Stem Cell Fate during Fracture Healing? Frontiers in Cell and Developmental Biology. 2017;5.
137. Murphy CL, Polak JM. Control of human articular chondrocyte differentiation by reduced oxygen tension. Journal of Cellular Physiology. 2004;199(3):451-9.
138. Rot C, Stern T, Blecher R, Friesem B, Zelzer E. A Mechanical Jack-like Mechanism Drives Spontaneous Fracture Healing in Neonatal Mice. Developmental Cell. 2014;31(2):159-70.
139. Alexander KA, Chang MK, Maylin ER, Kohler T, Muller R, Wu AC, et al. Osteal Macrophages Promote In Vivo Intramembranous Bone Healing in a Mouse Tibial Injury Model. Journal of Bone and Mineral Research. 2011;26(7):1517-32.
140. Hu DP, Ferro F, Yang F, Taylor AJ, Chang WH, Miclau T, et al. Cartilage to bone transformation during fracture healing is coordinated by the invading vasculature and induction of the core pluripotency genes. Development. 2017;144(2):221-34.
141. Schindeler A, McDonald MM, Bokko P, Little DG. Bone remodeling during fracture repair: The cellular picture. Seminars in Cell & Developmental Biology. 2008;19(5):459-66.
142. Li JL, Mori S, Kaji Y, Mashiba T, Kawanishi J, Norimatsu H. Effect of bisphosphonate (incadronate) on fracture healing of long bones in rats. Journal of Bone and Mineral Research. 1999;14(6):969-79.
143. Tarvainen R, Olkkonen H, Nevalainen T, Hyvonen P, Arnala I, Alhava E. Effect of clodronate on fracture healing in denervated rats. Bone. 1994;15(6):701-5.
144. Gao Y, Liu X, Gu Y, Song D, Ding M, Liao L, et al. The Effect of Bisphosphonates on Fracture Healing Time and Changes in Bone Mass Density: A Meta-Analysis. Frontiers in Endocrinology. 2021;12.
145. Yahara Y, Ma XY, Gracia L, Alman BA. Monocyte/Macrophage Lineage Cells From Fetal Erythromyeloid Progenitors Orchestrate Bone Remodeling and Repair. Frontiers in Cell and Developmental Biology. 2021;9.
146. Stewart SK. Fracture Non-Union: A Review of Clinical Challenges and Future Research Needs. Malaysian Orthopaedic Journal. 2019;13(2):1-10.
147. Tomecka MJ, Ethiraj LP, Sanchez LM, Roehl HH, Carney TJ. Clinical pathologies of bone fracture modelled in zebrafish. Disease Models & Mechanisms. 2019;12(9).
148. Panteli M, Pountos I, Jones E, Giannoudis PV. Biological and molecular profile of fracture non-union tissue: current insights. Journal of Cellular and Molecular Medicine. 2015;19(4):685-713.

149. Andrzejowski P, Giannoudis PV. The 'diamond concept' for long bone non-union management. Journal of Orthopaedics and Traumatology. 2019;20(1).
150. Giannoudis PV, Einhorn TA, Marsh D. Fracture healing: The diamond concept. Injury. 2007;38:S3-S6.
151. Roberts TT, Rosenbaum AJ. Bone grafts, bone substitutes and orthobiologics: the bridge between basic science and clinical advancements in fracture healing. Organogenesis. 2012;8(4):114-24.
152. Polo-Corrales L, Latorre-Esteves M, Ramirez-Vick JE. Scaffold Design for Bone Regeneration. Journal of Nanoscience and Nanotechnology. 2014;14(1):15-56.
153. Khatkar H, See A. Stem Cell Therapy in the Management of Fracture Non-Union - Evaluating Cellular Mechanisms and Clinical Progress. Cureus. 2021;13(3).
154. Xie Y, Zhang LC, Xiong Q, Gao YP, Ge W, Tang PF. Bench-to-bedside strategies for osteoporotic fracture: From osteoimmunology to mechanosensation. Bone Research. 2019;7.
155. Stark Z, Savarirayan R. Osteopetrosis. Orphanet Journal of Rare Diseases. 2009;4.
156. Xu Y, Yu XY, Huang MJ. A novel mutation in TNFRSF11A gene causes pediatric osteopetrosis: case report. Bmc Surgery. 2021;21(1).
157. Liu CY, Ajmal M, Akram Z, Ghafoor T, Farhan M, Shafique S, et al. Genetic analysis of osteopetrosis in Pakistani families identifies novel and known sequence variants. Bmc Medical Genomics. 2021;14(1).
158. Brunkow ME, Gardner JC, Van Ness J, Paeper BW, Kovacevich BR, Proll S, et al. Bone dysplasia sclerosteosis results from loss of the SOST gene product, a novel cystine knot-containing protein. American Journal of Human Genetics. 2001;68(3):577-89.
159. Van Wesenbeeck L, Cleiren E, Gram J, Beals RK, Benichou O, Scopelliti D, et al. Six novel missense mutations in the LDL receptor-related protein 5 (LRP5) gene in different conditions with an increased bone density. American Journal of Human Genetics. 2003;72(3):763-71.
160. Semenov MV, He X. LRP5 mutations linked to high bone mass diseases cause reduced LRP5 binding and inhibition by SOST. Journal of Biological Chemistry. 2006;281(50):38276-84.
161. Gregson CL, Bergen DJM, Leo P, Sessions RB, Wheeler L, Hartley A, et al. A Rare Mutation in SMAD9 Associated With High Bone Mass Identifies the SMAD-Dependent BMP Signaling Pathway as a Potential Anabolic Target for Osteoporosis. Journal of Bone and Mineral Research. 2020;35(1):92-105.
162. Giani AM, Gallo GR, Gianfranceschi L, Formenti G. Long walk to genomics: History and current approaches to genome sequencing and assembly. Computational and Structural Biotechnology Journal. 2020;18:9-19.
163. Zhu XW, Bai WY, Zheng HF. Twelve years of GWAS discoveries for osteoporosis and related traits: advances, challenges and applications. Bone Research. 2021;9(1).
164. Gregson CL, Newell F, Leo PJ, Clark GR, Paternoster L, Marshall M, et al. Genome-wide association study of extreme high bone mass: Contribution of common genetic variation to extreme BMD phenotypes and potential novel BMD-associated genes. Bone. 2018;114:62-71.
165. Davey Smith G, Hemani G. Mendelian randomization: genetic anchors for causal inference in epidemiological studies. Human Molecular Genetics. 2014;23:R89-R98.
166. McGowan LM, Davey Smith G, Gaunt TR, Richardson TG. Integrating Mendelian randomization and multiple-trait colocalization to uncover cell-specific inflammatory drivers of autoimmune and atopic disease. Human Molecular Genetics. 2019;28(19):3293-300.
167. Zheng J, Maerz W, Gergei I, Kleber M, Drechsler C, Wanner C, et al. Mendelian Randomization Analysis Reveals a Causal Influence of Circulating Sclerostin Levels on Bone Mineral Density and Fractures. Journal of Bone and Mineral Research. 2019;34(10):1824-36.
168. Zheng J, Frysz M, Kemp JP, Evans DM, Smith GD, Tobias JH. Use of Mendelian Randomization to Examine Causal Inference in Osteoporosis. Frontiers in Endocrinology. 2019;10.
169. Lelovas PP, Xanthos TT, Thoma SE, Lyritis GP, Dontasi IA. The Laboratory Rat as an Animal Model for Osteoporosis Research. Comparative Medicine. 2008;58(5):424-30.

170. Jilka RL. The Relevance of Mouse Models for Investigating Age-Related Bone Loss in Humans. Journals of Gerontology Series a-Biological Sciences and Medical Sciences. 2013;68(10):1209-17.
171. Brommage R, Ohlsson C. High Fidelity of Mouse Models Mimicking Human Genetic Skeletal Disorders. Frontiers in Endocrinology. 2020;10.
172. Maynard RD, Ackert-Bicknell CL. Mouse Models and Online Resources for Functional Analysis of Osteoporosis Genome-Wide Association Studies. Frontiers in Endocrinology. 2019;10.
173. Collier CD, Hausman BS, Zulqadar SH, Din ES, Anderson JM, Akkus O, et al. Characterization of a reproducible model of fracture healing in mice using an open femoral osteotomy. Bone Reports. 2020;12.
174. Haffner-Luntzer M, Kovtun A, Rapp AE, Ignatius A. Mouse Models in Bone Fracture Healing Research. Current Molecular Biology Reports. 2016;2(2):101-11.
175. Auregan JC, Coyle RM, Danoff JR, Burky RE, Akelina Y, Rosenwasser MP. The rat model of femur fracture for bone and mineral research: A n improved description of expected comminution, quantity of soft callus and incidence of complications. Bone & Joint Research. 2013;2(8):149-54.
176. Wong RMY, Thormann U, Choy MHV, Chim YN, Li MCM, Wang JY, et al. A Metaphyseal Fracture Rat Model for Mechanistic Studies of Osteoporotic Bone Healing. European Cells & Materials. 2019;37:420-30.
177. Hauser M, Siegrist M, Keller I, Hofstetter W. Healing of fractures in osteoporotic bones in mice treated with bisphosphonates - A transcriptome analysis. Bone. 2018;112:107-19.
178. Owen R, Reilly GC. In vitro Models of Bone Remodelling and Associated Disorders. Frontiers in Bioengineering and Biotechnology. 2018;6.
179. Liu YQ, Han XF, Liu TG, Cheng MC, Xiao HB. A cell-based model of bone remodeling for identifying activity of icarrin in the treatment of osteoporosis. Biotechnology Letters. 2015;37(1):219-26.
180. Czekanska EM, Stoddart MJ, Richards RG, Hayes JS. In Search of An Osteoblast Cell Model For In Vitro Research. European Cells & Materials. 2012;24:1-17.
181. Czekanska EM, Stoddart MJ, Ralphs JR, Richards RG, Hayes JS. A phenotypic comparison of osteoblast cell lines versus human primary osteoblasts for biomaterials testing. Journal of Biomedical Materials Research Part A. 2014;102(8):2636-43.
182. Ansari S, Ito K, Hofmann S. Cell Sources for Human In vitro Bone Models. Current Osteoporosis Reports. 2021;19(1):88-100.
183. Marolt D, Knezevic M, Novakovic GV. Bone tissue engineering with human stem cells. Stem Cell Research & Therapy. 2010;1.
184. de Wildt BWM, Ansari S, Sommerdijk N, Ito K, Akiva A, Hofmann S. From bone regeneration to three-dimensional in vitro models: tissue engineering of organized bone extracellular matrix. Current Opinion in Biomedical Engineering. 2019;10:107-15.
185. Cassar S, Adatto I, Freeman JL, Gamse JT, Iturria I, Lawrence C, et al. Use of Zebrafish in Drug Discovery Toxicology. Chemical Research in Toxicology. 2020;33(1):95-118.
186. Song YS, Dai MZ, Zhu CX, Huang YF, Liu J, Zhang CD, et al. Validation, Optimization, and Application of the Zebrafish Developmental Toxicity Assay for Pharmaceuticals Under the ICH S5(R3) Guideline. Frontiers in Cell and Developmental Biology. 2021;9.
187. Lieschke GJ, Currie PD. Animal models of human disease: zebrafish swim into view. Nature Reviews Genetics. 2007;8(5):353-67.
188. Gemberling M, Bailey TJ, Hyde DR, Poss KD. The zebrafish as a model for complex tissue regeneration. Trends in Genetics. 2013;29(11):611-20.
189. Weigele J, Franz-Odendaal TA. Functional bone histology of zebrafish reveals two types of endochondral ossification, different types of osteoblast clusters and a new bone type. Journal of Anatomy. 2016;229(1):92-103.
190. Witten PE, Hansen A, Hall BK. Features of mono- and multinucleated bone resorbing cells of the zebrafish Danio rerio and their contribution to skeletal development, remodeling, and growth. Journal of Morphology. 2001;250(3):197-207.

191. Tonelli F, Bek JW, Besio R, De Clercq A, Leoni L, Salmon P, et al. Zebrafish: A Resourceful Vertebrate Model to Investigate Skeletal Disorders. Frontiers in Endocrinology. 2020;11.
192. Spence R, Smith C. Mating preference of female zebrafish, Danio rerio, in relation to male dominance. Behavioral Ecology. 2006;17(5):779-83.
193. Li N, Felber K, Elks P, Croucher P, Roehl HH. Tracking Gene Expression During Zebrafish Osteoblast Differentiation. Developmental Dynamics. 2009;238(2):459-66.
194. Ogata S, Uhthoff HK. The Early Development and Ossification Of The Human Clavicle - An Embryologic Study Acta Orthopaedica Scandinavica. 1990;61(4):330-4.
195. Bergen DJM, Kague E, Hammond CL. Zebrafish as an Emerging Model for Osteoporosis: A Primary Testing Platform for Screening New Osteo-Active Compounds. Frontiers in Endocrinology. 2019;10.
196. Newham E, Kague E, Aggleton JA, Fernee C, Robson Brown KA, Hammond CL. Finite Element and deformation analyses predict pattern of bone failure in loaded zebrafish spines. bioRxiv2019.
197. Sousa S, Valerio F, Jacinto A. A new zebrafish bone crush injury model. Biology Open. 2012;1(9):915-21.
198. Geurtzen K, Knopf F, Wehner D, Huitema LFA, Schulte-Merker S, Weidinger G. Mature osteoblasts dedifferentiate in response to traumatic bone injury in the zebrafish fin and skull. Development. 2014;141(11):2225-34.
199. Knopf F, Hammond C, Chekuru A, Kurth T, Hans S, Weber CW, et al. Bone Regenerates via Dedifferentiation of Osteoblasts in the Zebrafish Fin. Developmental Cell. 2011;20(5):713-24.
200. Storer MA, Mahmud N, Karamboulas K, Borrett MJ, Yuzwa SA, Gont A, et al. Acquisition of a Unique Mesenchymal Precursor-like Blastema State Underlies Successful Adult Mammalian Digit Tip Regeneration. Developmental Cell. 2020;52(4):509-+.
201. Howe K, Clark MD, Torroja CF, Torrance J, Berthelot C, Muffato M, et al. The zebrafish reference genome sequence and its relationship to the human genome. Nature. 2013;496(7446):498-503.
202. Murayama E, Kissa K, Zapata A, Mordelet E, Briolat V, Lin HF, et al. Tracing hematopoietic precursor migration to successive hematopoietic organs during zebrafish development. Immunity. 2006;25(6):963-75.
203. Rosowski EE. Determining macrophage versus neutrophil contributions to innate immunity using larval zebrafish. Disease Models & Mechanisms. 2020;13(1).
204. Gore AV, Pillay LM, Galanternik MV, Weinstein BM. The zebrafish: A fintastic model for hematopoietic development and disease. Wiley Interdisciplinary Reviews-Developmental Biology. 2018;7(3).
205. Rauch F, Travers R, Parfitt AM, Glorieux FH. Static and dynamic bone histomorphometry in children with osteogenesis imperfecta. Bone. 2000;26(6):581-9.
206. Bensimon-Brito A, Cardeira J, Dionisio G, Huysseune A, Cancela ML, Witten PE. Revisiting in vivo staining with alizarin red S - a valuable approach to analyse zebrafish skeletal mineralization during development and regeneration. Bmc Developmental Biology. 2016;16.
207. Frost HM. Tetracycline-Based Histological Analysis of Bone Remodeling. Calcified Tissue Research. 1969;3(3):211-&.
208. Dempster DW, Compston JE, Drezner MK, Glorieux FH, Kanis JA, Malluche H, et al. Standardized Nomenclature, Symbols, and Units for Bone Histomorphometry: A 2012 Update of the Report of the ASBMR Histomorphometry Nomenclature Committee. Journal of Bone and Mineral Research. 2013;28(1):1-16.
209. de Bakker CMJ, Altman AR, Tseng WJ, Tribble MB, Li CN, Chandra A, et al. micro-CT-based, in vivo dynamic bone histomorphometry allows 3D evaluation of the early responses of bone resorption and formation to PTH and alendronate combination therapy. Bone. 2015;73:198-207.
210. Yeh SCA, Wilk K, Lin CP, Intini G. In Vivo 3D Histomorphometry Quantifies Bone Apposition and Skeletal Progenitor Cell Differentiation. Scientific Reports. 2018;8.

211. Hammond C, Moro E. Using transgenic reporters to visualize bone and cartilage signaling during development in vivo. Frontiers in Endocrinology. 2012;3.
212. Singh SP, Holdway JE, Poss KD. Regeneration of Amputated Zebrafish Fin Rays from De Novo Osteoblasts. Developmental Cell. 2012;22(4):879-86.
213. White RM, Sessa A, Burke C, Bowman T, LeBlanc J, Ceol C, et al. Transparent adult zebrafish as a tool for in vivo transplantation analysis. Cell Stem Cell. 2008;2(2):183-9.
214. Hur M, Gistelinck CA, Huber P, Lee J, Thompson MH, Monstad-Rios AT, et al. MicroCT-Based Phenomics in the Zebrafish Skeleton Reveals Virtues of Deep Phenotyping in a Distributed Organ System. Zebrafish. 2018;15(1):77-8.
215. Whittier DE, Boyd SK, Burghardt AJ, Paccou J, Ghasem-Zadeh A, Chapurlat R, et al. Guidelines for the assessment of bone density and microarchitecture in vivo using high-resolution peripheral quantitative computed tomography. Osteoporosis International. 2020;31(9):1607-27.
216. Shah AN, Davey CF, Whitebirch AC, Miller AC, Moens CB. Rapid Reverse Genetic Screening Using CRISPR in Zebrafish. Zebrafish. 2016;13(2):152-3.
217. Watson CJ, Monstad-Rios AT, Bhimani RM, Gistelinck C, Willaert A, Coucke P, et al. Phenomics-Based Quantification of CRISPR-Induced Mosaicism in Zebrafish. Cell Systems. 2020;10(3):275-+.
218. Ablain J, Durand EM, Yang S, Zhou Y, Zon LI. A CRISPR/Cas9 Vector System for Tissue-Specific Gene Disruption in Zebrafish. Developmental Cell. 2015;32(6):756-64.
219. Cox B, De Simone A, Tornini VA, Singh SP, Di Talia S, Poss KD. In Toto Imaging of Dynamic Osteoblast Behaviors in Regenerating Skeletal Bone. Current Biology. 2018;28(24):3937-+.
220. Kobayashi-Sun J, Yamamori S, Kondo M, Kuroda J, Ikegame M, Suzuki N, et al. Uptake of osteoblast-derived extracellular vesicles promotes the differentiation of osteoclasts in the zebrafish scale. Communications Biology. 2020;3(1).
221. Spoorendonk KM, Hammond CL, Huitema LFA, Vanoevelen J, Schulte-Merker S. Zebrafish as a unique model system in bone research: the power of genetics and in vivo imaging. Journal of Applied Ichthyology. 2010;26(2):219-24.
222. Ofer L, Zaslansky P, Shahar R. A comparison of the structure, composition and mechanical properties of anosteocytic vertebrae of medaka (O. latipes) and osteocytic vertebrae of zebrafish (D. rerio). Journal of Fish Biology. 2021;98(4):995-1006.
223. Mitchell RE, Huitema LFA, Skinner REH, Brunt LH, Severn C, Schulte-Merker S, et al. New tools for studying osteoarthritis genetics in zebrafish. Osteoarthritis and Cartilage. 2013;21(2):269-78.
224. Kague E, Turci F, Newman E, Yang YS, Brown KR, Aglan MS, et al. 3D assessment of intervertebral disc degeneration in zebrafish identifies changes in bone density that prime disc disease. Bone Research. 2021;9(1).
225. Ofer L, Dean MN, Zaslansky P, Kult S, Shwartz Y, Zaretsky J, et al. A novel nonosteocytic regulatory mechanism of bone modeling. Plos Biology. 2019;17(2).
226. Suniaga S, Rolvien T, vom Scheidt A, Fiedler IAK, Bale HA, Huysseune A, et al. Increased mechanical loading through controlled swimming exercise induces bone formation and mineralization in adult zebrafish. Scientific Reports. 2018;8.
227. Monma Y, Shimada Y, Nakayama H, Zang LQ, Nishimura N, Tanaka T. Aging-associated microstructural deterioration of vertebra in zebrafish. Bone Reports. 2019;11.
228. Hayes AJ, Reynolds S, Nowell MA, Meakin LB, Habicher J, Ledin J, et al. Spinal Deformity in Aged Zebrafish Is Accompanied by Degenerative Changes to Their Vertebrae that Resemble Osteoarthritis. Plos One. 2013;8(9).
229. Zhang SC, Cui PF. Complement system in zebrafish. Developmental and Comparative Immunology. 2014;46(1):3-10.

230. Muire PJ, Hanson L, Yoder J, Petrie-Hanson L. Transcript analysis of natural killer (NK) cell specific genes in the liver, kidney and spleen tissues of rag1(-/-) mutant zebrafish in response to in vivo administration of TLR ligands. Journal of Immunology. 2016;196.
231. Renshaw SA, Trede NS. A model 450 million years in the making: zebrafish and vertebrate immunity. Disease Models & Mechanisms. 2012;5(1):38-47.
232. Isles HM, Loynes CA, Alasmari S, Kon FC, Henry KM, Kadochnikova A, et al. Pioneer neutrophils release chromatin within in vivo swarms. Elife. 2021;10.
233. Lopez-Cuevas P, Deane L, Yang YS, Hammond CL, Kague E. Transformed notochordal cells trigger chronic wounds in zebrafish, destabilizing the vertebral column and bone homeostasis. Disease Models & Mechanisms. 2021;14(3).
234. Geurtzen K, Duseja A, Knopf F. Osteoblast cell death triggers a pro-osteogenic inflammatory response regulated by reactive oxygen species and glucocorticoid signaling in zebrafish. bioRxiv 2021.05.08.443237; doi: https://doi.org/10.1101/2021.05.08.443237 2021.
235. Zuniga-Traslavina C, Bravo K, Reyes AE, Feijoo CG. Cxcl8b and Cxcr2 Regulate Neutrophil Migration through Bloodstream in Zebrafish. Journal of Immunology Research. 2017;2017.
236. Wu YN, Wang S, Farooq SM, Castelvetere MP, Hou YN, Gao JL, et al. A Chemokine Receptor CXCR2 Macromolecular Complex Regulates Neutrophil Functions in Inflammatory Diseases. Journal of Biological Chemistry. 2012;287(8):5744-55.
237. Henry KM, Loynes CA, Whyte MKB, Renshaw SA. Zebrafish as a model for the study of neutrophil biology. Journal of Leukocyte Biology. 2013;94(4):633-42.
238. Bevan L, Lim ZW, Venkatesh B, Riley PR, Martin P, Richardson RJ. Specific macrophage populations promote both cardiac scar deposition and subsequent resolution in adult zebrafish. Cardiovascular Research. 2020;116(7):1357-71.
239. Elks PM, Loynes CA, Renshaw SA. Measuring Inflammatory Cell Migration in the Zebrafish. In: Wells CM, Parsons M, editors. Cell Migration: Developmental Methods and Protocols. Totowa, NJ: Humana Press; 2011. p. 261-75.
240. Gurevich DB, Severn CE, Twomey C, Greenhough A, Cash J, Toye AM, et al. Live imaging of wound angiogenesis reveals macrophage orchestrated vessel sprouting and regression. Embo Journal. 2018;37(13).
241. Lopez-Cuevas P, Cross SJ, Martin P. Modulating the Inflammatory Response to Wounds and Cancer Through Infection. Frontiers in Cell and Developmental Biology. 2021;9.
242. Renshaw SA, Loynes CA, Trushell DMI, Elworthy S, Ingham PW, Whyte MKB. A transgenic zebrafish model of neutrophilic inflammation. Blood. 2006;108(13):3976-8.
243. Mathias JR, Perrin BJ, Liu TX, Kanki J, Look AT, Huttenlocher A. Resolution of inflammation by retrograde chemotaxis of neutrophils in transgenic zebrafish. Journal of Leukocyte Biology. 2006;80(6):1281-8.
244. Hall C, Flores MV, Storm T, Crosier K, Crosier P. The zebrafish lysozyme C promoter drives myeloid-specific expression in transgenic fish. Bmc Developmental Biology. 2007;7.
245. Ellett F, Pase L, Hayman JW, Andrianopoulos A, Lieschke GJ. mpeg1 promoter transgenes direct macrophage-lineage expression in zebrafish. Blood. 2011;117(4):E49-E56.
246. Walton EM, Cronan MR, Beerman RW, Tobin DM. The Macrophage-Specific Promoter mfap4 Allows Live, Long-Term Analysis of Macrophage Behavior during Mycobacterial Infection in Zebrafish. Plos One. 2015;10(10).
247. Martins RR, Ellis PS, MacDonald RB, Richardson RJ, Henriques CM. Resident Immunity in Tissue Repair and Maintenance: The Zebrafish Model Coming of Age. Frontiers in Cell and Developmental Biology. 2019;7.
248. Moyse BR, Richardson RJ. A Population of Injury-Responsive Lymphoid Cells Expresses mpeg1.1 in the Adult Zebrafish Heart. ImmunoHorizons. 2020;4(8):464-74.

249. Ferrero G, Gomez E, Iyer S, Rovira M, Miserocchi M, Langenau DM, et al. The macrophage-expressed gene (mpeg) 1 identifies a subpopulation of B cells in the adult zebrafish. Journal of Leukocyte Biology. 2020;107(3):431-43.
250. Castranova D, Samasa B, Venero Galanternik M, Gore AV, Goldstein AE, Park JS, et al. Long-term imaging of living adult zebrafish. Development. 2022;149(4):dev199667.
251. Kettleborough RNW, Busch-Nentwich EM, Harvey SA, Dooley CM, de Bruijn E, van Eeden F, et al. A systematic genome-wide analysis of zebrafish protein-coding gene function. Nature. 2013;496(7446):494-+.
252. Dale RM, Topczewski J. Identification of an evolutionarily conserved regulatory element of the zebrafish col2a1a gene. Developmental Biology. 2011;357(2):518-31.
253. Yan YL, Willoughby J, Liu D, Crump JG, Wilson C, Miller CT, et al. A pair of Sox: distinct and overlapping functions of zebrafish sox9 co-orthologs in craniofacial and pectoral fin development. Development. 2005;132(5):1069-83.
254. Flores MV, Tsang VWK, Hu WJ, Kalev-Zylinska M, Postlethwait J, Crosier P, et al. Duplicate zebrafish runx2 orthologues are expressed in developing skeletal elements. Gene Expression Patterns. 2004;4(5):573-81.
255. Kwon RY, Watson CJ, Karasik D. Using zebrafish to study skeletal genomics. Bone. 2019;126:37-50.
256. Tachmazidou I, Hatzikotoulas K, Southam L, Esparza-Gordillo J, Haberland V, Zheng J, et al. Identification of new therapeutic targets for osteoarthritis through genome-wide analyses of UK Biobank data. Nature Genetics. 2019;51:231-6.
257. Zhang YL, Ji DR, Li L, Yang SQ, Zhang HW, Duan XH. ClC-7 Regulates the Pattern and Early Development of Craniofacial Bone and Tooth. Theranostics. 2019;9(5):1387-400.
258. Mahony C, Erskine L, Niven J, Greig NH, Figg WD, Vargesson N. Pomalidomide is nonteratogenic in chicken and zebrafish embryos and nonneurotoxic in vitro. Proceedings of the National Academy of Sciences of the United States of America. 2013;110(31):12703-8.
259. Duckworth AD, McQueen MM, Tuck CE, Tobias JH, Wilkinson JM, Biant LC, et al. Effect of Alendronic Acid on Fracture Healing: A Multicenter Randomized Placebo-Controlled Trial. Journal of Bone and Mineral Research. 2019;34(6):1025-32.
260. Richardson R, Slanchev K, Kraus C, Knyphausen P, Eming S, Hammerschmidt M. Adult Zebrafish as a Model System for Cutaneous Wound-Healing Research. Journal of Investigative Dermatology. 2013;133(6):1655-65.
261. Ohgo S, Ichinose S, Yokota H, Sato-Maeda M, Shoji W, Wada N. Tissue regeneration during lower jaw restoration in zebrafish shows some features of epimorphic regeneration. Development Growth & Differentiation. 2019;61(7-8):419-30.
262. Aman AJ, Fulbright AN, Parichy DM. Wnt/beta-catenin regulates an ancient signaling network during zebrafish scale development. Elife. 2018;7.
263. Zheng HF, Tobias JH, Duncan E, Evans DM, Eriksson J, Paternoster L, et al. WNT16 Influences Bone Mineral Density, Cortical Bone Thickness, Bone Strength, and Osteoporotic Fracture Risk. Plos Genetics. 2012;8(7).
264. Moverare-Skrtic S, Henning P, Liu XW, Nagano K, Saito H, Borjesson AE, et al. Osteoblast-derived WNT16 represses osteoclastogenesis and prevents cortical bone fragility fractures. Nature Medicine. 2014;20(11):1279-88.
265. Gori F, Lerner U, Ohlsson C, Baron R. A new WNT on the bone: WNT16, cortical bone thickness, porosity and fractures. Bonekey Reports. 2015;4.
266. Clements WK, Kim AD, Ong KG, Moore JC, Lawson ND, Traver D. A somitic Wnt16/Notch pathway specifies haematopoietic stem cells. Nature. 2011;474(7350):220-U62.

267. Bastian OW, Koenderman L, Alblas J, Leenen LPH, Blokhuis TJ. Neutrophils contribute to fracture healing by synthesizing fibronectin(+) extracellular matrix rapidly after injury. Clinical Immunology. 2016;164:78-84.
268. Kovtun A, Bergdolt S, Wiegner R, Radermacher P, Huber-Lang M, Ignatius A. The Crucial Role of Neutrophil Granulocytes in Bone Fracture Healing. European Cells & Materials. 2016;32:152-62.
269. Alestrom P, D'Angelo L, Midtlyng PJ, Schorderet DF, Schulte-Merker S, Sohm F, et al. Zebrafish: Housing and husbandry recommendations. Laboratory Animals.
270. Moro E, Ozhan-Kizil G, Mongera A, Beis D, Wierzbicki C, Young RM, et al. In vivo Wnt signaling tracing through a transgenic biosensor fish reveals novel activity domains. Developmental Biology. 2012;366(2):327-40.
271. DeLaurier A, Eames BF, Blanco-Sanchez B, Peng G, He XJ, Swartz ME, et al. Zebrafish sp7:EGFP: A Transgenic for Studying Otic Vesicle Formation, Skeletogenesis, and Bone Regeneration. Genesis. 2010;48(8):505-11.
272. Marjoram L, Alvers A, Deerhake ME, Bagwell J, Mankiewicz J, Cocchiaro JL, et al. Epigenetic control of intestinal barrier function and inflammation in zebrafish. Proceedings of the National Academy of Sciences of the United States of America. 2015;112(9):2770-5.
273. Brunt LH, Begg K, Kague E, Cross S, Hammond CL. Wnt signalling controls the response to mechanical loading during zebrafish joint development. Development. 2017;144(15):2798-809.
274. Keatinge M, Tsarouchas TM, Munir T, Porter NJ, Larraz J, Gianni D, et al. CRISPR gRNA phenotypic screening in zebrafish reveals pro-regenerative genes in spinal cord injury. Plos Genetics. 2021;17(4).
275. Tsarouchas TM, Wehner D, Cavone L, Munir T, Keatinge M, Lambertus M, et al. Dynamic control of proinflammatory cytokines Il-1 beta and Tnf-alpha by macrophages in zebrafish spinal cord regeneration. Nature Communications. 2018;9.
276. Labun K, Montague TG, Krause M, Cleuren YNT, Tjeldnes H, Valen E. CHOPCHOP v3: expanding the CRISPR web toolbox beyond genome editing. Nucleic Acids Research. 2019;47(W1):W171-W4.
277. Moreno-Mateos MA, Vejnar CE, Beaudoin J-D, Fernandez JP, Mis EK, Khokha MK, et al. CRISPRscan: designing highly efficient sgRNAs for CRISPR-Cas9 targeting in vivo. Nature Methods. 2015;12(10):982-8.
278. Koressaar T, Lepamets M, Kaplinski L, Raime K, Andreson R, Remm M. Primer3_masker: integrating masking of template sequence with primer design software. Bioinformatics. 2018;34(11):1937-8.
279. Carrington B, Varshney GK, Burgess SM, Sood R. CRISPR-STAT: an easy and reliable PCR-based method to evaluate target-specific sgRNA activity. Nucleic Acids Research. 2015;43(22).
280. Bergen DJM, Tong Q, Shukla A, Newham E, Zethof J, Lundberg M, et al. Regenerating zebrafish scales express a subset of evolutionary conserved genes involved in human skeletal disease. Bmc Biology. 2022;20(1).
281. Bergemann D, Massoz L, Bourdouxhe J, Pardo CAC, Voz ML, Peers B, et al. Nifurpirinol: A more potent and reliable substrate compared to metronidazole for nitroreductase-mediated cell ablations. Wound Repair and Regeneration. 2018;26(2):238-44.
282. Cvejic A, Hall C, Bak-Maier M, Flores MV, Crosier P, Redd MJ, et al. Analysis of WASp function during the wound inflammatory response - live-imaging studies in zebrafish larvae. Journal of Cell Science. 2008;121(19):3196-206.
283. Tommasini SM, Trinward A, Acerbo AS, De Carlo F, Miller LM, Judex S. Changes in intracortical microporosities induced by pharmaceutical treatment of osteoporosis as detected by high resolution micro-CT. Bone. 2012;50(3):596-604.
284. Schindelin J, Arganda-Carreras I, Frise E, Kaynig V, Longair M, Pietzsch T, et al. Fiji: an open-source platform for biological-image analysis. Nature Methods. 2012;9(7):676-82.
285. Cross SJ. Modular Image Analysis GitHub2021 [Available from: https://github.com/mianalysis/mia.
286. Cross SJ. SJCross/MIA: Version 0.9.30. Zenodo. 2019;2020(19/01):http://doi.org/10.5281/zenodo.2712750.

287. Cross SJ. mianalysis/mia: Version 0.21.2. 10.5281/zenodo.55845132021.
288. Faul F, Erdfelder E, Lang AG, Buchner A. G*Power 3: A flexible statistical power analysis program for the social, behavioral, and biomedical sciences. Behavior Research Methods. 2007;39(2):175-91.
289. Houschyar KS, Tapking C, Borrelli MR, Popp D, Duscher D, Maan ZN, et al. Wnt Pathway in Bone Repair and Regeneration - What Do We Know So Far. Frontiers in Cell and Developmental Biology. 2019;6.
290. Nusse R. Wnt signaling in disease and in development. Cell Research. 2005;15(1):28-32.
291. Jansson L, Kim GS, Cheng AG. Making sense of Wnt signaling-linking hair cell regeneration to development. Frontiers in Cellular Neuroscience. 2015;9.
292. Li ZQ, Xu ZM, Duan CC, Liu WW, Sun JC, Han B. Role of TCF/LEF Transcription Factors in Bone Development and Osteogenesis. International Journal of Medical Sciences. 2018;15(12):1415-22.
293. Rawadi G, Vayssiere B, Dunn F, Baron R, Roman-Roman S. BMP-2 controls alkaline phosphatase expression and osteoblast mineralization by a Wnt autocrine loop. Journal of Bone and Mineral Research. 2003;18(10):1842-53.
294. Kobayashi Y, Uehara S, Udagawa N. Roles of non-canonical Wnt signaling pathways in bone resorption. Journal of Oral Biosciences. 2018;60(2):31-5.
295. Nalesso G, Thomas BL, Sherwood JC, Yu J, Addimanda O, Eldridge SE, et al. WNT16 antagonises excessive canonical WNT activation and protects cartilage in osteoarthritis. Annals of the Rheumatic Diseases. 2017;76(1):218-26.
296. Koller DL, Zheng HF, Karasik D, Yerges-Armstrong L, Liu CT, McGuigan F, et al. Meta-analysis of genome-wide studies identifies WNT16 and ESR1 SNPs associated with bone mineral density in premenopausal women. Journal of Bone and Mineral Research. 2013;28(3):547-58.
297. Alam I, Alkhouli M, Gerard-O'Riley RL, Wright WB, Acton D, Gray AK, et al. Osteoblast-Specific Overexpression of Human WNT16 Increases Both Cortical and Trabecular Bone Mass and Structure in Mice. Endocrinology. 2016;157(2):722-36.
298. Alam I, Oakes D, Sbeta S, Billingsley C, Acton D, Reilly A, et al. Overexpression of WNT16 does not Rescue the Bone Loss due to Glucocorticoid Treatment in Mice. Journal of Bone and Mineral Research. 2017;32:S370-S.
299. Ohlsson C, Henning P, Nilsson KH, Wu JY, Gustafsson KL, Sjogren K, et al. Inducible Wnt16 inactivation: WNT16 regulates cortical bone thickness in adult mice. Journal of Endocrinology. 2018;237(2):113-22.
300. Loi F, Cordova LA, Pajarinen J, Lin TH, Yao ZY, Goodman SB. Inflammation, fracture and bone repair. Bone. 2016;86:119-30.
301. Nowalk JR, Flick LM. Visualization of different tissues involved in endochondral ossification with alcian blue hematoxylin and orange G/Eosin counterstain. Journal of Histotechnology. 2008;31(1):19-21.
302. Kim YH, Cho KA, Lee HJ, Park M, Kim HS, Park JW, et al. Identification of WNT16 as a Predictable Biomarker for Accelerated Osteogenic Differentiation of Tonsil-Derived Mesenchymal Stem Cells In Vitro. Stem Cells International. 2019;2019.
303. Jung YS, Lee HY, Kim SD, Park JS, Kim JK, Suh PG, et al. Wnt5a stimulates chemotactic migration and chemokine production in human neutrophils. Experimental and Molecular Medicine. 2013;45.
304. Janckila AJ, Yam LT. Biology and Clinical Significance of Tartrate-Resistant Acid Phosphatases: New Perspectives on an Old Enzyme. Calcified Tissue International. 2009;85(6):465-83.
305. Kobayashi Y, Thirukonda GJ, Nakamura Y, Koide M, Yamashita T, Uehara S, et al. Wnt16 regulates osteoclast differentiation in conjunction with Wnt5a. Biochemical and Biophysical Research Communications. 2015;463(4):1278-83.
306. Gibon E, Loi F, Cordova LA, Pajarinen J, Lin T, Lu L, et al. Aging Affects Bone Marrow Macrophage Polarization: Relevance to Bone Healing. Regenerative Engineering and Translational Medicine. 2016;2(2):98-104.

307. Kawane T, Qin X, Jiang Q, Miyazaki T, Komori H, Yoshida CA, et al. Runx2 is required for the proliferation of osteoblast progenitors and induces proliferation by regulating Fgfr2 and Fgfr3. Scientific Reports. 2018;8.
308. Zhong N, Gersch RP, Hadjiargyrou M. Wnt signaling activation during bone regeneration and the role of Dishevelled in chondrocyte proliferation and differentiation. Bone. 2006;39(1):5-16.
309. Kahler RA, Westendorf JJ. Lymphoid enhancer factor-1 and beta-catenin inhibit Runx2-dependent transcriptional activation of the osteocalcin promoter. Journal of Biological Chemistry. 2003;278(14):11937-44.
310. Zhang C. Transcriptional regulation of bone formation by the osteoblast-specific transcription factor Osx. Journal of Orthopaedic Surgery and Research. 2010;5.
311. Benhaj K, Akcali KC, Ozturk M. Redundant expression of canonical Wnt ligands in human breast cancer cell lines. Oncology Reports. 2006;15(3):701-7.
312. Farin HF, Van Es JH, Clevers H. Redundant Sources of Wnt Regulate Intestinal Stem Cells and Promote Formation of Paneth Cells. Gastroenterology. 2012;143(6):1518-+.
313. Chen BZ, Dodge ME, Tang W, Lu JM, Ma ZQ, Fan CW, et al. Small molecule-mediated disruption of Wnt-dependent signaling in tissue regeneration and cancer. Nature Chemical Biology. 2009;5(2):100-7.
314. Schulte-Merker S, Stainier DYR. Out with the old, in with the new: reassessing morpholino knockdowns in light of genome editing technology. Development. 2014;141(16):3103-4.
315. Hankenson KD, Dishowitz M, Gray C, Schenker M. Angiogenesis in bone regeneration. Injury-International Journal of the Care of the Injured. 2011;42(6):556-61.
316. Luo ZL, Shang XF, Zhang H, Wang GX, Massey PA, Barton SR, et al. Notch Signaling in Osteogenesis, Osteoclastogenesis, and Angiogenesis. American Journal of Pathology. 2019;189(8):1495-500.
317. Phan QT, Tan WH, Liu RR, Sundaram S, Buettner A, Kneitz S, et al. Cxcl9l and Cxcr3.2 regulate recruitment of osteoclast progenitors to bone matrix in a medaka osteoporosis model. Proceedings of the National Academy of Sciences of the United States of America. 2020;117(32):19276-86.
318. Qu XC, Liao M, Liu WW, Cai YS, Yi QR, Long JM, et al. Loss of Wnt16 Leads to Skeletal Deformities and Downregulation of Bone Developmental Pathway in Zebrafish. International Journal of Molecular Sciences. 2021;22(13).
319. Watson CJ, de Oca EMM, Fiedler IAK, Cronrath AR, Callies LK, Swearer AA, et al. wnt16 exerts pleiotropic effects on bone and lean mass in zebrafish. bioRxiv. 2021:2021.08.12.456120.
320. Simon SI, Kim MH. A day (or 5) in a neutrophil's life. Blood. 2010;116(4):511-2.
321. Pillay J, den Braber I, Vrisekoop N, Kwast LM, de Boer RJ, Borghans JAM, et al. In vivo labeling with (H2O)-H-2 reveals a human neutrophil lifespan of 5.4 days. Blood. 2010;116(4):625-7.
322. Andrews T, Sullivan KE. Infections in patients with inherited defects in phagocytic function. Clinical Microbiology Reviews. 2003;16(4):597-+.
323. Pittman K, Kubes P. Damage-Associated Molecular Patterns Control Neutrophil Recruitment. Journal of Innate Immunity. 2013;5(4):315-23.
324. Amarante-Mendes GP, Adjemian S, Branco LM, Zanetti LC, Weinlich R, Bortoluci KR. Pattern Recognition Receptors and the Host Cell Death Molecular Machinery. Frontiers in Immunology. 2018;9.
325. Bernhard S, Hug S, Stratmann AEP, Erber M, Vidoni L, Knapp CL, et al. Interleukin 8 Elicits Rapid Physiological Changes in Neutrophils That Are Altered by Inflammatory Conditions. Journal of Innate Immunity. 2021;13(4):225-41.
326. Cummings CJ, Martin TR, Frevert CW, Quan JM, Wong VA, Mongovin SM, et al. Expression and function of the chemokine receptors CXCR1 and CXCR2 in sepsis. Journal of Immunology. 1999;162(4):2341-6.
327. Rosales C. Neutrophil: A Cell with Many Roles in Inflammation or Several Cell Types? Frontiers in Physiology. 2018;9.

328. Lee WL, Harrison RE, Grinstein S. Phagocytosis by neutrophils. Microbes and Infection. 2003;5(14):1299-306.
329. Yang H, Biermann MH, Brauner JM, Liu Y, Zhao Y, Herrmann M. New insights into Neutrophil extracellular Traps: Mechanisms of Formation and Role in inflammation. Frontiers in Immunology. 2016;7.
330. Nguyen GT, Green ER, Mecsas J. Neutrophils to the ROScue: Mechanisms of NADPH Oxidase Activation and Bacterial Resistance. Frontiers in Cellular and Infection Microbiology. 2017;7.
331. Wang J. Neutrophils in tissue injury and repair. Cell and Tissue Research. 2018;371(3):531-9.
332. Wright HL, Moots RJ, Bucknall RC, Edwards SW. Neutrophil function in inflammation and inflammatory diseases. Rheumatology. 2010;49(9):1618-31.
333. Peiseler M, Kubes P. More friend than foe: the emerging role of neutrophils in tissue repair. Journal of Clinical Investigation. 2019;129(7):2629-39.
334. Xiong SM, Dong LL, Cheng L. Neutrophils in cancer carcinogenesis and metastasis. Journal of Hematology & Oncology. 2021;14(1).
335. Laforge M, Elbim C, Frere C, Hemadi M, Massaad C, Nuss P, et al. Tissue damage from neutrophil-induced oxidative stress in COVID-19. Nature Reviews Immunology. 2020;20(9):515-6.
336. Coelho FM, Pinho V, Amaral FA, Sachs D, Costa VV, Rodrigues DH, et al. The chemokine receptors CXCR1/CXCR2 modulate antigen-induced arthritis by regulating adhesion of neutrophils to the synovial microvasculature. Arthritis and Rheumatism. 2008;58(8):2329-37.
337. Heuer A, Stiel C, Elrod J, Konigs I, Vincent D, Schlegel P, et al. Therapeutic Targeting of Neutrophil Extracellular Traps Improves Primary and Secondary Intention Wound Healing in Mice. Frontiers in Immunology. 2021;12.
338. Nemeth T, Sperandio M, Mocsai A. Neutrophils as emerging therapeutic targets. Nature Reviews Drug Discovery. 2020;19(4):253-75.
339. Baht GS, Vi L, Alman BA. The Role of the Immune Cells in Fracture Healing. Curr Osteoporos Rep. 2018;16(2):138-45.
340. Bastian OW, Croes M, Alblas J, Koenderman L, Leenen LPH, Blokhuis TJ. Neutrophils Inhibit Synthesis of Mineralized Extracellular Matrix by Human Bone Marrow-Derived Stromal Cells In Vitro. Frontiers in Immunology. 2018;9.
341. Marin C, Luyten FP, Van der Schueren B, Kerckhofs G, Vandamme K. The Impact of Type 2 Diabetes on Bone Fracture Healing. Frontiers in Endocrinology. 2018;9.
342. Valderrabano RJ, Lui LY, Lee J, Cummings SR, Orwoll ES, Hoffman AR, et al. Bone Density Loss Is Associated With Blood Cell Counts. Journal of Bone and Mineral Research. 2017;32(2):212-20.
343. Ye XC, Jiang HW, Wang YL, Ji YF, Jiang XS. A correlative studies between osteoporosis and blood cell composition Implications for auxiliary diagnosis of osteoporosis. Medicine. 2020;99(26).
344. Bingol O, Ozdemir G, Kulakoglu B, Keskin OH, Korkmaz I, Kilic E. Admission neutrophil-to-lymphocyte ratio and monocyte-to-lymphocyte ratio to predict 30-day and 1-year mortality in geriatric hip fractures. Injury-International Journal of the Care of the Injured. 2020;51(11):2663-7.
345. Temiz A, Ersozlu S. Admission neutrophil-to-lymphocyte ratio and postoperative mortality in elderly patients with hip fracture. Ulusal Travma Ve Acil Cerrahi Dergisi-Turkish Journal of Trauma & Emergency Surgery. 2019;25(1):71-4.
346. Kuiper JWP, Forster C, Sun C, Peel S, Glogauer M. Zoledronate and pamidronate depress neutrophil functions and survival in mice. British Journal of Pharmacology. 2012;165(2):532-9.
347. Favot CL, Forster C, Glogauer M. The effect of bisphosphonate therapy on neutrophil function: a potential biomarker. International Journal of Oral and Maxillofacial Surgery. 2013;42(5):619-26.
348. Bischoff DS, Sakamoto T, Ishida K, Makhijani NS, Gruber HE, Yamaguchi DT. CXC receptor knockout mice: Characterization of skeletal features and membranous bone healing in the adult mouse. Bone. 2011;48(2):267-74.

349. Mizuno K, Mineo K, Tachibana T, Sumi M, Matsubara T, Hirohata K. The Osteogenetic Potential of Fracture Hematoma - Subperiosteal And Intramuscular Transplantation Of The Hematoma. Journal of Bone and Joint Surgery-British Volume. 1990;72(5):822-9.
350. Monti M, Iommelli F, De Rosa V, Carriero MV, Miceli R, Camerlingo R, et al. Integrin-dependent cell adhesion to neutrophil extracellular traps through engagement of fibronectin in neutrophil-like cells. Plos One. 2017;12(2).
351. Albrengues J, Shields MA, Ng D, Park CG, Ambrico A, Poindexter ME, et al. Neutrophil extracellular traps produced during inflammation awaken dormant cancer cells in mice. Science. 2018;361(6409):1353-+.
352. MacCarthy-Morrogh L, Martin P. The hallmarks of cancer are also the hallmarks of wound healing. Science Signaling. 2020;13(648).
353. Schauer C, Janko C, Munoz LE, Zhao Y, Kienhofer D, Frey B, et al. Aggregated neutrophil extracellular traps limit inflammation by degrading cytokines and chemokines. Nature Medicine. 2014;20(5):511-7.
354. Linnerz T, Hall CJ. The Diverse Roles of Phagocytes During Bacterial and Fungal Infections and Sterile Inflammation: Lessons From Zebrafish. Frontiers in Immunology. 2020;11.
355. Harvie EA, Huttenlocher A. Neutrophils in host defense: new insights from zebrafish. Journal of Leukocyte Biology. 2015;98(4):523-37.
356. Dixon G, Elks, P. M., Loynes, C. A., Whyte, M. K., Renshaw, S. A.,. A Method for the *In Vivo* Measurement of Zebrafish Tissue Neutrophil Lifespan. ISRN Hematol: 2012:915868. doi: 10.5402/2012/915868. Epub 2012 Jul 16.; 2012.
357. Singh SK, Sethi S, Aravamudhan S, Kruger M, Grabher C. Proteome Mapping of Adult Zebrafish Marrow Neutrophils Reveals Partial Cross Species Conservation to Human Peripheral Neutrophils. Plos One. 2013;8(9).
358. Oehlers SHB, Flores MV, Hall CJ, O'Toole R, Swift S, Crosier KE, et al. Expression of zebrafish cxcl8 (interleukin-8) and its receptors during development and in response to immune stimulation. Developmental and Comparative Immunology. 2010;34(3):352-9.
359. de Oliveira S, Reyes-Aldasoro CC, Candel S, Renshaw SA, Mulero V, Calado A. Cxcl8 (IL-8) Mediates Neutrophil Recruitment and Behavior in the Zebrafish Inflammatory Response. Journal of Immunology. 2013;190(8):4349-59.
360. Colucci-Guyon E, Batista AS, Oliveira SDS, Blaud M, Bellettini IC, Marteyn BS, et al. Ultraspecific live imaging of the dynamics of zebrafish neutrophil granules by a histopermeable fluorogenic benzochalcone probe. Chemical Science. 2019;10(12):3654-70.
361. Feng Y, Santoriello C, Mione M, Hurlstone A, Martin P. Live Imaging of Innate Immune Cell Sensing of Transformed Cells in Zebrafish Larvae: Parallels between Tumor Initiation and Wound Inflammation (vol 8, e1000562, 2010). Plos Biology. 2016;14(2).
362. Sipka T, Peroceschi R, Hassan-Abdi R, Gross M, Ellett F, Begon-Pescia C, et al. Damage-Induced Calcium Signaling and Reactive Oxygen Species Mediate Macrophage Activation in Zebrafish. Frontiers in Immunology. 2021;12.
363. Chen WJ, Zhao JJ, Mu D, Wang Z, Liu Q, Zhang YX, et al. Pyroptosis Mediates Neutrophil Extracellular Trap Formation during Bacterial Infection in Zebrafish. Journal of Immunology. 2021;206(8):1913-22.
364. Palic D, Andreasen CB, Ostojic J, Tell RM, Roth JA. Zebrafish (Danio rerio) whole kidney assays to measure neutrophil extracellular trap release and degranulation of primary granules. Journal of Immunological Methods. 2007;319(1-2):87-97.
365. Iorio V, Troughton LD, Hamill KJ. Laminins: Roles and Utility in Wound Repair. Advances in Wound Care. 2015;4(4):250-63.
366. Tang Y, Luo KY, Tan JL, Zhou R, Chen YQ, Chen C, et al. Laminin alpha 4 promotes bone regeneration by facilitating cell adhesion and vascularization. Acta Biomaterialia. 2021;126:183-98.

367. Klavert J, van der Eerden BCJ. Fibronectin in Fracture Healing: Biological Mechanisms and Regenerative Avenues. Frontiers in Bioengineering and Biotechnology. 2021;9.
368. Silva JC, Carvalho MS, Han XR, Xia K, Mikael PE, Cabral JMS, et al. Compositional and structural analysis of glycosaminoglycans in cell-derived extracellular matrices. Glycoconjugate Journal. 2019;36(2):141-54.
369. Gerlza T, Nagele M, Mihalic Z, Trojacher C, Kungl A. Glycosaminoglycans located on neutrophils and monocytes impact on CXCL8-and CCL2-induced cell migration. Cytokine. 2021;142.
370. Teijeira A, Garasa S, Gato M, Alfaro C, Migueliz I, Cirella A, et al. CXCR1 and CXCR2 Chemokine Receptor Agonists Produced by Tumors Induce Neutrophil Extracellular Traps that Interfere with Immune Cytotoxicity. Immunity. 2020;52(5):856-+.
371. Uddin M, Watz H, Malmgren A, Pedersen F. NETopathic Inflammation in Chronic Obstructive Pulmonary Disease and Severe Asthma. Frontiers in Immunology. 2019;10.
372. Pedersen F, Waschki B, Marwitz S, Goldmann T, Kirsten A, Malmgren A, et al. Neutrophil extracellular trap formation is regulated by CXCR2 in COPD neutrophils. European Respiratory Journal. 2018;51(4).
373. Stadtmann A, Zarbock A. CXCR2: from bench to bedside. Frontiers in Immunology. 2012;3.
374. Zhu YY, Huang YM, Ji Q, Fu SQ, Gu J, Tai NZ, et al. Interplay between Extracellular Matrix and Neutrophils in Diseases. Journal of Immunology Research. 2021;2021.
375. Zhu SN, Yu Y, Ren Y, Xu LY, Wang HL, Ling XM, et al. The emerging roles of neutrophil extracellular traps in wound healing. Cell Death & Disease. 2021;12(11).
376. McIlroy DJ, Jarnicki AG, Au GG, Lott N, Smith DW, Hansbro PM, et al. Mitochondrial DNA neutrophil extracellular traps are formed after trauma and subsequent surgery. Journal of Critical Care. 2014;29(6).
377. Palazzolo AM, Suquet C, Konkel ME, Hurst JK. Green fluorescent protein-expressing Escherichia coli as a selective probe for HOCl generation within neutrophils. Biochemistry. 2005;44(18):6910-9.
378. Xu SS, Xie FJ, Tian L, Manno SHC, Manno FAM, Cheng SH. Prolonged neutrophil retention in the wound impairs zebrafish heart regeneration after cryoinjury. Fish & Shellfish Immunology. 2019;94:447-54.
379. Powell D, Lou M, Becker FB, Huttenlocher A. Cxcr1 mediates recruitment of neutrophils and supports proliferation of tumor-initiating astrocytes in vivo. Scientific Reports. 2018;8.
380. Ribon M, Seninet S, Mussard J, Sebbag M, Clavel C, Serre G, et al. Neutrophil extracellular traps exert both pro- and anti-inflammatory actions in rheumatoid arthritis that are modulated by Clq and LL-37. Journal of Autoimmunity. 2019;98:122-31.
381. Jin R, Xu JJ, Gao QQ, Mao XN, Yin J, Lu KY, et al. IL-33-induced neutrophil extracellular traps degrade fibronectin in a murine model of bronchopulmonary dysplasia. Cell Death Discovery. 2020;6(1).
382. Heimroth RD, Casadei E, Benedicenti O, Amemiya CT, Munoz P, Salinas I. The lungfish cocoon is a living tissue with antimicrobial functions. Science Advances. 2021;7(47).
383. Neumann A, Brogden G, von Kockritz-Blickwede M. Extracellular Traps: An Ancient Weapon of Multiple Kingdoms. Biology-Basel. 2020;9(2).
384. Amulic B, Cazalet C, Hayes GL, Metzler KD, Zychlinsky A. Neutrophil Function: From Mechanisms to Disease. Annual Review of Immunology, Vol 30. 2012;30:459-89.
385. Carswell EA, Old LJ, Kassel RL, Green S, Fiore N, Williamson B. Endotoxin-Induced Serum Factor That Causes Necrosis Of Tumors. Proceedings of the National Academy of Sciences of the United States of America. 1975;72(9):3666-70.
386. Webster JD, Vucic D. The Balance of TNF Mediated Pathways Regulates Inflammatory Cell Death Signaling in Healthy and Diseased Tissues. Frontiers in Cell and Developmental Biology. 2020;8.
387. Aggarwal BB. Signalling pathways of the TNF superfamily: A double-edged sword. Nature Reviews Immunology. 2003;3(9):745-56.
388. Mannel DN, Moore RN, Mergenhagen SE. Macrophages As A Source Of Tumoricidal Activity (Tumor-Necrotizing Factor). Infection and Immunity. 1980;30(2):523-30.

389. Vroling AB, Duinsbergen D, Fokkens WJ, van Drunen CM. Allergen induced gene expression of airway epithelial cells shows a possible role for TNF-alpha. Allergy. 2007;62(11):1310-9.
390. Grell M, Douni E, Wajant H, Lohden M, Clauss M, Maxeiner B, et al. The Transmembrane Form Of Tumor-Necrosis-Factor Is The Prime Activating Ligand Of The 80 Kda Tumor-Necrosis-Factor Receptor. Cell. 1995;83(5):793-802.
391. Tartaglia LA, Ayres TM, Wong GHW, Goeddel DV. A Novel Domain Within The 55 Kd Tnf Receptor Signals Cell-Death. Cell. 1993;74(5):845-53.
392. Hsu HL, Xiong J, Goeddel DV. The Tnf Receptor 1-Associated Protein Tradd Signals Cell-Death And Nf-Kappa-B Activation. Cell. 1995;81(4):495-504.
393. Wajant H, Scheurich P. TNFR1-induced activation of the classical NF-kappa B pathway. Febs Journal. 2011;278(6):862-76.
394. Wajant H, Siegmund D. TNFR1 and TNFR2 in the Control of the Life and Death Balance of Macrophages. Frontiers in Cell and Developmental Biology. 2019;7.
395. Moatti A, Cohen JL. The TNF-alpha/TNFR2 Pathway: Targeting a Brake to Release the Anti-tumor Immune Response. Frontiers in Cell and Developmental Biology. 2021;9.
396. Brenner D, Blaser H, Mak TW. Regulation of tumour necrosis factor signalling: live or let die. Nature Reviews Immunology. 2015;15(6):362-74.
397. Schliemann M, Bullinger E, Borchers S, Allgower F, Findeisen R, Scheurich P. Heterogeneity reduces sensitivity of cell death for TNF-Stimuli. Bmc Systems Biology. 2011;5.
398. Fahlman C, Jacobsen FW, Veiby OP, McNiece IK, Blomhoff HK, Jacobsen SEW. Tumor-Necrosis-Factor-Alpha (TNF-Alpha) Potently Enhances In-Vitro Macrophage Production From Primitive Murine Hematopoietic Progenitor Cells In Combination With Stem-Cell Factor And Interleukin-7 - Novel Stimulatory Role Of P55 TNF Receptors. Blood. 1994;84(5):1528-33.
399. Taylor DJ. Interleukin-4 (Il-4) Induces Down-Modulation And Shedding Of The P55 Tumor-Necrosis-Factor Receptor And Inhibits Tnf-Alpha-S Effect On Rheumatoid Synovial Fibroblasts. Rheumatology International. 1994;14(1):21-5.
400. Havell EA. Evidence That Tumor Necrosis Factor Has An Important Role In Antibacterial Resistance. Journal of Immunology. 1989;143(9):2894-9.
401. Parameswaran N, Patial S. Tumor Necrosis Factor-a Signaling in Macrophages. Critical Reviews in Eukaryotic Gene Expression. 2010;20(2):87-103.
402. Atri C, Guerfali FZ, Laouini D. Role of Human Macrophage Polarization in Inflammation during Infectious Diseases. International Journal of Molecular Sciences. 2018;19(6).
403. Marino MW, Dunn A, Grail D, Inglese M, Noguchi Y, Richards E, et al. Characterization of tumor necrosis factor-deficient mice. Proceedings of the National Academy of Sciences of the United States of America. 1997;94(15):8093-8.
404. Pfeffer K, Matsuyama T, Kundig TM, Wakeham A, Kishihara K, Shahinian A, et al. Mice Deficient For The 55kd Tumor-Necrosis-Factor Receptor Are Resistant To Endotoxic-Shock, Yet Succumb To L-Monocytogenes Infection. Cell. 1993;73(3):457-67.
405. Erickson SL, Desauvage FJ, Kikly K, Carvermoore K, Pittsmeek S, Gillett N, et al. Decreased Sensitivity To Tumor-Necrosis-Factor But Normal T-Cell Development In TNF Receptor-2-Deficient Mice. Nature. 1994;372(6506):560-3.
406. Pasparakis M, Alexopoulou L, Episkopou V, Kollias G. Immune and inflammatory responses in TNF alpha-deficient mice: A critical requirement for TNF alpha in the formation of primary B cell follicles, follicular dendritic cell networks and germinal centers, and in the maturation of the humoral immune response. Journal of Experimental Medicine. 1996;184(4):1397-411.
407. Ritsu M, Kawakami K, Kanno E, Tanno H, Ishii K, Imai Y, et al. Critical role of tumor necrosis factor-alpha in the early process of wound healing in skin. Journal of Dermatology Dermatologic Surgery-Jdds. 2017;21(1):14-9.

408. Das A, Sinha M, Datta S, Abas M, Chaffee S, Sen CK, et al. Monocyte and Macrophage Plasticity in Tissue Repair and Regeneration. American Journal of Pathology. 2015;185(10):2596-606.
409. Gurevich DB, French KE, Collin JD, Cross SJ, Martin P. Live imaging the foreign body response in zebrafish reveals how dampening inflammation reduces fibrosis. Journal of Cell Science. 2020;133(5).
410. Montfort A, Colacios C, Levade T, Andrieu-Abadie N, Meyer N, Segui B. The TNF Paradox in Cancer Progression and Immunotherapy. Frontiers in Immunology. 2019;10.
411. Ahmad S, Azid NA, Boer JC, Lim J, Chen X, Plebanski M, et al. The Key Role of TNF-TNFR2 Interactions in the Modulation of Allergic Inflammation: A Review. Frontiers in Immunology. 2018;9.
412. Ashcroft GS, Jeong MJ, Ashworth JJ, Hardman M, Jin WW, Moutsopoulos N, et al. Tumor necrosis factor-alpha (TNF-a) is a therapeutic target for impaired cutaneous wound healing. Wound Repair and Regeneration. 2012;20(1):38-49.
413. Manara M, Sinigaglia L. Bone and TNF in rheumatoid arthritis: clinical implications. Rmd Open. 2015;1.
414. Bamias G, Dahman MI, Arseneau KO, Guanzon M, Gruska D, Pizarro TT, et al. Intestinal-Specific TNF alpha Overexpression Induces Crohn's-Like Ileitis in Mice. Plos One. 2013;8(8).
415. Roulis M, Armaka M, Manoloukos M, Apostolaki M, Kollias G. Intestinal epithelial cells as producers but not targets of chronic TNF suffice to cause murine Crohn-like pathology. Proceedings of the National Academy of Sciences of the United States of America. 2011;108(13):5396-401.
416. Lis K, Kuzawinska O, Balkowiec-Iskra E. Tumor necrosis factor inhibitors - state of knowledge. Archives of Medical Science. 2014;10(6):1175-85.
417. Orti-Casan N, Wu YY, Naude PJW, De Deyn PP, Zuhorn IS, Eisel ULM. Targeting TNFR2 as a Novel Therapeutic Strategy for Alzheimer's Disease. Frontiers in Neuroscience. 2019;13.
418. Harris J, Hope JC, Keane J. Tumor Necrosis Factor Blockers Influence Macrophage Responses to Mycobacterium tuberculosis. Journal of Infectious Diseases. 2008;198(12):1842-50.
419. Keane J, Gershon S, Wise RP, Mirabile-Levens E, Kasznica J, Schwieterman WD, et al. Tuberculosis associated with infliximab, a tumor necrosis factor (alpha)-neutralizing agent. New England Journal of Medicine. 2001;345(15):1098-104.
420. Ferraro S, Leonardi L, Convertino I, Blandizzi C, Tuccori M. Is There a Risk of Lymphoma Associated With Anti-tumor Necrosis Factor Drugs in Patients With Inflammatory Bowel Disease? A Systematic Review of Observational Studies. Frontiers in Pharmacology. 2019;10.
421. Solomon DH, Mercer E, Kavanaugh A. Observational studies on the risk of cancer associated with tumor necrosis factor inhibitors in rheumatoid arthritis: A review of their methodologies and results. Arthritis and Rheumatism. 2012;64(1):21-32.
422. McMillan D, Martinez-Fleites C, Porter J, Fox D, Davis R, Mori P, et al. Structural insights into the disruption of TNF-TNFR1 signalling by small molecules stabilising a distorted TNF. Nature Communications. 2021;12(1).
423. Zhao BH. TNF and Bone Remodeling. Current Osteoporosis Reports. 2017;15(3):126-34.
424. Gough P, Myles IA. Tumor Necrosis Factor Receptors: Pleiotropic Signaling Complexes and Their Differential Effects. Frontiers in Immunology. 2020;11.
425. Yao ZQ, Li P, Zhang Q, Schwarz EM, Keng P, Arbini A, et al. Tumor necrosis factor-alpha increases circulating osteoclast precursor numbers by promoting their proliferation and differentiation in the bone marrow through up-regulation of c-Fms expression. Journal of Biological Chemistry. 2006;281(17):11846-55.
426. Zhang Q, Guo R, Schwarz EM, Boyce BF, Xing LP. TNF inhibits production of stromal cell-derived factor 1 by bone stromal cells and increases osteoclast precursor mobilization from bone marrow to peripheral blood. Arthritis Research & Therapy. 2008;10(2).

427. Kitaura H, Kimura K, Ishida M, Kohara H, Yoshimatsu M, Takano-Yamamoto T. Immunological Reaction in TNF-alpha-Mediated Osteoclast Formation and Bone Resorption In Vitro and In Vivo. Clinical & Developmental Immunology. 2013.
428. Phan QT, Liu, R., Tan, W. H., Imangali, N., Cheong, B., Schartl, M., & Winkler, C. Macrophages Switch to an Osteo-Modulatory Profile Upon RANKL Induction in a Medaka (Oryzias latipes) Osteoporosis Model. JBMR Plus. 2020;4(11):e10409.
429. Gulyas K, Horvath A, Vegh E, Pusztai A, Szentpetery A, Petho Z, et al. Effects of 1-year anti-TNF-alpha therapies on bone mineral density and bone biomarkers in rheumatoid arthritis and ankylosing spondylitis. Clinical Rheumatology. 2020;39(1):167-75.
430. Anandarajah AP, Schwarz EM, Totterman S, Monu J, Feng CY, Shao T, et al. The effect of etanercept on osteoclast precursor frequency and enhancing bone marrow oedema in patients with psoriatic arthritis. Annals of the Rheumatic Diseases. 2008;67(3):296-301.
431. Gilbert L, He XF, Farmer P, Boden S, Kozlowski M, Rubin J, et al. Inhibition of osteoblast differentiation by tumor necrosis factor-alpha. Endocrinology. 2000;141(11):3956-64.
432. Lee HL, Woo KM, Ryoo HM, Baek JH. Tumor necrosis factor-alpha increases alkaline phosphatase expression in vascular smooth muscle cells via MSX2 induction. Biochemical and Biophysical Research Communications. 2010;391(1):1087-92.
433. Lee SS, Sharma AR, Choi BS, Jung JS, Chang JD, Park S, et al. The effect of TNF alpha secreted from macrophages activated by titanium particles on osteogenic activity regulated by WNT/BMP signaling in osteoprogenitor cells. Biomaterials. 2012;33(17):4251-63.
434. Huang H, Zhao N, Xu X, Xu Y, Li S, Zhang J, et al. Dose-specific effects of tumor necrosis factor alpha on osteogenic differentiation of mesenchymal stem cells. Cell Proliferation. 2011;44(5):420-7.
435. Feng XM, Feng GJ, Xing J, Shen BY, Li LR, Tan W, et al. TNF-alpha triggers osteogenic differentiation of human dental pulp stem cells via the NF-kappa B signalling pathway. Cell Biology International. 2013;37(12):1267-75.
436. Kubota A, Hasegawa K, Suguro T, Koshihara Y. Tumor necrosis factor-alpha promotes the expression of osteoprotegerin in rheumatoid synovial fibroblasts. Journal of Rheumatology. 2004;31(3):426-35.
437. Briolay A, Lencel P, Bessueille L, Caverzasio J, Buchet R, Magne D. Autocrine stimulation of osteoblast activity by Wnt5a in response to TNF-alpha in human mesenchymal stem cells. Biochemical and Biophysical Research Communications. 2013;430(3):1072-7.
438. Seriolo B, Paolino S, Sulli A, Ferretti V, Cutolo M. Bone metabolism changes during anti-TNF-alpha therapy in patients with active rheumatoid arthritis. Basic and Clinical Aspects of Neuroendocrine Immunology in Rheumatic Diseases. 2006;1069:420-7.
439. Al-Bogami M, Bystrom J, Clanchy F, Taher TE, Mangat P, Williams RO, et al. TNF alpha inhibitors reduce bone loss in rheumatoid arthritis independent of clinical response by reducing osteoclast precursors and IL-20. Rheumatology. 2021;60(2):947-57.
440. Kang KY, Ju JH, Park SH, Kim HY. The paradoxical effects of TNF inhibitors on bone mineral density and radiographic progression in patients with ankylosing spondylitis. Rheumatology. 2013;52(4):718-26.
441. van der Weijden MAC, van Denderen JC, Lems WF, Nurmohamed MT, Dijkmans BAC, van der Horst-Bruinsma IE. Etanercept Increases Bone Mineral Density in Ankylosing Spondylitis, but Does Not Prevent Vertebral Fractures: Results of a Prospective Observational Cohort Study. The Journal of Rheumatology. 2016;43(4):758.
442. Maldonado-Pérez MB, Castro-Laria L, Caunedo-Álvarez A, Montoya-García MJ, Giner-García M, Argüelles-Arias F, et al. Does the Antitumor Necrosis Factor-α Therapy Decrease the Vertebral Fractures Occurrence in Inflammatory Bowel Disease? Journal of Clinical Densitometry. 2019;22(2):195-202.

443. Sakunrangsit N, Metheepakornchai P, Kumpunya S, Greenblatt MB, Leelahavanichkul A, Pisitkun P, et al. Etanercept prevents TNF-alpha mediated mandibular bone loss in Fc gamma RIIb(-/-) lupus model. Plos One. 2021;16(4).
444. Chen JF, Hsu CY, Yu SF, Ko CH, Chiu WC, Lai HM, et al. The impact of long-term biologics/target therapy on bone mineral density in rheumatoid arthritis: a propensity score-matched analysis. Rheumatology. 2020;59(9):2471-80.
445. Timmen M, Hidding H, Wieskotter B, Baum W, Pap T, Raschke MJ, et al. Influence of antiTNF-alpha antibody treatment on fracture healing under chronic inflammation. Bmc Musculoskeletal Disorders. 2014;15.
446. Lehmann W, Edgar CM, Wang K, Cho TJ, Barnes GL, Kakar S, et al. Tumor necrosis factor alpha (TNF-alpha) coordinately regulates the expression of specific matrix metalloproteinases (MMPS) and angiogenic factors during fracture healing. Bone. 2005;36(2):300-10.
447. Glass GE, Chan JK, Freidin A, Feldmann M, Horwood NJ, Nanchahal J. TNF-alpha promotes fracture repair by augmenting the recruitment and differentiation of muscle-derived stromal cells. Proceedings of the National Academy of Sciences of the United States of America. 2011;108(4):1585-90.
448. Chan JK, Glass GE, Ersek A, Freidin A, Williams GA, Gowers K, et al. Low-dose TNF augments fracture healing in normal and osteoporotic bone by up-regulating the innate immune response. Embo Molecular Medicine. 2015;7(5):547-61.
449. Paunovic Z, Milutinovic S, Stankovic N, Abazovic D, Stanojevic I, Rakic M, et al. Association of fracture configuration and callus formation with a concentration of proinflammatory cytokines in children with long bone fractures. Vojnosanitetski Pregled. 2021;78(4):397-402.
450. Li YG, Xiao TY, Zou J. Fish TNF and TNF receptors. Science China-Life Sciences. 2021;64(2):196-220.
451. Duan YL, Wang YW, Li ZB, Ma LZ, Wei XH, Yang JQ, et al. The unique structure of the zebrafish TNF-alpha homotrimer. Developmental and Comparative Immunology. 2021;122.
452. Clay H, Volkman HE, Ramakrishnan L. Tumor necrosis factor signaling mediates resistance to mycobacteria by inhibiting bacterial growth and macrophage death. Immunity. 2008;29(2):283-94.
453. Nguyen-Chi M, Laplace-Builhe B, Travnickova J, Luz-Crawford P, Tejedor G, Lutfalla G, et al. TNF signaling and macrophages govern fin regeneration in zebrafish larvae. Cell Death & Disease. 2017;8.
454. Espin R, Roca FJ, Candel S, Sepulcre MP, Gonzalez-Rosa JM, Alcaraz-Perez F, et al. TNF receptors regulate vascular homeostasis in zebrafish through a caspase-8, caspase-2 and P53 apoptotic program that bypasses caspase-3. Disease Models & Mechanisms. 2013;6(2):383-96.
455. Candel S, de Oliveira S, Lopez-Munoz A, Garcia-Moreno D, Espin-Palazon R, Tyrkalska SD, et al. Tnfa Signaling Through Tnfr2 Protects Skin Against Oxidative Stress-Induced Inflammation. Plos Biology. 2014;12(5).
456. Muller GW, Chen R, Huang SY, Corral LG, Wong LM, Patterson RT, et al. Amino-substituted thalidoimide analogs: Potent inhibitors of TNF-alpha production. Bioorganic & Medicinal Chemistry Letters. 1999;9(11):1625-30.
457. Jung YJ, Tweedie D, Scerba MT, Kim DS, Palmas MF, Pisanu A, et al. Repurposing Immunomodulatory Imide Drugs (IMiDs) in Neuropsychiatric and Neurodegenerative Disorders. Frontiers in Neuroscience. 2021;15.
458. Pasqualetti S, Banfi G, Mariotti M. Osteoblast and osteoclast behavior in zebrafish cultured scales. Cell and Tissue Research. 2012;350(1):69-75.
459. Ding J, Ghali O, Lencel P, Broux O, Chauveau C, Devedjian JC, et al. TNF-alpha and IL-1 beta inhibit RUNX2 and collagen expression but increase alkaline phosphatase activity and mineralization in human mesenchymal stem cells. Life Sciences. 2009;84(15-16):499-504.
460. Ando K, Shibata E, Hans S, Brand M, Kawakami A. Osteoblast Production by Reserved Progenitor Cells in Zebrafish Bone Regeneration and Maintenance. Developmental Cell. 2017;43(5):643-+.

461. Sousa S, Afonso N, Bensimon-Brito A, Fonseca M, Simoes M, Leon J, et al. Differentiated skeletal cells contribute to blastema formation during zebrafish fin regeneration. Development. 2011;138(18):3897-905.
462. Liu T, Zhang L, Joo D, Sun S-C. NF-kappa B signaling in inflammation. Signal Transduction and Targeted Therapy. 2017;2.
463. Mishra R, Sehring I, Cederlund M, Mulaw M, Weidinger G. NF-kappa B Signaling Negatively Regulates Osteoblast Dedifferentiation during Zebrafish Bone Regeneration. Developmental Cell. 2020;52(2):167-+.
464. Jerez HE, Altube MJ, Gandola YB, Gonzalez L, Gonzalez MC, Morilla MJ, et al. Macrophage apoptosis using alendronate in targeted nanoarchaeosomes. European Journal of Pharmaceutics and Biopharmaceutics. 2021;160:42-54.
465. Sehring IM, Weidinger G. Recent advancements in understanding fin regeneration in zebrafish. Wiley Interdisciplinary Reviews-Developmental Biology. 2020;9(1).
466. Poss FD, Shen JX, Nechiporuk A, McMahon G, Thisse B, Thisse C, et al. Roles for Fgf signaling during zebrafish fin regeneration. Developmental Biology. 2000;222(2):347-58.
467. Tornini VA, Thompson JD, Allen RL, Poss KD. Live fate-mapping of joint-associated fibroblasts visualizes expansion of cell contributions during zebrafish fin regeneration. Development. 2017;144(16):2889-95.
468. Wei H, Xu Y, Wang Y, Xu L, Mo C, Li L, et al. Identification of Fibroblast Activation Protein as an Osteogenic Suppressor and Anti-osteoporosis Drug Target. Cell Reports. 2020;33(2).
469. Chung K-M, Hsu S-C, Chu Y-R, Lin M-Y, Jiaang W-T, Chen R-H, et al. Fibroblast Activation Protein (FAP) Is Essential for the Migration of Bone Marrow Mesenchymal Stem Cells through RhoA Activation. Plos One. 2014;9(2).
470. Hlushchuk R, Broennimann D, Shokiche CC, Schaad L, Triet R, Jazwinska A, et al. Zebrafish Caudal Fin Angiogenesis Assay-Advanced Quantitative Assessment Including 3-Way Correlative Microscopy. Plos One. 2016;11(3).
471. Bayliss PE, Bellavance KL, Whitehead GG, Abrams JM, Aegerter S, Robbins HS, et al. Chemical modulation of receptor signaling inhibits regenerative angiogenesis in adult zebrafish. Nature Chemical Biology. 2006;2(5):265-73.
472. Loeffler J, Duda GN, Sass FA, Dienelt A. The Metabolic Microenvironment Steers Bone Tissue Regeneration. Trends in Endocrinology and Metabolism. 2018;29(2):99-110.
473. Xu G, Xue M, Wang H, Xiang C. Hypoxia-inducible factor-1 alpha antagonizes the hypoxia-mediated osteoblast cell viability reduction by inhibiting apoptosis. Experimental and Therapeutic Medicine. 2015;9(5):1801-6.
474. Tang WJ, Yang F, Li Y, de Crombrugghe B, Jiao HL, Xiao GZ, et al. Transcriptional Regulation of Vascular Endothelial Growth Factor (VEGF) by Osteoblast-specific Transcription Factor Osterix (Osx) in Osteoblasts. Journal of Biological Chemistry. 2012;287(3):1671-8.
475. Regan JN, Lim J, Shi Y, Joeng KS, Arbeit JM, Shohet RV, et al. Up-regulation of glycolytic metabolism is required for HIF1 alpha-driven bone formation. Proceedings of the National Academy of Sciences of the United States of America. 2014;111(23):8673-8.
476. Khatib AM, Lahlil R, Hagedorn M, Delomenie C, Christophe O, Denis C, et al. Biological outcome and mapping of total factor cascades in response to HIF induction during regenerative angiogenesis. Oncotarget. 2016;7(11):12102-20.
477. Moss JJ, Hammond CL, Lane JD. Zebrafish as a model to study autophagy and its role in skeletal development and disease. Histochemistry and Cell Biology. 2020;154(5):549-64.
478. Zheng LW, Wang WC, Ni JD, Mao XZ, Song DY, Liu T, et al. Role of autophagy in tumor necrosis factor-alpha-induced apoptosis of osteoblast cells. Journal of Investigative Medicine. 2017;65(6):1014-20.

479. Schmidt JR, Geurtzen K, von Bergen M, Schubert K, Knopf F. Glucocorticoid Treatment Leads to Aberrant Ion and Macromolecular Transport in Regenerating Zebrafish Fins. Frontiers in Endocrinology. 2019;10.
480. Wehner D, Cizelsky W, Vasudevaro MD, Oezhan G, Haase C, Kagermeier-Schenk B, et al. Wnt/beta-Catenin Signaling Defines Organizing Centers that Orchestrate Growth and Differentiation of the Regenerating Zebrafish Caudal Fin. Cell Reports. 2014;6(3):467-81.
481. Stoick-Cooper CL, Weidinger G, Riehle KJ, Hubbert C, Major MB, Fausto N, et al. Distinct Wnt signaling pathways have opposing roles in appendage regeneration. Development. 2007;134(3):479-89.
482. Stewart S, Gomez AW, Armstrong BE, Henner A, Stankunas K. Sequential and Opposing Activities of Wnt and BMP Coordinate Zebrafish Bone Regeneration. Cell Reports. 2014;6(3):482-98.
483. Chen DF, Li Y, Zhou ZY, Xing YG, Zhong Y, Zou XN, et al. Synergistic Inhibition of Wnt Pathway by HIF-1 alpha and Osteoblast-Specific Transcription Factor Osterix (Osx) in Osteoblasts. Plos One. 2012;7(12).
484. Buono L, Corbacho J, Naranjo S, Almuedo-Castillo M, Moreno-Marmol T, de la Cerda B, et al. Analysis of gene network bifurcation during optic cup morphogenesis in zebrafish. Nature Communications. 2021;12(1).
485. Loontiens S, Depestel L, Vanhauwaert S, Dewyn G, Gistelinck C, Verboom K, et al. Purification of high-quality RNA from a small number of fluorescence activated cell sorted zebrafish cells for RNA sequencing purposes. Bmc Genomics. 2019;20.
486. Gerlach GF, Morales EE, Wingert RA. Microbead Implantation in the Zebrafish Embryo. Jove-Journal of Visualized Experiments. 2015(101).
487. McDonald GLK, Wang MD, Hammond CL, Bergen DJM. Pharmacological Manipulation of Early Zebrafish Skeletal Development Shows an Important Role for Smad9 in Control of Skeletal Progenitor Populations. Biomolecules. 2021;11(2).
488. Jonz MG, Nurse CA. Development of oxygen sensing in the gills of zebrafish. Journal of Experimental Biology. 2005;208(8):1537-49.
489. Kague E, Karasik D. Functional Validation of Osteoporosis Genetic Findings Using Small Fish Models. Genes. 2022;13(2).
490. Todd H, Galea GL, Meakin LB, Delisser PJ, Lanyon LE, Windahl SH, et al. Wnt16 Is Associated with Age-Related Bone Loss and Estrogen Withdrawal in Murine Bone. Plos One. 2015;10(10).
491. O'Byrne PM, Metev H, Puu M, Richter K, Keen C, Uddin M, et al. Efficacy and safety of a CXCR2 antagonist, AZD5069, in patients with uncontrolled persistent asthma: a randomised, double-blind, placebo-controlled trial. Lancet Respiratory Medicine. 2016;4(10):797-806.
492. Wenisch C, Patruta S, Daxbock F, Krause R, Horl W. Effect of age on human neutrophil function. Journal of Leukocyte Biology. 2000;67(1):40-5.
493. Josephson AM, Bradaschia-Correa V, Lee S, Leclerc K, Patel KS, Lopez EM, et al. Age-related inflammation triggers skeletal stem/progenitor cell dysfunction. Proceedings of the National Academy of Sciences of the United States of America. 2019;116(14):6995-7004.
494. Kylmaoja E, Nakamura M, Turunen S, Patlaka C, Andersson G, Lehenkari P, et al. Peripheral blood monocytes show increased osteoclast differentiation potential compared to bone marrow monocytes. Heliyon. 2018;4(9).
495. King AC, Gut M, Zenker AK. Shedding new light on early sex determination in zebrafish. Archives of Toxicology. 2020;94(12):4143-58.
496. Maack G, Segner H. Morphological development of the gonads in zebrafish. Journal of Fish Biology. 2003;62(4):895-906.
497. Ahi EP, Walker BS, Lassiter CS, Jonsson ZO. Investigation of the effects of estrogen on skeletal gene expression during zebrafish larval head development. Peerj. 2016;4.

498. Kim YI, Lee JN, Bhandari S, Nam IK, Yoo KW, Kim SJ, et al. Cartilage development requires the function of Estrogen-related receptor alpha that directly regulates sox9 expression in zebrafish. Scientific Reports. 2015;5.
499. Chen Y, Tang HP, Wang L, He JN, Guo Y, Liu Y, et al. Fertility Enhancement but Premature Ovarian Failure in esr1-Deficient Female Zebrafish. Frontiers in Endocrinology. 2018;9.
500. Takatsu K, Miyaoku K, Roy SR, Murono Y, Sago T, Itagaki H, et al. Induction of Female-to-Male Sex Change in Adult Zebrafish by Aromatase Inhibitor Treatment. Scientific Reports. 2013;3.
501. Rahaman MM, Kumagai R, Tokumoto T. Rapid Induction of Female-to-Male Sex Change in Adult Zebrafish by Injection of an Aromatase Inhibitor. Zebrafish. 2020;17(4):261-7.
502. Gorelick DA, Halpern ME. Visualization of Estrogen Receptor Transcriptional Activation in Zebrafish. Endocrinology. 2011;152(7):2690-703.
503. Damdimopoulou P, Treuter E. Reporter Zebrafish: Endocrine Disruption Meets Estrogen Signaling. Endocrinology. 2011;152(7):2542-5.